UNIVERSITAT ROVIRA i VIRGILI

Dynamic Covalent Capsules based on Calix[4]pyrrole Scaffolds

CHIARA FRANCESCA MARIA MIRABELLA

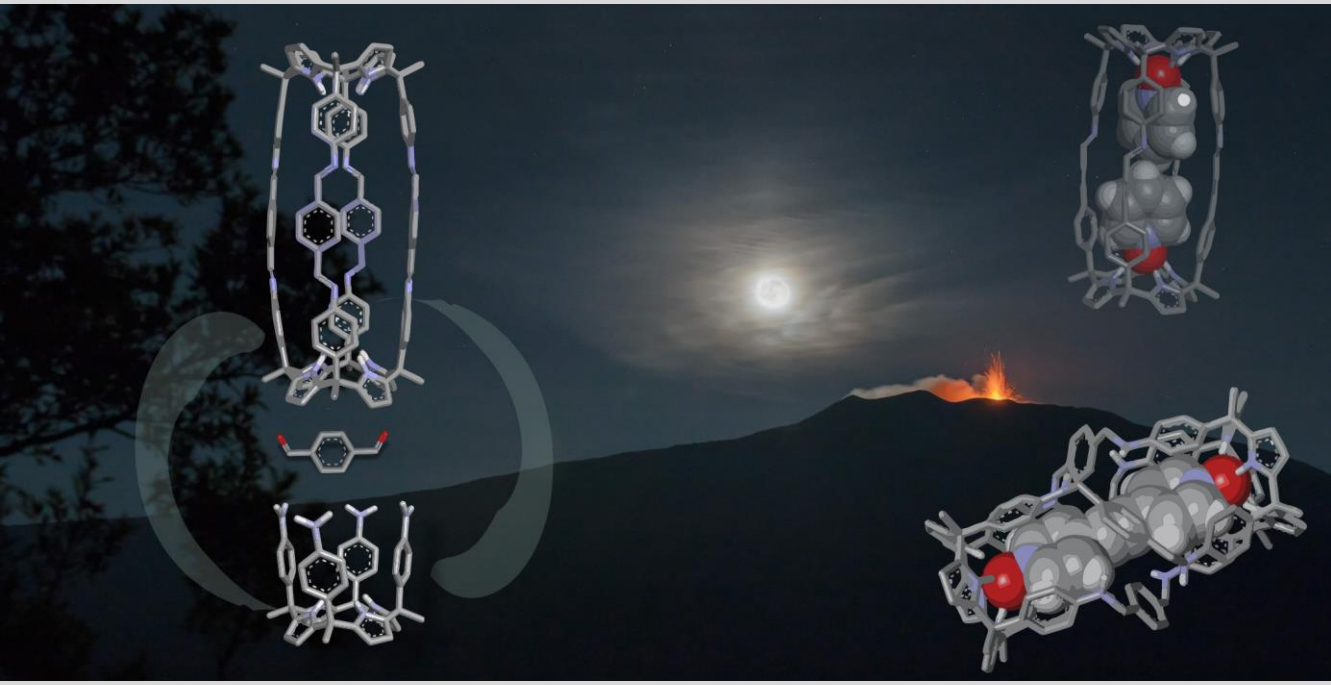

DOCTORAL THESIS
2022

DOCTORAL THESIS

Chiara Francesca Maria Mirabella

DYNAMIC COVALENT CAPSULES BASED ON CALIX[4]PYRROLE SCAFFOLDS

Supervised by Prof. Pablo Ballester Balaguer

UNIVERSITAT
ROVIRA i VIRGILI

Tarragona

2022

Institut Català d'Investigació Química

Av. Països Catalans, 16
43007 Tarragona, Spain
Tel. (+34) 977 920 200
email: iciq@iciq.es

UNIVERSITAT ROVIRA i VIRGILI
Dept. de Química Analítica i Química Orgànica

Carrer de Marcel·lí Domingo, 1
43007 Tarragona, Spain
Tel. (+34) 977 55 97 69
email: sdn4@urv.cat

I STATE that the present study, entitled "Dynamic Covalent Capsules based on Calix[4]pyrrole Scaffolds", presented by Chiara Francesca Maria Mirabella for the award of the degree of Doctor, has been carried out under my supervision at the Institute of Chemical Research of Catalonia (ICIQ).

Tarragona, June 2022

Doctoral Thesis Supervisor

Prof. Pablo Ballester Balaguer

Dissi lu surci a la nuci: "dammi tempu ca ti perciu"

Said the maggot to the tree:

"Lend me time and I'll pierce thee"

Proverbio siciliano

Sicilian proverb

"Which is more important," asked Big Panda, "the journey or the destination?"

"The company". Said Tiny Dragon

James Norbury

Acknowledgements

In the following pages I try to acknowledge all the people who in some ways contributed to my arrival at this destination. Who with a big or small help participated in this short and at the same time long frame of my professional and emotional journey.

I would like to say thanks to my thesis supervisor, **Prof. Pau Ballester** for the scientific knowledge he transferred to me. I know his research group was the best I could choose to professionally improve as researcher and acquire a critical point of view on the scientific phenomena around me.

I also say thanks to **Gemma Aragay** for the precious advice received during these years and the experimental help I needed. Thanks for having introduced me to this amazing NOAH ITN, to all the opportunities and the activities involved in it. We shared very pleasant moments during our schools and groups activities, included our recent walk in the Grunewald forest in Berlin. Thanks for making me discover the world of outreach through our funny and creative NOAH Lab.

I want to acknowledge **Beatriz Martin** for the help in the most annoying but also important part, the bureaucrat and papeleo. Also thanks for being always ready to help us in whatever we needed and for your infinite kindness.

Many thanks to all my **lab mates**. As reported at the very beginning of the thesis, the important part of the trip is not the destination but the company. Without your constant support anything would have been the same! Thanks for having shared with me lots of your different cultures and habits. That made me a richer person than I was at the beginning of this journey. Thanks to the new members of the lab **Tamal**, **Evgeny**, **Karen**, **Eva**, **Esteban**. We did not spend lot of time together but I am glad to have met you guys and have learned something from all of you.

Thanks to **Hayley**, the first PhD student I supervised. I hope I could properly pass on the secrets and pains of wonderful imine capsules to you.

Thanks to the "loquisimo" **Lluis Martinez**, the postdoc of my heart. With you friendly and funny behaviours you taught me a lot, not only about liposomes but about chemistry in general.

Thanks to **Giulia Moncelsi**, my first friend in Tarragona. You welcomed me in the warmest way you could making me feel immediately at home, bringing me to the

Arrabbassada or wherever you were going. Even if just a bit older than me, you always have represented for me a wise older sister. You taught me to forget about fears and shyness and instead enjoy every aspects of life, people and places. I will never forget our crazy nights dancing between El Cau and Highland at rhythm of "dej… dej… dej…"and or just walking through the city and the beach talking about our lives and "tazza monofiato".

Thanks to my friend and dj of PB4 **Ricardo Molina**! "Please, don't let me be misunderstood"…but we had never more listened to such good music in the lab without you there. You made PB4 an happier lab just running to Corte Ingles to buy the cable for the speakers! Thanks for letting me enter in your circle of selected good friends and letting me share with you afternoons in Raffa and exciting games nights (especially playing Katan)!
Thanks a lot to **Felipe Sierra**, for your infinite kindness and your wise Colombian beliefs. Your warm and happy attitude always gave me the positive vibes to get through the worst days. You taught me to always look for the best side of people and things.
Thanks to **Dragos Dabuleanu** for the crazy experiments in the lab and the brilliant ideas about chemistry!
Thanks to **Guillem Peñuelas** for the unforgettable lessons of Catalan folklore and the nice afternoons all together laying on the sofa of your home.
Thanks to **Luis Escobar** for having transferred to me some practical knowledge during my first months in PB4.

Many thanks to my PhD husband, the unique **Pedro Ferreira**! Impossible to summarize in some words all the amazing experiences we lived together. Thanks for withstanding me literally every day for the last 4 years. All the laughs and the tears, lunches and dinners, the columns and the preparative TLCs and the tetranitrocalix[4]pyrrole pain… all of this with you! And the best… our long walks in the forests between Leverkusen, Köln and Duesseldorf trying to not get lost during the sunset… and then arrive safe to Netto to buy your favourite Oreo snacks and recover our strengths. Ainda me lembro daquele dia in Duesseldorf…. "Justineeee!" All memories that I will always bring with me. OBRIGADA pela tua amizade e por todo o bacalhau a braz!

Thanks to **Yifan** and **Qing Qing**! I really enjoyed your delicious hot pots and your stories about Chinese cousin and habits.

And I have to say thanks to Andrea… just because you are Andrea! Thanks for accompanying me in every step of this journey called life.
Thanks to all visiting students and researcher who passed by PB4: **Kaisa, Jorn, Inma, Alicia, Sebastian, Anna, Martina, Maria** for giving me the opportunity to borrow from you a bit of chemistry and lend mine. Special thanks to **Stefania Gambaro**, incredible concentrate of energy and laughs. You made that sad COVID times a better period for all of us. I will never forget all the efforts we made to NOT get our resorcinarenes!
Thanks to all **NOAH network**! It was a pleasure to travel with you and participate to our schools. Especially thanks to **Quentin Bouvier** and **Arturo Llamosi**, who spent some times in PB4 with us. I really enjoyed the nights in Quentin's terrace and Arturo's classes on " How to be a perfect nerd"! Thanks to **Daniel Sanchez** and **Santiago Pons**, for having shared with me more than just NOAH Schools and meetings.

Thanks to **Prof. Christopher Schalley** and **Daniel Stares** for having introduced me to the world of gas phase in Berlin. Thanks for your lessons about supra chem in gas phase and for giving me the opportunity to learn how to use a mass spectrometer.

I also remember with particular pleasure the time spent in Covestro Leverkusen with **Irene Latorre**, **Laura Woods, Anne Kutz**, **Britta Doebler**. I really appreciated the time you spent teaching to me a bit of polymer science and introducing me to the industry world. For this I also want to say thanks to **Stefanie Eiden** for the amazing opportunity to join Covestro Leverkusen for a while.

And remembering German times, I want to acknowledge **Susanne Simon** and **Fergus the cat**. Susanne, you really saved me from grey and sad winter days in Berlin, just putting me on the car and guiding me through the city in the night to explore the secret corners of Berlin. And you Fergus, I can say you have been my first (and last) cat. Thanks for being a silent but good mate during the snowy afternoons of work.

Grazie a **Rita Di Masi**, per aver altrettanto contribuito alla mia salute mentale durante le grigie giornate a Berlino. Grazie per avermi accolto a casa tua come una sorella e per le nostre serate da leoni con tv, divano e "Doppio Passo Primitivo"!

Thanks to all my friends from ICIQ: **Andrea**, **Alberto**, **Sarita**, **Alessandra**, **Elena**, **Matteuccio**, **Davide**, **Julian**, **Resepe**, **Julia**, **Justine, Klaudia**. Thanks for sharing your time out of chemistry, the days at the beach, the parties at **Matteo**'s house, the wild

outdoor experiences and the climbing afternoons. I will remember you as one of the best things of Tarragona.

I want to acknowledge **Prof. Sebastiano Pappalardo** for having transferred to me his love for supramolecular chemistry. Without your good advice I would have not reached this point. Many thanks!

Un caloroso grazie alle mie amiche dottoresse **Francesca**, **Maria** e **Rosa** per essere state per me una piccola famiglia dal primo momento a Tarragona. Grazie per le mille cene italiane e le serate passate semplicemente a scherzare e cantare insieme. Grazie alle mie amiche del cuore da una vita, **Giulia** e **Lidia**. Vi ringrazio per rendermi lieve e gioioso ogni grande e tedioso passo, tenendomi sempre stretta per mano.
Grazie a **mamma** e **papà** per avermi spinto fin qui, incoraggiandomi a cercare di migliorare sempre senza pormi limiti. Grazie ad **Elisa**, per il supporto psicologico gratuito ed i mille incoraggiamenti a suon di "sei babba" ogni volta che la sindrome dell'impostore prendeva il sopravvento.
Thanks to my friend **©Nunzio Santisi Photographer** for the amazing picture in the cover. Mother Etna, symbol of my land, always reminds to be powerful, active and live each experience of this life to the fullest.

Finally thanks to my inspiring muse, the music. My "quite" friend always present to alleviate the hard days writing this book.

The work contained in this thesis has been made possible thanks to the financial support from the European Union's Horizon 2020 research and innovation programme under Marie Sklodowska-Curie grant agreement No 765297.

A Ciccia e Cetty,

Table of Contents

Chapter 1

General Introduction

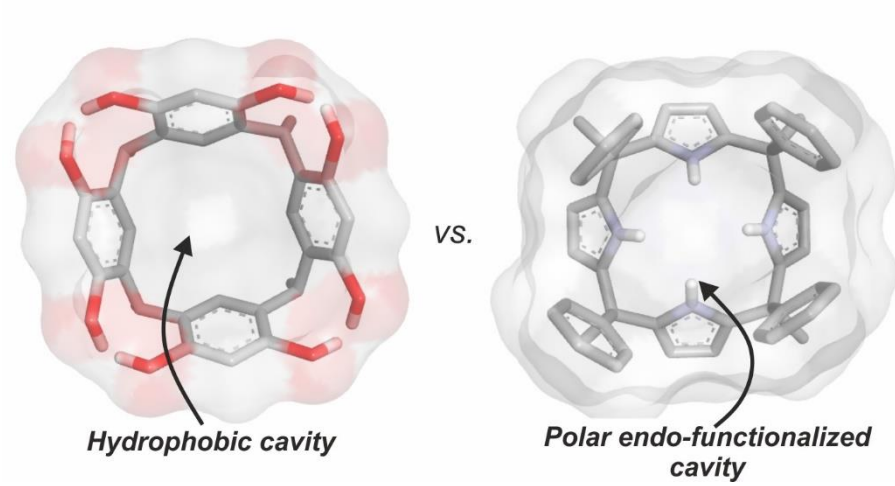

1.1 Calix[4]pyrrole receptors

Calix[4]pyrroles[1,2] are a class of supramolecular receptors having considerable relevance[3,4,5,6] owing to their application in diverse fields including molecular sensing,[7,8] anion recognition[9,10] and transport,[11,12,13,14] catalysis[15] and the design of smart materials.[16]

Meso-octamethyl calix[4]pyrrole was first synthesized in 1886[17] by the acid catalyzed condensation reaction of acetone and pyrrole.

The macrocycle containing four pyrrole rings linked together through the α-positions via tetra-substituted sp^3-hybridized carbon atoms resulted stable to oxidation compared to the porphyrinogen counterpart -bearing *meso*-hydrogen substituted atoms. Notably, the *meso*-octamethyl calix[4]pyrrole and derivatives displayed binding properties for the recognition of anions[1] and electron-rich neutral molecules.[18]

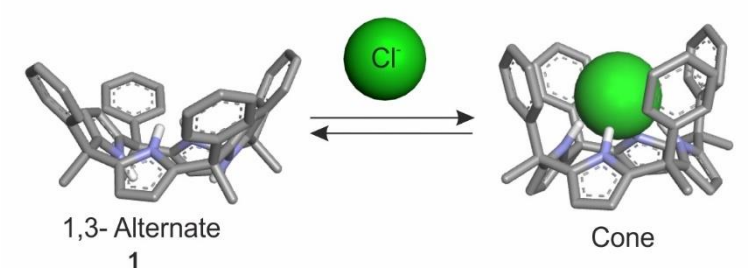

Figure 1.1. Conformational switch from the 1,3 alternate to the cone conformation of the α,α,α,α aryl-extended calix[4]pyrrole induced by chloride binding.

X-ray crystal analyses revealed that in the solid state structures of the TBACl and TBAF complexes of *meso*-octamethyl and *meso*-tetraspiro cyclohexyl-calix[4]pyrroles, the receptor adopted the cone conformation. In both cases, the anion established four convergent hydrogen bonds with the four NH protons of the receptor. In contrast, the free calix[4]pyrrole receptors adopted the 1,3-alternate conformation. Likewise, an analogous hydrogen-bonding interaction between electron-rich atoms of neutral guests *i.e*. *N*-oxides with the calix[4]pyrrole receptors produced the conformational switch of the latter from the 1,3-alternate conformer in the free state to the bound cone conformation (Figure 1.1).

The binding properties of the calix[4]pyrrole receptors towards a series of anions (*i.e*. Cl^-, Br^-, I^-, $H_2PO_4^-$, and HSO_4^-) were also investigated in solution using ^1H NMR spectroscopy. Titration experiments performed in CD_2Cl_2 solution, evidenced the formation of 1:1 ion-paired complexes, displaying high binding affinities (with

stability constants larger than 10^3 M^{-1} in the case of F^- and Cl^-) with a remarkable selectivity for F^{-1}.

Along recent years, the structures of calix[4]pyrrole based receptors evolved by functionalization in the β pyrrole positions[19,20] and the insertion of *meso*-substituents other than methyl groups. The latter synthetic approximation involved the use of di-alkyl ketones, bearing different or identical substituents and alkyl-phenyl ketones instead of acetone in the acid-catalyzed condensation with pyrrole.[21,22] The more elaborated structures of the calix[4]pyrrole receptors led to tunable aromatic cavities (*i.e.* depth cavity and electronic properties) displaying modulated binding affinities.[19]

The substitution of one methyl group in each one of the four *meso*-carbons of the octa-methyl calix[4]pyrrole scaffold with an aryl counterpart produced "four-wall" aryl-extended calix[4]pyrroles.[23]

The two possible orientations (up *α* or down *β*) of the *meso*-aryl groups with respect to the plane defined by the *meso*-carbons of the receptor's cone conformation led to the existence of "four wall" calix[4]pyrrole as four configurational isomers (*α,α,α,α; α,α,α,β*; *α,α,β,β*; *α,β,α,β*). In turn, each configurational isomer can adopt different conformations of the calix[4]pyrrole core: 1,2- and 1,3-alternate, cone and half-cone (Figure 1.2).[23]

In the cone conformation, the *α,α,α,α*-isomer defines a polar and deep aromatic cavity with an open-end that is suitable for the inclusion of mono- and polyatomic anions[24] , as well as electron-rich neutral guests.[25]

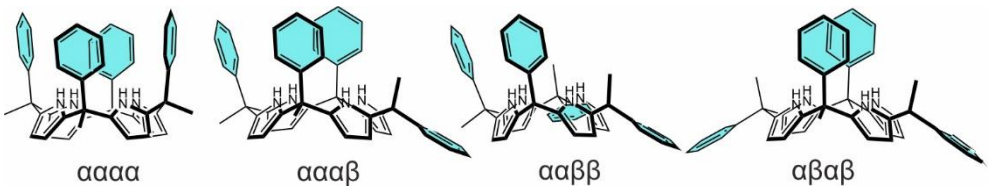

Figure 1.2. Configurational isomers of "four-wall" aryl-extended calix[4]pyrrole in cone conformation.

In addition, the introduction of different substituents in the meso-aromatic panels allows the modulation of its electronic properties and the tuning of the non-covalent interactions in which they might be involved: anion-π, π-π, CH-π interactions.

Our group demonstrated the existence of a linear free-energy relationship between the electronic properties of the *meso*-aromatic units in tetra-α aryl-extended calix[4]pyrroles and the binding strength of mono- and poly-atomic anions (*i.e*. halides and nitrate).[26,27,28] Different *para* substituents were used to modify the

density and charge distribution of the *meso*-aromatic walls. The main non-covalent interaction in the complexes of anions with "four wall" calix[4]pyrroles is due to hydrogen bonding with the pyrrole NHs. In addition, the results of the binding studies performed for the halides with a series of "four wall" receptors (analyzed using ^{1}H NMR titrations and ITC experiments) demonstrated that the halide-π interactions became progressively more attractive as the electron withdrawing character of the *para*-substituent in the aromatic walls was increased.

A special case of doubly opposed *meso*-functionalization of calix[4]pyrroles produces "strapped" receptors.[29,30] Compared to the simple di-substituted counterparts, "strapped" calix[4]pyrroles displayed higher binding affinities towards anions and ion pairs. This design allowed the incorporation of additional cooperative binding sites (*i.e*. amide and carbamates functional groups, heteroaromatic moieties) in the strap of the calix[4]pyrrole. Moreover, the strap endows the receptor with an enhanced preorganization (conformational locking) and substrate complementarity. It also allows to increase the contact surface of the bi- or multi-macrocyclic receptor and the bound guest (molecule **3**, Figure 1.3).[31]

The covalent synthetic strategies are rather demanding. In contrast, molecular self-assembly[32] approaches can produce molecular receptors based on calix[4]pyrrole, with a significantly reduced synthetic cost.

For instance, metal coordination and hydrogen bonding interactions were also applied in the self-assembly of calix[4]pyrrole aggregates. Our group investigated the self-assembly of tetraurea-calix[4]pyrroles in hydrogen bonded dimeric capsules. In non-polar solvents, the dimeric capsules were stabilized by the formation of an array of 16-hydrogen bonds between the unidirectionally oriented 8-urea groups. Notably, the presence of suitable guests that acted as encapsulation templates was necessary for the emergence of the capsular dimer. For example, the ditopic 4,4'-bipyridine bis-*N*,*N*'-oxide and the pairwise encapsulation of trimethylamine *N*-oxide and trimethyl phosphine oxide induced the self-assembly of the dimer.[33,34] Simultaneously to the hydrogen bonded belt of the urea groups, the encapsulated guests established additional hydrogen-bonding and CH-π interactions with the polar calix[4]pyrrole hemispheres of the supramolecular capsules (molecule **2**, Figure 1.3).

The singularity of "four wall" calix[4]pyrrole receptors emerges from their deep aromatic cavity that is functionalized with four NH at its closed end. There is significant interest in the development of synthetic biomimetic receptors with functionalized polar aromatic cavities. These receptor constructs are analogues of biological counterparts. The study of their binding properties is expected to increase

our understanding of the molecular recognition mechanisms operating in biological systems. In addition, synthetic polar receptors may overcome some of the limitations of the natural receptors: reduced availability, high-cost, limited shelf life

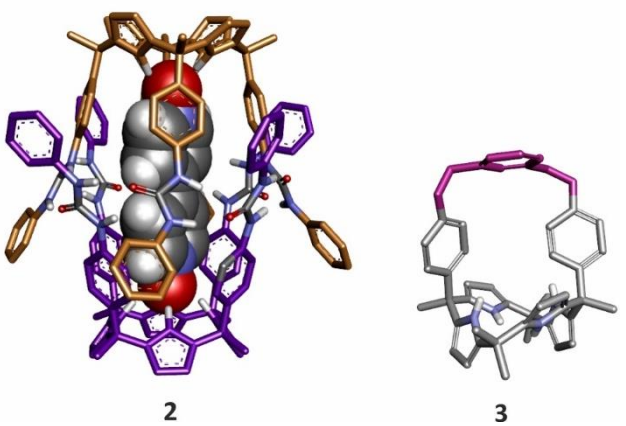

Figure 1.3. Energy minimized structure (MM3) of the complex of a dimeric capsule based on a tetra-urea "four wall" calix[4]pyrrole **2** and single crystal structure of a strapped "two wall" α,α-calix[4]pyrrole **3**. The latter receptor displays the 1,3-alternate conformation (adapted from ref. 31).

and suboptimal function in extreme weather conditions. The extensive use of aromatic panels in shaping the cavities of synthetic receptors makes their functionalization with convergent functional groups synthetically challenging. This inner functionalization is a must for the encapsulation/inclusion of polar substrates.

In this introductory chapter, we generally describe relevant examples of supramolecular containers that are assembled using dynamic covalent chemistry approaches. Cavitand-based capsules, supramolecular macrocycles, interlocked molecules and supramolecular polymers have been constructed under thermodynamic control using weak, reversible, non-covalent interactions such as hydrogen bonds, metal coordination, ionic interactions, and solvophobic interactions. As an alternative strategy in supramolecular syntheses, dynamic covalent chemistry offers great advantages because it combines the robustness of covalent bonds with the reversibility of non-covalent interactions.
We will then specially focus on *endo* functionalized supramolecular capsules and cages assembled by imine condensation reaction.

1.2 Dynamic covalent chemistry in supramolecular assemblies

Dynamic covalent chemistry (DCC) deals with the use of reversible covalent bonds allowing the combination of multiple molecular components into complex

supramolecular aggregates. For systems working under thermodynamic control, the resulting aggregate or mixture of aggregates correspond to the energy minimum of the system at equilibrium. This synthetic strategy opens the way towards an adaptive and evolutive chemistry of covalent molecular objects responding to external demands by changing their composition and structure.[35,36] Thanks to the reversibility of the reactions operating in thermodynamically driven dynamic covalent chemistry approaches, via "proof-reading" and "error-checking" mechanisms, intricate molecular architectures and responsive materials can be obtained often in a one-pot synthesis (Figure 1.4 a).[37]

In kinetically controlled reactions, the products' distribution is determined by the difference in free energy between the transition states. In contrast in chemical reactions operating under thermodynamic control, the difference between the energetic stabilities of the products is what controls their distribution.

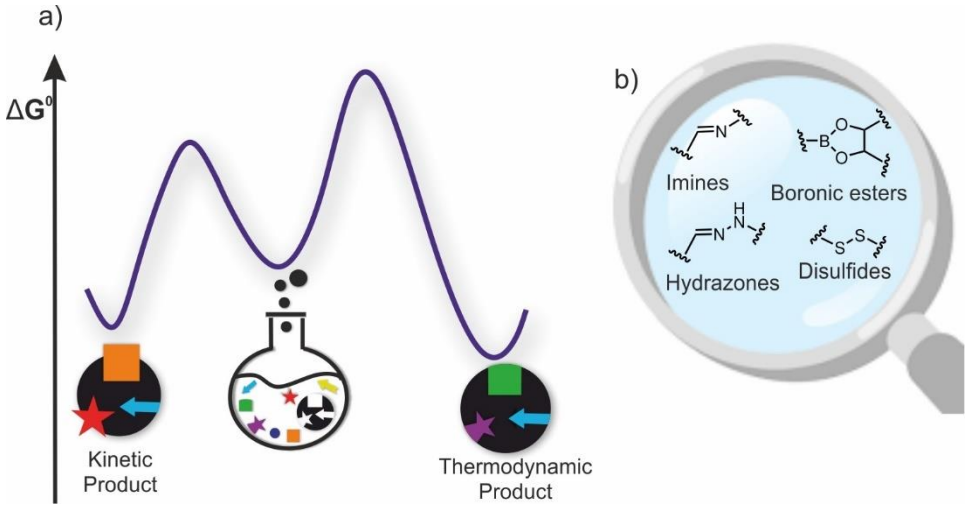

Figure 1.4. a) Schematic representation of the energetic diagram for the kinetic and thermodynamic products resulting from a supramolecular assembly; the energies of the products' transition states are directly related to their relative stabilities; b) most common functional groups used in dynamic covalent supramolecular chemistry.

As a consequence, the distribution of products in dynamical covalent systems can be controlled by endowing the starting materials with certain features (*i.e.* constitutional, steric and electronic effects that will stabilize the desired product and so encourage equilibration to the thermodynamically most stable product). Likewise, the formation of a specific molecular aggregate in the equilibrium can be driven by using one of the starting materials in excess or by removing a product resulting from the reversible condensation reaction (precipitation).[35] The products of a dynamic covalent reaction are dynamically covalent libraries (DCL) of

compounds. The compositions of these libraries are responsive to external influences, such as reaction medium (solvent), physical factors (temperature, light, electric, mechanical stress, etc.) and the presence of stabilizing species (templates, metal ions, protons, etc.). In short, dynamically covalent chemistry enables applications of covalent adaptable chemistry.[38]

There is a range of different organic functional groups resulting from the formation of dynamic covalent bonds. The chemical reactions producing imines, hydrazones, boronic esters, disulfides, alkyne metathesis *etc*. have been extensively used in the assembly of dynamic covalent supramolecular architectures (Figure 1.4 b). Below we present some particular examples.

1.2.1 Boronic esters based supramolecular systems

Boronate esters are formed by reacting boronic acids with alcohols under neutral conditions. When 1,2- or 1,3-diols are employed as alcohols the equilibrium favors the boronic ester. Such boronic esters are reliable synthons for dynamic covalent chemistry and the construction of supramolecular architectures. One of the advantages of the boronic esters is that their formation does not require the addition of an acid or a base as catalysts.[39] Another attractive feature of the boronate esters resides in the Lewis acidity of the boron atoms. Boronic esters are known to form 1:1 adducts with various Lewis bases. The geometry of the boron atom changes from planar-trigonal to tetrahedral upon coordination with the Lewis base.[40]

Between 2008 and 2010, Kobayashi and co-workers reported the synthesis and binding properties of boronic esters based capsules containing resorcin[4]arene scaffolds (Figure 1.5).[41,42] They demonstrated that mixture in 2:4 molar ratio of the tetra-boronic acid cavitand **4** with 1,2-bis(3,4-dihydroxyphenyl)ethane **5**, in $CHCl_3$ or C_6H_6 solution, quantitatively afforded capsule **6** upon heating at 50 °C for 3 h.[43]

The capsule's cavity had approximate dimensions of 8.4 Å× 19.4 Å. It accommodated and discriminated between a variety of aromatic guests (*i.e.* diacetyl derivative **7**) according to size and shape complementarity, as well as the establishment of complementary interactions with the interior surface of the capsule (*i.e*. via CH-π and C=O-CH interactions). The authors also showed the reversibility of the boronic ester bonds and its coupling with the assembly/disassembly and guest uptake/release processes. Addition of an excess of CD_3OD to a C_6D_6 solution of the **7**⊂**6** complex caused the immediate methanolysis of the boronic ester bonds with the concomitant disassembly of capsule **6** and the release of **7** to the bulk solution.

The produced mixture was completely restored to the original **7⊂6** capsular

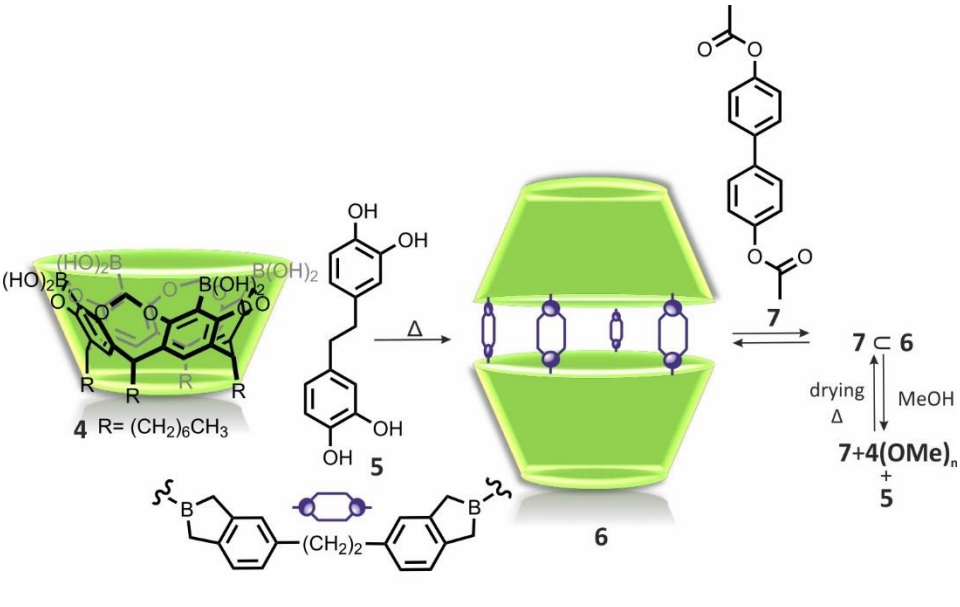

Figure 1.5. Reversible assembly and disassembly of boronic ester capsule **6** based on the tetra-boronic acid resorcin[4]arene cavitand **4**.

by vacuum drying at room temperature, treating the obtained solid with C_6D_6 and heating the of the solution at 50 °C.

Recently, the dynamic transformation between covalent organic frameworks (COFs)[44,45] and discrete cages was reported. The used strategy relied on a dynamic covalent chemistry (DCC)-induced linker exchange (Figure 1.6). COF-**11** was put into a flask containing THF and molecular sieves (MS).[46] Next, *o*-terphenyl-4-4"-bisboronic acid **10** was added to the suspension. The acquisition of time-dependent ^{1}H NMR spectra of the suspension, revealed the gradual emergence of the characteristic signals for the protons of cage **12** (in light blue and red). In addition, diagnostic signals of the *p*-phenylene bis-boronic acid **8** were detected. Pure cage **12** was obtained after solvent evaporation and purification of the solid mixture by recrystallization. However, it was not possible to assemble COF **11** starting from cage **12**.

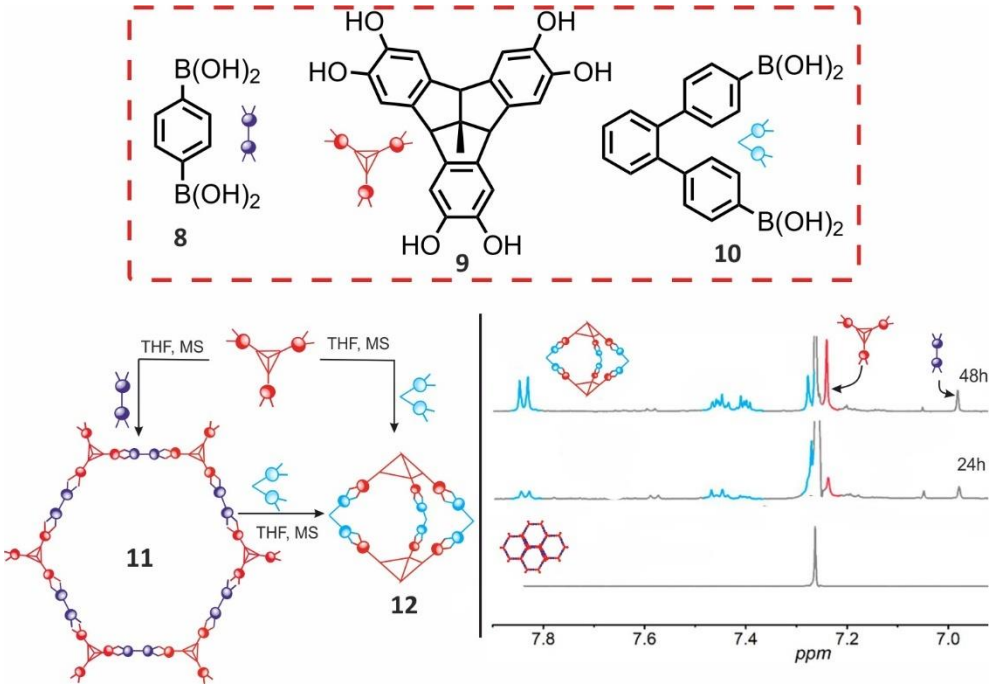

Figure 1.6. (Left) Schematic representation of reversible assembly of COF **11** and cage **12**; (right) ^{1}H NMR spectra in $CDCl_3$ representing the disassembly of COF **11** upon addition of **10** to give cage **12** (adapted from ref 46).

1.2.2 Hydrazones based supramolecular systems

Hydrazones are formed by condensation of an aldehyde or ketones with hydrazines. In contrast to imines which quickly hydrolyze at neutral to acidic pH and are quite unstable in water, hydrazones are thermodynamically stable even at low pH. They tend to be kinetically inert under neutral conditions. Acidic conditions (pH 4 or below) and high temperatures are usually required for the hydrolysis and exchange of hydrazones. The high stability of hydrazones towards hydrolysis and exchange is due to the mesomeric effect. The conjugation of the nitrogen lone pair with the adjacent pi double bond (-NH-N=CH-) reduces the electrophilic character of the carbon atom. Most of the applications of hydrazone groups in dynamic combinatorial chemistry feature acyl hydrazone derivatives. The acyl group moderates the stabilizing influence played by the nitrogen atom adjacent to the imine bond, R-CO-NH-N=CH-. Indeed, in the absence of electron withdrawing groups, the hydrazones tend to be too stable to be used in dynamic covalent libraries.[37]

In 2011 Warmuth and co-workers reported the assembly of di, tetra- and hexa-cavitand-based polyacyl hydrazone nanocapsules. The nanocapsules were formed

by reacting tetraformyl resorcin[4]arene cavitands with aromatic dihydrazides (isophthalic and terephthalic) and trigonal planar trihydrazides in presence of TFA.[47] The authors demonstrated that the reaction outcome not only depended on the ratio cavitand/ linker used but also on their structural features. They were able to assemble [2+4]-,[4+8]- and [6+12]-nanocapsules using dihydrazide linkers (**17**, **18**) and [2+4], [6+8]- nanocapsules using a trihydrazide counterpart (**19**) (Figure 1.7 b).

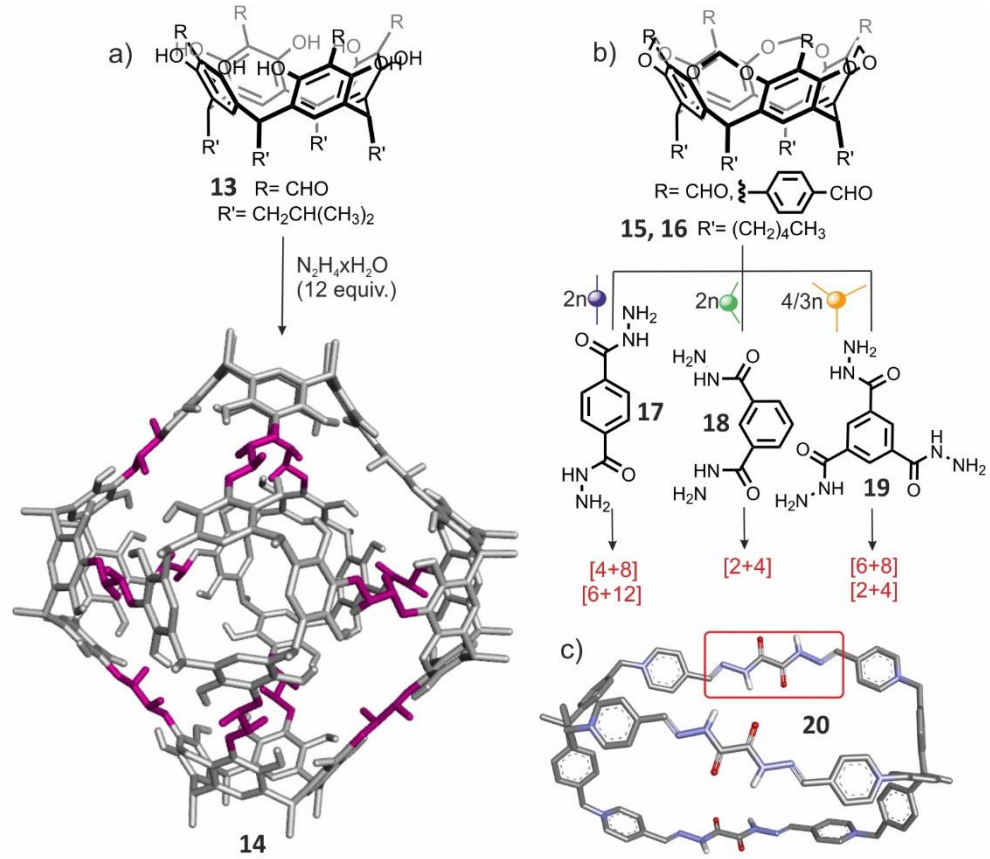

Figure 1.7. a) X-ray structure of polyhydrazone capsule **14** (adapted from ref. 50) based on tetra-formyl resorcin[4]arene **13**; b) assembly of polyhydrazone capsules based on tetra-formyl resorcin[4]arenes **15** and **16**; c) energy minimized structure (MM3) of olive-like cage **20**.

Careful analysis of the crystal structures of the nanocapsules assisted by molecular modeling studies, allowed the authors to rationalize that the final composition of the reaction mixtures depended on the conformational strain of the acyl hydrazone linkages and the tendency to maximize the number of intramolecular hydrazone linkages. The possibility to employ similar capsular systems in the selective elimination of radionuclide waste, toxic heavy metal ions, and organic

micropollutant from water was explored.[48] In this way, the stability of poly-acyl hydrazone capsules in aqueous media was also proved.[49]

In the same line, Szumna and co- workers successfully assembled a hexameric poly-hydrazone capsule by condensation of 6 equiv. of tetra-formyl resorcin[4]arene **13** with 12 equiv. of hydrazine (Figure 1.7 a). The pinwheel-shaped directional arrangement of the hydrazone groups endowed the cubic capsule with inherent chirality.[50]

Recently, two olive-like organic cages (**20**, Figure 1.7c) were fully assembled in water solution through [2+3] hydrazone condensation of two pyridinium-derived tri-aldehydes and three oxalohydrazide.[51]
The organic cages efficiently encapsulated and solubilized in water linear molecular guests (aldehydes and acyl hydrazines).They were applied as reactor vessels to promote the two- and three-components hydrazone condensation in water. The yields of the products increased from zero in the absence of the cage to up to 90% when the capsules were present in solution.

1.2.3 Imine based supramolecular systems

Imine bonds[52] are readily formed by the condensation reaction of an aldehyde with an amine. They are one of the oldest and most used motifs in dynamic covalent chemistry for the self-assembly of molecular capsules.[53]
Imine condensation reaction typically takes place in mild acidic conditions and the equilibrium between starting materials and product can be easily altered by several external factors (*i.e*. solvents, pH, temperature, concentration), as well as internal factors (*i.e*. electronic features and steric bulk of the building blocks).
In addition, considering that imines can participate in hydrolysis, exchange and metathesis reactions, the involved equilibria can be manipulated not only for the purpose to study their dynamic nature but also to force them to produce a desired product.[52]
Cram and co-workers reported the first example of an octa-imine hemicarcerand. The compound was produced in 45% yield from the condensation reaction of the tetra-formyl resorcin[4]arene cavitand **15** (2 equiv.) and *m*-phenylenediamine (4 equiv.) in dry pyridine at 65 °C (Figure 1.7 b).[54] A few years later, Stoddart and co-workers investigated the dynamic nature of the hemicarcerand through exchange reactions of the imine linkers and the release of the included guest promoted by the addition of trifluoro acetic acid (TFA).[55]

Following these pioneering works, imine chemistry was extensively exploited to develop multiple organic cages that were applied for the separation of small molecules,[56] or as building blocks for polymers[57]and materials.[58]

For example, Moore and co-workers reported the tetrahedral poly-imine molecular cage **24**, that was prepared using two orthogonal covalent dynamic bonds (Figure 1.8). Cage **24** was designed in order to respond to external chemical stimuli in a controlled manner.[59] The condensation reaction of 1 equiv. of tris-formyl **21** with 3 equiv. of the amine-bis-alkynyl **22** produced the cage precursor **23** having six methyl-alkynyl groups. The intramolecular alkyne metathesis reaction of **23** promoted by a Mo catalyst yielded the tetrahedral cage **24**.

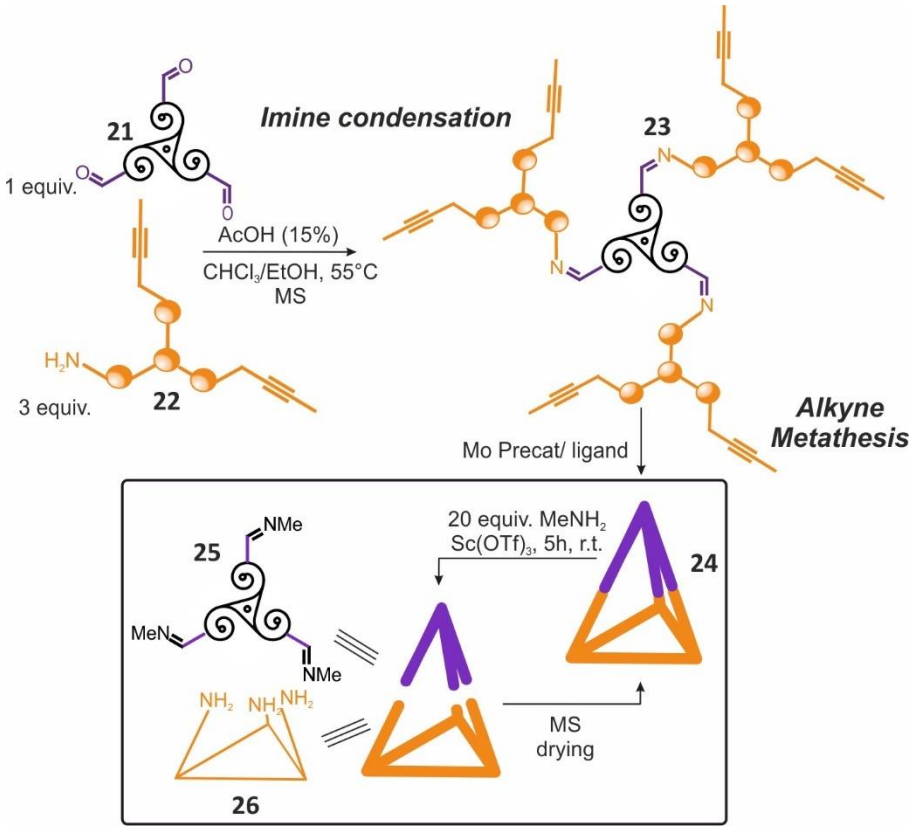

Figure 1.8. Schematic representation of the assembly of cage **24** through imine chemistry followed by alkyne metathesis. The cage was disassembled into the tris-imine **25** and the tris-amino macrocycle **26** upon addition of methyl amine and a Lewis acid.

The authors were particularly interested in demonstrating that the assembly of cage **24** could take place from different starting points and going through different reaction products. To this end, they investigated the dynamic nature of the imine bonds present in **24** in trans-imination reactions triggered by a chemical stimuli.

Thus, the addition of 20 equiv. of methylamine in the presence of a Lewis acid ($Sc(OTf)_3$) induced, after stirring for 5h at r.t., the disassembly of cage **24** and produced two new building blocks **25** and **26**. The reversibility of the condensation reaction and the reassembly of cage **24** from the two formed building blocks required the evaporation of the solvent to remove residual methylamine followed by addition of molecular sieves to a 3 mM chloroform: acetonitrile solution of the obtained solid.

1.2.4 Template assisted synthesis in dynamic covalent chemistry

The rational and strategic use of templates as a useful tool for the assembly of supramolecular architectures was investigated and exploited. Specifically, templates have played an important role in the amplification of molecular components of dynamic combinatorial libraries (DCL) relying on dynamic combinatorial chemistry (DCC)[37,60] for the serendipitous discovery of receptors, catalysts and materials.[61,62]

Dynamic combinatorial libraries (DCL) operating under thermodynamic control are composed of multiple dynamic members. The members of a combinatorial library interconvert between them because their molecular building blocks interact through reversible bonds (either non-covalent or covalent).

Rather than influencing the intrinsic properties of a product, a template is used to manipulate its overall geometry and structure. When a template preferentially binds to a specific library member, this species (complex) becomes energetically stabilized and the equilibrium of the mixture shifts towards the complex, normally resulting in an increase in the concentration of the selected library member (amplification).

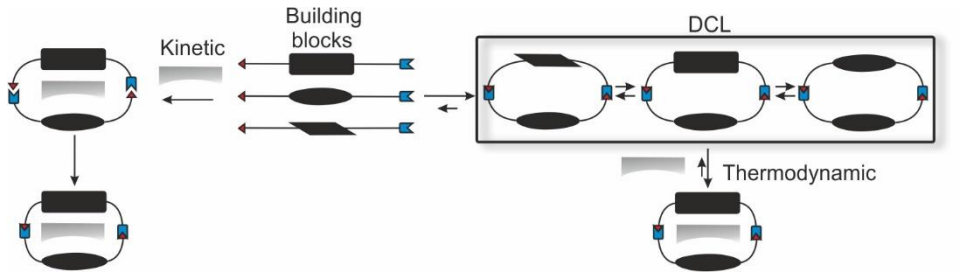

Figure 1.9. Thermodynamic templation vs. kinetic templation.

It is useful to distinguish between kinetic and thermodynamic templating (Figure 1.9), for example in relation to macrocycle or capsule formation:

- kinetic templating involves the template binding to linear species and the collection or preorganization of irreversibly reacting groups. In this way the transition state energy is lowered by reducing the entropic penalty from collecting reactants and freezing out rotational degrees of freedom during the macrocyclization step. This results in an increase in the reaction rate of ring formation for a particular size of a macrocycle;
- thermodynamic templating relies on the binding of the template inside the already formed capsule (or macrocycle) forming a stabilized complex. In other words, the equilibrium involving a range of preformed and different size macrocycles would be shifted towards the formation of one of them in presence of the template.[35,52]

A remarkable example of thermodynamic templation was reported by Sanders and co-workers, showing that acetylcholine was able to selectively amplify one component (a [2]-catenane consisting of two interlocked macrocyclic trimers assembled by hydrazone bonds) of a DCL (Figure 1.10 a). The catenane was isolated in 67% yields from the amplified DCL.[63]
HPLC analysis showed that in absence of acetylcholine **28**, the dipeptide **27** self-assembled producing a DCL of oligomers and various macrocycles. The mixture reached thermodynamic equilibrium after 3 days. However, the addition of acetylcholine to the DCL, first amplified the dimer species, which slowly interconverted into a single diastereoisomer of the [2]-catenane **29** (completely absent in the DCL) and its hexameric macrocyclic isomer.

Isothermal titration calorimetry (ITC) experiments confirmed the existence of a strong and selective binding of acetylcholine with the [2]-catenane. This interaction produced the amplification of the [2]-catenane in the DCL. The K_a calculated for the 1:1 complex of the [2]-catenane and acetylcholine was $1.4\times 10^{7}M^{-1}$ in 95:5 $CHCl_3$/DMSO. In this complex, the trimethyl ammonium group of the acetylcholine was involved in the more important intermolecular interactions (cation-π). The K_a values for the 1:1 complexes of acetylcholine with other macrocycles present in the DCL were of the order of $10^{3}M^{-1}$ in the same solvent. As explained above, templation not only allows the amplification of molecular components of a DCL but also favors the formation of macrocyclic and capsular species (intramolecular reactions) over their oligomeric counterparts (intermolecular reactions). In this case, the template stablishes non-covalent interactions with precursor species. For instance, aromatic dicarboxylates preorganized the open intermediate species of pseudo-peptidic macrocycles by establishing H-bonding interactions and π-π stacking interactions. In

the formed complex, the reaction groups of the open precursors are brought close in space.[64,65]

Contrasting studies, showed how template effects, in combination to a selected solvent,[66] functionalization of the dynamic library and amount of template employed,[67] can also contribute to amplify weaker binders or achieve kinetic products.

For example, experimental and DFT studies demonstrated the quantitative assembly of the highly strained [2+3] trigonal-bipyramidal boronate cage **32** by

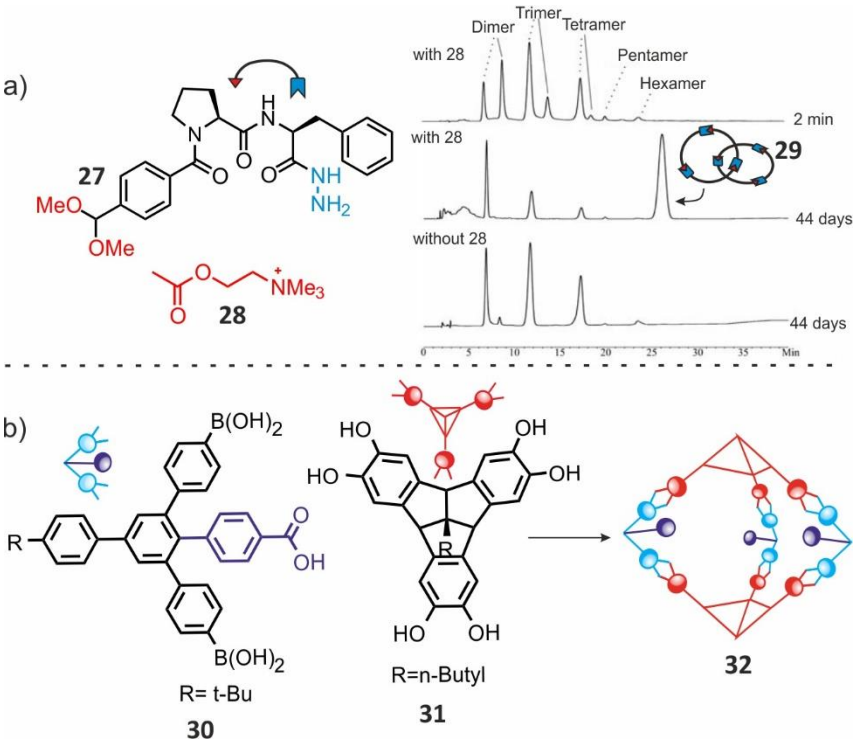

Figure 1.10. a) HPLC chromatogram demonstrating the templating effect of acetylcholine **28** in the amplification of [2]-catenane **29** (adapted from ref. 63); b) template-directed assembly of boronate cage **32**.

reacting hexahydroxy **31** with diboronic acid **30** in 2:3 molar ratio in CH_3CN solution (Figure 1.10 b).[68] Formation of cage **32** was non-expected because the use of unsubstituted bis-boronic acids having a bite angle of 120° favored the formation of [4+6] cage assemblies. Cage **32** was considered to be the kinetically trapped product owing to its low solubility in this solvent compared to other possible boronate species. Contrarily, in THF solution the reaction of **30** and **31** produced a complex equilibrium mixture. Pre-organization in dimers or trimers of the products formed by reaction of **30** and **31**, via intermolecular hydrogen-bonding between the COOH

groups induced the formation of strained boronate ester bonds in smaller macrocycles and cages including **32**.

In many cases, changes in the solvent used for the assembly can favor the formation of cyclic and capsular species over polymeric and linear counterparts.
This proves that solvents can also play the role of templating agent. Solvent molecules can indeed interact via non-covalent forces with the interior of the cage, stabilizing some products over a complex mixture of species.[69,70,71]

1.2.4.1 *Metal-ion assisted sub-component assembly*

One of the most widely used strategy for the organization of molecular building blocks into well-defined supramolecular arrays, consists on the use of transition metals and its coordination chemistry.[72]

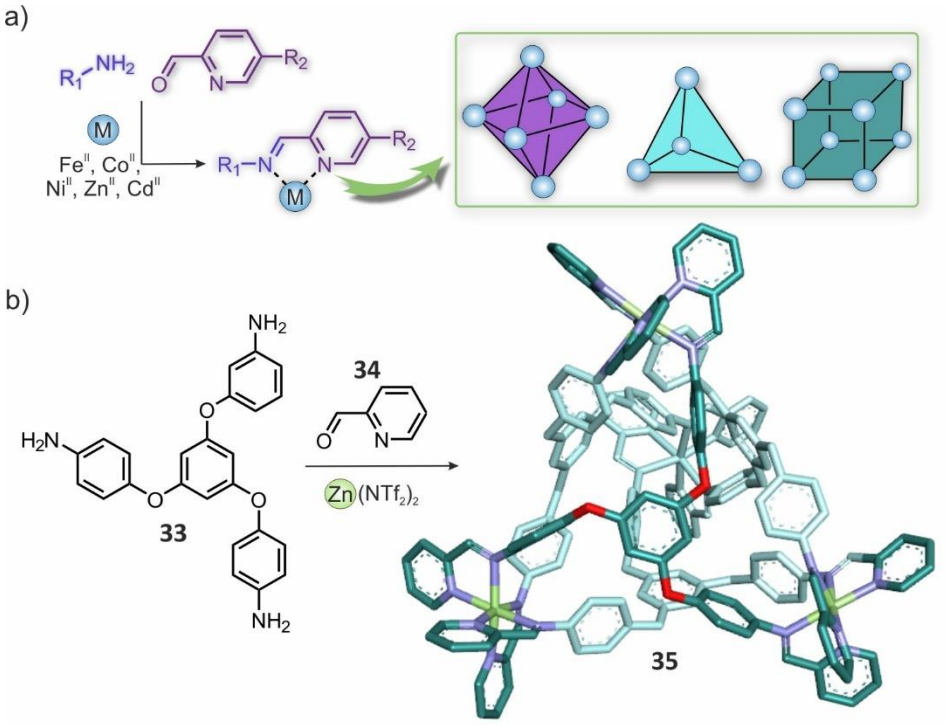

Figure 1.11. a) Sub-component metal-assisted synthesis of polyhedral supramolecular structures; b) assembly of imine-Zn (II) cage **35** (X-ray structure adapted from ref. 74).

Schiff base chemistry is particularly suited for the synthesis of directionally dynamic covalent nanocapsules. The imine bond is a “quasi-linear” connection substituting a metal–ligand dative bond in coordination capsules.[52]

One of the advantages arising from the combination of dynamic imine bonds with dynamic coordination bonds is the high water stability imparted on the former by the latter. This exceptional stability was exploited by Nitschke *et al.* in preparing metal-organic capsules, stable even in water, via the simultaneous formation of dynamic coordination bonds (N→metal) with dynamic covalent bonds (N=C).[73]

This synthetic strategy employs multidentate pyridyl-imine ligands to define either the edges or the faces of polyhedral structures. In turn, octahedral metal ions, such as Fe(II), Co(II), Ni(II), Zn(II) and Cd(II), constitute the vertices of the polyhedron (Figure 1.11).[74,75,76] Covalent coordination bonds have an intermediate strength between the weak non-covalent interactions and the strong covalent bonds defining the structure of most organic compounds. Significantly, most heteroatom-metal bonds are thermally labile. This property allows to intentionally select either a thermodynamic or a kinetic product through the rational choice of ligands, transition metals and reaction conditions correcting the defects of the structures.[77]

1.3 Endo- functionalized cages and capsules assembled via imine bonds

Many synthetic capsular assemblies take inspiration from biological recognition and catalysts and are designed to mimic the active sites of enzymes. This not only allows a better understanding of the molecular recognition mechanisms operating in biological systems but also the development of new therapeutic and diagnostic tools for medicine.[78]

Enzyme's active sites are endowed with functional groups to bind the substrate, transfer protons, stabilize charges, coordinate metal ions and act as nucleophiles/electrophiles.[79] In the same line, biomimetic synthetic receptors/catalysts should be *endo*-functionalized with polar groups similar to those encountered in the catalytic sites of biological counterparts, for instance amino acid residues (Figure 1.12).

Binding between the enzyme mimic and the substrate is key for the success of biomimetic catalyst. Improving the properties of the binding event means optimizing the active site of the synthetic enzyme, its shape and charge distribution in order to maximize the interactions with the target substrate and its recognition.

The synthesis of molecular containers endowed with polar functionalized cavities requires substantial synthetic efforts. This explains the reduced number of examples of this type of molecular containers described in literature.

One of the synthetic challenges faced during the synthesis of container molecules with a polar cavity is related to the possible interference between the polar groups

installed in the skeleton of building blocks to drive the assembly of the container

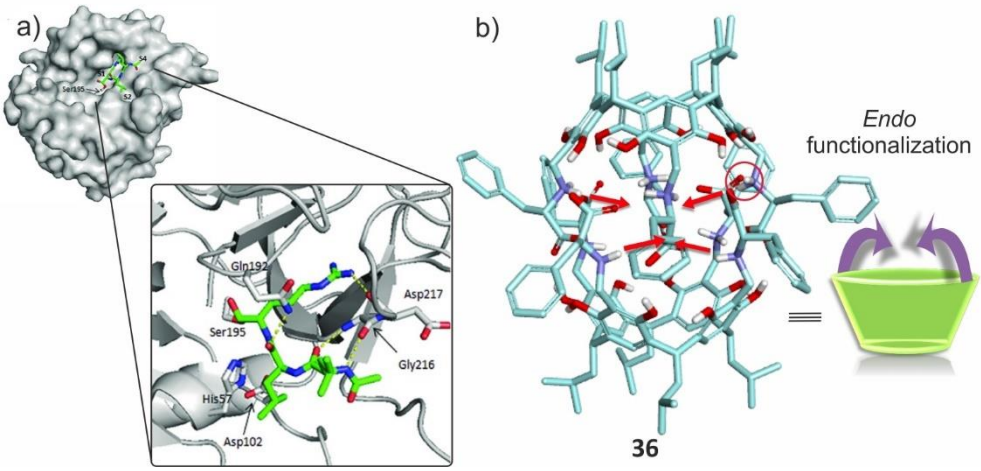

Figure 1.12. a) Example of enzyme binding pocket and enzyme-substrate interactions (co-crystallized structure of leupeptin and a Kallikrein-related peptidase (KLK5) adapted from ref. 80); b) X-ray structure of a resorcinarene based *endo*-functionalized receptor **36** (adapted from ref. 81).

and those that are supposed to be endohedrally located in the container's interior.[82] As mentioned above, dynamic covalent chemistry (DCC) is considered to be a useful alternative to covalent chemistry in the synthesis of molecular containers with polar interiors. DCC working under thermodynamic control allows the equilibration of complex libraries of assemblies into a single compound: the thermodynamically more stable one.

We describe below some selected representative examples of capsules and cages having polar groups inwardly directed and assembled using imine chemistry. We comment the details of their synthesis and post-assembly modifications directed to stop the chemical reversibility of their structures. The molecular recognition properties of the produced assemblies and their applications in innovative research fields are also outlined.

1.3.1 Synthesis and post-assembly modifications of poly-imine containers

Relatively complex and large container structures are accessible by simple imine bond formation from rather readily available molecular building blocks. The assembly of these architectures, in a straightforward and predictable manner, requires a deep understanding of the fundamental structural and geometrical properties of the molecular building blocks.[83]

As described by Lehn, the careful choice of the structural features of molecular components (*e.g.* electronic properties, flexibility, presence of heteroatoms) had a strong influence in their self-sorting processes in poly-imine cryptand like cages.[84] For example, in the competitive condensation reaction between tris-(aminoethyl)amine (TREN) and two dialdehyde linkers, pyridine-2,6-dicarbaldehyde and isophthalaldehyde, the former outperformed the latter in the self-sorting process producing [2+3]-hexa-imine cryptand-type cages. In both cages, fully conjugated systems of the aromatic ring of the spacer and its substituents are obtained. However, the lone pair of the N-atom in the pyridine-2,6-dicarbaldehyde spacer is suitable for interaction with the imine (and aldehyde) C-H bonds.
Warmuth *et al*. investigated the role of the solvent in the assembly of different poly-imine cages using the same molecular building blocks. They demonstrated that the outcome of the thermodynamically controlled reactions can be fine-tuned by the used solvent. In short, the same molecular building blocks gave cages of different geometry in different solvents.[85]

Recently, Mastalerz and co-workers were also interested in analyzing the influence of the reaction conditions in the preferential obtention of a kinetically or a thermodynamically controlled shape-persistent poly-imine cage.[66] There are many examples supporting the thermodynamically controlled formation of imine cages. However, there are also observation suggesting that imine cages are rather kinetically controlled products. To gain some insight into the reversibility of the imine bond and to avoid driving forces derived from electronic differences and solubility of the starting materials, intermediates or cages, Mastalerz investigated the scrambling of [2+3] imine cages, derived from the condensation of triamines (TREN **39** and (2,4,6-triethylbenzene-1,3.5-triyl)-trimethanamine **38**) with 5-tert-butyl-isophthalaldhyde **37** and their *tert*-butyl deuterated congeners (Figure 1.13). The formation of the imine cages was studied using different reaction conditions (*i.e*. $CHCl_3$, CH_2Cl_2, EtOH, MeOH, CH_3CN and in the presence and absence of TFA). The 1,3,5-benzene-triyl trimethaneamine cage **40** precipitated out from most solvents, underlaying that its formation is mainly kinetically driven by precipitation. Conversely, the TREN derived cage **41** was soluble in most solvents. Higher yields were obtained for cage **41** that did not precipitate, suggesting that it was thermodynamically more stable than the triethyl benzene counterpart. Once formed both cages do not scramble with the deuterated congeners, neither with or without acid or/and water addition.
For the TREN cage **41**, no scramble was observed in any solvent even with deuterated isophthalaldehyde **37- d9** except THF. The addition of TFA favored the

scrambling process in all solvents, except EtOH or MeOH -solvents that are most often used for its synthesis. The benzyl amine derived cage **40**, had again a different behavior. The addition of acid induced the scrambling with the aldehyde **37- d9** in EtOH and MeOH. The benzyl amine cage **40** was thermodynamically favored over the TREN counterpart **41**. However, based on the knowledge gained in these studies and in order to demonstrate the role of kinetics in imine cage chemistry, the benzyl cage **40** was converted into the TREN counterpart **41** using a MeOH solution of the former and adding of 20 equiv. of TREN. The TREN cage **41** precipitated from solution and was isolated in 87% yield.

In short, the solvent played an important role in the synthesis and scrambling of components of imine cages. The lack of scrambling does not necessarily means that the cage is the kinetic product, especially when it precipitates. When theoretical heats of formation of imine cages and experimental data do not provide a coincident

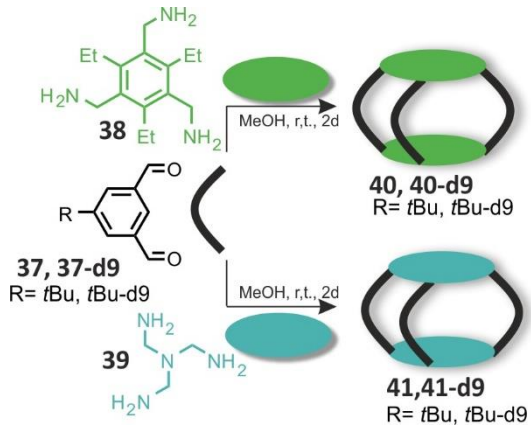

Figure 1.13. Assembly of [2+3] imine cages derived from the condensation of triamines with 5-tert-butyl-isophthalaldhyde **37** used to investigate their scrambling.

picture, with respect to their thermodynamic or kinetic nature, more tedious computations of their kinetic pathways may be useful in solving the issue.

The issue of kinetic *vs* thermodynamic nature of imine cages can also be addressed by synthesizing soluble congeners of prior insoluble cages. This allows the study of their formation, as well as the reversibility of the reactions, by investigating the exchange of building blocks between cages and with their deuterated derivatives.

For example, the condensation of triptycene triamine **42** with tri-aldehyde **44** in dry DMF at 120 °C resulted in the formation of the *endo*-functionalized shape-persistent cubic [4+4] cage **45**. This cage simply precipitated from the reaction media and at no time oligomeric side products were detected in solution by MS analysis. These results indicated that **45** might be a kinetically trapped product.[86]

The same authors also studied the influence on the cage's formation of the hydroxyl substituent in the dialdehyde precursor **47**, **48**. The condensation of four tris-amino triptycene **42** and six salicylic dialdehydes **48** resulted in the formation of the OH *endo*-functionalized [4+6] cage **49** in 58 % yield in THF at room temperature (Figure 1.14). It was suggested that the salicylic hydroxy group promoted the formation of the cage **49** by activating the aldehyde moieties through the formation of intramolecular hydrogen bonds. When a salicylic dialdehyde derivative bearing a protected OH group was used in the cage's assembly a solid precipitated from the solution (most likely polymers). Similarly, the use of iso-phthalaldehyde produced a complex mixture of species after 14 days of reaction. These findings supported the hypothesis that the hydroxyl substituent of the dialdehyde component had a preorganization effect in the cage's assembly. The hydroxyl groups pointed synergistically into the center of the cage's cavity, thus making the compound a potential host for the recognition of smaller polar guest molecules.[87]

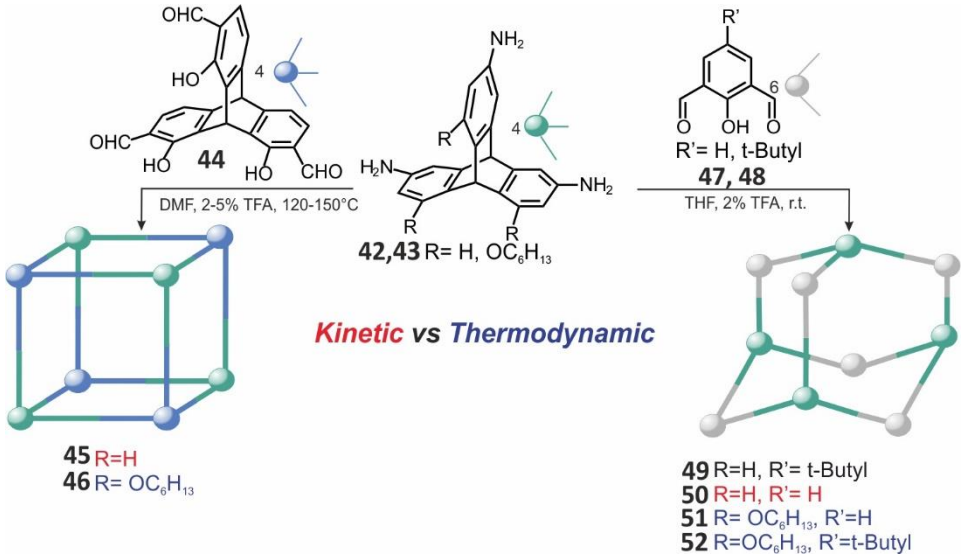

Figure 1.14. Assembly of poly-imine [4+4] and [4+6] cages from differently functionalized tris-amino triptycenes and di-aldehydes.

The fact that the [4+4] and [4+6] cages, **45** and **50**, are collected as precipitates of the reaction solution and no polymeric species were detected as side products, complicated the assignment of the cages as kinetic or thermodynamic products. To study more in detail their nature, soluble congeners (**46**, **51** and **52**) were assembled using the same conditions. The increase in solubility of the new imines cages was endowed by the presence of three sidechains in the triptycene diamine precursor unit, **43**.[88] By monitoring the reaction of the cages' assembly by gel permeation

chromatography (GPC) the authors concluded that the imine cages were the thermodynamic products. Indeed, for the soluble [4+4] cage **46**, they observed the formation of polymeric species at beginning of the reaction. With time the peaks of the polymers decreased in intensity, while a new peak corresponding to the cage **46** increased until reaction completion (after 3 days). These results contrasted with the original observations made for the unsubstituted cubic [4+4] cage **45**, which was not soluble and its formation was suggested to be mainly kinetically driven due to precipitation. For the soluble [4+6] cages, **51** and **52**, shorter reaction times were observed (the reactions were completed after 1 h) compared to the insoluble congeners. In these cases, oligomeric intermediates were also detected at the very beginning of the reaction (especially when the reaction was performed in absence of TFA). The results of this study demonstrated that small variations in the cage structures (*i.e.* [4+6] *endo* and *exo*-cages), can lead to large differences in the formation mechanisms.

1.3.1.1 *Reductive amination*

Imine-based cages offer the possibility for post-synthetic transformations of the imine functional groups by means of different reactions. Some of these reactions allow the conversion of labile imine bonds into chemically more stable covalent bonds.

Among the post-synthetic transformations of imine cages, the most common one is the reduction of the imines to amines. Amines play a paramount role in medicinal chemistry owing to their ubiquitous presence in biologically active compounds.[89]

The transformation of the sp^2-nitrogen atoms into the sp^3-hybridized counterparts produces a conformationally more flexible cage scaffold.

An advantage of the amine cages is that their flexibility allows their adaptation to the guest structure. However, as a consequence of the conformational flexibility, amine cages tend to lose shape persistency and material porosity.

The most popular options of reductive agents for imine bonds include borohydride salts ($NaBH(OAc)_3$, $NaBH_3CN$, $NaBH_4$) and hydrogenation with hydrogen gas using various catalysts. Considering its availability, facility to handle and degree of functional group tolerance (*e.g.* esters, lactones, amides, nitriles, etc.) $NaBH_4$ is the preferred reductive agent used in supramolecular organic cages.[90]

Warmuth and co-workers used $NaBH_4$ to stop imine bonds lability of organic cages. The final amine capsules were isolated via reverse phase chromatography owing to the difficulty of purification of the strongly basic amine cage by silica column chromatography.[91]

Mastalerz and co-workers extensively studied the post-functionalization of imine bonded cages using reductive amination.

For example, [4+6] salicylimine cages were easily transformed into the amine derivatives by treatment with $NaBH_4$ in MeOH at r.t. (Figure 1.15). The gain in chemical stability of the resulting amine cage is accompanied by a reduction in the gas sorption properties due to the collapse of the cavity in the solid state caused by an increase in conformational flexibility.[92]

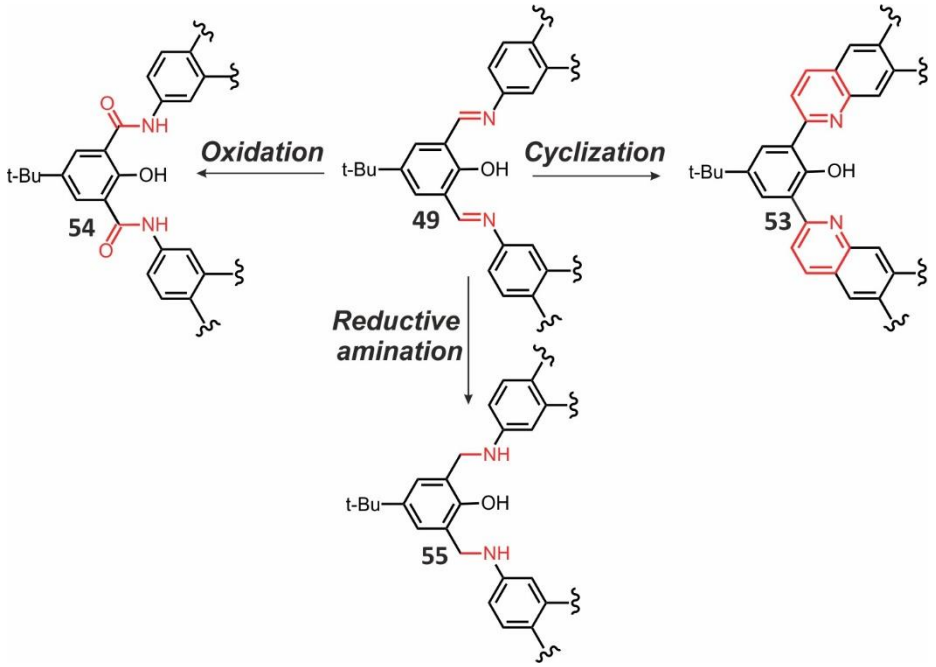

Figure 1.15. Different post-assembly modifications of cage **49** directed to increase chemical stability.

1.3.1.2 *Amidation and cyclization*

Amide bonds are chemically robust. As a result of the partial double bond character of the C−N bond, amides are comparable to imines in terms of directionality and rigidity. Large amide based cages are usually obtained in low overall yields, considering their stepwise syntheses involving the formation of multiple amide bonds and macrocyclization reactions. Because the formation of the amide bond is not reversible, self-correction processes are not possible during the synthesis of amide based cages.

Notably, the twelve imine bonds of the rigid and shape-persistent [4+6] salicylimine cage **49**, were transformed by Pinnick oxidation[93,94] into chemically much more robust amide counterparts **54** (Figure 1.15). The hydroxy groups of the phenols were protected as methyl ethers to avoid oxidation. The resulting cage contains two types

of amide groups. In some amides, the carbonyl oxygen atoms point outside of the cavity while its amide NH group is hydrogen bonded to the adjacent methoxy-O atom. Other amide groups direct the carbonyl oxygen atom inwardly with respect to the cage's cavity.[95]
Cage **49** can be post-modified without previous protection of the phenol OH groups. The treatment of the imine cage **49** in neat phenylacetylene as solvent, with scandium triflate as Lewis acid and chloranil as oxidant, at 100 °C for 20 hours, afforded the robust quinoline cage **53** in 25% yield in a single synthetic step.[96]

After the Povarov[97] cyclization, the conformational flexibility of the quinoline cage **53** is substantially reduced compared to that of the parent poly-imine **49**. In addition, all electron lone-pairs of the nitrogen atoms of **53** are inwardly directed with respect to its cavity (Figure 1.15).
The flexibility of the post-functionalized cages maintains its shape persistence and the porosity of the materials thereof. These are crucial features for applications in gas sorption and separation.

1.3.2 Structural features and recognition properties of *endo*-functionalized organic poly-imine cages

In the next section, we will describe the structural features of *endo*-functionalized organic cages assembled via imine chemistry. We will relate their structures to their molecular recognition properties. We decided to classify the selected examples according to the chemical composition and functionalization of the cages' cavity.

1.3.2.1 *Cages functionalized with amide-imine and amide/amine groups*

Considering their hydrogen bond donating character, amide groups are one of the most used binding motifs in supramolecular chemistry for the recognition of anions.

Recently Badjic and co-workers reported the synthesis, characterization and binding properties of the hexapodal cage **58** assembled by imine bonds (Figure 1.16). The cage was endowed with eighteen hydrogen bond donor groups (6 CONH, 6 N=CH and 6 Ar C-H) able to effectively bind oxyanions and halides.[98,99]
The novelty of cage **58** resides on the possibility to force the interaction of six functional groups instead of three above the benzene platform.[100,101] The conformational change of the cage structure should be favored by entropic and enthalpic contributions due to the release of solvent molecules in presence of an anionic guest. Attempts to assemble the capsule **58** in the absence of a template, by the condensation reaction of equimolar amounts of **56** and **57** in DMSO solution, led

to polymeric aggregates.[98] However, the addition of an excess of Na_2HPO_4 salt (1.5 equiv.) induced the observation of sharp and well defined proton signals in the ^1H NMR spectrum of the mixture indicating the assembly of cage **58**. Most likely, the hydrogen phosphate anion acted as a template. Other anions were also investigated as template (TBACl, TBA_2SO_4, $NaCO_3$, $NaHCO_3$, TBA_2HPO_4). The template strategy allowed to synthesize and isolate cage **58** in yields ranging from 43 and 67%. Interestingly, when Cl^-⊂**58** was placed in DCM and the organic phase washed with water, capsule **58** without chloride was obtained.

X-ray diffraction analysis of single crystals of the [HPO_4⊂**58**]TMA_2 complex showed that all six amides had their NH groups pointing towards the cage's interior and were

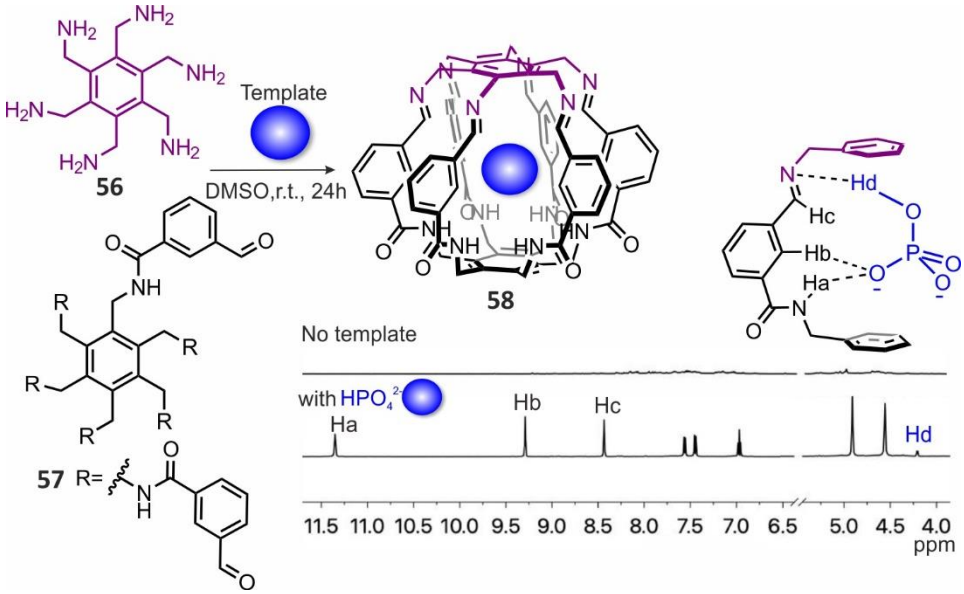

Figure 1.16. Selected regions of the ^{1} H NMR spectra in DMSO (solution 10% DMSO-d_6) showing the diagnostic peaks of the assembly of cage **58** in the presence of an anionic template and the lack of proton signals in the absence of template (adapted from ref.98) .

participating in six HN···OP hydrogen bonds. Six aromatic CH groups formed six CH···OP hydrogen bonding contacts. Finally, five imine protons formed a pocket of positively polarized hydrogens holding the oxygen atom of the hydrogen phosphate group HO-P. The same HO-P group formed a weak hydrogen bond with an imine nitrogen (Figure 1.16 shows a schematic representation of the intermolecular interactions).

The association constant values for the cage complexes with different anions were evaluated in DMSO-d_6 by ^1H NMR titration experiments and competitive displacements. Using incremental amounts TBACl as anion precursor, the authors determined a K_a of 2 ×10^5 M^{-1} for the Cl^-⊂**58** complex. On the other hand, the

addition of 1 equiv. TBA_2SO_4, as sulfate precursor, produced the quantitative formation of the $SO_4^{-}\subset$**58**, for which a $K_a > 10^7\ M^{-1}$ was estimated.

It is worth nothing that when 1.5 equiv. of Na_2SO_4 or TBA_2HPO_4 were added to a DMSO-d_6 solution containing the [$Cl^-\subset$**58**]TBA complex, the complete displacement of the Cl^- required one week for SO_4^- and even a longer period of time for HPO_4^{2-}. These results suggested that the encapsulation kinetics depend on the mechanism of guest uptake requiring less or more time as a function of the relative sizes of the cage portals and guest's dimensions.[102]

In trying to clarify the kinetic selectivity of anion encapsulation by cage **58**, other anions were tested as templates for the cage's synthesis.[99] Some of them (*i.e.* BF_4^-, ClO_4^-, CF_3COO^-, PF_6^-) were not good templates. This was due not only to a reduced size and shape complementarity between the cage's interior and the anion but also to the lack of establishing efficient intermolecular interactions with it. This conclusion was evidenced during the ^1H NMR titration experiments in DMSO-d_6, in which a minimal magnetic perturbation of the proton resonances of **58** was observed upon addition of BF_4^-, ClO_4^-, CF_3COO^-or PF_6^- salts.

Anions	K_a [M^{-1}]	Kinetic
	$10^3<K_a<10^6$	Seconds
	$10^5<K_a<10^7$	Minutes/hours
	$10^6<K_a<10^8$	Days
	–	–

Table 1.1. Estimated K_a of **58** for anions of different geometries measured in DMSO-d_6 by ^1H NMR spectroscopy and relative kinetics of encapsulation.

For small, spherical and cylindrical anions (*i.e.* F^-, N_3^-, CN^-), the gating through the cage portals is fast (seconds). However, the formed 1:1 inclusion complexes are thermodynamically less stable ($10^3\ M^{-1} < K_a < 10^6\ M^{-1}$) than those obtained with larger tetrahedral and basic anions (*i.e.* SO_4^{2-}, HPO_4^{2-} ,$HAsO_4^{2-}$; $10^6\ M^{-1} < K_a < 10^8\ M^{-1}$). The larger tetrahedral and basic anions forming the most stable inclusion complexes, were very slow in trafficking to and from the cage (hours to days). Trigonal planar anions such as CO_3^{2-}, $HCOO^-$, CH_3COO^-, NO_3^- (Table 1.1) could enter sideways into the cage and provide medium incoming rates that were proportional to the thermodynamic stability ($10^5\ M^{-1} < K_a < 10^7\ M^{-1}$) of the corresponding complexes.

The result of a competitive experiment in which equimolar amounts of twelve anions (between the ones listed above) and cage **58** were mixed in DMSO-d_6 solution evidenced the selectivity of the cage for CO_3^{2-} binding. Larger anions remained free in solution. On the other hand, if $HCOO^-$ was also included in the list of competing anions, a mixture of $[CO_3\subset\mathbf{58}]^{2-}$ and $[HCOO\subset\mathbf{58}]^-$complexes was obtained. The composition of the mixture changed with time.

It was possible to change the kinetic selectivity observed for **58** in the binding of carbonate and formate from the mixture of 16 anions to a composition of anion complexes that was related to the thermodynamic selectivity of the cage. To do so, the imine complexes $[CO_3\subset\mathbf{58}]^{2-}$ and $[HCOO\subset\mathbf{58}]^-$ were hydrolyzed by adding an excess of TsOH in a mixture containing the other competing anions. Next, the solution was neutralized by adding TBAOH. This induced reassembly of cage **58** leads to the formation of the most thermodynamically stable inclusion complexes, which involved SO_4^{2-}, HPO_4^{2-}, $HAsO_4^{2-}$ anions. In summary, cage **58** can be considered a kinetically selective host for the encapsulation of carbonate and formate anions, considering the vastly different time scales required for the encapsulation of larger tetrahedral oxyanions anions producing the thermodynamically more stable complexes.

In 2013, Ghosh *et al.* described the tripodal cage **61** featuring two polar binding sites (Figure 1.17). Amine and amide groups can be presented to the included guests in the cavity of **61**. The ditopic cage **61** was assembled via the imine condensation reaction between **59** and **60** and the further post- assembly reduction of the imines groups to the amine counterparts.[103]

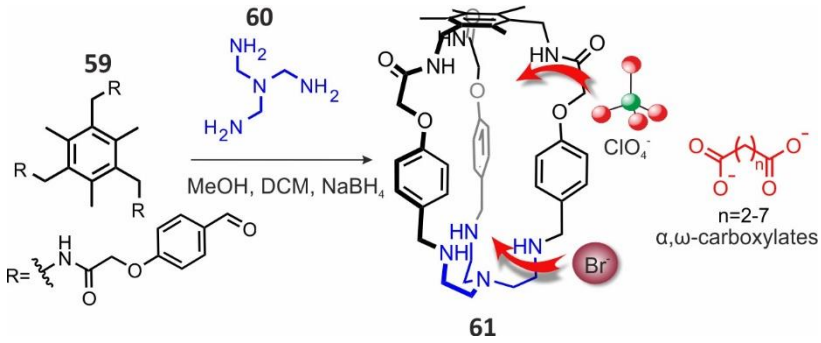

Figure 1.17. Assembly and binding mode of capsule **61** towards Br^-, ClO_4^- and α, ω-dicarboxylates.

The potential of the macro-bicyclic cage **61** resided in the possibility to exploit both hydrogen bonding and electrostatic interactions in the complexation of anions. Many synthetic receptors containing amine groups are used for the binding of anions in aqueous medium.[104,105] The amine groups can be protonated providing the

necessary positive charge to interact with the anions through coulombic interactions and also to impart water solubility to the receptor. The non-protonated amino group can also act as hydrogen bond acceptor, which may be useful for the binding of anions having hydroxyl groups such as phosphates. The tri-protonated form of the cage ($[H_3\mathbf{61}](PF_6)_3$) was used in the evaluation of the binding properties towards spherical and tetrahedral anions (*i.e.* Cl^-, Br^-, ClO_4^-, HSO_4^-) using ITC experiments in DMSO solution. The binding isotherms were analyzed using a three sets of sites sequential binding model and returned overall K_T values in the order of $10^8 M^{-3}$ for all the anions. The binding with halides was endothermic and entropy driven. Conversely, the tetrahedral anions showed exothermic binding that was both entropy-and enthalpy driven. The binding studies also revealed the selectivity of $[H_3\mathbf{61}](PF_6)_3$ towards the binding of HSO_4^-.

Interestingly, crystal structures demonstrated that both amide and amine groups were inwardly oriented with respect to the cage's cavity. Anions of different sizes and shapes were discriminated by the two binding site of the cage, most likely due to its preorganization and reduced conformational flexibility. This was observed for the binding of Br^- and ClO_4^- which formed 1:1 inclusion complexes with different binding geometries. On the one hand, ClO_4^- was located in the amide pocket establishing two hydrogen bonding interactions through two of its oxygen atoms. A water molecule was co-encapsulated and located in the amine binding site. On the other hand, in the case of Br^- the anion was located in the protonated amines binding pocket, forming three hydrogen bonding interactions with the protonated amine groups. In this case a molecule of acetonitrile resided in the amide's binding site.

The $[H_3\mathbf{61}](PF_6)_3$ cage also works as a ditopic receptor for biologically relevant α, ω-dicarboxylates (n= 2–7) in a mixture of H_2O: DMSO (1:1).[106]
Using potentiometric titrations and the mathematical analysis of the multiple equilibria that can be established between the different protonated states of the cage and the bis-carboxylates allowed the quantification of the K_a values of the formed complexes. The results of the titrations indicated that for the 1:1 complexes formed between $[H_3\mathbf{61}](PF_6)_3$ and the bis-carboxylate series, the binding affinity increased from glutaric to adipic (which showed the best fit for the capsule's dimensions). After the adipate, the binding affinity decreased with the increase of the length of the aliphatic chain of the dicarboxylate.
Not surprisingly, the larger *Ka* values resulted from the fully protonated host and the di-anionic forms of the carboxylic acids. In these conditions the electrostatic

interactions are maximized. Nevertheless, the amide groups of $[H_3\mathbf{61}](PF_6)_3$ also provided important contributions in the stabilization of the bis-carboxylate complexes in highly competitive solvents (such as H_2O and DMSO).

1.3.2.2 *Pyrrole based cages*

The use of versatile building blocks bearing functional groups converging in the interior cavity of cage molecules is an appealing strategy for the design of containers with polar cavities that are suitable for the recognition of ions and polar molecules.[107] Among these building blocks, pyrrole was extensively used in the assembly of polar cryptand like receptors[108] showing selective recognition of anions.[109,110]

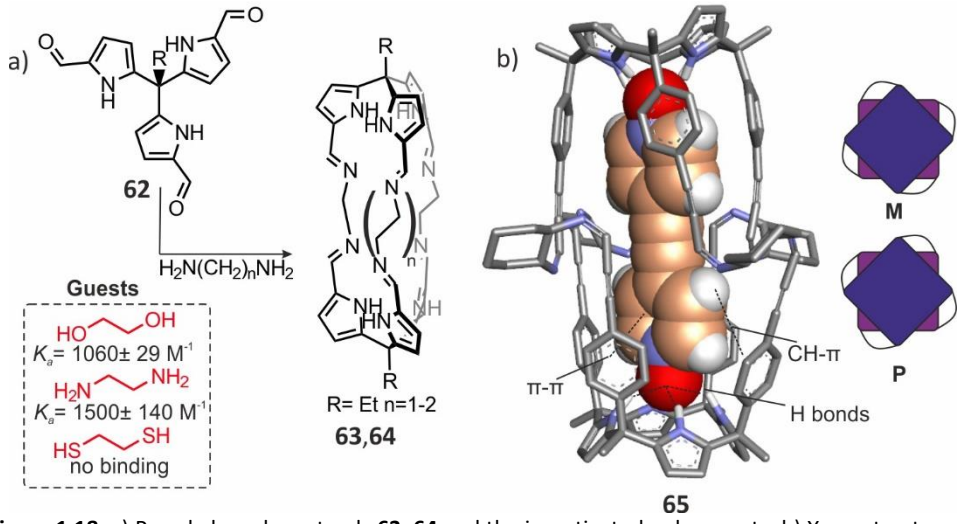

Figure 1.18. a) Pyrrole based cryptands **63**, **64** and the investigated polar guests; b) X-ray structure of **65** (adapted from ref. 112) and cartoon representations of the two possible diastereomers raising from the combination between the two senses of bis-imine covalent bonds and stereogenic carbon of diamino linker.

In 2001, Beer and co-workers developed the hexa-pyrrole cryptands **63** and **64** (Figure 1.18 a) from the [2+3] condensation of methyl- and ethyl-triformyl pyrrole with diamines (ethylenediamine and butylenediamine).[111] The resulting Schiff bases cryptands-like receptors had functionalized interiors with six convergent hydrogen bond donors deriving from the pyrrole NHs. The X-ray crystal structure of the cages revealed that the diamine linkers played the role of a template in the assembly of the cryptand receptors. One molecule of the diamine was included in the cage by stablishing multiple hydrogen bonds between its nitrogen atom and four of the six

pyrrole NHs acting as hydrogen donor. Evidence for the encapsulation of 1,2-ethanediamine and 1,2-ethanediol in solution was obtained via ^{1}H NMR titrations of the cryptands in $CDCl_3$ solution. The binding constants determined for the two 1:1 complexes were similar.

More recently, our group reported the synthesis of the chiral octa-imine capsule **65** based on calix[4]pyrrole components. The assembled capsule featured a large polar interior (Figure 1.18 b)[112] able to encapsulate 4-(4-pyridinylethynyl)pyridine-*N,N'*-dioxide. The pyridyl-*N*-oxide interacted with calix[4]pyrrole capsule's hemispheres through hydrogen bonding interactions, CH-π and π-π interactions. The bis-*N*-oxide acted as a template for the capsule's assembly. Interestingly, the use of enantiomerically pure (1R,2R)-(-)-1,2-diaminecyclohexane as linker endowed the capsule with chirality. The combination of the stereogenic carbon atoms of the diamine with the two possible senses of the unidirectional orientation of the imine bonds produced the possible existence of **65** as a mixture of *P* and *M* diastereoisomers. Notably, only one of the two diastereomers was observed in the X-ray crystal structure of **65**. This result highlighted the existence of a supramolecular point chirality transfer in the assembly of the cage.

Pyrrole has been also exploited as cage component for the recognition of carbohydrates. Roelens *et al*. investigated the binding affinity of the cryptand-like cage **67** towards α and β-glucopyranosides (Figure 1.19).[113] The amine cage **67** was synthesized by reduction of the parent imine counterpart **66** using $NaBH_4$.

The X-ray structure of **67** showed C_{3h} symmetry. In the solid state, the amine NH groups and the pyrrole NHs of cage **67** were inwardly directed with respect to its cavity.

The polar cavity of **67** was useful for the selective binding in $CDCl_3$ solution of octyl-β-D-glucopyranoside (OctβGlc) in front of the α isomer (OctαGlc). A binding constant value in the order of 10^4 M^{-1} was determined for the OctβGlc⊂**67** complex. Interestingly, although the interior of the imine-cage precursor **66** is very similar, the addition of an equimolar amount of OctβGlc did not produce the encapsulation complex in significant amounts. Instead, the imine cage **66** transformed into oligomeric species. Not surprisingly, the use of OctβGlc as template for the synthesis of the imine cage also produced a mixture of oligomers. Most probably, this is due to structural restrictions imparted by the rigidity of the imine bonds.

ESI-MS experiments supported the results obtained in solution. That is, the ESI-MS spectra of separate equimolar solutions of **67** with OctβGlc and OctαGlc displayed an intense ion-peak for the 1:1 complex only in the case of OctβGlc (Figure 1.19 a,b).

Further studies of the same authors focused on quantitative comparison between the pyrrole cage **67** and the pyridine cage **69** for the molecular recognition of OctβGlc.[114] ITC experiments in $CDCl_3$ solution revealed a trend in the K_a values of the 1:1 complexes with OctβGlc for cages **67**, **69** and **68** (K_a= 4.0× 10^4 M^{-1}, 3.6× 10^3 M^{-1} and 1.9× 10^2 M^{-1}, respectively). The authors attributed the lower K_a of cage **69** for the OctβGlc binding compared to the K_a of cage **67**, to the hydrogen bonding acceptor nature of the pyridine nitrogen atom of the former compared to the pyrrole NHs hydrogen bonding donating properties in the latter. Using molecular mechanic calculations, the authors selected a family of conformers for the OctβGlc⊂**67** complex that were compatible with the experimentally observed

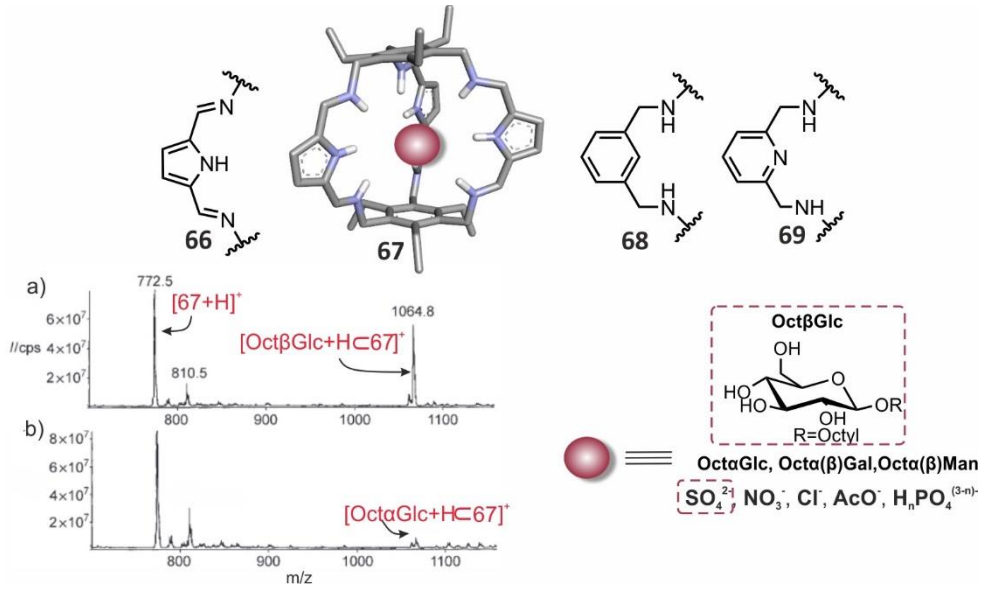

Figure 1.19. Energy minimized structure (MM3) of **67**; ESI-MS spectra showing a) an intense ion-peak for the OctβGlc⊂**67** complex and b) a low intensity ion-peak in the case of the OctαGlc⊂**67** complex (adapted from ref. 113)

^{1}H NMR chemical shifts and NOEs. They concluded that in the complexes with the pyridine cage **69** only one hydrogen bonding interaction was established with the glucopyranoside. In contrast, the pyrrole cage **67** interacted with the OctβGlc through three hydrogen bonding interactions.

A somewhat related comparison was reported by Delgado and co-workers who investigated the binding behavior of two hexa-amine cages towards different anions with a particular focus on phosphate and sulfate. These anions are of special interest due to their ubiquitous presence in biological systems and also because of their well-known toxic effects in the environment (especially in potable and waste water).

The results of potentiometric titrations of protonated **67** in H_2O-MeOH with a series of anions (SO_4^{2-}, NO_3^-, Cl^-, AcO^-, $H_nPO_4^{(3-n)-}$)[115] showed that, at pH=4, SO_4^{2-} was strongly bound and the only competitor was $H_nPO_4^{(3-n)-}$, even if in a negligible extent. Considering that in these pH conditions the cage is in the hexaprotonated form, the high association constant obtained for SO_4^{2-} (K_a= 2.6 ×10^6 M^{-1}) is mainly due to the four positive charges of the receptor and the two negative charges of the anion, so the electrostatic contribution to binding was maximized. However, a comparison between this experiment and the experiment performed in presence of cage **68**, demonstrated that also hydrogen bond interactions due to the pyrrole NHs (hydrogen bonding donors) contributed to the binding affinity. Indeed, the K_a value calculated for **68** was 9.5× 10^4 M^{-1}, which was smaller than the K_a value determined for **67** (2.6× 10^6 M^{-1}). The X-ray structure of the SO_4^{2-}⊂**67** complex confirmed the interaction of the anion with the host through a network of nine hydrogen bonds, three of them involving the pyrrole NHs.

1.3.2.3 *Pseudo-peptidic cages*

The reasonable introduction of amino acid derived components (peptide-like or pseudopeptides) in the structures of macrobicyclic receptors would endow their inner cavities with polar functional groups. This structural modification was expected to increase the functional variability of the receptors for future biological applications.

Alfonso and co- workers explored the synthesis of pseudo-peptidic macrocycles taking advantage of the designed preorganization of the linkers and the dynamic covalent approach.[116,117,118] They achieved the preorganization of amide-amine unit, **71**, in a U shaped conformation by combining two chiral building blocks (1,2-*R,R*-diamine-cyclohexyl and *S*-amino acids). The condensation of the bis-amines **71** having a cyclohexyl spacer with the aromatic tri-aldehyde **70** in MeOD solution produced the corresponding hexa-imine cages featuring D_3 symmetry. The "in situ" reduction of the hexa-imine cages produced the hexa-amine cage derivatives (**72**, **73**, **74** Figure 1.20).

The assembly of structurally related hexa-imine cages was also studied using U-shaped units **71** having an aliphatic flexible spacer, both in the presence and in the absence of benzene 1,3,5-tricarboxylate as template. The obtained results demonstrated that in the presence of the template imine cages were assembled in shorter times (3h *vs* 27h in absence of template). The tri-carboxylate template was able to interact with the amide functional groups of the spacers through the formation of hydrogen bonds. These interactions stabilized the structure of the

hexa-imine-cages, as well as that of the hexa-amine derivatives during the reduction reaction of the former. The versatile synthetic approach described above allowed the insertion of U-shaped cyclic and linear aliphatic spacers functionalized with polar side chains. The different substitutions of the cages conferred them on different solubilities in polar solvents. It was also shown that the polar substituents of the spacers participated in the binding of *N*-protected dipeptides.[119]

The X-ray structure of the perchlorate salt of cage **72** revealed the complete protonation of the amino groups and the partial encapsulation of the perchlorate. The perchlorate anions formed a network of hydrogen bonds with the ammonium groups and the amide NHs of the cage.

Competitive binding experiments analyzed by ESI-MS allowed the selection of the best hexa-amine cage for the binding of *N*-protected dipeptides. The hexa-amine cage **72**, having cyclohexane spacers with serine amino acids, was identified. This

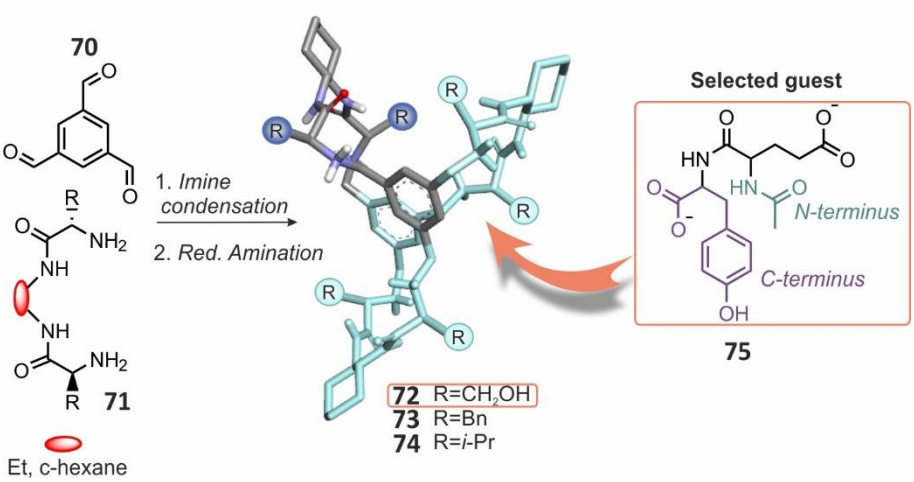

Figure 1.20. X-ray structure of protonated pseudo-peptidic cage **72** (adapted from ref. 118). Cage **72** and guest **75** formed the thermodynamically more stable 1:1 complex.

result supported that the rigidity of the spacer improved the binding features of the cage. ^{1}H NMR studies in $CDCl_3$ solution and in mixtures of polar solvents such as CD_3CN: CD_3OD, which prevented self-aggregation processes, allowed to screen the binding affinities of cage **72** towards a library of *N*-protected dipeptides. The following conclusions were drawn from the results of these studies: a) the serine OH group present as side chains of the cage's spacers contributed to the binding selectivity of the guests through hydrogen bonding interactions; b) the selective recognition of *N*-protected dipeptidic guests demanded the presence of an aromatic residue at the C-terminus and an acetyl group at the opposite *N*- terminus. The aromatic group of the guest was involved in hydrophobic interactions with the

spacer substituents of the pseudo-peptidic cage. The carboxylate groups of the di-peptide established charged hydrogen bonding interactions with the amine/ amide functions of the cage.

1.3.3 Applications of imine and amine based cages

The large majority of shape-persistent organic cages have been synthesized by exploiting the reversible bond breaking and bond making characteristics offered by dynamic covalent chemistry reactions. These cages present accessible both intrinsic and extrinsic voids created through the packing of cage molecules in the solid-state. Within the class of porous materials, shape persistent cage compounds are superior, because they maintain the voids and porosity even upon desolvation of the crystals.[120,121,122] The presence of permanent cavities motivated chemists to explore the porosity of the cages and study the applications in gas sorption and gas separation processes.

Discrete organic molecules as precursors for porous materials provided very high specific surface areas of approx. 3000 m^2g^{-1}, as well as good gas sorption properties.[123]

Mastalerz and co-workers investigated the sorption properties of salicyl bisimine cage **49** and its *exo* and *endo*-functionalized derivatives, towards CO_2, N_2 and CH_4. These studies considered that the sorption properties of solids are influenced by the chemical environment of their surfaces (Figure 1.21).

The X-ray structure of **49** showed that the six hydroxyl groups were inwardly directed towards the cavity of the cage. The cage cavity had a slightly distorted octahedron shape with a volume of roughly 550 $Å^3$. In the packing of the lattice, the cages self-assembled through π–π interactions between their phenolic arene rings. This resulted in additional voids in the material with a diameter of approximately 22.3 $Å^3$. The material showed a high surface area (1377 m^2g^{-1}) and was able to take up 9.4 wt% CO_2 and 0.94 wt% CH_4. The sorption selectivity for CO_2 might be a consequence of the hydroxyl functional groups placed inside the cage's cavity.[124]

To further investigate the influence of the *endo*-functionalization on the adsorption properties, cage **49**'s derivatives in which the hydroxyl groups were functionalized with methyl, propyl, allyl and benzyl substituents were also studied.[125]

N_2 sorption experiments at 77K showed that the specific surface area (determined by the Brunauer-Emmett-Teller (BET) model) decreased as the bulkiness of the internal substituents was increased. For instance, the propylated cage **77** gave a lower BET surface area (491 $m^2\,g^{-1}$) than the methylated cage **76** (824 $m^2\,g^{-1}$). In

addition, the heat adsorption curves of CH_4 were very similar for cages **49** (R'= hydrogen) and **76** (R'= methyl). However, very different heat adsorption curves were obtained for the more polar CO_2. The pore surface of cage **49**, containing hydroxy groups, is more polar than that of **76**. Pore polarity had a small but recognizable effect on the sorption of CO_2.

Additional interactions of the hydroxyl groups of **49** with CO_2 molecules can occur through hydrogen bonding. This will explain the higher heats of adsorption

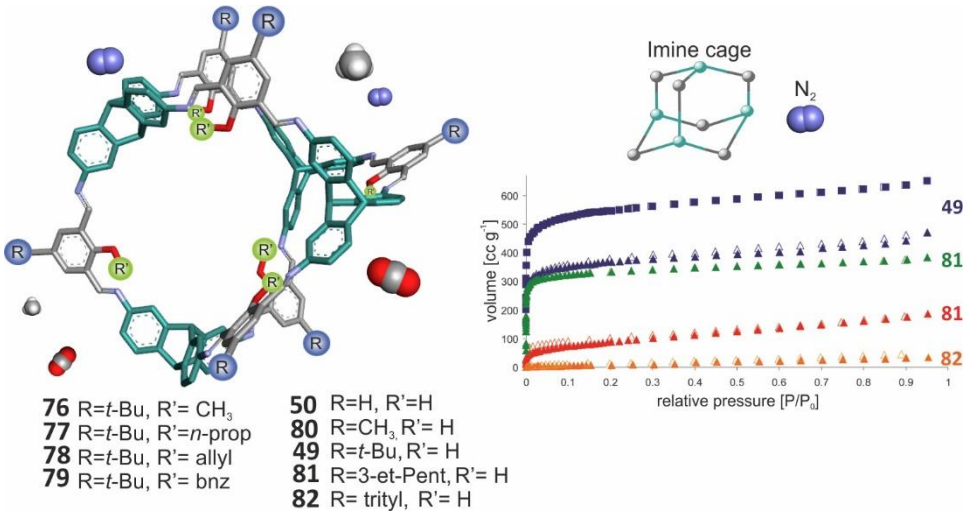

Figure 1.21. X-ray structure of cage **49** (adapted from ref. 124); (on the right) N_2 adsorption (filled symbols) and desorption (empty symbols) profiles at 77K for cage **49** and derivatives in their crystalline states (adapted from ref. 126).

measured for cage **49** (R'= hydrogen) compared to cage **76** (R'= methyl) that is not capable to form hydrogen bonds. These examples clearly showed that *endo*-functionalization of shape persistent cages not only led to the modification of the pores in terms of specific surface area and volume but also in terms of functional complementarity during the sorption of molecules.

The functionalization of cage **49** periphery resulted in cages **80**– **82**. The authors did not detect relevant changes in sorption properties of N_2 for the two cages, **80** (R= methyl) and **82** (R= trithyl), in their amorphous states.[126] However, in their crystalline states, the accessible surface area for N_2 significantly dropped for cage **49** functionalized with sterically more demanding groups (309 $m^2\ g^{-1}$ for **81** (with 3-ethylpentyl groups) and to 22 $m^2\ g^{-1}$ for **82** (with trityl groups))(Figure 1.21).

Similarly, the polar cavity of a [2+3] imine cage endowed with two inwardly directed phosphate groups showed selective sorption of polar CO_2 over CH_4. In this case, the polar inner functionalization and the partition of the cavity in three subunits, due to

the introduction of the two phosphate groups, played a role in the selective sorption.[127]

Very recently, Sessler and co-workers presented two shape persistent cryptand like pyrrole based imine cages (**83**, **84** Figure 1.22) as gas adsorption materials.[128] Similarly to what was observed in the systems described above, the polar nature of pyrrole based cages should confer selectivity for the sorption of polar gases. Indeed, the two cages preferentially adsorbed CO_2 and O_2 over H_2, CH_4 and N_2. In addition, cage **83** showed a higher uptake of all gases, which was indicative of a more ordered and accessible pore structure.

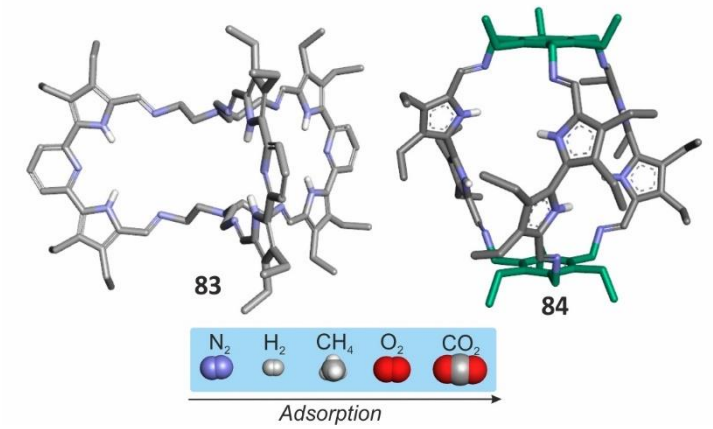

Figure 1.22.(On the top) X-ray structures of pyrrole based cages **83** and **84** (adapted from ref. 128); (on the bottom) selective adsorption of polarizable gases.

In summary, the examples analyzed in this section demonstrate that the rational design of imine based cages can lead to shape persistent systems with interesting gas sorption properties. Taking into account that gas sorption is influenced by the chemical environment of the surface, the *endo* functionalization of the cavity with polar groups can fine-tune the gas absorptivity properties leading to selectivity towards different gases.

Organic endo functionalized organic cages assembled by DCC also find applications in biological fields.

Derivatives of the pseudo- peptidic cage **72**, in particular those functionalized with histidine, ornithine and aspartic acid side chains, were used in biological applications as peptide protectors against tyrosine kinase-mediated phosphorylation. Alfonso and co-workers showed that these derivatives of **72** were able to selectively bind tyrosine residues in peptides and that the action of tyrosine kinase can be inhibited upon encapsulation of the residue in the cage.[129] The inhibition of the tyrosine kinase mediated phosphorylation depended on the peptide sequence and the side

chain of the cage. Importantly, the magnitudes of the binding affinities of the cage derivatives (determined by fluorescence emission titrations considering the different equilibria present in the reaction media) strongly correlated with their inhibitory efficiency.

1.4 Conclusions

Along the years, many researchers developed small molecules able to partially mimic complex biomolecules function. On the one hand, the aim of these studies was to improve our understanding of the molecular behavior of the more complex biological systems. On the other hand, they exploited the structural and mechanistic knowledge derived from the biological systems to inspire the design of smaller molecules with defined properties and specific applications.

One successful strategy to build bioinspired molecules is to combine natural building blocks, which provide functional elements, with abiotic fragments serving as structural scaffolds.

All the functional synthetic receptors whose self-assembly and binding properties were summarized in the last sections of this chapter (endowed with polar aminoacidic moieties, amide and amine groups, pyrroles, pyridines, hydroxy and carboxylic groups, etc.) took advantage of dynamic covalent chemistry. “In situ” reductive amination and other post-assembly modifications allowed to evolve their structures into chemically more stable derivatives and inserting additional functional polar groups in their cavity (*i.e*. amine groups).

The reviewed synthetic receptors showed relevant structural features and properties for the molecular recognition of biologically interesting targets (*i.e*. carbohydrates, peptides and dicarboxylate anions). In addition, other polar molecules and anions, which are ubiquitous in the natural world and play essential roles in the environment and in biology, were also bound by some of the synthetic receptors.

When the synthetic capsules and cages are decorated with inwardly directed protonated amines or other positively charged groups, the binding of anionic guest is mainly driven by coulombic interactions (charge-charge). We consider the synthetic receptors displaying neutral polar groups in their cavities (*i.e*. functionalized with amide or pyrrole moieties) better candidates for the selective binding of charged and neutral electron rich substrates.

We showed that the inner functionalization of the cavities of synthetic receptors with polar groups was necessary to design of bio-mimetic analogues with potential bio-chemical applications. The presence of polar groups influenced the inner

surfaces of shape persistent cages and produced a relevant impact in the development of new functional materials for gas storage and separation.

1.5 Aims of the thesis

The general aim of this thesis is the design, synthesis of the molecular components and study of the self-assembly processes of supramolecular poly-imine capsules and cages. For this purpose we will use calix[4]pyrrole scaffolds providing a sizeable polar cavity suitable for the encapsulation of small polar guests.

We are also interested in studying the recognition and binding properties of the prepared self-assembled poly-imine cages and capsules towards polar pyridyl-*N*-oxide guest derivatives. We aim at unveiling the mechanisms of the encapsulation and release processes of the guests by the capsules. The partial rupture of the dynamic covalent bonds holding together the molecular components of the capsular assemblies might be involved in the uptake and release of esoterically demanding guests that are too large to cross the open portals of the capsules.

Finally, we want to evaluate the application of these large capsular containers as supramolecular nano-reactors.

In order to achieve our aims, we proposed the following specific goals:

1) Self-assembly of [1+1] and [4+2] poly-imine dynamic covalent cages and capsules based on calix[4]pyrrole scaffolds: study of the condensation reaction conditions and post- assembly modifications to yield poly-amine derivatives.

We previously reported the synthesis of poly-imine [4+2] capsules through the condensation reaction of a tetra-α aryl extended calix[4]pyrrole, functionalized with aldehyde groups at the upper rim and a diamine linker. This methodology represents a convenient strategy for the self-assembly of poly-imine capsular aggregates under thermodynamic equilibrium conditions. In this thesis, we propose the use of a similar synthetic strategy to assemble [1+1] poly-imine cages through the condensation reaction of tetra-α aryl extended calix[4]pyrrole bearing at the upper rims aldehyde and amine groups, respectively. Alternatively, we also propose the self-assembly of unprecedented [4+2] poly-imine capsules by the condensation reaction of two copies of a tetra-α-tetra-amino aryl-extended calix[4]pyrrole and four copies of a phenyl-dialdehyde linker.

The self-assembly processes of the poly-imine capsules will be investigated under thermodynamic equilibrium conditions. We plan to investigate different reaction

conditions *i.e*. solvents and presence of template in order to assemble the capsules in good yields. We will evaluate the role of bis-pyridyl-*N*-oxides as templates for the self-assembly of the capsules. We will also attempt the self-assembly of the capsular systems in pure chloroform and in a chloroform: acetonitrile solvent mixtures. It is well-known that one molecule of acetonitrile is included in the polar cavity of calix[4]pyrrole receptors via hydrogen-bonding interactions. We foresee that the binding of an acetonitrile molecule will lock the receptor in the cone conformation and pre-organize the reacting amino groups in a favorable orientation for the imine condensation reaction leading to the capsular aggregates.

Finally, we will study the conversion of the chemically labile poly-imine capsules into more robust covalently bonded amino-capsules by a post-assembly modification of the imine bonds (*i.e.* reductive amination).

2) Evaluation of the binding properties of the self-assembled poly-imine and tetra-imine capsules and cages towards *N*-oxides and study of the kinetics of encapsulation processes in different solvents.

We plan to study the binding properties of the poly-imine and tetra-amine capsules and cages towards monotopic and ditopic *N*-oxides by means of ^{1}H NMR spectroscopy. The self-assembly of the capsular aggregates in the absence of templates or even in the presence of a weakly bound templates (*i.e.* acetonitrile) would provide "empty" containers suitable for the assessment of their binding features.
In addition, we plan to study the kinetics of the encapsulation processes of the guests. We expect that the shape and dimensions of the guest, as well as the solvent nature will play a role. The obtained results will serve to gain some insights into the mechanisms of the uptake and release of the guests occurring in the covalent dynamic and fully covalent capsular systems.

3) Study of a cycloaddition reaction mediated by the poly-imine and poly-amine capsules.

We plan to evaluate the effect played by the [4+2] poly-imine and poly-amine self-assembled capsules in mediating the Huisgen 1,3-dipolar cycloaddition of adequately substituted pyridine-*N*-oxide derivatives.
The pyridine-*N*-oxides will bind into the polar capsules' cavity mainly through hydrogen interactions. In the hetero-capsular complex, we expect that the reactants will be positioned in a favorable orientation to achieve the geometry of the transition state of the cycloaddition reaction in the confined space.

1.6 Outline of the thesis

This thesis is divided in four chapters: the introduction (chapter 1), three chapters describing the results and their discussion (chapters 2–4) and a final section dedicated to the general conclusions of the work.

Chapter 1 represents a revision of the state of art focusing on *endo*- functionalized capsules and cages assembled by imine bonds. It also contains general and fundamental concepts related to dynamic covalent chemistry that will be useful for the reader of the thesis. Each chapter will also contain its own introduction in which a more specific background on the topic will be provided.

Chapter 2 describes the synthesis of tetra-aldehyde and tetra-amino functionalized calix[4]pyrrole derivatives used as molecular components in the self-assembly of the [1+1] tetra-imine cages. The optimal conditions for the self-assembly of [1+1] tetra-imine capsular aggregates are also reported. These include the use of a di-topic pyridyl-*N*-oxide acting as a template, as well as the exclusive use of pure solvents and solvent mixtures ($CDCl_3$, CD_2Cl_2, $CDCl_3$:CD_3CN).

The chapter also discloses the binding properties of the [1+1] tetra-imine cages towards planar (2D) and sterically demanding (3D) *N*-oxides. The binding properties were investigated using ^1H NMR spectroscopy. We provide our insights on the mechanisms operating for the encapsulation of the guests. Our knowledge is derived from the kinetics measured for the encapsulation processes in pure $CDCl_3$ and $CDCl_3$:CD_3CN mixtures.

Chapter 3 deals with the self-assembly of [4+2] octa-imine capsules displaying a large polar cavity and their post-assembly modifications. The reductive amination of the imine functionalities provided the corresponding octa-amine capsule endowed with a fully covalent backbone that was conformationally more flexible than the parent capsule. In this chapter, we also evaluated the differences in the structures of the encapsulation complexes of the conformationally more rigid octa-imine capsules with respect to that of the flexible octa-amine counterpart.

Finally, **Chapter 4** describes the application of the [4+2] octa-imine capsule and its amino derivative as supramolecular nanoreactors. We disclose the important role played by the capsules in accelerating the Huisgen 1,3-dipolar cycloaddition between encapsulated pyridine-*N*-oxides bearing azide and alkyne groups. We calculated the initial rates of the reaction using different experimental conditions.

Finally, we compare the initial rate values of the reaction occurring in the capsules with that observed in the bulk solution.

1.7 References and notes

[1] P. A. Gale, J. L. Sessler, V. Král, V. Lynch, *J. Am. Chem. Soc.* **1996**, *118*, 5140-5141.
[2] P. A. Gale, P. Anzenbacher Jr, J. L. Sessler, *Coord. Chem. Rev.* **2001**, *222*, 57-102.
[3] F. H. Kohnke, *Eur. J. Org. Chem.* **2020**, *2020*, 4261-4272.
[4] I. A. Rather, S. A. Wagay, M. S. Hasnain, R. Ali, *RSC Adv.* **2019**, *9*, 38309-38344.
[5] I. Saha, J. T. Lee, C.-H. Lee, *Eur. J. Org. Chem.* **2015**, *2015*, 3859-3885.
[6] S. Peng, Q. He, G. I. Vargas-Zúñiga, L. Qin, I. Hwang, S. K. Kim, N. J. Heo, C.-H. Lee, R. Dutta, J. L. Sessler, *Chem. Soc. Rev.* **2020**, *49*, 865-907.
[7] A. F. Sierra, D. Hernández-Alonso, M. A. Romero, J. A. González-Delgado, U. Pischel, P. Ballester, *J. Am. Chem. Soc.* **2020**, *142*, 4276-4284.
[8] A. F. Sierra, G. Aragay, G. Peñuelas-Haro, P. Ballester, *Org. Chem. Front.* **2021**, *8*, 2402-2412.
[9] E. Mulugeta, Q. He, D. Sareen, S.-J. Hong, J. H. Oh, V. M. Lynch, J. L. Sessler, S. K. Kim, C.-H. Lee, *Chem* **2017**, *3*, 1008-1020.
[10] D. Villarón, M. A. Siegler, S. J. Wezenberg, *Chem. Sci.* **2021**, *12*, 3188-3193.
[11] D. S. Kim, J. L. Sessler, *Chem. Soc. Rev.* **2015**, *44*, 532-546.
[12] P. A. Gale, *Chem* **2020**, *6*, 2873-2875.
[13] L. Martínez-Crespo, J. L. Sun-Wang, A. F. Sierra, G. Aragay, E. Errasti-Murugarren, P. Bartoccioni, M. Palacín, P. Ballester, *Chem* **2020**, *6*, 3054-3070.
[14] L. Martínez-Crespo, J. L. Sun-Wang, P. Ferreira, C. F. M. Mirabella, G. Aragay, P. Ballester, *Chem.–Eur. J.* **2019**, *25*, 4775-4781.
[15] C. Maeda, S. Sasaki, K. Takaishi, T. Ema, *Catal. Sci. Technol.* **2018**, *8*, 4193-4198.
[16] X. Wang, L. Xie, K. Lin, W. Ma, T. Zhao, X. Ji, M. Alyami, N. M. Khashab, H. Wang, J. L. Sessler, *Angew. Chem. Int. Ed.* **2021**, *60*, 7188-7196.
[17] A. Baeyer, *Ber. Dtsch. Chem. Ges.* **1886**, *19*, 2184-2185.
[18] W. E. Allen, P. A. Gale, C. T. Brown, V. M. Lynch, J. L. Sessler, *J. Am. Chem. Soc.* **1996**, *118*, 12471-12472.
[19] P. A. Gale, J. L. Sessler, W. E. Allen, N. A. Tvermoes, V. Lynch, *Chem. Commun. (Cambridge, U. K.)* **1997**, 665-666.
[20] P. Anzenbacher, A. C. Try, H. Miyaji, K. Jursíková, V. M. Lynch, M. Marquez, J. L. Sessler, *J. Am. Chem. Soc.* **2000**, *122*, 10268-10272.
[21] L. Bonomo, E. Solari, G. Toraman, R. Scopelliti, C. Floriani, M. Latronico, *Chem. Commun. (Cambridge, U. K.)* **1999**, 2413-2414.
[22] P. Anzenbacher, K. Jursíková, V. M. Lynch, P. A. Gale, J. L. Sessler, *J. Am. Chem. Soc.* **1999**, *121*, 11020-11021.
[23] A. Díaz-Moscoso, D. Hernández-Alonso, L. Escobar, F. A. Arroyave, P. Ballester, *Org. Lett.* **2017**, *19*, 226-229.
[24] S. Camiolo, P. A. Gale, *Chem. Commun. (Cambridge, U. K.)* **2000**, 1129-1130.
[25] C. Guo, H. Wang, V. M. Lynch, X. Ji, Z. A. Page, J. L. Sessler, *Chem. Sci.* **2020**, *11*, 5650-5657.
[26] L. Adriaenssens, C. Estarellas, A. Vargas Jentzsch, M. Martinez Belmonte, S. Matile, P. Ballester, *J. Am. Chem. Soc.* **2013**, *135*, 8324-8330.
[27] L. Adriaenssens, G. Gil-Ramírez, A. Frontera, D. Quiñonero, E. C. Escudero-Adán, P. Ballester, *J. Am. Chem. Soc.* **2014**, *136*, 3208-3218.

[28] G. Gil-Ramírez, E. C. Escudero-Adán, J. Benet-Buchholz, P. Ballester, *Angew. Chem. Int. Ed.* **2008**, *47*, 4114-4118.
[29] N. J. Heo, J. H. Yang, V. M. Lynch, B. J. Ko, J. L. Sessler, S. K. Kim, *Chem. Sci.* **2020**, *11*, 8288-8294.
[30] D. Villarón, M. A. Siegler, S. J. Wezenberg, *Chem. Sci.* **2021**, *12*, 3188-3193.
[31] S. Peng, Q. He, G. I. Vargas-Zúñiga, L. Qin, I. Hwang, S. K. Kim, N. J. Heo, C.-H. Lee, R. Dutta, J. L. Sessler, *Chem. Soc. Rev.* **2020**, *49*, 865-907.
[32] G. Cafeo, F. H. Kohnke, L. Valenti, A. J. P. White, *Chem.–Eur. J.* **2008**, *14*, 11593-11600.
[33] P. Ballester, G. Gil-Ramirez, *PNAS* **2009**, *106*, 10455-10459.
[34] G. Gil-Ramírez, M. Chas, P. Ballester, *J. Am. Chem. Soc.* **2010**, *132*, 2520-2521.
[35] S. J. Rowan, S. J. Cantrill, G. R. L. Cousins, J. K. M. Sanders, J. F. Stoddart, *Angew. Chem. Int. Ed.* **2002**, *41*, 898-952.
[36] J.-M. Lehn, *Chem. Soc. Rev.* **2007**, *36*, 151-160.
[37] P. T. Corbett, J. Leclaire, L. Vial, K. R. West, J.-L. Wietor, J. K. M. Sanders, S. Otto, *Chem. Rev. (Washington, DC, U. S.)* **2006**, *106*, 3652-3711.
[38] Y. Jin, C. Yu, R. J. Denman, W. Zhang, *Chem. Soc. Rev.* **2013**, *42*, 6634-6654.
[39] K. Kobayashi, M. Yamanaka, *Chem. Soc. Rev.* **2015**, *44*, 449-466.
[40] N. Iwasawa, K. Ono, *Chem. Rec.* **2022**, *22*, e202100214.
[41] N. Nishimura, K. Kobayashi, *J. Org. Chem.* **2010**, *75*, 6079-6085.
[42] N. Nishimura, K. Yoza, K. Kobayashi, *J. Am. Chem. Soc.* **2010**, *132*, 777-790.
[43] N. Nishimura, K. Kobayashi, *Angew. Chem. Int. Ed.* **2008**, *47*, 6255-6258.
[44] A. P. Côté, A. I. Benin, N. W. Ockwig, M. O'Keeffe, A. J. Matzger, O. M. Yaghi, *Science* **2005**, *310*, 1166-1170.
[45] K. Geng, T. He, R. Liu, S. Dalapati, K. T. Tan, Z. Li, S. Tao, Y. Gong, Q. Jiang, D. Jiang, *Chem. Rev. (Washington, DC, U. S.)* **2020**, *120*, 8814-8933.
[46] Z. Shan, X. Wu, B. Xu, Y.-l. Hong, M. Wu, Y. Wang, Y. Nishiyama, J. Zhu, S. Horike, S. Kitagawa, G. Zhang, *J. Am. Chem. Soc.* **2020**, *142*, 21279-21284.
[47] Z. Lin, T. J. Emge, R. Warmuth, *Chem.–Eur. J.* **2011**, *17*, 9395-9405.
[48] M. Yang, F. Qiu, E.-S. M. El-Sayed, W. Wang, S. Du, K. Su, D. Yuan, *Chem. Sci.* **2021**, *12*, 13307-13315.
[49] T. Jiao, G. Wu, Y. Zhang, L. Shen, Y. Lei, C.-Y. Wang, A. C. Fahrenbach, H. Li, *Angew. Chem. Int. Ed.* **2019**.
[50] M. Wierzbicki, A. A. Głowacka, M. P. Szymański, A. Szumna, *Chem. Commun. (Cambridge, U. K.)* **2017**, *53*, 5200-5203.
[51] Y.-Y. Xu, H.-K. Liu, Z.-K. Wang, B. Song, D.-W. Zhang, H. Wang, Z. Li, X. Li, Z.-T. Li, *J. Org. Chem.* **2021**, *86*, 3943-3951.
[52] M. E. Belowich, J. F. Stoddart, *Chem. Soc. Rev.* **2012**, *41*, 2003-2024.
[53] N. M. Rue, J. Sun, R. Warmuth, *Isr. J. Chem.* **2011**, *51*, 743-768.
[54] M. L. C. Quan, D. J. Cram, *J. Am. Chem. Soc.* **1991**, *113*, 2754-2755.
[55] S. Ro, S. J. Rowan, A. R. Pease, D. J. Cram, J. F. Stoddart, *Org. Lett.* **2000**, *2*, 2411-2414.
[56] A. Jiménez, R. A. Bilbeisi, T. K. Ronson, S. Zarra, C. Woodhead, J. R. Nitschke, *Angew. Chem. Int. Ed.* **2014**, *53*, 4556-4560.
[57] S. Vu, G. Nagesh, N. Yousefi, J. F. Trant, D. S. K. Ting, M. J. Ahamed, S. Rondeau-Gagné, *Mat. Adv.* **2021**, *2*, 6676-6683.

[58] A. F. M. El-Mahdy, A. M. Elewa, S.-W. Huang, H.-H. Chou, S.-W. Kuo, *Adv. Optical Mater.* **2020**, *8*, 2000641.
[59] C. C. Pattillo, J. S. Moore, *Chem. Sci.* **2019**, *10*, 7043-7048.
[60] J. Li, P. Nowak, S. Otto, *J. Am. Chem. Soc.* **2013**, *135*, 9222-9239.
[61] C. D. Meyer, C. S. Joiner, J. F. Stoddart, *Chem. Soc. Rev.* **2007**, *36*, 1705-1723.
[62] K. Das, L. Gabrielli, L. J. Prins, *Angew. Chem. Int. Ed.* **2021**, *60*, 20120-20143.
[63] R. T. S. Lam, A. Belenguer, S. L. Roberts, C. Naumann, T. Jarrosson, S. Otto, J. K. M. Sanders, *Science* **2005**, *308*, 667-669.
[64] M. Bru, I. Alfonso, M. I. Burguete, S. V. Luis, *Angew. Chem. Int. Ed.* **2006**, *45*, 6155-6159.
[65] I. Alfonso, M. Bolte, M. Bru, M. I. Burguete, S. V. Luis, J. Rubio, *J. Am. Chem. Soc.* **2008**, *130*, 6137-6144.
[66] T. H. G. Schick, F. Rominger, M. Mastalerz, *J. Org. Chem.* **2020**, *85*, 13757-13771.
[67] K. C. F. Leung, F. Aricó, S. J. Cantrill, J. F. Stoddart, *J. Am. Chem. Soc.* **2005**, *127*, 5808-5810.
[68] N. Schäfer, M. Bühler, L. Heyer, M. I. S. Röhr, F. Beuerle, *Chem.–Eur. J.* **2021**, *27*, 6077-6085.
[69] J. Zhu, Y. Han, Y. Ni, S. Wu, Q. Zhang, T. Jiao, Z. Li, J. Wu, *J. Am. Chem. Soc.* **2021**, *143*, 14314-14321.
[70] N. Iwasawa, H. Takahagi, *J. Am. Chem. Soc.* **2007**, *129*, 7754-7755.
[71] H. Takahagi, N. Iwasawa, *Chem.–Eur. J.* **2010**, *16*, 13680-13688.
[72] F. Aricó, J. D. Badjic, S. J. Cantrill, A. H. Flood, K. C. F. Leung, Y. Liu, J. F. Stoddart, in *Templates in Chemistry II: -/-* (Eds.: C. A. Schalley, F. Vögtle, K. H. Dötz), Springer Berlin Heidelberg, Berlin, Heidelberg, **2005**, pp. 203-259.
[73] B.-N. T. Nguyen, A. B. Grommet, A. Tron, M. C. A. Georges, J. R. Nitschke, *Adv. Mater. (Weinheim, Ger.)* **2020**, *32*, 1907241.
[74] D. Zhang, T. K. Ronson, J. R. Nitschke, *Acc. Chem. Res.* **2018**, *51*, 2423-2436.
[75] L. Xu, D. Zhang, T. K. Ronson, J. R. Nitschke, *Angew. Chem. Int. Ed.* **2020**, *59*, 7435-7438.
[76] D. Zhang, Q. Gan, A. J. Plajer, R. Lavendomme, T. K. Ronson, Z. Lu, J. D. Jensen, B. W. Laursen, J. R. Nitschke, *J. Am. Chem. Soc.* **2022**, *144*, 1106-1112.
[77] B. J. Holliday, C. A. Mirkin, *Angew. Chem. Int. Ed.* **2001**, *40*, 2022-2043.
[78] Z. Dong, Q. Luo, J. Liu, *Chem. Soc. Rev.* **2012**, *41*, 7890-7908.
[79] P. Dramou, N. Tarannum, *Molecularly Imprinted Catalysts: Synthesis and Applications*, **2016**.
[80] N. Masurier, D. P. Arama, C. El Amri, V. Lisowski, *Med. Res. Rev.* **2018**, *38*, 655-683.
[81] B. Kuberski, A. Szumna, *Chem. Commun. (Cambridge, U. K.)* **2009**, 1959-1961.
[82] L. Adriaenssens, P. Ballester, *Chem. Soc. Rev.* **2013**, *42*, 3261.
[83] G. Zhang, M. Mastalerz, *Chem. Soc. Rev.* **2014**, *43*, 1934-1947.
[84] M. Kołodziejski, A. R. Stefankiewicz, J.-M. Lehn, *Chem. Sci.* **2019**, *10*, 1836-1843.
[85] X. Liu, R. Warmuth, *J. Am. Chem. Soc.* **2006**, *128*, 14120-14127.
[86] S. M. Elbert, F. Rominger, M. Mastalerz, *Chem.–Eur. J.* **2014**, *20*, 16707-16720.
[87] M. Mastalerz, *Chem. Commun. (Cambridge, U. K.)* **2008**, 4756-4758.
[88] M. Holsten, S. Feierabend, S. M. Elbert, F. Rominger, T. Oeser, M. Mastalerz, *Chem.–Eur. J.* **2021**, *27*, 9383-9390.
[89] O. I. Afanasyev, E. Kuchuk, D. L. Usanov, D. Chusov, *Chem. Rev. (Washington, DC, U. S.)* **2019**, *119*, 11857-11911.

[90] M. B. Smith, in *Organic Synthesis (Fourth Edition)* (Ed.: M. B. Smith), Academic Press, Boston, **2017**, pp. 483-518.
[91] X. Liu, Y. Liu, G. Li, R. Warmuth, *Angew. Chem. Int. Ed.* **2006**, *45*, 901-904.
[92] M. Mastalerz, M. W. Schneider, I. M. Oppel, O. Presly, *Angew. Chem. Int. Ed.* **2011**, *50*, 1046-1051.
[93] M. A. Mohamed, K.-i. Yamada, K. Tomioka, *Tetrahedron Lett.* **2009**, *50*, 3436-3438.
[94] P. J. Waller, S. J. Lyle, T. M. Osborn Popp, C. S. Diercks, J. A. Reimer, O. M. Yaghi, *J. Am. Chem. Soc.* **2016**, *138*, 15519-15522.
[95] A. S. Bhat, S. M. Elbert, W.-S. Zhang, F. Rominger, M. Dieckmann, R. R. Schröder, M. Mastalerz, *Angew. Chem. Int. Ed.* **2019**, *58*, 8819-8823.
[96] P.-E. Alexandre, W.-S. Zhang, F. Rominger, S. M. Elbert, R. R. Schröder, M. Mastalerz, *Angew. Chem. Int. Ed.* **2020**, *59*, 19675-19679.
[97] V. V. Kouznetsov, *Tetrahedron* **2009**, *65*, 2721-2750.
[98] H. Xie, T. J. Finnegan, V. W. Liyana Gunawardana, R. Z. Pavlović, C. E. Moore, J. D. Badjić, *J. Am. Chem. Soc.* **2021**, *143*, 3874-3880.
[99] H. Xie, V. W. L. Gunawardana, T. J. Finnegan, W. Xie, J. D. Badjić, *Angew. Chem. Int. Ed.* **2022**, *61*, e202116518.
[100] K. V. Kilway, J. S. Siegel, *J. Am. Chem. Soc.* **1991**, *113*, 2332-2333.
[101] D. Das, L. J. Barbour, *J. Am. Chem. Soc.* **2008**, *130*, 14032-14033.
[102] M. L. C. Quan, D. J. Cram, *J. Am. Chem. Soc.* **1991**, *113*, 2754-2755.
[103] S. Saha, B. Akhuli, S. Chakraborty, P. Ghosh, *J. Org. Chem.* **2013**, *78*, 8759-8765.
[104] J. M. Llinares, D. Powell, K. Bowman-James, *Coord. Chem. Rev.* **2003**, *240*, 57-75.
[105] E. García-España, P. Díaz, J. M. Llinares, A. Bianchi, *Coord. Chem. Rev.* **2006**, *250*, 2952-2986.
[106] S. Chakraborty, S. Saha, L. M. P. Lima, U. Warzok, S. Sarkar, B. Akhuli, M. Nandi, S. Bej, N. N. Adarsh, C. A. Schalley, R. Delgado, P. Ghosh, *J. Org. Chem*. **2017**, *82*, 10007-10014.
[107] O. D. Fox, T. D. Rolls, M. G. B. Drew, P. D. Beer, *Chem. Commun. (Cambridge, U. K.)* **2001**, 1632-1633.
[108] F. Wang, E. Sikma, Z. Duan, T. Sarma, C. Lei, Z. Zhang, S. M. Humphrey, J. L. Sessler, *Chem. Commun. (Cambridge, U. K.)* **2019**, *55*, 6185-6188.
[109] J. H. Oh, J. H. Kim, D. S. Kim, H. J. Han, V. M. Lynch, J. L. Sessler, S. K. Kim, *Org. Lett.* **2019**, *21*, 4336-4339.
[110] H. J. Han, J. H. Oh, J. L. Sessler, S. K. Kim, *Chem. Commun. (Cambridge, U. K.)* **2019**, *55*, 10876-10879.
[111] O. D. Fox, T. D. Rolls, M. G. B. Drew, P. D. Beer, *Chem. Commun. (Cambridge, U. K.)* **2001**, 1632-1633.
[112] A. Galán, E. C. Escudero-Adán, P. Ballester, *Chem. Sci.* **2017**, *8*, 7746-7750.
[113] O. Francesconi, A. Ienco, G. Moneti, C. Nativi, S. Roelens, *Angew. Chem.* **2006**, *118*, 6845-6848.
[114] O. Francesconi, M. Gentili, S. Roelens, *J. Org. Chem.* **2012**, *77*, 7548-7554.
[115] P. Mateus, R. Delgado, P. Brandão, V. Félix, *J. Org. Chem.* **2009**, *74*, 8638-8646.
[116] I. Alfonso, M. I. Burguete, F. Galindo, S. V. Luis, L. Vigara, *J. Org. Chem.* **2009**, *74*, 6130-6142.
[117] I. Alfonso, M. Bolte, M. Bru, M. I. Burguete, S. V. Luis, C. Vicent, *Org. Biomol. Chem.* **2010**, *8*, 1329-1339.

[118] A. Moure, S. V. Luis, I. Alfonso, *Chem.–Eur. J.* **2012**, *18*, 5496-5500.
[119] E. Faggi, A. Moure, M. Bolte, C. Vicent, S. V. Luis, I. Alfonso, *J. Org. Chem.* **2014**, *79*, 4590-4601.
[120] G. Zhang, O. Presly, F. White, I. M. Oppel, M. Mastalerz, *Angew. Chem. Int. Ed.* **2014**, *53*, 1516-1520.
[121] K. E. Jelfs, X. Wu, M. Schmidtmann, J. T. A. Jones, J. E. Warren, D. J. Adams, A. I. Cooper, *Angew. Chem. Int. Ed.* **2011**, *50*, 10653-10656.
[122] M. Brutschy, M. W. Schneider, M. Mastalerz, S. R. Waldvogel, *Adv. Mater. (Weinheim, Ger.)* **2012**, *24*, 6049-6052.
[123] M. A. Little, A. I. Cooper, *Adv. Funct. Mater.* **2020**, *30*, 1909842.
[124] M. Mastalerz, M. W. Schneider, I. M. Oppel, O. Presly, *Angew. Chem. Int. Ed.* **2011**, *50*, 1046-1051.
[125] M. W. Schneider, I. M. Oppel, A. Griffin, M. Mastalerz, *Angew. Chem. Int. Ed.* **2013**, *52*, 3611-3615.
[126] M. W. Schneider, I. M. Oppel, H. Ott, L. G. Lechner, H.-J. S. Hauswald, R. Stoll, M. Mastalerz, *Chem.–Eur. J.* **2012**, *18*, 836-847.
[127] G. Feng, W. Liu, Y. Peng, B. Zhao, W. Huang, Y. Dai, *Chem. Commun. (Cambridge, U. K.)* **2016**, *52*, 9267-9270.
[128] F. Wang, E. Sikma, Z. Duan, T. Sarma, C. Lei, Z. Zhang, S. M. Humphrey, J. L. Sessler, *Chem. Commun. (Cambridge, U. K.)* **2019**, *55*, 6185-6188.
[129] L. Tapia, N. Solozabal, J. Solà, Y. Pérez, W. T. Miller, I. Alfonso, *Chem.–Eur. J.* **2021**, *27*, 9542-9549.

Chapter 2

Self-assembly of [1+1] tetra-imine cages and kinetic studies of inclusion of polar guests

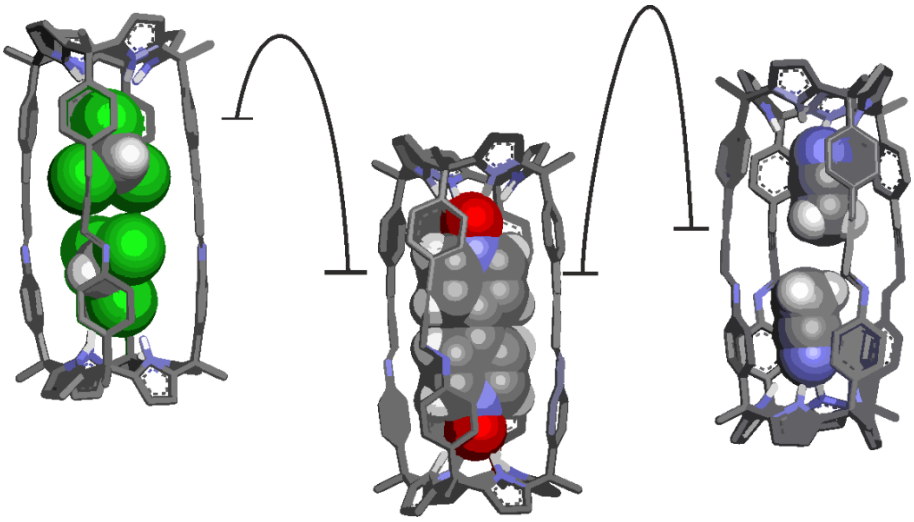

Unpublished results

2.1 Introduction

The assembly of supramolecular capsules has been a topic of interest for many researchers in the last decades. Their inner space shows unique properties, different from the bulk solution, making them attractive for specific functions (*i.e*. guest encapsulation,[1,2] stabilization of reactive species[3,4,5] and catalysis[6,7,8]).
The first examples of molecular capsules emerged from the pioneering work of Prof. Donald Cram on covalent molecular containers (named *carcerands* and *hemicarcerands*). These containers were synthesized by covalently linking two resorcin[4]arene units (Figure 2.1 a).[9] The advantage of this family of containers resided in their kinetic stability owing to the exclusive involvement of covalent bonds. However, their low synthetic yields and the difficulties encountered for the reversible encapsulation of specific guests, forced the researchers to develop and study self-assembly processes for the construction of more versatile molecular containers. For example, different reversible interactions like hydrogen bonding,[10,11] halogen bonding[12],chalcogen bonding,[13] and metal mediated coordination[14,15] were used. Likewise, dynamic covalent approaches were also investigated.[16,17,18]

As commented in Chapter 1, dynamic covalent chemistry can provide the thermodynamically most stable product, in a one-step reaction, via "proof-reading" and "error checking" mechanisms, thanks to the reversibility of the driving reactions.[19]
C=N imine bonds, formed through the condensation reaction of an aldehyde with an amine, are one of the oldest and most used motifs in dynamic covalent chemistry for the self-assembly of molecular capsules.[20,21,22]
Several examples of imine bonded capsules based on different building blocks have been reported in literature showing different geometries. For example, resorcin[4]arene have been widely used.[23 ,24,25,26]
Recently, fully π-conjugated truncated tetrahedral[27] having eight-membered [1,5] diazocine rings (Figure 2.1 b) and "cucurbitimine"[28] molecular containers were described. Most of these molecular containers showed recognition properties towards neutral molecules, which were driven by π-π interactions, CH-π interactions and the hydrophobic effect (mainly in water).

Notably, encapsulation studies of alkylammonium cations with a series of different size truncated tetrahedral nona-imine cages showed binding selectivity.[29] The observed binding selectivity was related to the size of the cage portals and the dimensions of the cation.

The “kinetic selectivity” displayed by the cages seems to be related to the preferred mechanism of guest encapsulation. The uptake of the cations is most likely favored by a squeezing mechanism rather than by a gate-opening mechanism. These findings are also in agreement with the previous observation assigning a kinetically controlled nature to the capsules.

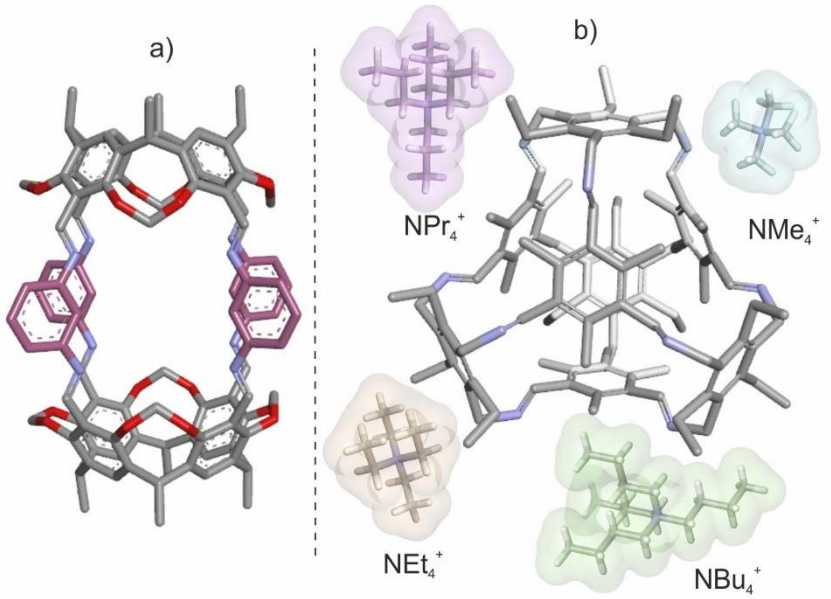

Figure 2.1. (a) Energy minimized structure (MM3) of an octa-imine capsule based on two tetra-carbaldehyde resorcin[4]arene units (the benzyl groups at the lower rims of the resorcinarene are omitted for clarity); (b) X-ray structure of a truncated tetrahedral nona-imine cage (adapted from ref. 29) and stick representation of the ammonium salts used as guests.

In the same vein and as anticipated in Chapter 1, carbonate anion was selectively encapsulated in the hexapodal poly-imine-amide cage described by Badjic and co-workers.[30] The observed kinetic selectivity for carbonate, resulted from the cage possessing narrow portals that “squeeze”[31] the guest upon its entrance and release. The resulting carbonate encapsulation complex was stable for hours even in the presence of competing anions forming more thermodynamically stable complexes (*i.e.* sulfate).

The lack of polar functional groups in the cavity of the molecular containers often restricts their inclusion properties to non-polar guests being size and shape complementary. Thus, the inclusion of polar guests is not favorable with a consequent reduction in selectivity and binding affinity.[32]

The incorporation of pyrrole units in the container's molecular scaffolds is a useful strategy to endow their cavities with polar functions. This provides a closer mimicking of the binding properties exhibited by the biological receptors.[33,34]

The polar interior of aryl-extended calix[4]pyrroles[35] in the cone-conformation and its bowl-like aromatic cavity makes them versatile candidates for the construction not only of polar supramolecular containers but also of the covalently bonded counterparts.

The template-directed synthesis of a chiral poly-imine capsule was successfully achieved by combining two units of an aryl-extended tetra-aldehydecalix[4]pyrrole with four diamine linkers and a suitable bis-*N*-oxide as a template.[36] The template effect exerted by *N*-oxides of different sizes and geometries was investigated. The obtained results revealed the importance of using a suitable bis-*N*-oxide template for the efficient assembly of the poly-imine bonded capsules.

The used template *N*-oxide established strong intermolecular interactions with the calix[4]pyrrole units and formed a thermodynamically and kinetically highly stable complex with the cage.

The strong interaction of the template with the cage hampered the release of the template after the formation of the capsule and we could not perform additional studies on its recognition properties.

The aim of this work is to extend the use of dynamic covalent chemistry based on imine-bonds to the self-assembly of cage-like aggregates composed of two different "four wall" calix[4]pyrrole units.[36] In this chapter we will describe the template-assisted self-assembly of [1+1] tetra-imine cages based on calix[4]pyrrole units. In addition, we will disclose our results on the self-assembly of the cages in the absence of templating guests.

We will report the binding properties of the calix[4]pyrrole precursor units and the imine bonded cages towards planar monotopic and ditopic pyridyl-*N*-oxides, as well as with the sterically more demanding *N*-oxide of quinuclidine. We will focus on determining the kinetics of the encapsulation processes of the guests in $CDCl_3$ and $CDCl_3$:CD_3CN mixtures. Based on the obtained results, we derived that the encapsulation/release of the guests is more likely to occur through a "French doors" mechanism than a gate-opening alternative implying the partial cleavage of some imine bonds.

2.2 Results and discussion

2.2.1 Design and synthesis

First, we investigated the synthesis of tetra-imine bonded cages **6**, **7** and **8** (Scheme 2.1), based on two different calix[4]pyrroles scaffolds: a tetra-aldehyde calix[4]pyrrole (**1** or **2**) and a tetra-amino calix[4]pyrrole (**3** or **4**). Initially, we used 4',4'-bipyridyl *N,N'*dioxide **5** as template. In doing so, we investigated the template-assisted assembly of calix[4]pyrrole based cages. On the other hand, we studied the use of $CDCl_3$, CD_2Cl_2 and a $CDCl_3$:CD_3CN 9:1 solvent mixture for the self-assembly of analogous solvent template cages (Scheme 2.1).

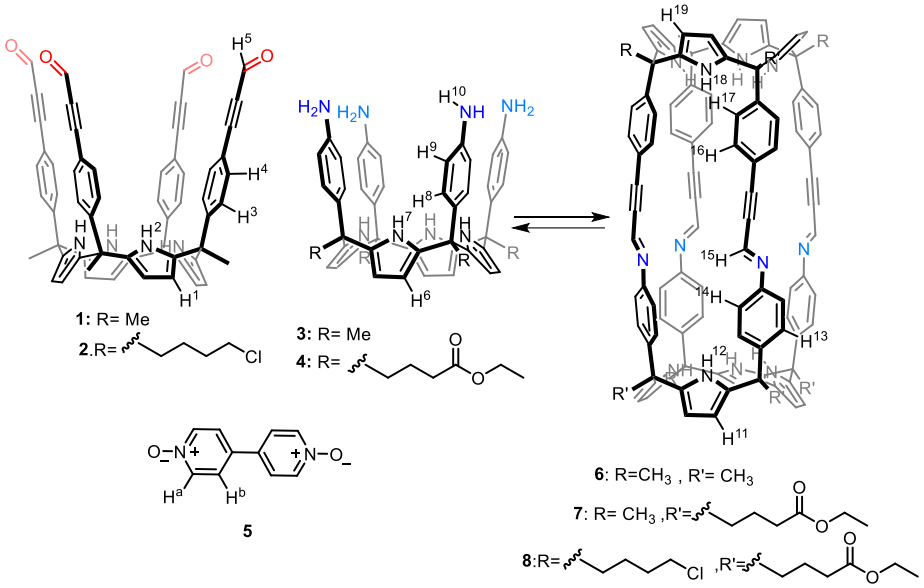

Scheme 2.1. General synthetic scheme of calix[4]pyrrole based tetra-imine cages **6**, **7** and **8** with the corresponding protons assignment. The molecular structure of bis-pyridine *N*-oxide **5**, used as template in the template-directed approach, is also shown with the corresponding protons assignment.

Tetra-aldehyde calix[4]pyrroles **1**[36] and **2** were synthesized from the corresponding tetra-iodo calix[4]pyrrole precursors (see experimental section). In turn, the tetra-iodo calix[4]pyrrole precursors were obtained from the acid-catalyzed condensation reactions of pyrrole and the *p*-iodoacetophenone derivatives using slightly modified synthetic procedures.[37,38] The four-fold Sonogashira reaction[39] of the tetra-iodo calix[4]pyrroles with 2-propargylaldehyde diethyl acetal in a 1:1 mixture of DIPA/THF yielded the acetal protected calix[4]pyrrole building blocks. Deprotection of the aldehyde groups with trifluoroacetic acid (TFA), followed by trituration of the

reaction crudes with CH_2Cl_2/MeOH mixtures, afforded the tetra-aldehyde calix[4]pyrroles **1** and **2** as white powders in 80 and 53% yield respectively.

The tetra-amino calix[4]pyrrole **3** and the lipophilic tetra-amino tetra-ester analogue **4** were also synthesized following previously reported procedures.[40,41] First, the acid-catalysed condensation of pyrrole with the corresponding *p*-nitroacetophenone allowed the isolation of the tetra-α isomers of the tetra-nitro-calix[4]pyrrole derivatives as yellow solids in 9-10% yields.
The purification procedure for tetra-nitro calix[4]pyrrole precursor of **4** was slightly modified. In short, the reaction crude was filtered over a short silica path using as eluent a mixture DCM-1% MTBE in DCM. The solvent was removed and the resulting solid was dissolved again in 0.5 ml of MTBE. The addition of MeOH (1.5 mL) produced the precipitation of the pure product. Second, the catalytic hydrogenation of the tetra-nitro calix[4]pyrroles with Pd/C in ethyl acetate, provided the corresponding tetra-amino calix[4]pyrroles **3** and **4** as beige solids.

With the aim of obtaining water-soluble imine cages, we also attempted the synthesis of water-soluble calix[4]pyrroles.
Aryl-extended calix[4]pyrroles possessing terminal alkylchloride groups at their *meso*-alkyl substituents can be easily derivatized into their water soluble counterparts.
Specifically, the nucleophilic substitution of the terminal chloride groups of the *meso*-alkyl chains of tetra-aldehyde calix[4]pyrrole **2** with pyridine affords four charged pyridinium groups that may impart water solubility to the derivative[38] and eventually to the imine cages assembled from it.[42,43,44]
We studied the transformation of the *meso*-alkyl chloride substituents into the pyridinium ions. We heated the protected tetra-aldehyde calix[4]pyrrole with freshly distilled pyridine at 95-100 °C. We isolated the tetra-pyridinium derivative in a reduced yield and purity. Notably, the compounds resulted to be soluble in neutral water at mM concentration. Nevertheless, the reaction conditions need to be optimized.

2.2.1.1 *Study of the template-assisted self-assembly of tetra-imine cage **6**: **5**⊂**6** cage complex.*

Based on our previous results on the self-assembly of dynamically covalent octa-imine capsules containing calix[4]pyrrole scaffolds, we assumed that the encapsulation of a ditopic template was essential for the emergence of the tetra-imine aggregate. Firstly, we studied the self-assembly of 1 equiv. of tetra-aldehyde

1 with 1 equiv. of tetra-amino tetra-methyl **3** in the presence of 1 equiv. of a bis-pyridyl-bis-*N*,*N*'-oxide **5** in chloroform solution. Simple molecular modelling (MM3) studies showed a good size, shape and function complementarity between the bis-*N*-oxide **5** and the cavity of the tetra-imine cages **6**, **7** and **8** (Figure 2.2).

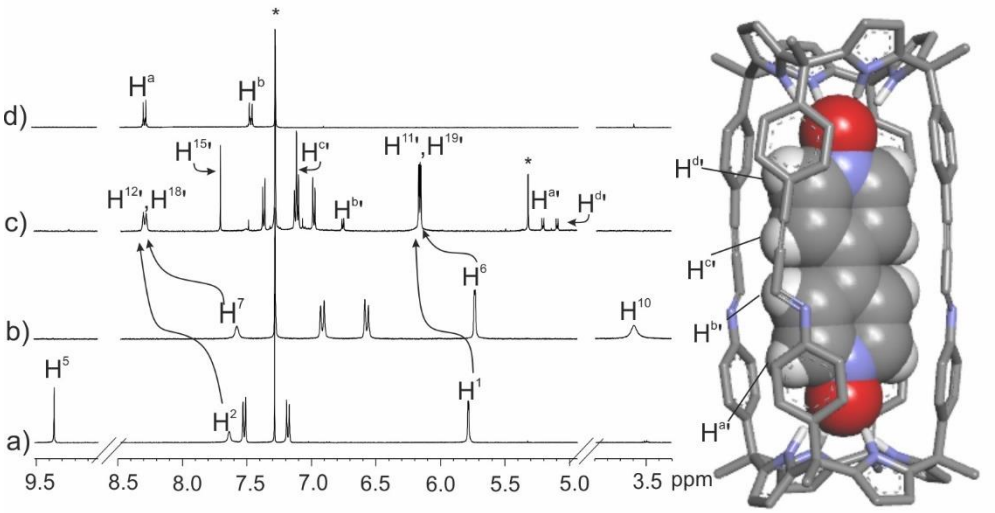

Figure 2.2. (Left) Selected regions of the ^{1}H NMR spectra (400 MHz, at 298 K, $CDCl_3$) of (a) tetra-aldehyde calix[4]pyrrole **1**, (b) tetra-amino calix[4]pyrrole **3**, (c) equimolar mixture of **1**, **5** and **3** after reaction at r.t for 24h to give imine capsular complex **5⊂6**, d) bis-pyridyl *N*-oxide **5**. See Scheme 2.1 for protons assignment. Primed letters indicate the signals of the complex. (*) Indicates residual solvents. (Right) Energy minimized (MM3) structure of imine capsular complex **5⊂6**.

The template-directed (bis-*N*-oxide **5**) condensation reaction of tetra-aldehyde **1** and tetra-amine **3** was monitored using ^{1}H NMR spectroscopy. We used 1,3,5-trimethoxy-benzene as internal standard (i.s.) to quantify the yield of the reaction.
The ^{1}H NMR spectrum of the suspension obtained by adding equimolar amounts of solids **1**, **3** and template **5** to $CDCl_3$, showed broad and ill-defined proton signals. Notably, after 24 hours a clear yellow solution was obtained. The ^{1}H NMR spectrum of the solution showed well-defined and sharp proton signals. We observed the appearance of sharp singlet resonating at δ = 7.7 ppm that was assigned to the imine protons (Figure 2.2).
We also observed the disappearance of the singlet attributed to the aldehyde proton of **1**, H^5, resonating at δ = 9.4 ppm.
The remaining proton signals are in agreement with C_{4V} symmetry and diagnostic of the assembly of the cage complex **5⊂6** containing two different calix[4]pyrrole hemispheres. The β-pyrrole protons appeared as two overlapping doublets and the aromatic protons of the *meso*-phenyl groups as two sets of separate doublets.

In addition, the pyrrole NHs, $H^{12'}$ and $H^{18'}$, moved downfield ($\Delta\delta$= 0.46) suggesting their involvement in hydrogen bonding interactions with the *N*-oxide knobs of the template **5**. The downfield shifts experienced by the pyrrole NHs were smaller than the ones observed for typical inclusion complexes of the pyridyl-*N*-oxides with calix[4]pyrrole receptors.[45] This observation suggested that the formed hydrogen bonds were probably weaker and that most likely the template **5** was too short for establishing an ideal ditopic interaction with the two calix[4]pyrrole binding sites of the cage. We also observed four upfield shifted doublets for the aromatic protons of the included guest ($H^{a'}$, $H^{b'}$, $H^{c'}$, $H^{d'}$). This located the template **5** included in the polar cavity of the cage and experiencing the shielding effect of its π-systems. Template **5** also establishes CH-π and π-π interactions with the aromatic walls of the cage. Using integral values of selected proton signals of the cage and those of an i.s. we determined that the **5⊂6** cage complex was formed in a 50% yield after 24 h at room temperature.

The cage complex **5⊂6** was characterized by a complete set of high-resolution spectra (1D and 2D NMR experiments and by MS spectrometry). The DOSY experiment[46] of the cage complex in $CDCl_3$ solution assigned identical diffusion constant values of *ca.* 4.11× 10^{-10} m^2s^{-1} for the decays of the proton signals of the cage **6** and the template **5**. This result indicated that the two species were involved in the same supramolecular complex. The diffusion constant determined for monomer **1** in $CDCl_3$ solution was 5.94× 10^{-10} m^2s^{-1}. The measured difference in diffusion constant values supported the larger dimensions of the inclusion cage complex **5⊂6**.

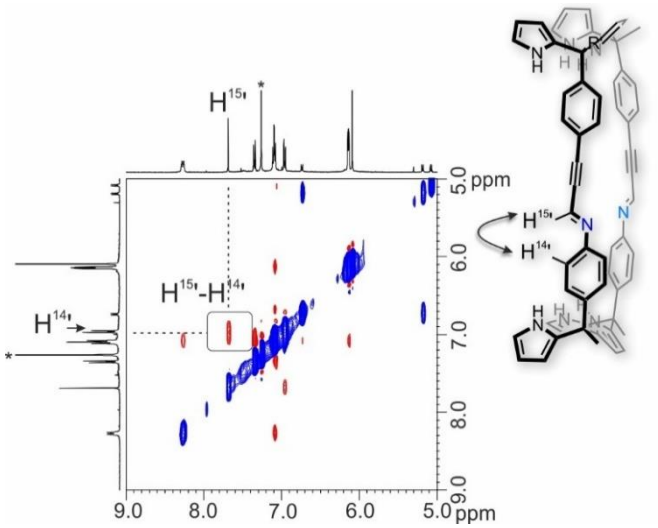

Figure 2.3. 2D ROESY NMR (400 MHz, at 298 K, $CDCl_3$) of a solution containing imine cage complex **5⊂6**. See Scheme 2.1 for protons assignment. (*) Indicates residual solvents.

Remarkably, a 2D-ROESY experiment of the **5⊂6** cage complex showed the existence of nOe cross peaks between the imine proton $H^{15'}$ and the aromatic protons of the *meso*-phenyl $H^{14'}$ that were in agreement with the assembly of the cage (Figure 2.3).

The synthesis of the **5⊂6** cage complex was scaled-up.
All our attempts to reduce imine bonds of the **5⊂6** cage complex to amine groups, using $NaBH_4$ as reducing agent, failed. We screened different reaction conditions (r.t and 313 K). We used MeOH to solubilize the $NaBH_4$. We also employed mixtures of $CHCl_3$/MeOH solubilizing the cage complex **5⊂6** and $NaBH_4$. We investigated the use of different ratios of capsule-reducing agent. However, the analyses of the reaction crudes using MS and ^1H NMR spectroscopy revealed the exclusive presence of unreacted cage complex **5⊂6**. Most likely, the conjugation of triple bond with the imine bond prevented its reduction.[47]

2.2.1.2 *Study of the template-assisted self-assembly of tetra-imine cages **7** and **8**: **5⊂7** and **5⊂8** cage complexes*

In order to self-assemble cage complexes structurally analogous to **5⊂6** but having an increased solubility we used the more lipophilic tetra-ester tetra-amine building block calix[4]pyrrole **4**.

In contrast to the long reaction time (*i.e*. 24 h) required for the self-assembly of the octa-methyl analogue **5⊂6** complex, the ^1H NMR spectrum of an equimolar mixture of tetra-amine calix[4]pyrroles **1**, **4** and template **5** (2 mM) revealed the exclusive observation of the proton signals diagnostic of the **5⊂7** cage complex after 4h (Figure 2.4). It is worthy to note that although the ^1H NMR spectrum displays a single set of proton signals, we cannot claim that the assembly of the **5⊂7** cage complex is quantitative. Using integral values of selected proton signals of the cage ($H^{14'}$ and $H^{16'}$) and those of an i.s. we determined that the **5⊂7** cage complex was formed in a 65% yield after 12 h at room temperature. Most likely, the remaining 35% of the molecular components of the cage are involved in the formation of large polymeric aggregates that are not visible in the ^1H NMR spectrum of the mixture (*i.e*. signals broad beyond detection).

The cage complex **5⊂7** was characterized by a complete set of high-resolution 1D and 2D NMR experiments. The ROESY experiment of the **5⊂7** cage complex revealed the existence of nOe cross peaks between the imine proton $H^{15'}$ and the aromatic protons $H^{14'}$ of the amine hemisphere, as observed for the **5⊂6** cage complex analogue (Figure 2.38).

Not surprisingly, the DOSY NMR experiment of the cage complex **5⊂7** in $CDCl_3$ solution assigned the same diffusion constant to the proton signals of the cage and the included template. The decay of the protons with respect to the gradient strength showed a good fit to the corresponding mono-exponential Stejskal–Tanner function[48] (Figure 2.39), returning a diffusion constant value of D= 3.58×10^{-10} m^2s^{-1}, which is in good agreement with the one determined for the **5⊂6** counterpart (*vide supra*).

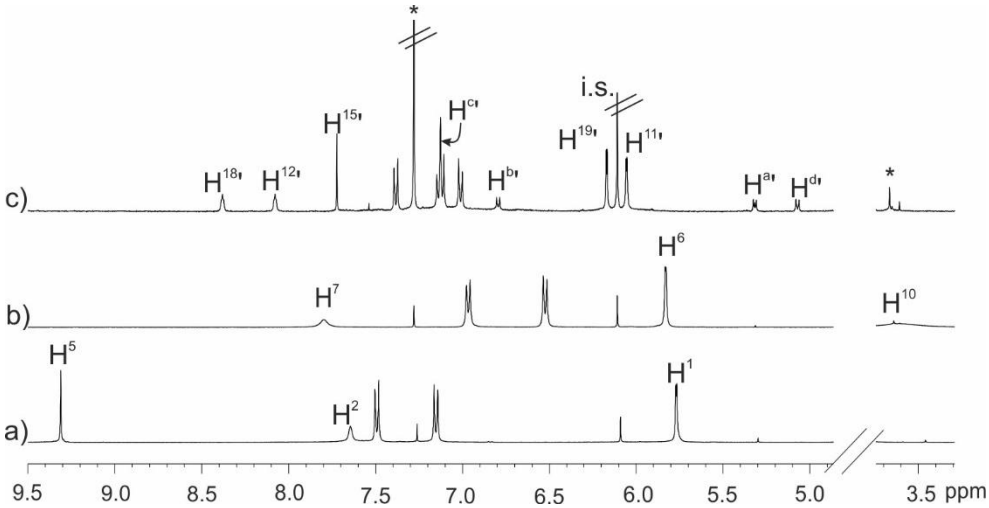

Figure 2.4. Selected regions of the ^{1}H NMR spectra (400 MHz, at 298 K, $CDCl_3$) of (a) tetra-aldehyde calix[4]pyrrole **1**, (b) tetra-amino calix[4]pyrrole **4**, (c) equimolar mixture of **1**, **4** and **5** after reaction at r.t for 4h to give imine capsular complex **5⊂7**. See Scheme 2.1 for protons assignment. Primed letters indicate the signals of the complex. (*) Indicates residual solvents.

Similarly, an equimolar (2 mM) mixture of **2**, **4** and **5** in $CDCl_3$ produced a clear solution. The analysis of the mixture using ^{1}H NMR spectroscopy revealed a single set of sharp and well-defined proton signals that were diagnostic of the self-assembly of the **5⊂8** cage complex (Figure 2.5).

The **5⊂8** cage complex was characterized by a set of high-resolution 1D and 2D NMR spectra.

After 24h, the extent of the assembly of the tetra-imine cage complex **5⊂8** was calculated to be about 55%. To this end, we used the integral values of selected proton signals of the cage complex and those of 1,3,5-trimethoxybenzene used as i.s. During the studies of the self-assembly processes of the cage complexes described above, we learned that the purity of the calix[4]pyrrole components was key in obtaining high yields.

In line to what was discussed in Chapter 1, most likely, the bis-pyridyl *N*-oxide **5** initially plays the role of a kinetic template agent for the assembly of the imine cages. Bis-*N*-oxide **5** binds two calix[4]pyrrole units and organizes their reacting

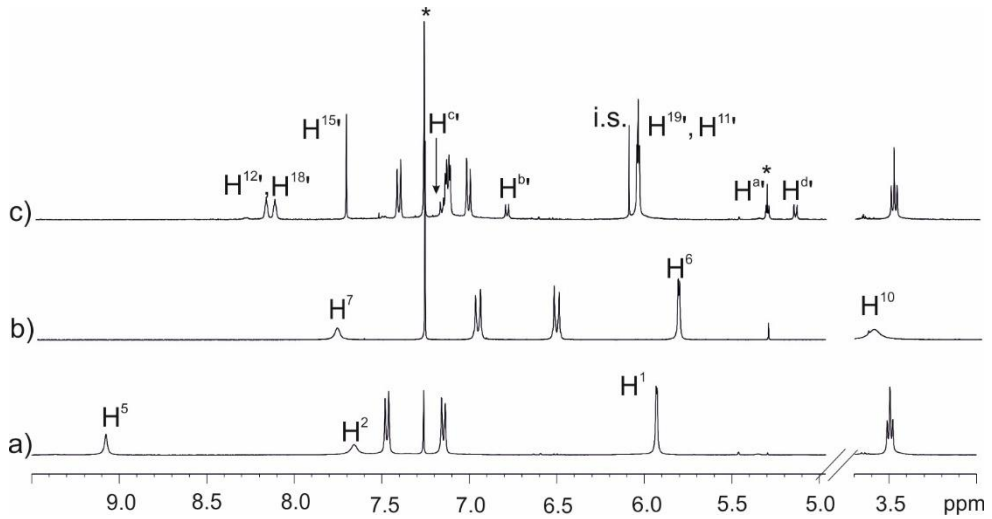

Figure 2.5. Selected regions of the ^{1}H NMR spectra (400 MHz, at 298 K, $CDCl_3$) of (a) tetra-aldehyde calix[4]pyrrole **2**, (b) tetra-amino calix[4]pyrrole **4**, (c) equimolar mixture of **2**,**4** and **5** after reaction at r.t for 12h to give imine capsular complex **5⊂8**. See Scheme 2.1 for proton assignment. Primed letters indicate the signals of the complex. (*) Indicates residual solvents.

groups (amine and aldehyde) in proximity allowing the reaction to occur (Schiff base).[16,22] However, the *N*-oxide **5** also acts as a thermodynamic template favoring the formation of the thermodynamic more stable cage resulting from the reaction.

2.2.1.3 Solvent-assisted self-assembly of tetra-imine cages **7** and **8**

2.2.1.3.1 Self-Assembly in a chloroform: acetonitrile 9:1 mixture

We explored the possibility of self-assembling the tetra-imine cages in the absence of a specific template agent. We attempted the self-assembly of the cage in a chloroform:acetonitrile mixture of solvents. Previously, we described that polar non-protic solvents such as acetonitrile were included in the cavity of α,α,α,α-tetra-aryl extended calix[4]pyrroles. The nitrogen atom of the bound acetonitrile established four convergent hydrogen-bonds with the pyrrole NHs locking the receptor in the cone conformation.[35,49] We hypothesized that this preorganization of the calix[4]pyrrole units in cone conformation will facilitate the self-assembly of the tetra-imine cage.

Firstly, we attempted the self-assembly of the tetra-imine cage **6** deriving from the calix[4]pyrrole units **1** and **3** in a 9:1 mixture of $CDCl_3$:CD_3CN. The equimolar mixture of the two molecular components led to the formation of a suspension. Most likely, this is due to the low solubility of the tetra-amine calix[4]pyrrole **3**, as well as its Schiff based derived products (oligomers and cage) in the mixture of solvents.

Swapping the tetra-amine calix[4]pyrrole **3** with its more lipophilic counterpart **4**, produced a solution for the 2 mM equimolar mixture of calix[4]pyrroles **1** and **4** in 9:1 $CDCl_3$:CD_3CN mixture of solvents. The ^{1}H NMR spectrum of the solution acquired 20 min after mixing the two calix[4]pyrrole components displayed sharp and well-defined proton signals (Figure 2.7 a) diagnostic of the self-assembly of the tetra-imine cage **7**. The observation of a sharp singlet resonating at δ= 7.9 ppm was indicative of the formation of the imine bonds.

The yield of the self-assembly of the tetra-imine **7** was calculated to be close to 65% after 24h of reaction. To this end, we used the integral value of the imine proton signal and those of the proton signals of 1,3,5-trimethoxybenzene used as i.s. This result indicated that the yield of the self-assembly process of cage **7** in the 9:1 $CDCl_3$:CD_3CN mixture of solvents was very similar to that obtained for the template **5⊂7** cage inclusion complex.

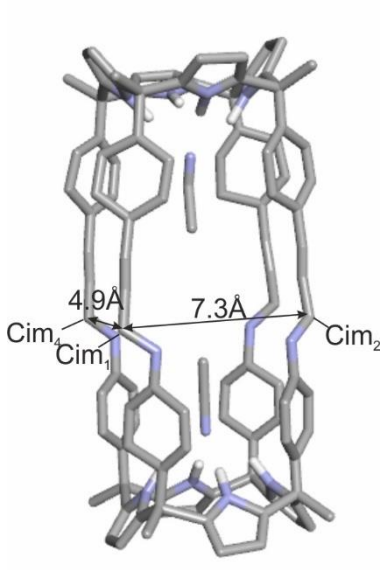

Figure 2.6. Preliminary X-ray structure of acetonitrile solvated cage **7**. Alkyl chains with terminal ester groups were truncated to methyl groups for clarity. Non-polar protons were omitted for clarity.

Single crystals suitable for X-ray diffraction grew from the slow diffusion of *p*-xylene into the $CDCl_3$:CD_3CN 9:1 mixture of solvents containing the tetra-imine cage **7**.

The analysis of the diffraction data showed the solid-state structure of tetra-imine cage **7** with two acetonitrile molecules included in its polar cavity (Figure 2.6). The two acetonitrile molecules established four convergent hydrogen bonds with the pyrrole NHs of the two non-equivalent cage hemispheres in cone conformation. All imine bonds featured *E*-configuration and did not orient in a unidirectional manner. Instead, the convergence of the imine CHs in two pairs defined two different sized portals for the solid-state structure of cage **7** (Portal1: $d(C_{im1}\cdots C_{im2})$ = 7.3 Å; Portal2: $d(C_{im1}\cdots C_{im4})$ = 4.9 Å).
Notably, the CH imine protons are outwardly directed with respect to the cage's cavity.

Similarly, the equimolar mixture of the lipophilic calix[4]pyrroles, tetra-aldehyde **2** ($R=(CH_2)_4Cl$) and tetra-amine **4** ($R=(CH_2)_3CO_2Et$), in a 9:1 mixture of $CDCl_3$:CD_3CN at 2 mM concentration produced a clear solution. The ^1H NMR spectrum of the obtained solution displayed the ears-signals of the self-assembly of cage **8** (Figure 2.60).

The quick self-assembly of cages **7** and **8** and the lack of detection of intermediate aggregates might suggest that they are kinetic products. However, the fact that the cages are stable in solution for long periods of time (weeks) indicated their thermodynamic nature.[50]

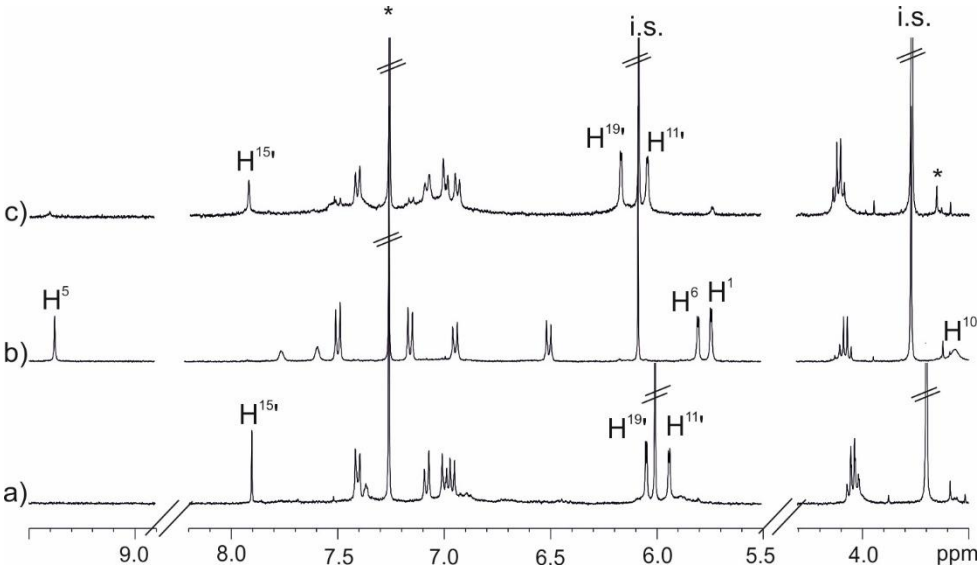

Figure 2.7. Selected regions of the ^1H NMR spectra (400 MHz, at 298 K) of an equimolar mixture of tetra-aldehyde calix[4]pyrrole **1** and tetra-amino calix[4]pyrrole **4**: (a) in $CDCl_3$:CD_3CN 9:1 solution; (b) in $CDCl_3$ solution after mixing the components, and (c) in $CDCl_3$ solution after heating the previous solution at 308 K for 48 h. See Scheme 2.1 for protons assignment. (*) Indicates residual solvents.

Interestingly, cage **7** self-assembled in $CDCl_3$:CD_3CN 9:1 mixture showed good structural stability upon addition of 1-10% of MeOH. Even after 7 days of the addition of 1% of MeOH, we did not observe new proton signals in the ^{1}H NMR spectrum of the solution, nor the diminution of the intensity of the proton signals of cage **7** (Figure 2.49). We were expecting that the addition of MeOH had a deleterious effect on the stability of the imine bonds. However, it has been demonstrated that MeOH prevented the insertion of new diamines into poly-imine capsular assemblies.[51]

These findings confirmed that dynamic covalent bonds, even being reversible and less stable than covalent bonds, conferred a rather relevant structural stability to poly-imine assemblies owing to the multivalent effect.[52]

2.2.1.3.2 Self-Assembly in pure chlorinated solvents

The good results obtained in the self-assembly of the tetra-imine cages in a 9:1 $CDCl_3$:CD_3CN mixture, encouraged us to explore the cage self-assembly exclusively in pure chlorinated solvents: chloroform and dichloromethane.

The ^{1}H NMR spectrum of a freshly prepared equimolar mixture of tetra-aldehyde **1** (R= CH_3) and tetra-amine **4** (R=$(CH_2)_3CO_2Et$), either in $CDCl_3$ or CD_2Cl_2 solution at 2 mM concentration, showed exclusively the proton signals of the two building blocks (**1** and **4**) (Figure 2.7 b). The ^{1}H NMR spectrum of the standing mixture at r.t. for several days showed the formation of imine cage aggregates in equilibrium with the starting materials. However, after 4 days of reaction, the rate of reaction significantly slowed down. In contrast, heating the $CDCl_3$ and CD_2Cl_2 solutions of the equimolar mixtures at 308 K and 303 K respectively, produced the observation of the proton signals assigned to the tetra-imine cage as the main species in solution (*e.g.* imine protons) (Figure 2.7 c).

After heating for 48 and 72 hours, the $CDCl_3$ and CD_2Cl_2 solutions of the equimolar mixtures of **1** and **4**, respectively, we quantified that the tetra-imine cage **7** was assembled in an extent close to 50% in both cases (Figure 2.50, Figure 2.56). Evidence of the assembly of cage **7** in pure chlorinated solvents was also derived from ^{1}H DOSY NMR experiments. We calculated a diffusion constant value of 3.72×10^{-10} m^2s^{-1} for proton signals of cage **7** assembled in pure $CDCl_3$ solution. This value is very similar to the one determined in the same solvent for the **5⊂7** cage inclusion complex (where **5** is 4,4'-bipyridine-*N,N'*-dioxide).

It is worthy to note that the ^{1}H NMR spectrum of cage **7** in pure $CDCl_3$ showed broader proton signals than those of the same assembly in the 1:9 CD_3CN:$CDCl_3$

solvents mixture and the corresponding cage inclusion complex **5⊂7**. This observation together with the reduction in the calculated yield of the self-assembly process, suggested that in pure $CDCl_3$ solution, cage **7** was thermodynamically less stable and possibly conformationally more flexible than the obtained cage inclusion complexes (**CD_3CN)$_2$⊂7** and **5⊂7**. In addition, the reduction of the thermodynamic stability of **7** is accompanied by the increase of the amount of polymeric aggregates formed in solution. This finding is in good agreement with the thermodynamic nature of the tetra-imine cage **7**.

Molecular modelling studies of the tetra-imine cage **7** showed a nice fit of two chlorinated solvent molecules ($CHCl_3$ or CH_2Cl_2, Figure 2.68) in its cavity providing sensible PC values (about 50%) for the resulting three-particles cage inclusion complexes. Aiming at providing experimental evidence for the inclusion of the solvent molecules, we performed 1D GOESY ^{1}H NMR experiments in $CHCl_3$ solution. Unfortunately, at room temperature, the selective irradiation of the $CHCl_3$ signals did not provide any indication of the putative included solvent molecules. If these latter molecules were involved in a chemical exchange process with those of the bulk solvent, showing slow dynamics on the chemical shift time scale, we should observe peaks due to magnetization transfer in the 1D GOESY spectrum. In addition, we did not detect GOESY peaks in experiments carried at lower (253 K) and higher temperatures (323 K). Most likely, the chemical exchange between free and bound solvent molecules is fast on the chemical shift time scale in the range of studied temperatures.

2.2.2 Binding properties of tetra-imine cage **7** and its calix[4]pyrrole molecular precursors towards *N*-oxides

The assembly of cage **7** in the absence of templates that strongly bind the cavity opens the possibility to study its binding properties with a series of polar guests **5**, **9**, **10** and **11** (Figure 2.8). Considering that the non-cage aggregates are also formed in solution and that they can also bind *N*-oxide guests, we performed our binding experiments using an excess of guest with respect to the calculated amount of cage assembled (calculated yield). We monitored the kinetics of the uptake of guests **5** and **9** by cage **7** using ^{1}H NMR spectroscopy in $CDCl_3$: CD_3CN 9:1 mixture.
We also became interested in studying the kinetics of the inclusion and dissociation processes of these *N*-oxide guests. According to the results obtained in previous studies of guest exchange mechanisms and kinetics in mono-nuclear Pd/Pt cages,

we expected to measure dissimilar kinetics for the inclusion and exchange processes of cage **7** in response to the size and shape of the involved guests.[53]

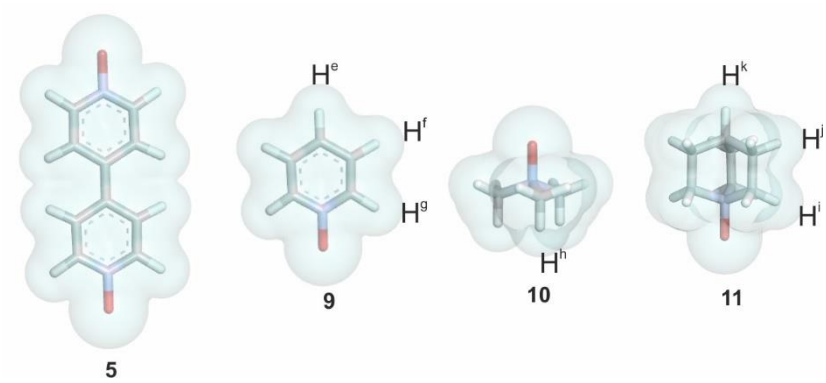

Figure 2.8. Ditopic (**5**) and monotopic (**9**, **10** and **11**) *N*-oxide guests used in the study of the binding properties of calix[4]pyrroles **1**, **4** and the self-assembled cage **7**.

Before characterizing kinetically and thermodynamically the inclusion complexes of cage **7**, we decided to investigate the binding properties of its molecular components: the tetra-aldehyde calix[4]pyrrole **1** and tetra-amino calix[4]pyrrole **4**. For the sake of brevity, below we only describe in detail the results of the binding studies of the ditopic 4',4'-bipyridyl *N,N'*-dioxide **5** with the two calix[4]pyrrole scaffolds. The results of the binding studies performed with the other *N*-oxide guests are included in the experimental section of this chapter (pyridine *N*-oxide **9**, trimethylamine *N*-oxide **10**, quinuclidine *N*-oxide **11**).

2.2.2.1 *^{1}H NMR titration of the tetra-aldehyde calix[4]pyrrole **1** with 4',4'-bipyridyl N,N'-dioxide **5***

The ^{1}H NMR titration of the tetra-aldehyde **1** with incremental amounts of bis-*N*-oxide **5** (Figure 2.9) showed significant chemical shift changes in the proton signals of the calix[4]pyrrole receptor. This observation indicated that the exchange between the bound and free receptor was fast on the NMR chemical shift timescale. The downfield shifts experienced by the pyrrole NHs of **1** ($H^{1'}$) upon addition of incremental amounts of **5**, suggested the formation of hydrogen bonding interactions between the binding partners. The chemical shift changes suffered by the aromatic and, especially, by the β-pyrrole proton signals of **1** were indicative of a conformation change: from 1,3 alternate in the free state to cone in the complex. In the presence of 0.6 equiv. of **5**, the signals of the protons of the bis-*N*-oxide broadened beyond detection (Figure 2.9 c).

The ^{1}H NMR spectrum of the mixture at 213 K previously reported by the group[36] showed two separate sets of proton signals for the calix[4]pyrrole **1**. One set of signals corresponded to free **1**, the other set of signals was assigned to the 1:1 **5⊂1** complex. The absence of proton signals that could be assigned to a putative 2:1 complex suggested that the length of the *N*-oxide **5** was too short to bind simultaneously two copies of **1** without producing significant steric clashes.

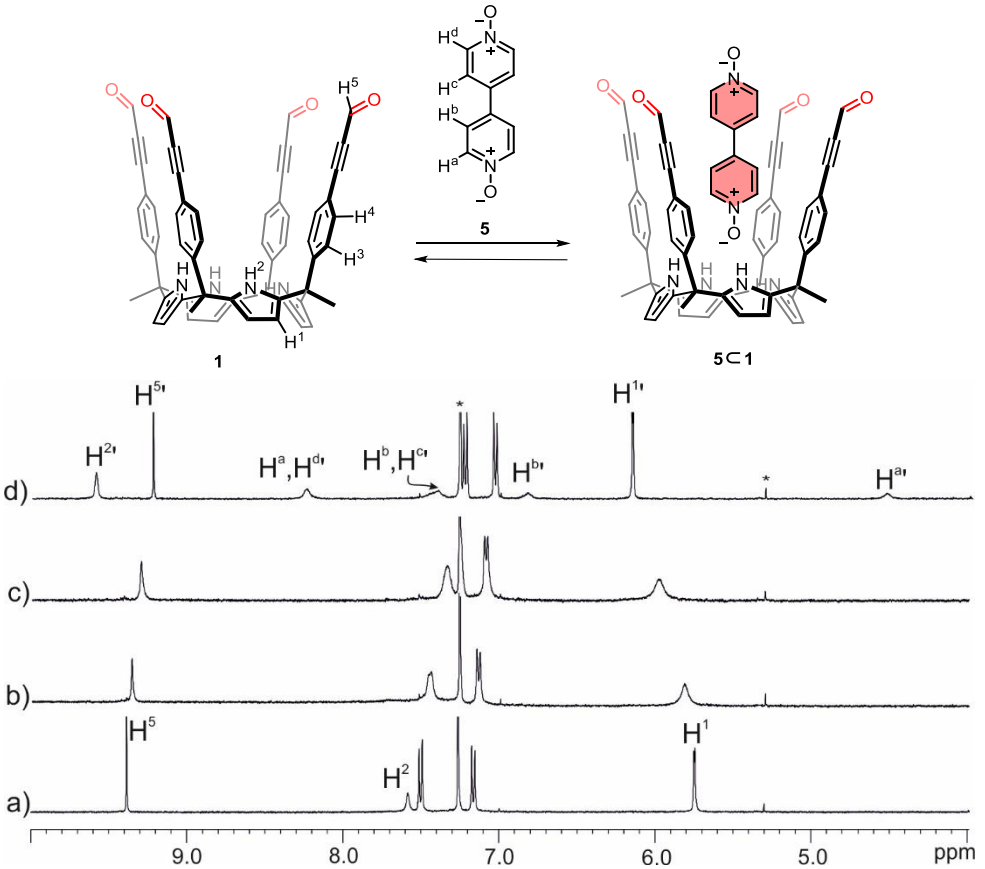

Figure 2.9. Selected region of ^{1}H NMR spectra (400 MHz, at 298 K, $CDCl_3$) acquired during the titration of tetra-aldehyde calix[4]pyrrole [**1**]= 1 mM; a) free **1**; (b) **1** with *ca*. 0.2 equiv. of **5**, (c) **1** with ca. 0.6 equiv. of **5**, (d) **1** with ca. 1.1 equiv. of **5**. Primed letters indicate the proton signals in the bound host and guest. (*) Indicates residual solvents.

The addition of 1.1 equiv. of the *N*-oxide **5** to the solution of **1** provoked the sharpening of all the proton signals. We also observed four sets of separate signals for the aromatic protons of the bound *N*-oxide **5** ($H^{a\prime}$, $H^{b\prime}$, $H^{c\prime}$, $H^{d\prime}$). These observations indicated the quantitative formation of the 1:1 **5⊂1** complex. We

estimated that the association constant value of the **5⊂1** complex was larger than 10^4 M^{-1}.

2.2.2.2 *^{1}H NMR titration of tetra-amino calix[4]pyrrole **4** with 4',4'-bipyridyl N,N'-dioxide **5***

The initial phase of the ^{1}H NMR titration of the tetra-amine calix[4]pyrrole **4** with incremental amounts of the bis-*N*-oxide **5** (<0.5 equiv.) showed two set of signals for the protons of **4**. One set of signals corresponded to free **4**. The other set of signals was assigned to the receptor **4** in the 1:2 complex **5⊂(4)$_2$**. The observation of two separate sets of proton signals indicated that the exchange between free and bound **4** was slow on the proton chemical shift timescale. When *ca.* 0.5 equiv. of **5** were added to the solution of **4**, we only observed the proton signals assigned to the **5⊂(4)$_2$** complex (Figure 2.10 c). The pyrrole NHs protons ($H^{7''}$) in the **5⊂(4)$_2$** complex appeared downfield shifted in comparison to the free **4**. This observation indicated that hydrogen bonding interactions between **5** and **4** were present in the complex. The β-pyrrole protons also moved downfield (H^6, from 5.80 to 5.94 ppm) in response to the conformational change experienced by **4** in the **5⊂(4)$_2$** complex. The bound bis-*N*-oxide **5** in the **5⊂(4)$_2$** complex showed two signals for its aromatic protons ($H^{a''}$, $H^{b''}$) that were significantly upfield shifted. This is in agreement to the D_{4h} symmetry of the 1:2 complex and the shielding effect exerted by the aromatic walls of **4** to the included pyridyl-*N*-oxide knobs of **5**.

The integral values of proton signals of **4** and **5** are also in agreement with the formation of the 1:2 complex. The incremental addition of more than 0.5 equiv. of **5** produced the appearance of a new set of signals for the protons of **4** and **5**. The intensity of the new set of signals grew at the expenses of that of the 1:2 complex. We assigned the new set of signals to the formation of a 1:1 **5⊂4** inclusion complex (Figure 2.10 d, e).

Even in the presence of 2.5 equiv. of **5**, the **5⊂4** inclusion complex was not quantitatively formed (Figure 2.10 e). This finding indicated that the assembly of the **5⊂(4)$_2$** complex was cooperative.

The length of the bis-*N*-oxide **5**, is suitable for the simultaneous binding of two copies of calix[4]pyrrole **4**, as shown in energy minimization structure (Figure 2.11). Most likely, the amine groups are involved in direct or solvent mediated favorable

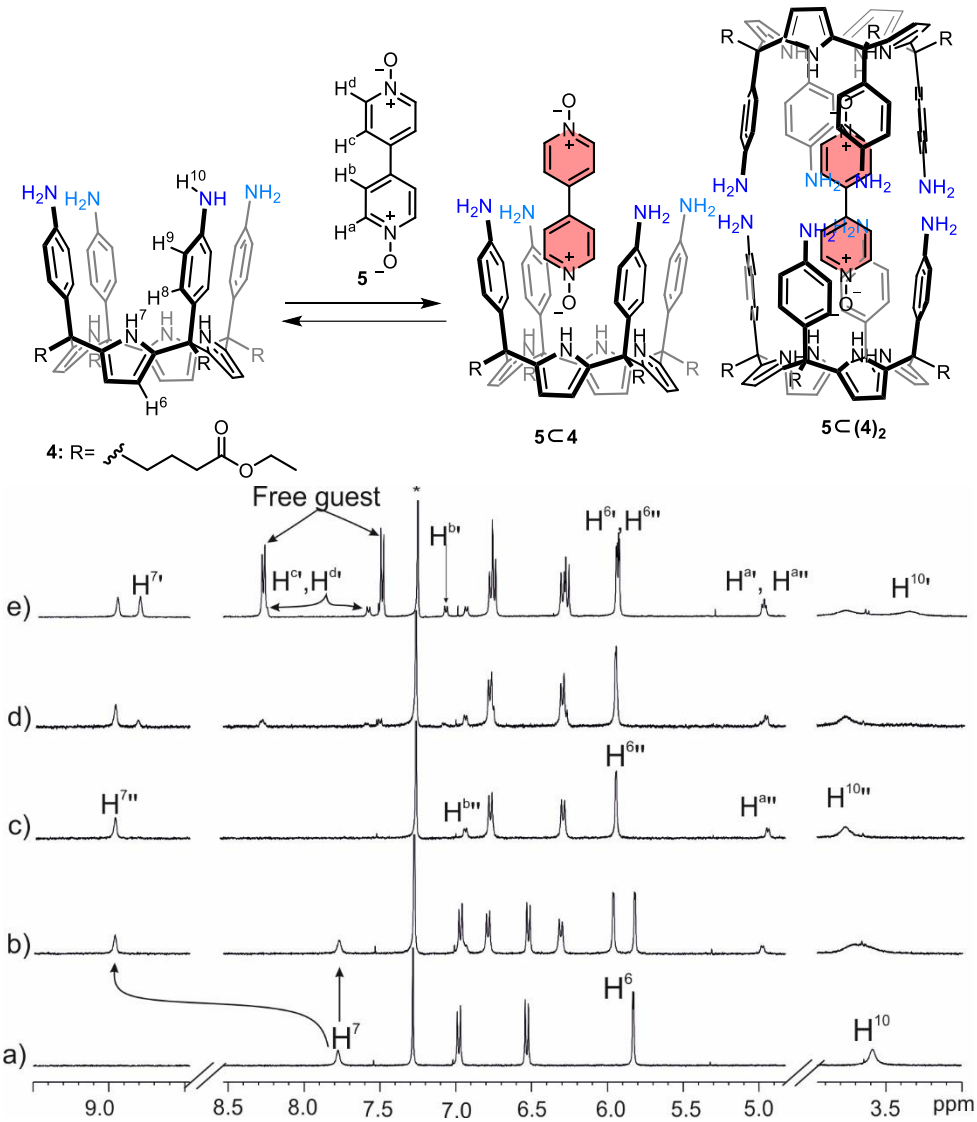

Figure 2.10. Selected region of ^{1}H NMR (400 MHz, at 298 K, $CDCl_3$) spectra acquired during the titration of tetra-amino calix[4]pyrrole [4]= 1.5 mM with **5**: (a) free**4**; (b) **4** in the presence of *ca.* 0.25 equiv. of **5**; (c) **4** in the presence of ca. 0.5 equiv. of **5**; (d) **4** in the presence of ca. 1 equiv. of **5**, (e) **4** in the presence of ca. 2.5 equiv. of **5**. Primed letters indicate the proton signals of the host and guest in the 1:1 complex; double primed letters indicate the proton signals of the host and guest in the 2:1 complex. (*) Indicates residual solvents.

interactions. This is in contrast to the 1:2 **5⊂(1)$_2$** complex, which seemed to experience steric clashes of alkynyl-aldehyde substituents energetically disfavoring its formation with respect to the 1:1 **5⊂1** counterpart.

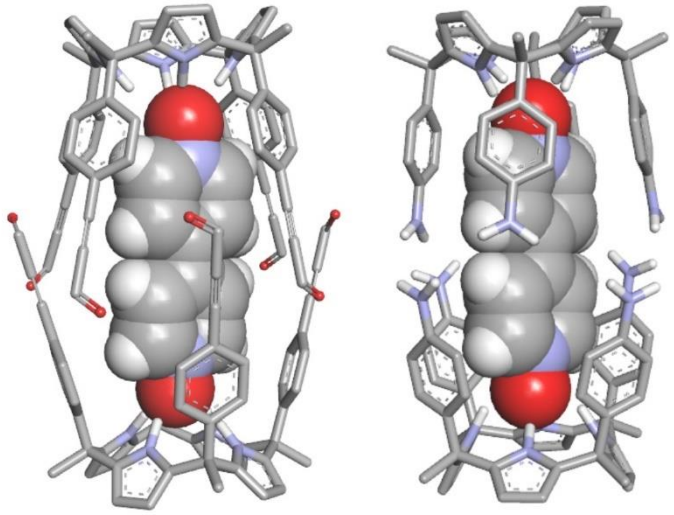

Figure 2.11. Energy minimized (MM3) structures of **5⊂(1)$_2$** and **5⊂(4)$_2$** cage-like complexes.

2.2.2.3 *Binding properties of cage **7** with N-oxide guests **5**–**10** in a 9:1 chloroform: acetonitrile mixture*

*2.2.2.3.1 Kinetic studies of the inclusion of the bis-N-oxide **5** by the (CD$_3$CN)$_2$⊂**7** cage complex*

As described above, we self-assembled cage **7** in a $CDCl_3$:CD_3CN 9:1 mixture of solvents obtaining a final concentration close to 1.2 mM (the yield of the self-assembly is roughly 65%). Next, we added an excess. of bis-*N*-oxide **5** with respect to the initial concentrations of the cage components (2.6 mM). The ^{1}H NMR spectrum of the mixture immediately after the addition of the *N*-oxide showed exclusively the proton signals corresponding to **7** and **5** free in solution (Figure 2.12). The mixture was left for 24 h at r.t. and reanalysed. The ^{1}H NMR spectrum evidenced the appearance of a new set of proton signals corresponding to the **5⊂7** complex. Notably, the proton signals of free **7** and **5** were still visible. In the $CDCl_3$:CD_3CN 9:1 mixture of solvents, the **5⊂7** complex was formed only in a 20% extent. We observed that the intensity of the proton signals of the **5⊂7** cage complex increased with time at the expenses of those of free **7** and **5**. After 18 days we observed a reduction of the uptake rate. At this point, the integral values of selected proton signals of the bound (**5⊂7**) and free (**7** and **5**) species, allowed the calculation of the molar ratio at equilibrium as 80:20. We also fit the observed changes in the concentrations of the free/bound species during the inclusion experiment to a

reversible theoretical kinetic model A + B ⇌ C + 2D using the Parameter Estimation module in the COPASI Software Version 4.25:[54]

$$(\mathbf{CH_3CN})_2\subset\mathbf{7} \;+\; \mathbf{5} \;=\; \mathbf{5}\subset\mathbf{7} \;+\; \mathbf{2CH_3CN}$$

$$\boldsymbol{Ka} = \frac{[\mathbf{5}\subset\mathbf{7}]\,[\mathbf{CH_3CN}]^2}{[(\mathbf{CH_3CN})_2\subset\mathbf{7}\,]\,[\mathbf{5}]} = \frac{\boldsymbol{kon}}{\boldsymbol{koff}}$$

The fit of the experimental data to the theoretical model was good and returned the

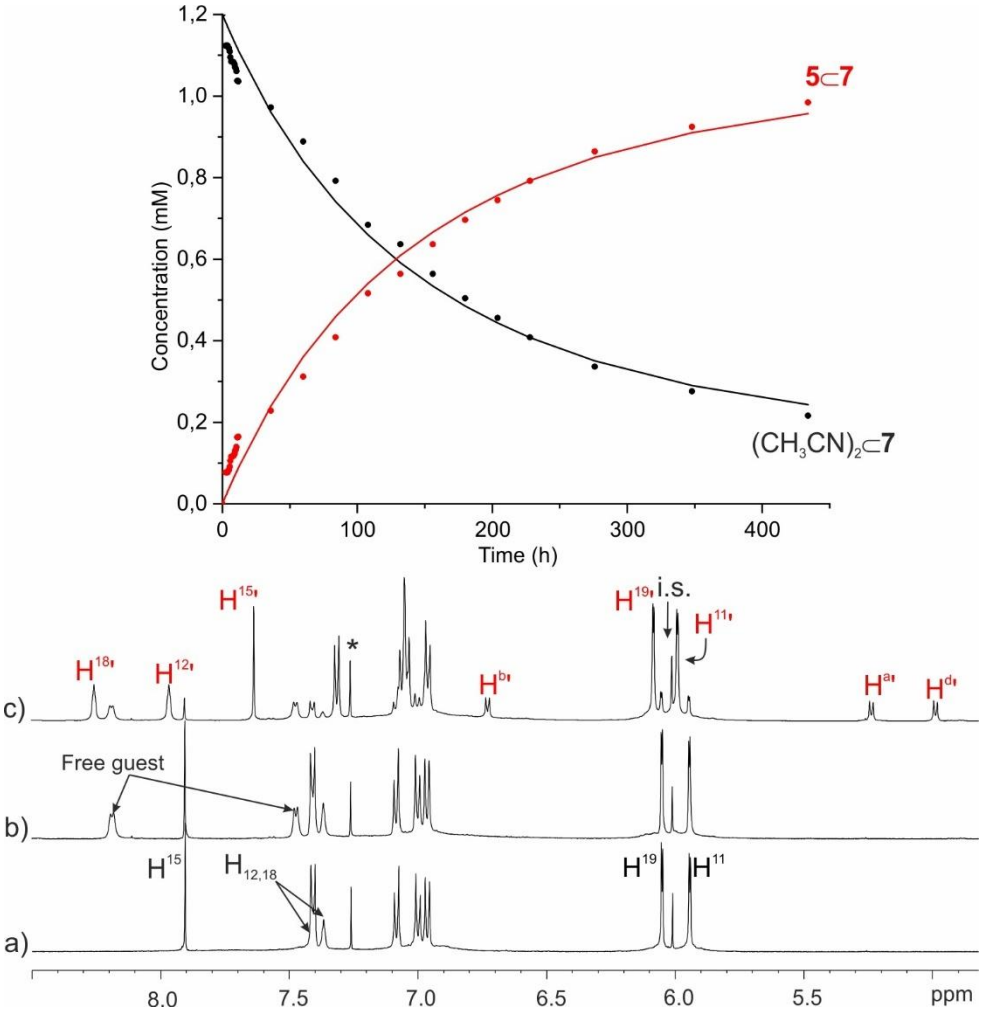

Figure 2.12. (Top) Kinetic data for encapsulation of **5** in tetra-imine cage **7** in a $CDCl_3$:CD_3CN 9:1 mixture to form **5⊂7**. (Bottom) Selected regions of the ^1H NMR spectra (500 MHz with cryoprobe, at 298 K, $CDCl_3$:CD_3CN 9:1) of (a) an equimolar mixture of tetra-aldehyde calix[4]pyrrole **1** and tetra-amino calix[4]pyrrole **4** after 24h at r.t. to give capsule **7**, (b) immediately after addition of **5** (2.6 mM), (c) 18 days after addition of **5**. Primed letters indicate bound host and guest in the 1:1 cage complex. See Scheme 2.1 for protons assignment.(*) Indicates residual solvents.

rate constant values as: $k_{on} = 7.0 \times 10^{-4}$ $M^{-1}s^{-1}$ and $k_{off} = 4.7 \times 10^{-8}$ $M^{-2}s^{-1}$. From these values we could derive the equilibrium constant as $K_a = 1.5 \times 10^4$ M. We performed analogous inclusion experiments in a solution containing a larger amount of acetonitrile: 80:20 $CDCl_3$:CD_3CN mixture. As could be expected, the increase in the acetonitrile concentration led to the formation of the **5⊂7** cage inclusion complex to a reduced extent. We calculated that the molar ratio of cage **7** and the inclusion complex **5⊂7** was 45:55, respectively after 18 days (*i.e*. 450 h).

Nevertheless, the rate constant values determined previously produced a good fit of the experimental kinetic data. These results provided an indication of the quality and the fit of the used theoretical kinetic model.

Taken together, obtained results suggested that the acetonitrile molecules act as solvent and efficient template guest. The inclusion of two molecules of acetonitrile in the initial cage **7** affected the kinetics of the binding/inclusion of the bis-*N*-oxide **5** and the final distribution of the two species, **7** and **5⊂7**, at equilibrium compared to the results obtained in pure $CDCl_3$ (see section 2.2.2.4)

*2.2.2.3.2 Kinetic study of the inclusion of pyridine-N-oxide **9** by the $(CD_3CN)_2$⊂**7** cage complex*

The ^{1}H NMR spectrum acquired immediately after (~ 5 min) the addition of pyridine *N*-oxide **9** (1.3 mM, 0.3 equiv. in respect to the total concentration of calix[4]pyrrole in solution) to a solution of the tetra-imine capsule $(CD_3CN)_2$⊂**7** (~ 1.3 mM) assembled in a $CDCl_3$:CD_3CN 9:1 mixture displayed two sets of proton signals for the protons of the cage. One set of signals corresponded to free **7** and the other was assigned to the **9⊂7** inclusion complex. After 4h, we observed that the ratio of the intensities of the two sets of signals changed (Figure 2.13 b).

The different chemical nature of the hemispheres of the tetra-imine cage **7** provided two different binding sites for the included *N*-oxide **9**. This could lead to the formation of two possible isomers for the 1:1 **9⊂7** complex. These isomers might be involved in either slow or fast chemical exchange process. However, the observation of two separate pyrrole NHs, resonating at δ = 9.6 and 7.45 ppm, for the **9⊂7** complex indicated the preferential formation of a single isomer in which *N*-oxide **9** was preferentially included in the hemisphere displaying the downfield-shifted pyrrole NHs. A 2D ROESY experiment of the solution containing the **9⊂7** complex revealed the existence of nOe cross-peaks (proximity in space) between the pyrrole

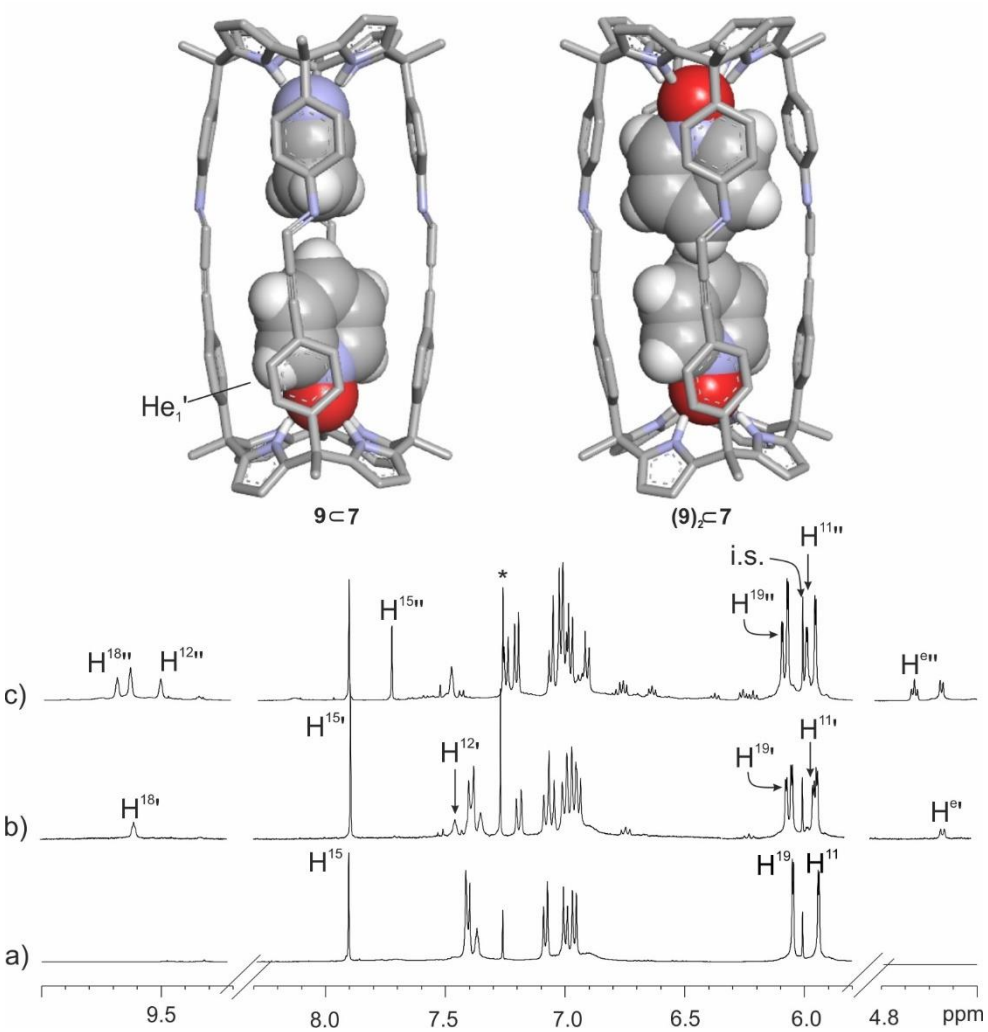

Figure 2.13. (Top panel) Energy minimized structures (BP86-D3-def2-TZVP DFT level of theory using Turbomole v7.0) of **9⊂7** and **(9)$_2$⊂7**. (Bottom panel) Selected regions of the ^{1}H NMR spectra (500 MHz with cryoprobe, at 298 K, $CDCl_3$:CD_3CN 9:1) of: (a) tetra-imine cage **7** (assembled from 2 mM concentration of **1** and **4**); (b) **9⊂7** complex after 4h of the addition of 0.3 equiv. of **9** (1.3 mM concentration), (c) a mixture of **9⊂7** and **(9)$_2$⊂7** obtained 1.5 h after the addition of 2 equiv. of **9**. Primed letters indicate the proton signals of bound cage and *N*-oxide in the 1:1 complex; double primed letters indicate the proton signals of bound cage and *N*-oxide in the 2:1 complex. (*) Indicates residual solvents.

NHs of the hemisphere having the *meso-p*-phenyl alkynyl substituents ($H^{18'}$) and the aromatic protons of the bound *N*-oxide **9** alpha to the nitrogen atom ($H^{e'}$) (Figure 2.81, Figure 2.82). This located *N*-oxide **9** exclusively included in this hemisphere of the **9⊂7** complex. Most likely, the opposite hemisphere of the **9⊂7** complex is occupied by one molecule of acetonitrile. We performed DFT calculations at the BP86[55,56]-D3[57]-def2-TZVP level of theory using

Turbomole v7.0[58,59] of the two potential 1:1 isomeric complexes of **9⊂7**. In contrast to the experimental observations, the computational results assigned similar energies to the two isomeric 1:1 geometries of the **9⊂7** complex.

In pure chloroform solution, the equimolar mixture of **7** and **9** produced a close to statistical mixture of free **7** and its 1:1 and 2:1 complexes (no cooperativity or slightly positive cooperativity). Most likely, the co-inclusion of one molecule of CD_3CN with **9** in the cavity of cage **7**, which takes place in the formation of the **9⊂7** complex in $CDCl_3$:CD_3CN 9:1 solvent mixture, is energetically favoured (negative cooperativity) with respect to the formation of the $(\mathbf{9})_2\subset\mathbf{7}$ counterpart.

Instead, the addition of two equiv. of pyridine *N*-oxide **9** to a solution containing cage **7** produced the instantaneous appearance of two new sets of signals that were attributed to the 1:1 and the 2:1 complexes, **9⊂7** and $(\mathbf{9})_2\subset\mathbf{7}$, respectively. The ^{1}H NMR spectrum registered immediately after the addition of the guest showed residual proton signals of free **7** in solution. However, after 1.5 h only the signals of the 1:1 and 2:1 complexes were observed. The inclusion processes of the *N*-oxide **9** in cage **7** yielding the 1:1 and 2:1 complexes are slow on the human timescale (Figure 2.13 c). The integral values of selected proton signals of the **9⊂7** and $(\mathbf{9_2})\subset\mathbf{7}$ complexes gave a 60:40 molar ratio. We did not detect proton signals for free **9**. Either the formation of the 2:1 complex showed a negative cooperativity or the added equivalents of **9** with respect to cage **7** were less than 2 equiv.

*2.2.2.3.3 Kinetic study of the inclusion of quinuclidine-N-oxide **11** by the $(CD_3CN)_2\subset$**7** cage complex*

After 24 h of the addition of 2 equiv. of quinuclidine *N*-oxide **11** to a solution of the tetra-imine capsule **7** in $CDCl_3$:CD_3CN 9:1 mixture, the ^{1}H NMR spectrum of the solution displayed exclusively the protons signals of the free cage and the free *N*-oxide (Figure 2.14 b). The solution was heated at 308 K for 24 h and reanalyzed using ^{1}H NMR spectroscopy. We observed the appearance of new signals with very low intensity in the regions of the imine and the bound pyrrole NH protons (Figure 2.14 c, highlighted in light blue and orange). We surmised that the new set of proton signals corresponded to the **11⊂7** complex.

In order to increase the concentration of the inclusion complex in the equilibrium, we thermally equilibrated the mixture at 308 K during three additional days. After

this time, the ^{1}H NMR spectrum of the mixture showed an increase of the imine and NH protons assigned to the **11**⊂**7** complex (Figure 2.14 c and d). The observation of a single pyrrole NH in the downfield region of the spectrum supported the formation of the 1:1 complex as a single isomer. The proton of the free cage provided the more intense signals.

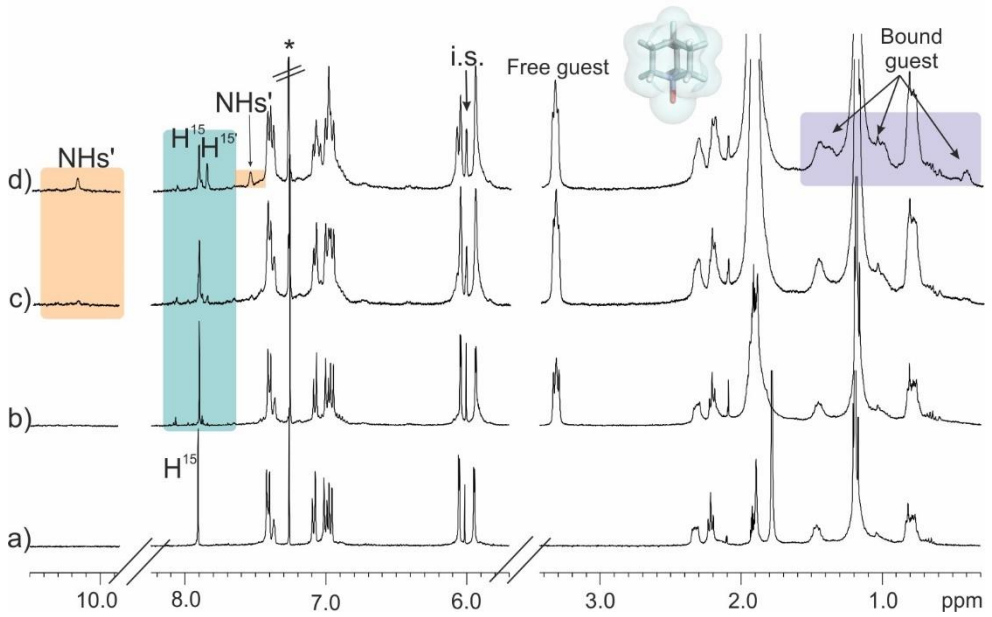

Figure 2.14. Selected regions of the ^{1}H NMR spectra (400 MHz, at 298 K, $CDCl_3$:CD_3CN 9:1 mixture) of (a) cage **7**; (b) 24 h after addition of 2 equiv. of **11**, (c) after addition of 2 equiv. of **11** and equilibration at 308 K for one day; (d) after addition of 2 equiv. of **11** and equilibration at 308 K for 3 days. Primed letters indicate bound host and guest in the 1:1 complex. (*) Indicates residual solvents.

The lack of signals related to the **11**⊂**7** encapsulation complex in the ^{1}H NMR spectrum of the mixture of **11** and **7** in $CDCl_3$:CD_3CN 9:1 mixture after 24 h at room temperature suggested that the encapsulation of the sterically demanding *N*-oxide **11** required the partial dissociation of the tetra-imine cage **7**. The cleavage of one or more imine bonds of cage **7** is associated with a higher energy barrier than the "French doors" alternative mechanisms postulated for the inclusion of the pyridyl-*N*-oxide derivatives **5** and **9**. It is worth mentioning, that the inclusion barriers of the *N*-oxides by cage **7** are always larger in the $CDCl_3$:CD_3CN solvent mixture than in pure $CDCl_3$ solution. This is due to the additional energy required for the displacement of the polar and hydrogen-bonded acetonitrile molecules included in cage **7** assembled in the solvent mixture compared to the chloroform molecules bound by **7** when the pure chlorinated is used. Considering the volume of **11** (91 Å^3) and the dimensions of the portals of **7** ($dCim_1$-Cim_2= 7.3 Å, dNH_{12}-NH_{18}= 12.5 Å, 7.3 Å× 12.5 Å= 91.3 Å^2, calculated from single crystal structure in $CDCl_3$:CD_3CN), the simultaneous rotation

of the *meso*-phenyl walls at both hemispheres does not allow the passage of the former through the latter.

As reported in literature, the constrictive binding of a guest[60] associated with a free energy barrier larger than 26 kcal/mol, will require several days at room temperature.[61] A thermal stimulus might cause conformational modifications of covalent structures leading to gate enlarging. Consequently, the energy barrier will diminish and the kinetic of guest entrance favoured. In our case, most probably, the inclusion mechanism of **11** by **7** involves a stepwise process with a rate-determining step related to energy barrier of the hydrolysis of the imine bond. The partial dissociation of cage **7** produced larger openings in the scaffold allowing the inclusion of bulky guest like **11** followed by shell closing.[24,63] However, we cannot rule out the possibility that the thermal stimulus causes conformational changes on the tetra-imine walls large enough to allow the entrance of the guest without affecting the covalent structure of the cage.

2.2.2.4 *Binding properties of cage **7** with N-oxide guests **5**–**10** in pure chloroform solution*

We mixed $CDCl_3$ solutions of tetra-aldehyde calix[4]pyrrole **1** and tetra-amino calix[4]pyrrole **4** in equimolar amounts to produce a final 2 mM concentration of each component. The resulting solution was heated at 308 K for 48 h. The thermally stabilized mixture was analyzed by ^{1}H NMR spectroscopy revealing the exclusive observation of the proton signals assigned to cage **7**. Nevertheless, the calculated yield for the self-assembly process using an internal standard was close to 50% (*vide supra*). Next, we added a slight excess of *N*-oxides **5**–**10** (2.5 mM for ditopic guest and 5 mM for monotopic guests) to separate $CDCl_3$ solutions containing the self-assembled cage **7**. The inclusion of the *N*-oxides in cage **7** was also monitored using ^{1}H NMR spectroscopy. The acquired ^{1}H NMR spectra revealed that cage **7** quantitatively included all *N*-oxides. Moreover, the uptake of the *N*-oxides was complete within 20 min after the addition.

These results contrast with the ones described for $CDCl_3$:CD_3CN 9:1 mixture of solvents, in which starting from **7** the encapsulation complexes required several weeks to achieve the equilibrium.

Notably, the chemical exchange between the free and the bound *N*-oxides was slow on the proton chemical shift and EXSY timescales. We concluded that the weakly bound $CDCl_3$ molecules occupying the interior of cage **7** must be readily replaced (low energy barrier) by the incoming *N*-oxides forming thermodynamically and

kinetically highly stable inclusion complexes. The *N*-oxides interacted with the cavity of cage **7** mainly by establishing hydrogen bonding interactions with its two calix[4]pyrrole hemispheres. In addition, CH-π and π-π interactions were also involved in the stabilization of the inclusion complexes.

Not surprisingly, the ^{1}H NMR spectrum of the **5⊂7** inclusion complex obtained in $CDCl_3$ starting from cage **7** and adding the bis-*N*-oxide **5** (Figure 2.15 b) was identical to the one obtained in the self-assembly of **7** using **5** as template (Figure 2.4c).

In the case of the inclusion cage complexes obtained with pyridine-*N*-oxide **9** and trimethyl-*N*-oxide **10**, the careful analyses of their ^{1}H NMR spectra led us to conclude that their stoichiometries were 2:1. That is, in the complexes **(9)$_2$⊂7** and **(10)$_2$⊂7** each hemisphere of cage **7** include a hydrogen-bonded *N*-oxide. Because the two hemispheres are different the protons of the bound guests split in two different sets of signals (Figure 2.15 c, d).

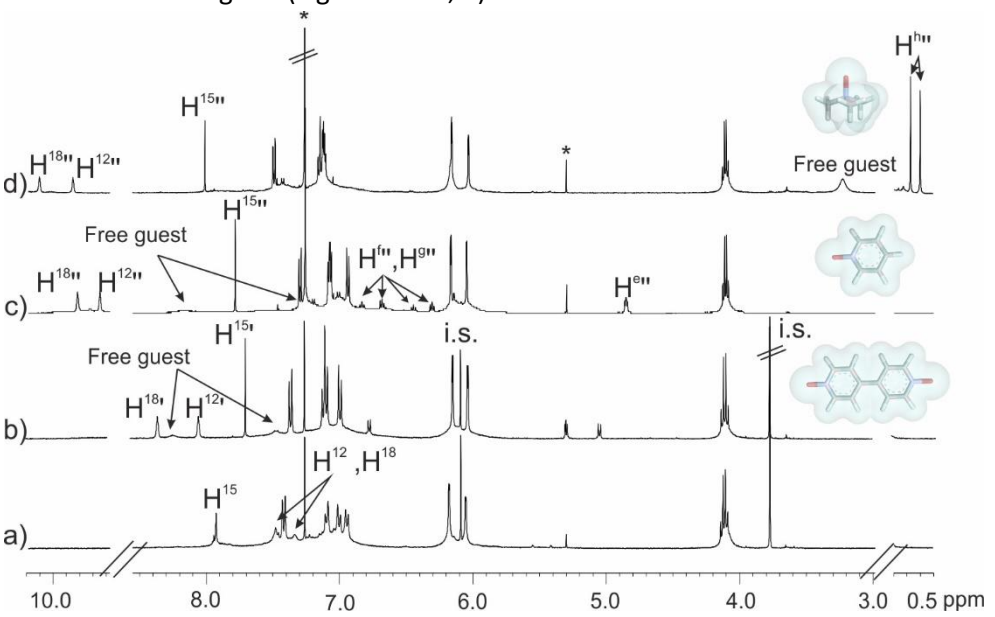

Figure 2.15. Selected regions of the ^{1}H NMR spectra (400 MHz, at 298 K, $CDCl_3$) of (a) imine cage **7**, (b) after addition of 1.2 equiv. of **5**, (c) after addition of 2.2 equiv. of **9**, (d) of 2.2 equiv. of **10**. Primed letters indicate bound host and guest in the 1:1 complex; double primed letters indicate the bound host and guest in the 2:1 complex. See Scheme 2.1 for protons assignment. (*) Indicates residual solvents.

Interestingly, the pyrrole NHs in the **(9)$_2$⊂7** and **(10)$_2$⊂7** cage complexes (H$^{18''}$ and H$^{12''}$) experienced larger downfield shifts, compared to free **7**, than those observed for the **5⊂7** counterpart. This observation suggested that the hydrogen bonds in the latter complex are longer than in the two former ones. We also compared the $\Delta\delta$ value experienced by the NHs in the **5⊂7** complex with that of 1:1 inclusion

complexes of pyridyl-*N*-oxide with "four wall" aryl extended calix[4]pyrroles and reached an identical conclusion.

We surmised that the length of bis-*N*-oxide **5** is not adequate to establish simultaneously eight optimal hydrogen bonding interactions with the two hemispheres of **7**.

The calculated packing coefficients (PC) for the cage complexes **(9)$_2$⊂7** and **(10)$_2$⊂7** were 60% and 55%, respectively. Packing coefficients larger than the ideal 55% established by Rebek's rule[62] are common for inclusion complexes of polar molecules in molecular containers featuring functionalized cavities.[29]

The proton signals of the *N*-oxide⊂**7** complexes were sharper than those of free **7**. Surprisingly to us, the addition of the *N*-oxides did not have a significant thermodynamic template effect. In short, the amount of cage **7** did not significantly increase in the presence of the template. We hypothesized that the mixture of oligomers formed by the condensation of calix[4]pyrroles **1** and **4** not leading to the cage assembly may be trapped in a kinetic minimum.

We detected that the time required to obtain the quantitative formation of the **5⊂7** and **(9)$_2$⊂7**, through the addition of the *N*-oxides to the self-assembled cage **7** in $CDCl_3$ solution, was slightly different. The 5⊂**7** complex required longer times than the **(9)$_2$⊂7** counterpart. We hypothesized that the guest uptake mechanism involves a gating process. That is, the incoming guest is squeezed on passing through the enlarged portals of cage **7** experiencing a "french doors" mechanism of the *meso*-phenyl substituents. Because cage **7** contains two "four wall" calix[4]pyrrole units, the entrance of the bis-*N*-oxide **5** may require an almost synchronous "french doors" process of the two hemispheres. The inclusion of the pyridine-*N*-oxide **9** to form the **(9)$_2$⊂7** complex is known to be stepwise leading to the formation of an initial 1:1 complex. Consequently, only one of the two hemispheres of **7** must experience the "french doors" mechanism. The energy barrier of the latter process is probably lower than that of the simultaneous gating of the two hemispheres. This will explain the different times required for the quantitative formation of the two inclusion complexes. We consider the partial cleavage of imine bonds is not likely to occur during the uptake of the guests owing to the fast kinetics observed for the formation of the inclusion complexes.[63]

2.2.2.4.1 *Exchange experiment of the two included pyridine-N-oxides in the* ***(9)$_2$⊂7*** *complex by addition of bis-N-oxide* ***5***

We investigated the exchange of the two pyridine-*N*-oxide molecules included in the **(9)$_2$⊂7** complex by addition of 1 equiv. of the bis-*N*-oxide **5**. Firstly, we assembled the **(9)$_2$⊂7** complex in pure $CDCl_3$ at a concentration close to 1 mM. Next, we added to the solution approximately 1 equiv. of the 4',4'-bipyridyl-*N,N'*-dioxide **5**. The resulting mixture was analysed at different time intervals using ^{1}H NMR spectroscopy.

Despite the reduced fit of the bis-*N*-oxide **5** in the cavity of **7** commented above, we expected that the two-particles **5⊂7** complex would be energetically more favourable than the initial three particles aggregate **(9)$_2$⊂7**.

After 192h, the reaction mixture seemed to have reached equilibrium. The ^{1}H NMR spectrum of the mixture showed two sets of proton signals for the proton signal of the cage that corresponded to the **5⊂7** and **(9)$_2$⊂7** inclusion complexes. Based on the integral values of selected proton signals, we determined that the two complexes were present in solution in a 60: 40 ratio. The two-particles cage complex **5⊂7** was the major species but not the exclusive one (Figure 2.16).
However, with time we observed the slow evolution of the spectrum until the quantitative formation of **5⊂7** encapsulation complex is reached after one month.
The energy minimized structures of the two complexes at the BP86-D3-def2-TZVP DFT level of theory using Turbomole v7.0 are shown in Figure 2.16. The average distances of the hydrogen bonding interactions in the **5⊂7** complex is $d_{average(H\text{-}N\cdots O\text{-}N)}$ = 3.25 ± 0.07 Å). However, for the three-particles **(9)$_2$⊂7** cage complex the analogous hydrogen bonding interactions are shorter($d_{(H\text{-}N\cdots O\text{-}N)}$ =2.88 ± 0.02 Å).

In short, the two pyridine-*N*-oxide molecules included in the **(9)$_2$⊂7** seems to form more favourable hydrogen bonding interactions with the two calix[4]pyrrole hemispheres of the cage. However, the entropic advantage deriving from the **5⊂7** complex formation compensates the reduced enthalpic gain leading to its formation, making the two particles aggregates **5⊂7** energetically competent.

This hypothesis was further confirmed by a reverse experiment. More specifically, we investigated the exchange of one molecule of bis-*N*-oxide **5** involved in the **5⊂7** complex by addition of 2 equiv. of the pyridine-*N*-oxide **9**. We observed in this case that after equilibration at r.t for 700 h, the ditopic guest was not replaced by two molecules of pyridine-*N*-oxide **9** even after addition of an excess of **9**. The outcome of this simple experiment confirmed our initial expectation that the two-particles

5⊂7 complex is energetically more favourable than the three particles aggregate **$(9)_2$⊂7**.

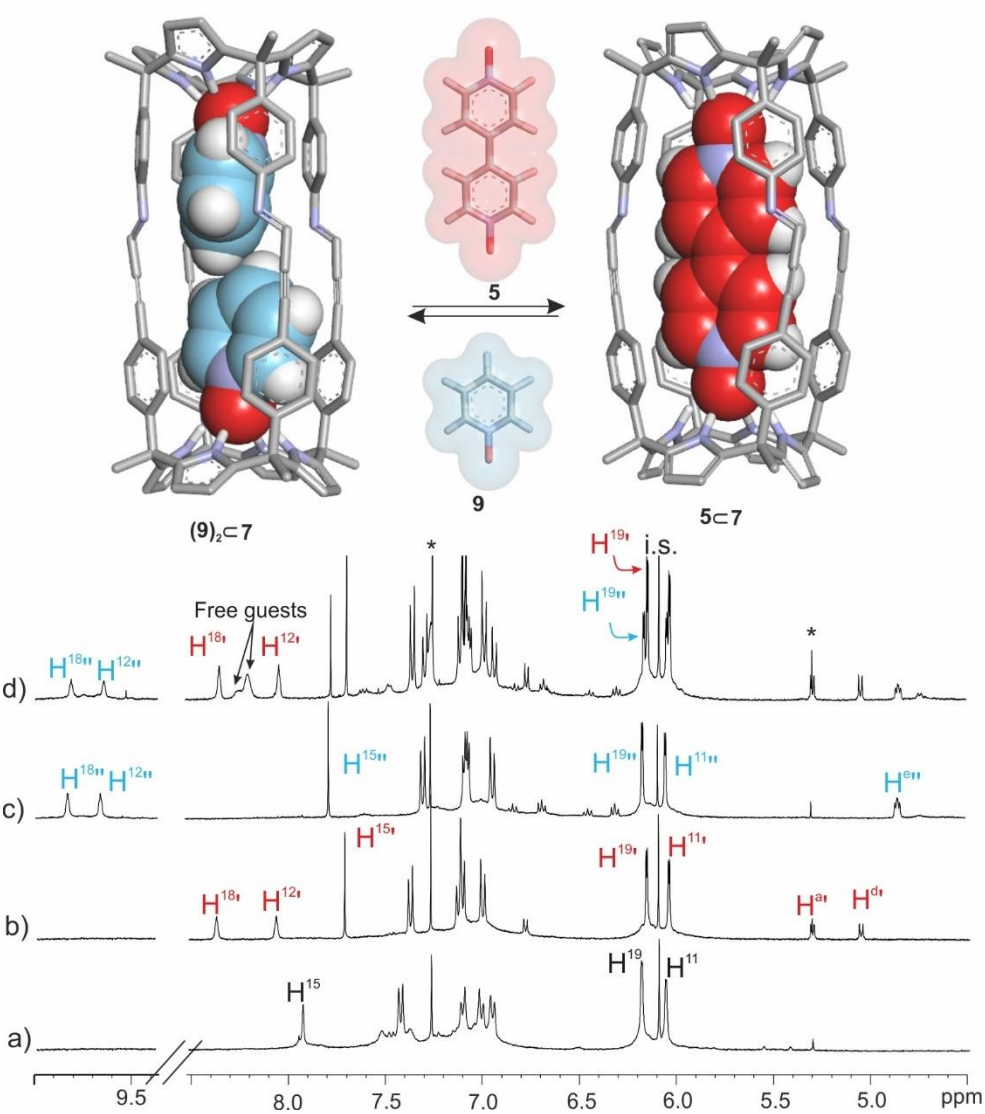

Figure 2.16. (Top) Energy minimized structures (BP86-D3-def2-TZVP DFT level of theory using Turbomole v7.0) of **$(9)_2$⊂7** and **5⊂7.** (Bottom) Selected regions of the ^{1}H NMR spectra (400 MHz, at 298 K, $CDCl_3$) of: (a) self-assembled cage **7** (thermally equilibrated equimolar mixture of tetra-aldehyde calix[4]pyrrole **1** and tetra-amino calix[4]pyrrole **4**); (b) **5⊂7**cage complex; (c) **$(9)_2$⊂7** cage complex; (d) the mixture obtained after 192h of the addition of 1 equiv. of **5** to a solution of **$(9)_2$⊂7** in $CDCl_3$. Primed letters indicate proton signals of bound host and guest in the **5⊂7**cage complex; double primed letters indicate the bound host and guest in the **$(9)_2$⊂7** complex. See Scheme 2.1 for protons assignment. (*) Indicates residual solvents.

*2.2.2.4.2 Kinetics of the inclusion of quinuclidine-N-oxide **11** by cage **7** in $CDCl_3$ solution*

The ^{1}H NMR spectrum acquired immediately after (~ 5 min) the addition of 1 equiv. of the sterically demanding quinuclidine-*N*-oxide **11** to a thermally stabilized $CDCl_3$ solution containing cage **7** (Figure 2.17 b) showed some small changes with respect to that of the free cage (Figure 2.17 a). The number of signals for the aromatic and β-pyrrole protons of cage **7** increased. We also observed the appearance of a sharp singlet resonating at δ= 8 ppm and two humps in the region of 10.5 ppm. The mixture was left standing at r.t. for 24 h and reanalyzed using ^{1}H NMR spectroscopy.

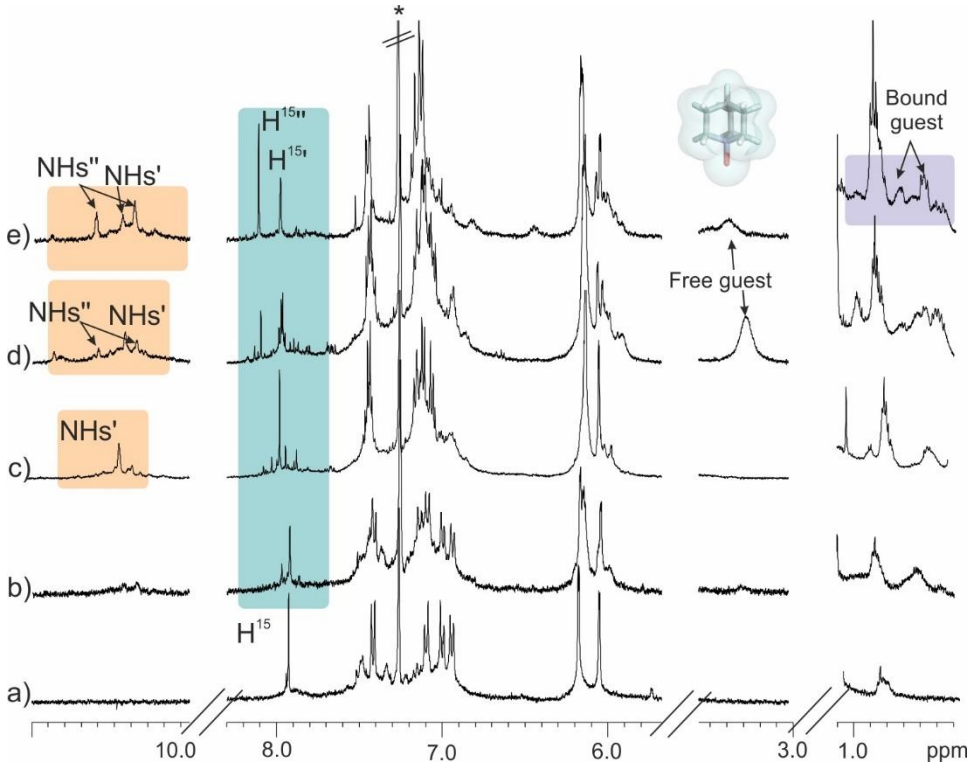

Figure 2.17. Selected regions of the ^{1}H NMR spectra (400 MHz, at 298 K, $CDCl_3$) of solutions containing: (a) self-assembled cage **7**; (b) cage **7** and 1 equiv. of **11**, 5 min after the addition of **11**; (c) same as (b) 24h after the addition of **11**; (d) thermal equilibration (308 K, 48h) of the mixture in (c) after adding another equivalent of **11**; (e) an equimolar mixture of **11⊂1** and **11⊂4** after 24h at r.t. Primed letters indicate proton signals for the bound host and guest in the putative 1:1 **11⊂7** complex; double primed letters indicate proton signals for the bound host and guest in the putative 2:1 (**11**)$_2$**⊂7** complex. See Scheme 2.1 for protons assignment (*) Indicates residual solvents.

After this time, the new signals had increased in intensity at the expenses of those of free **7**. We hypothesized that the new signals corresponded to the 1:1 inclusion cage complex **11⊂7**. At this point, we also detected a new multiplet resonating at δ

= 0.7 ppm that was assigned to the protons of the encapsulated *N*-oxide **11**. In order to induce the formation of the 2:1 complex, **(11)$_2$⊂7**, we added another equiv. of **11** to the mixture above and thermally equilibrated it during 24 h at 308 K. This treatment provoked the emergence of new signals in the regions of the ^{1}H NMR spectrum where the imine and pyrrole NHs of cage **7** typically appeared. We tentatively assigned these new signals to the formation of the **(11)$_2$⊂7** complex to a reduced extent.

Alternatively, we evaluated the self-assembly of the **11⊂7** and **(11)$_2$⊂7** complexes by mixing equimolar solutions of the 1:1 complexes of the cage components with the *N*-oxide **11**: **11⊂1** and **11⊂4**. The resulting solution was left at r.t. for 24 h. The ^{1}H NMR spectrum of the equilibrated mixture displayed the proton signals assigned to the **11⊂7** and **(11)$_2$⊂7** complexes (Figure 2.17 e). Using these conditions, the **(11)$_2$⊂7** complex was the major species assembled in solution.

On one hand, the observations of coinciding protons signals in the ^{1}H NMR spectra of the solutions used to assemble the cage complexes, **11⊂7** and **(11)$_2$⊂7**, starting from different conditions supported their formation. On the other hand, the fact that the ratio of the **11⊂7** and **(11)$_2$⊂7** complexes is different depending on the methodology used for their self-assembly suggested that the formation of the **(11)$_2$⊂7** complex from the **11⊂7** counterpart occurred through a high energy barrier. We surmised that the uptake of a second *N*-oxide **11** by the self-assembled **11⊂7** complex required the partial cleavage of the imine bonds. Thus, the extent of formation of the **(11)$_2$⊂7** complex starting from the self-assembled cage **7** is reduced and slow on the human time-scale even when the solution is heated at 308 K. We cannot rule out that the extended thermal equilibration of the mixture starting from **7** produced a partial decomposition/degradation of the molecular components of the cage complexes. This will explain the complexity of the ^{1}H NMR spectrum in comparison to the one registered from the equilibrated mixture of the 1:1 complexes: **11⊂1** and **11⊂4**.

The calculated packing coefficients for the $CDCl_3$·**11⊂7** and **(11)$_2$⊂7** complexes were 48% and 78%, respectively. We expected the formation of the **(11)$_2$⊂7** complex not to be energetically favored. However, as commented above exceptions of the 55% Rebek's rule are known for inclusion complexes of polar molecules in *endo*-functionalized containers hydrogen- bond donor or acceptor guests.

2.2.3 Gas phase characterization

We also became interested in characterizing cage **7** and its inclusion complexes in the gas phase. Mass spectrometry offers the possibility to study supramolecular architectures under solvent-free conditions and as isolated ions (charged species are formed under high vacuum (below 10^{-9} mbar)). The stability of charged complexes formed by polar interactions is expected to be affected by the absence of solvent molecules.[64,65,66]

We performed ESI-MS analysis of solutions of **7** and solution mixtures containing **7** and the series of *N*-oxides **5**, **9**, **10** and **11**, both in positive and negative mode. We further studied the complexes' stabilities using collision induced dissociation (CID) experiments,[67] which partially reflected what observed in solution.

We prepared $CHCl_3/CH_3CN$ solutions at μM concentration of **7** in the presence of excess of **5**, **9**, **10**, **11** and 0.5% of TFA when operating in positive mode. The positive monocharged ion $[M+H]^+$ and the double charged $[M+2H]^{2+}$ were frequently detected, most probably due to protonation of one or two imine functionalities.

First of all, we wanted to investigate the structural stability of cage **7** in the gas phase. To this end, we selected the parent ion [**7**+H]$^+$ (m/z= 1949.9166) and induced

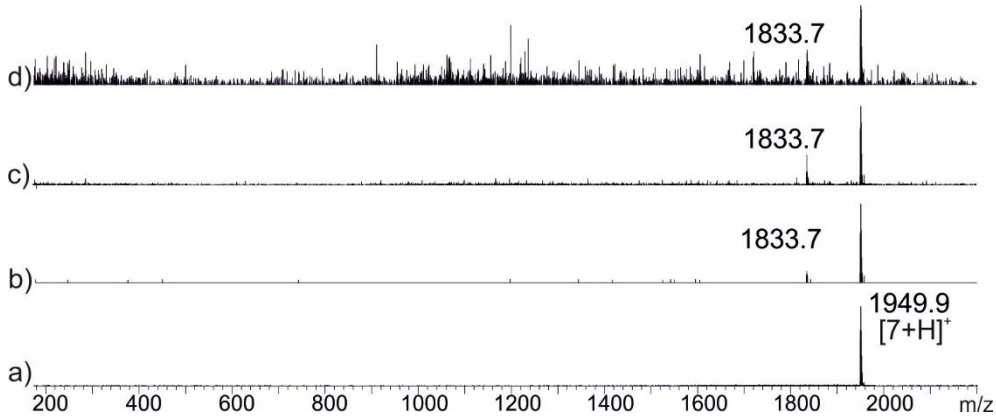

Figure 2.18. CID experiment performed with the mass selected ion [**7**+H]$^+$ with CE of (a) 5V, (b)40 V, (c) 60 V, (d) 70 V.

its fragmentation by rapid collision with N_2 through the application of an increasing voltage at the entrance of the hexapole. We expected that cage ion of **7** disassemble as consequence of imine bonds dissociation. However, instead we observed the loss of an ester chain. The intensity of the selected ion peak decreased and a new peak at m/z= 1833.764 was generated (Figure 2.18 b). Only when the voltage was further increased (up to 70 V) the intensity of the selected ion peak was drastically reduced by secondary fragmentations of the entire backbone. This reflected the stability of

the imine bonds in the gas phase and in the absence of residual water molecules that can promote its cleavage.

When we performed CID experiments in the positive mode for the selected ion of the inclusion complex of bis-*N*-oxide with tetra-imine cage [**5**⊂**7**+H]$^+$ (m/z= 2137.945), the applied voltage caused a significant loss of encapsulated **5** only at around 40V and generated the ion peak of the protonated cage [**7**+H]$^+$ (m/z= 1949.9166) (Figure 2.19). This result is interesting because it highlights that the voltage required for the disassembly of **5**⊂**7** complex is lower than those required for the disassembly of the cage.

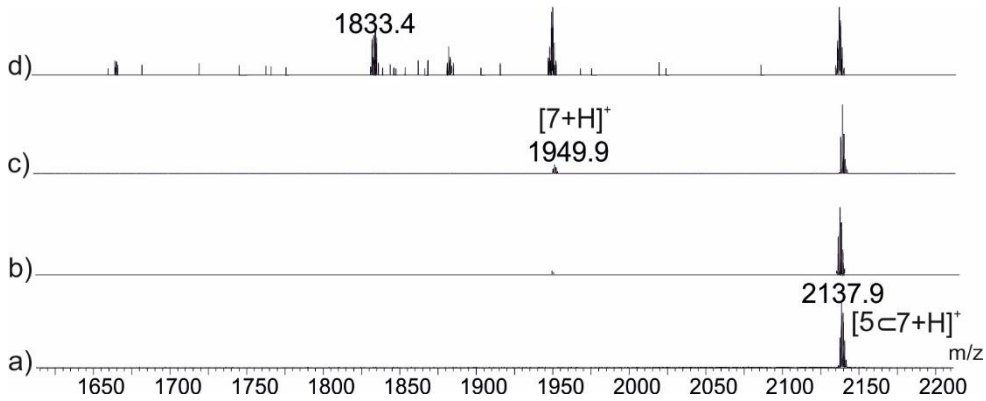

Figure 2.19. CID experiment performed with the mass selected ion [**5**⊂**7**+H]$^+$ with CE of (a) 0V, (b) 25 V, (c) 40 V, (d) 60 V.

Analogous CID experiments with the selected ion [(**9**)$_2$⊂**7**+H]$^+$ (m/z= 2139.933) showed that already at low voltages the ion of the 1:1 complex [**9**⊂**7**+H]$^+$ (m/z= 2044.932) generated from the loss of one molecule of pyridine *N*-oxide was produced (Figure 2.20). A small increase of the applied voltage showed that almost

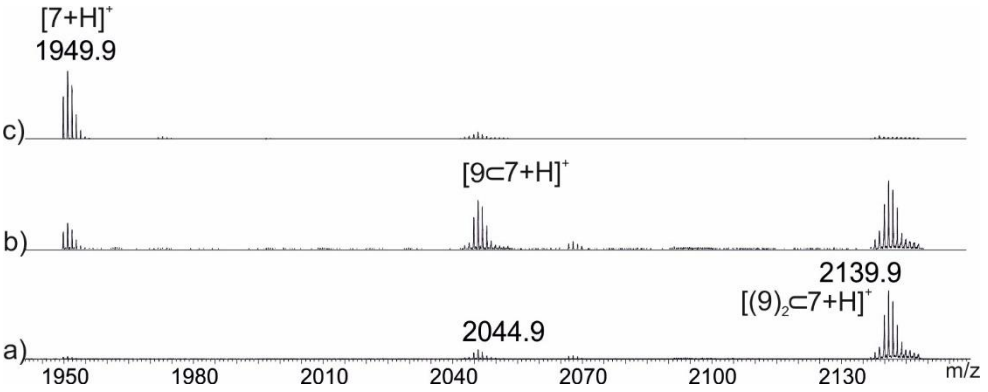

Figure 2.20. CID experiment performed with the mass selected ion [(**9**)$_2$⊂**7**+H]$^+$ with CE of (a) 0V, (b) 5 V, (c) 15 V.

50% of the parent ion is fragmented in [**9**⊂**7**+H]$^+$ and [**7**+H]$^+$. At 15 V the peak corresponding to the dissociation of the two guest molecules is detected.Taken together, the results of CID experiments for monotopic and ditopic planar *N*-oxides guests reflected our findings in solution: the guests can enter/exit the cage through its portals giving rise to the formation and disassembly of the inclusion complexes. This process is energetically less costly for **9** than for **5**. In addition, as we also observed in solution, **5**⊂**7** is slightly more stable than (**9**)$_2$⊂**7**.

Interestingly in the case of cage complex of quinuclidine *N*-oxide **11** an ion peak at the *m/z* ratio corresponding to [(**11**)$_2$⊂**7**+H]$^+$ was observed in the ESI-MS spectrum. We also performed Ion Mobility Mass Spectrometry (IMS)[68] CID experiments in order to have more insights into the size of the complexes once increasing voltages are applied. We observed the appearance of a second signal with a smaller arrival time when the selected parent ion [(**11**)$_2$⊂**7**+H]$^+$ was subjected to fragmentation

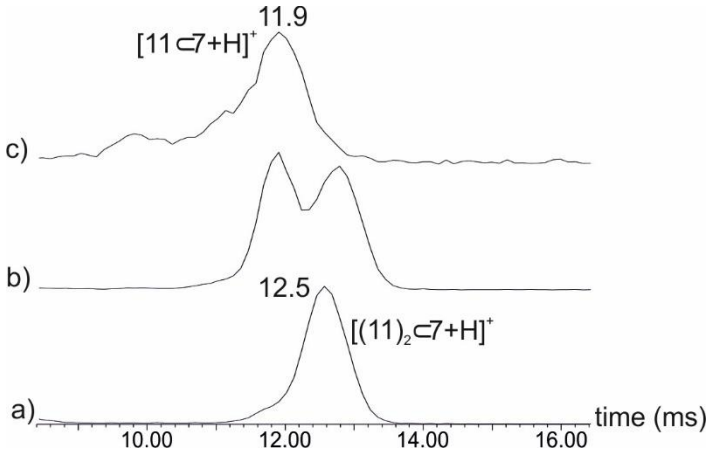

Figure 2.21. Arrival time distribution of ions [(11)$_2$⊂7+H]$^+$ and [11⊂7+H]$^+$ obtained in IMS-CID experiments of [(11)$_2$⊂7+H]$^+$at (a) 0V, (b)40V and (c)80V.

(Figure 2.21). At a voltage of 80 V, in the gas phase, this second peak was exclusively present. We attributed the second peak to the mono-protonated ion of the 1:1 complex [**11**⊂**7**+H]$^+$. The difference in arrival time is directly related to a difference in size of the two ions, meaning that after the release of one guest molecule from the cavity of the cage [(**11**)$_2$⊂**7**+H]$^+$ to give [**11**⊂**7**+H]$^+$, the size of the supramolecular ion changes.

Unfortunately, this information did not allow us to clarify whether both guest molecules are co-encapsulated in the capsule cavity or the second molecule of **11** can somehow interact outside the cavity.

The CID experiments on the $[(\mathbf{11})_2 \subset \mathbf{7}+H]^+$ ion showed that to reduce the intensity of this ion peak, it is necessary to increase the voltage above that required to reduce the intensity of $[\mathbf{5} \subset \mathbf{7}+H]^+$ and $[(\mathbf{9})_2 \subset \mathbf{7}+H]^+$ ions (Table 2.1).

Most probably this can be due to the fact that the sterically more demanding encapsulated quinuclidine *N*-oxide can only escape from the capsule cavity when high voltages are applied to the parent ions and producing the partial disassembly of the cage.

Parent ion	CE (V)
$\mathbf{[7+H]^+}$	50
$\mathbf{[5 \subset 7+H]^+}$	24
$\mathbf{[(9)_2 \subset 7+H]^+}$	8
$\mathbf{[(10)_2 \subset 7+H]^+}$	18
$\mathbf{[(11)_2 \subset 7+H]^+}$	38

Table 2.1. CE values determined via CID experiments necessary to reduce of 50% the intensity of parent ions.

2.3 Conclusions

We described the synthesis of imine bonded cages via condensation reaction between tetra-aldehyde calix[4]pyrroles and tetra-amino calix[4]pyrroles in pure chlorinated solvents and in solvent mixtures (*i.e.* $CDCl_3$:CD_3CN 9:1). We demonstrated that in the presence of a templating guest or a solvent able to pre-organize the cavity of the calix[4]pyrrole precursors in the cone conformation (*e.g*. acetonitrile), higher yields of capsular assembly can be achieved compared to pure chlorinated solvents (*e.g*. chloroform or dichloromethane). We demonstrated their stability at r.t. and studied their binding properties towards a series of *N*-oxides. In short, the weakly bound solvent molecules are displaced by the *N*-oxide guests which establish hydrogen bond interactions with the pyrrole NH protons of the calix[4]pyrrole core and complementary CH-π and π-π interactions.

Interestingly, the binding studies with monotopic or ditopic planar or sterically more demanding *N*-oxide guests showed that the kinetic of encapsulation is not only influenced by the nature of the guest but also by the solvent. Indeed, in the presence of CD_3CN molecules in the media we observed a slow kinetic of encapsulation for all the studied *N*-oxide guests. We assume that this observation is attributed to the competition between the coordinating solvent and the polar guest for hydrogen bond interactions with the capsule's binding site.

We observed that the formation of the 1:1 complex of the tetra imine capsule with the most sterically demanding quinuclidine *N*-oxide guest required more time and

temperature to be formed either in $CDCl_3$ or $CDCl_3$:CD_3CN 9:1 compared to the planar pyridine *N*-oxide guests. We surmised that the encapsulation mechanisms operating with planar (2D guest) and tridimensional guests are different. Most likely, the entrance of quinuclidine *N*-oxide requires the partial dissociation of the tetra imine cage (*i.e.* cleavage of some imine bonds). On the other hand, we propose a French doors mechanism operating in the case of the planar guests.

The stability of the tetra imine capsule **7** and its encapsulation complexes (**5**⊂**7**, (**9**)$_2$⊂**7**, (**10**)$_2$⊂**7**, (**11**)$_2$⊂**7**) was also investigated in the gas phase by means ESI-MS experiments. The values of CE obtained to reduce a 50% the intensity of parent ions are in good agreement with our findings in solution using ^{1}H NMR spectroscopy.

2.4 Experimental section

2.4.1 General information and instruments

Starting materials and reagents were purchased from commercial suppliers and used without any further purification. All reactions were performed under argon atmosphere unless specified. Anhydrous solvents were obtained from a solvent purification system SPS-400-6 from Innovative Technologies. All solvents were of HPLC grade quality, commercially obtained and used without further purification.
^{1}H NMR and 2D NMR spectra were recorded on a Bruker Avance 400(400 MHz for ^{1}H NMR) and Bruker Avance500 (500 MHz for ^{1}H NMR). Deuterated solvents from Sigma Aldrich were used for NMR studies, previously dried for the synthesis of dynamic covalent capsules. Chemical shifts are given in ppm, relative to residual solvents.
Tetra-aldehyde calix[4]pyrrole **1**[36], tetra-amino calix[4]pyrroles **3**, **4**[40,41] and quinuclidine *N*-oxide **11**[53] were synthesized adapting previously reported procedures.
Mass spectrometric experiments were performed in a Synapt G2-S HDMS (Waters Co., Milford, MA, USA) travelling wave ion mobility mass spectrometer. All ions were generated by electrospray ionization (ESI) in the positive and negative mode. The parameters were optimized to obtain the maximum abundance of the ions of interest.

2.4.2 Synthesis and characterization

2.4.2.1 *Synthesis of tetra-aldehyde calix[4]pyrroles **1** and **2***

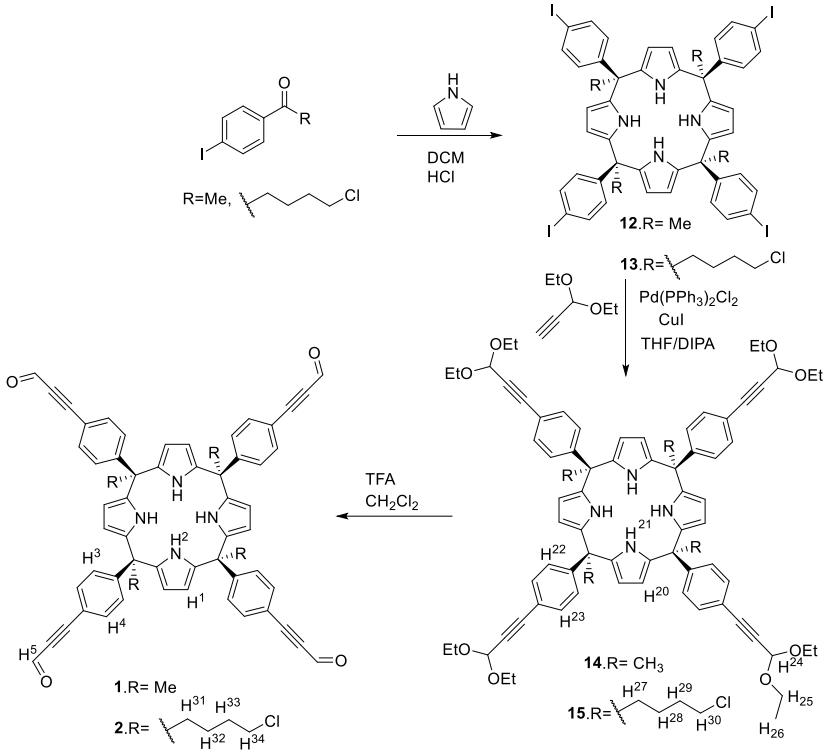

Scheme 2.2. Synthesis of calix[4]pyrroles **1** and **2** starting from differently functionalized *p*-iodo acetophenones.

Calix[4]pyrroles **14** and **15** were synthesized adapting reported procedures.[38] Tetra-iodo calix[4]pyrroles **12**[37] or **13**[38] (1 equiv., 0.054 mmol), CuI (0.2 equiv., 10.8 µmol) and $Cl_2Pd(PPh_3)_2$ (0.12 equiv., 6.5 µmol) were dried in a Schlenk tube for 1 h and then propargyl-aldehyde diethyl acetal (20 equiv., 1.1 mmol) was added. A 1:1 mixture (14 mL) of dry and degassed DIPA and THF was added to the mixture under Ar and the reaction heated at 45˚C for 3 h covered by an Al foil. The reaction was the stirred at 35˚C overnight.

The reaction crude was brought to dryness and later dissolved in DCM (30 ml) and washed with HCl 1N (2x30 ml) and with water (30 ml). The organic phase was dried with anhydrous Na_2SO_4, filtered and the solvent was evaporated under reduced pressure.

The crude was purified by column chromatography on silica gel (DCM-->DCM/MTBE 1%) and further purified by precipitation from DCM/MeOH (1:3) at low

temperature, to obtain the pure compounds **14** and **15** as white powders (in 80% and 53 % yield respectively).
Spectroscopic data for **14** are in agreement with that reported in literature.[36]
15: ^{1}H NMR (400 MHz, $CDCl_3$): 7.33 (d ,8H), 7.28 (b.s, 4H), 7.06 (d, 8H), 5.80 (d, 8H), 5.49 (s, 4H), 3.86- 3.62 (m, 16 H), 3.49 (t, 8H), 2.27 – 2.23 (m, 8H), 1.74 (quint., 8H), 1.42- 1.34 (m, 8 H), 1.27 (t, 24H, overlapped with grease).
^{13}C [^{1}H]NMR (100 MHz, $CDCl_3$) δ(ppm): 145. 6, 135.5, 131.4, 128.4, 106.7, 92.0, 85.0, 84.8, 61.1, 48.9, 44.8, 39.5, 32.9, 22.7, 15.3.

HR MS (ESI- TOF) m/z: $[M+Na]^+$ Calculated for $C_{88}H_{104}Cl_4N_4O_8Na^+$= 1507.6500; found 1507.6518.

The reaction crude from the synthesis of **15** using the above described procedure was analyzed by HPLC (method: Spherisorb silica gel column (80 Å, 5 µm, 4.6 mm × 250 mm); CH_2Cl_2; flux = 1 mL/min; injections of 20 µL; detection at 245 nm).

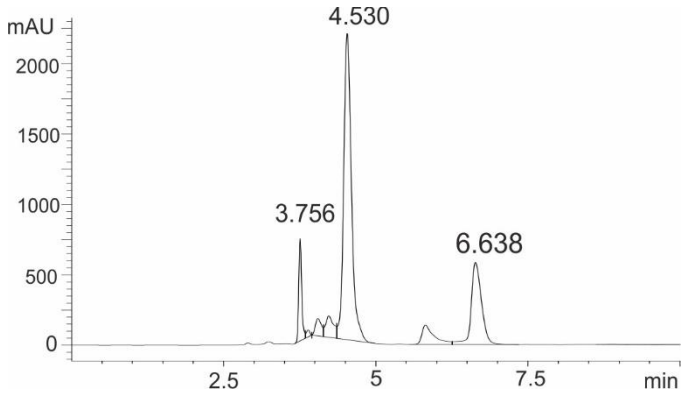

Figure 2.22. Chromatogram of the reaction crude of **15** (1 mg/mL solution) using the detection wavelengths 245 nm. The target compound is eluted after 4.53 min.

Tetra-aldehyde calix[4]pyrroles **1** and **2** were synthesized adapting a reported procedure.[36] Calix[4]pyrrole **14** or **15** (0.013 mmol) were dissolved in DCM (12 mL) and then a solution of TFA (0.40 mmol, 30 equiv.) in DCM (12 mL) was slowly added dropwise during 1h. Once the addition was completed, the solution was kept under stirring for 4 h under Ar and protected from the light. The mixture was then washed with $NaHCO_3$ (5x 30 ml) and water (40 ml), dried over anhydrous Na_2SO_4, filtered and concentrated, affording the product as a orange sticky solid (97% yield).
Spectroscopic data for **1** are in agreement with what reported in literature.[36]
2:^{1}H NMR (400 MHz, $CDCl_3$) δ(ppm): 9.16 (s ,4H), 7.51 (b.s., 4H), 7.47 (d, 8H), 7.16 (d, 8H), 5.9 (s, 8H), 3.5 (t, 8H), 2.35–2.29 (m, 8H), 1.75 (quint., 8H), 1.41–1.3 (m, 8 H).

^{13}C [^{1}H]NMR (100 MHz, $CDCl_3$) δ(ppm): 117.1, 149.2, 135.7,132.9, 129.3, 118.1, 106.9, 88.9, 49.3, 45.0, 39.4, 32.8, 29.8, 25.2.

2.4.2.2 *Synthesis of imine cage complex **5⊂6***

Procedure A (NMR scale): Tetra-amino calix[4]pyrrole **3** (0.51 mg, 0.69 µmol), 4',4'-bipyridyl *N,N'*-dioxide **5** (0.135 mg, 0.71 µmol) and tetra-aldehyde calix[4]pyrrole **1** (0.61 mg, 0.69 µmol), in a molar ratio of 1:1:1, were dissolved in 0.6 mL of a 3 mM solution of the internal standard 1,3,5-trimethoxybenzene (1.07 mg in 2 mL of dry degassed $CDCl_3$).
Initially, a suspension was formed (especially the guest **4** and tetra-amino calix[4]pyrrole **2** are not very soluble in $CDCl_3$). After 24 h the solution was clear and the ^{1}H NMR showed the diagnostic peaks for the formation of the cage in a 45% yield according to the internal standard.
^{1}H NMR (500 MHz, $CDCl_3$) δ(ppm): 8.28 (br s, 4H), 8.26 (br s, 4H), 7.69 (s, 4H), 7.35 (d, *J* = 8.4 Hz, 8H), 7.12–7.06 (m, 18H), 6.96 (d, *J* = 8.5 Hz , 8H), 6.74 (d, *J* = 7.3 Hz, 2H), 6.14 (d, *J* = 2.6 Hz, 8H), 6.13 (d, *J* = 2.6 Hz, 8 H), 5.18 ppm (d, *J* = 7.3 Hz, 2H), 5.08 (d, *J* = 7.3 Hz, 2H), 1.96 (s, 12H), 1.94 (s, 12H).

MS (ESI TOF) m/z: $[M+K]^+$ Calculated for $C_{118}H_{92}N_{14}O_2K^+$ =1775.7159; found 1775.8545.

Procedure B (large scale): Tetra-amino calix[4]pyrrole **3** (23 mg, 0.032 mmol) and 4',4'-bipyridyl **5** (7.2 mg, 0.038 mmol) were suspended in dry degassed $CDCl_3$ (8 mL) in a round bottom flask under Ar atmosphere. A chloroform solution (8 mL) of tetra-aldehyde calix[4]pyrrole **1** (28.2 mg, 0.032 mmol) was added dropwise to the reaction mixture under Ar atmosphere. The resulting yellow suspension was stirred at 35˚C under Ar atmosphere for 3 days. After 3 days, the insoluble precipitate was filtered off and washed with chloroform. Imine cage complex **5⊂6** was obtained from evaporation of the chloroform solution.

2.4.2.3 *Synthesis of imine cage complex **5⊂7***

In a NMR tube, tetra-amino calix[4]pyrrole **4** (0.73 mg, 0.64 µmol), 4',4'-bipyridyl *N,N'*-dioxide **5** (0.11 mg, 0.60 µmol) and tetra-aldehyde calix[4]pyrrole **1** (0.57 mg, 0.64 µmol) in molar ratio of 1:1:1, were dissolved in 0.6 mL of a 3 mM solution of the internal standard 1,3,5-trimethoxybenzene (1.07 mg in 2 mL of dry degassed $CDCl_3$). Then, tetra-aldehyde calix[4]pyrrole **1** (0.55 mg, 0.62 µmol) was added. The

^{1}H NMR of the reaction mixture acquired after 15 hours at room temperature, showed the formation of the cage in a 65% yield according to the internal standard.
^{1}H NMR (400 MHz, $CDCl_3$) δ(ppm): 8.36 (br s, 4H), 8.06 (br s, 4H), 7.70 (s, 4H), 7.36 (d, *J*= 8.3 Hz, 8H), 7.14–7.05 (m, 18H), 6.99 (d, *J* = 8.3 Hz, 8H), 6.77 (d, *J* = 7.3 Hz, 2H), 6.15 (d, *J* = 2.6 Hz, 8H), 6.04 (d, *J* = 2.6 Hz, 8H), 5.29 (d, *J* = 7.3 Hz, 2H), 5.05 (d, *J* = 7.3 Hz, 2H), 4.10 (q, *J* = 7.1, Hz 8H), 2.44–2.36 (m, 8H), 2.25 (t, *J* = 7.3 Hz 8H), 1.94 (s, 12H), 1.51–1.41 (m, 8H), 1.25 (t, *J* = 7.1 Hz, 12H).
HR MS (ESI TOF) m/z: $[M+Cl]^-$ Calculated for $C_{138}H_{124}N_{14}O_{10}Cl^-$=2171.9318; found 2171.9070.

2.4.2.4 *Synthesis of imine cage **7***

Procedure A (1:9 CD_3CN:$CDCl_3$): In a NMR tube, tetra-amino calix[4]pyrrole **4** (0.73 mg, 0.64 µmol) was dissolved in 0.6 mL of a 1:9 CD_3CN:$CDCl_3$. Then, tetra-aldehyde calix[4]pyrrole **1** (0.55 mg, 0.62 µmol) was added. The ^{1}H NMR of the reaction mixture after 12 hours shows the signals corresponding to formation of the capsule in a 65 % yield, according to the presence of the internal standard in solution (1,3,5-trimethoxybenzene, see previous synthetic procedures).
Alternatively, the cage could be assembled by mixing equimolar amounts of **1** and **4** in a 1:9 CD_3CN:$CDCl_3$ mixture at r.t. (2-4 mM).
^{1}H NMR (500 MHz, 1:9 CD_3CN:$CDCl_3$) δ(ppm): 7.86 (s, 4H), 7.36 (d, *J* = 8.2 Hz, 8H), 7.34 (bs, 4H), 7.32 (bs, 4H), 7.05 (d, *J* = 8.5 Hz, 8H), 6.94 (d, *J* = 8.5 Hz, 8H), 6.91 (d, *J* = 8.2 Hz, 8H), 5.99 (d, *J* = 2.6 Hz 8H), 5.89 (d, *J* = 2.6 Hz, 8H), 3.98 (q, *J* = 7.1 Hz 8H), 2.27–2.24 (m, 8H), 2.15 (t, *J* = 7.2, Hz 8H), 1.83 (s, 12H), 1.42–1.35 (m, 8H), 1.12 (t, *J* = 7.1 Hz, 12 H).
MS (ESI TOF) m/z: $[M+H]^+$ Calculated for $C_{128}H_{116}N_{12}O_8H^+$=1949.9112; found 1949.9166

Procedure B ($CDCl_3$): In a NMR tube, tetra-amino calix[4]pyrrole **4** (1.39 mg, 1.22 µmol) was dissolved in 0.6 mL $CDCl_3$. Then, tetra-aldehyde calix[4]pyrrole **1** (1.11 mg, 1.24 µmol) was added and the mixture was heated at 308 K. The ^{1}H NMR of the reaction mixture after 48 hours shows the signals corresponding to formation of the capsule in a 48% yield , according to the presence of an internal standard in solution (1,3,5-trimethoxybenzene).
Alternatively, the cage could be assembled by mixing equimolar solution (2-4 mM) of **1** and **3** in $CDCl_3$ and heating at 308 K for 48h.
^{1}H NMR (400 MHz, $CDCl_3$) δ(ppm): 7.92 ppm (s, 4H), 7.48 (bs, 4H), 7.42 (d, *J* = 8.3 Hz, 8H), 7.33 (bs, 4H), 7.09 (d, *J* = 8.2 Hz, 8H), 7.00 (d, *J* = 8.3 Hz, 8H), 6.94 (d, *J* = 8.2 Hz,

8H), 6.17 (d, *J* = 2.5 Hz, 8H), 6.05 (d, *J* = 2.6 Hz, 8H), 4.11 (q, *J* = 7.1 Hz, 8H), 2.46–2.37 (m, 8H), 2.26 (t, *J* = 7.3 Hz, 8H), 1.95 (s, 12H), 1.55–1.45 (m, 8H), 1.25 (t, *J* = 7.1 Hz, 12H).

Procedure C (CD_2Cl_2): In a NMR tube, tetra-amino calix[4]pyrrole **4** (0.76 mg, 0.67μmol) was dissolved in 0.6 mL CD_2Cl_2 solution. Then, tetra-aldehyde calix[4]pyrrole **1** (0.6 mg, 0.68 μmol) was added and the mixture was heated at 303 K. The ^{1}H NMR of the reaction mixture after 72 hours shows the signals corresponding to formation of the cage in a 48 % yield, according to the presence of an internal standard in solution (1,3,5-trimethoxybenzene).

Alternatively, the cage could be assembled by mixing equimolar amounts of **1** and **4** in CD_2Cl_2 and heating at 35ºC for 72 h (2-4 mM).

^{1}H NMR (500 MHz, CD_2Cl_2) δ(ppm): 7.93 (s,4H), 7.48 (d, *J* = 8.1 Hz, 8H), 7.30 (bs, 4H), 7.17 (bs, 4H) 7.14 (d, *J* = 8.3 Hz, 8H), 7.02 (d, *J* = 8.3 Hz, 8H), 6.98 (d, *J* = 8.1 Hz, 8H), 6.19 (d, *J* = 2.6 Hz, 8H), 6.09 (d, J = 2.6 Hz, 8H), 4.08 (q, *J* = 7.1 Hz, 8H), 2.43–2.37 (m, 8H), 2.29 (t, *J* = 7.4 Hz, 8H), 1.99 (s, 12H), 1.55–1.45 (m, 8H, overlap. with water), 1.25 (t, *J* = 7.1 Hz, 12H).

2.4.2.5 *Synthesis of imine cage complex* ***5⊂8***

In a NMR tube, tetra-amino calix[4]pyrrole **4** (1.6 mg, 1.36 μmol), 4',4'-bipyridyl *N,N'*-dioxide **5** (1.6 mg, 1.36 μmol) and tetra-aldehyde calix[4]pyrrole **1** (1.7 mg, 1.39 μmol), were dissolved in 0.6 mL of dry degassed $CDCl_3$. The ^{1}H NMR of the reaction mixture acquired after 24 hours at room temperature, showed formation of the cage in a 55% yield according to an internal standard (1,3,5-trimethoxybenzene) added in solution.

^{1}H NMR (400 MHz, $CDCl_3$) δ(ppm): 8.16 (s,4H), 8.11 (s,4H), 7.70 (s,4H), 7.40 (d, *J* = 8.4 Hz, 8H), 7.14 (d, *J* = 7.3 Hz, 2H), 7.14-7.11 (m, 16H), 7.0 (d, *J* = 8.4 Hz, 8H), 6.78 (d, *J* = 7.3 Hz, 2H), 6.04 (d partially overlapped, *J* = 2.8 Hz, 8H), 6.03 (d partially overlapped, *J* = 2.8 Hz, 8H), 5.29 (d, *J* = 7.3 Hz, 2H), 5.13 (d, *J* = 7.3 Hz, 2H), 4.11 (q, *J* = 7.3 Hz, 8H), 3.47 (t, *J* = 6.6 Hz, 8H), 2.44–2.36 (m, 16H), 2.25 (t, *J* = 7.3 Hz, 8H), 1.73 (quint., *J* = 6.6 Hz, 8H), 1.51–1.41 (m, 8H), 1.26–1.22 (m, 16H).

2.4.2.6 *Synthesis of imine cage* ***8***

In a NMR tube, tetra-amino calix[4]pyrrole **4** (1.6 mg, 1.36 μmol) was dissolved in 0.6 mL of a 1:9 CD_3CN:$CDCl_3$ mixture. Then, tetra-aldehyde calix[4]pyrrole **2** (1.7 mg, 1.39 μmol) was added. The ^{1}H NMR of the reaction mixture after 24 hours shows

the signals corresponding to formation of the capsule in a 65 % yield, according to the presence of an internal standard in solution (1,3,5-trimethoxybenzene).
Alternatively, the cage could be assembled by mixing equimolar amounts of **2** and **4** in a 1:9 CD_3CN:$CDCl_3$ mixture at r.t. (2-4 mM).
^{1}H NMR (400 MHz, $CDCl_3$) δ(ppm): 7.93(s,4H), 7.46 (d, *J*= 8.3 Hz, 8H), 7.37 (s,4H), 7.29 (s,4H), 7.10 (d, *J*= 8.5 Hz, 8H), 7.0 (d, *J* = 8.5 Hz, 8H), 7.0 (d, *J*= 8.3 Hz, 8H), 5.98–5.90 (m, 16H), 4.04 (q, *J*= 7.0 Hz, 8H), 3.45 (t, *J*= 6.5 Hz, 8H), 2.37–2.28 (m, 16H), 2.21 (t, *J*= 7.0 Hz, 8H), 1.7 (quint., *J*= 7.0 Hz, 8H), 1.51–1.4 (m, 8H), 1.31–1.21 (m partially overlapped, 8H), 1.20–1.15 (m partially overlapped, 8H).

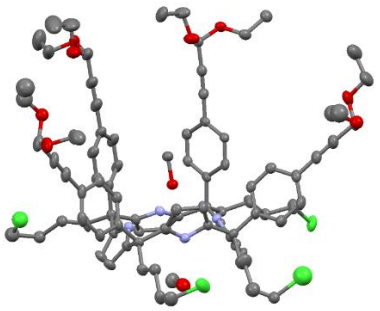

Figure 2.23. Single crystal structure of **15** (grown from slow evaporation from MeOH) in partial cone conformation. One MeOH molecule is interacting with three pyrrole NHs while the second molecule is interacting with one pyrrole NHs from the opposite side. Hydrogen atoms and additional solvent molecules were omitted for clarity.

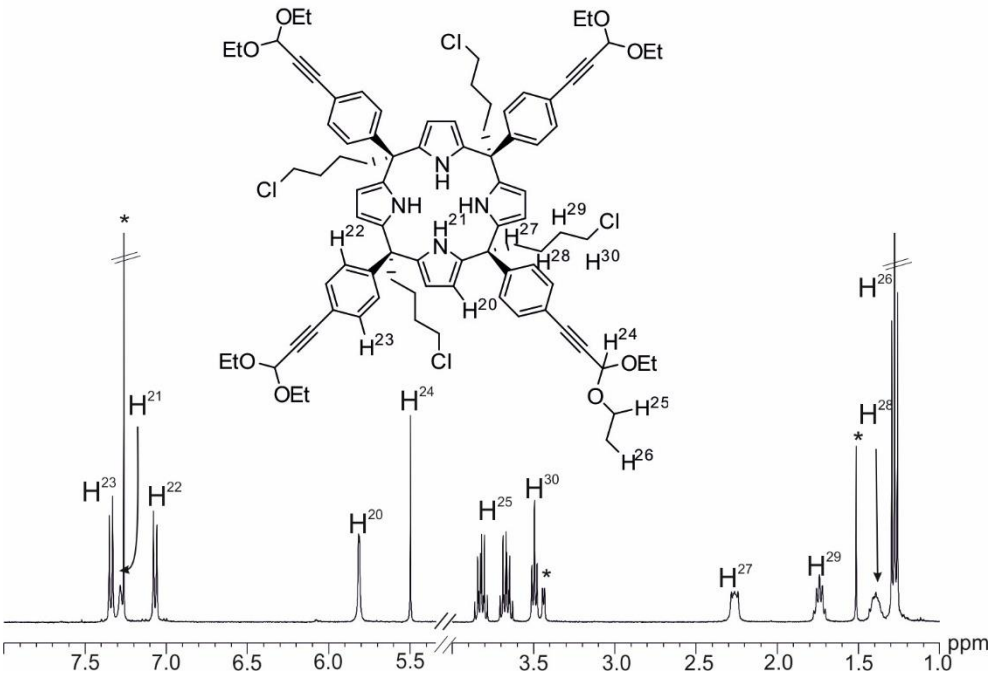

Figure 2.24. ^{1}H NMR spectrum (400 MHz, at 298 K, $CDCl_3$) of calix[4]pyrrole **15.** (*) Indicates residual solvents.

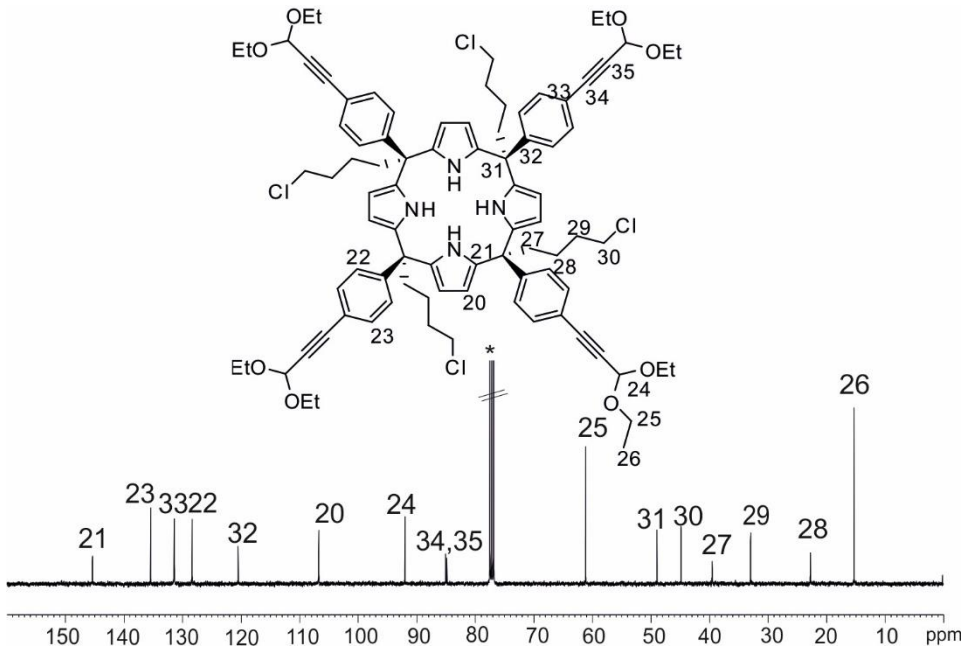

Figure 2.25. ^{13}C NMR (100 MHz, at 298 K, $CDCl_3$) of calix[4]pyrrole **15** in $CDCl_3$. (*) Indicates residual solvents.

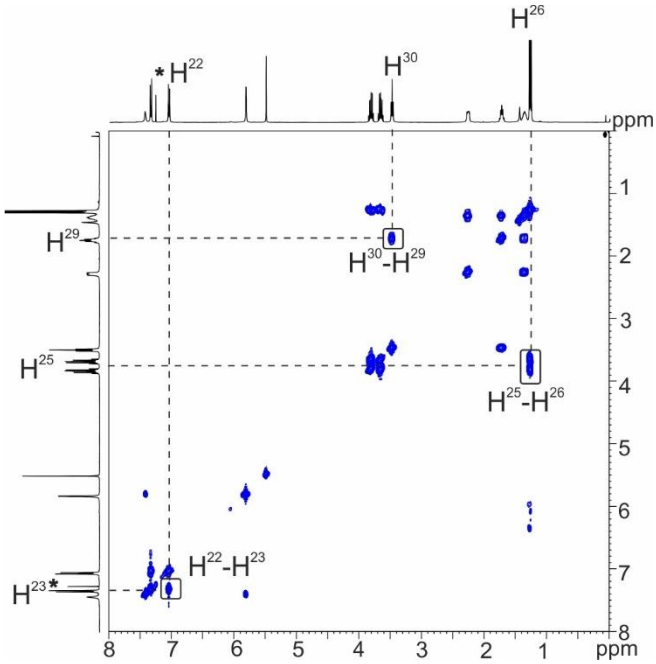

Figure 2.26. Selected region of 2D COSY NMR (400 MHz, at 298 K, $CDCl_3$) of calix[4]pyrrole **15.** See Figure 2.24 for protons assignment. (*) Indicates residual solvents.

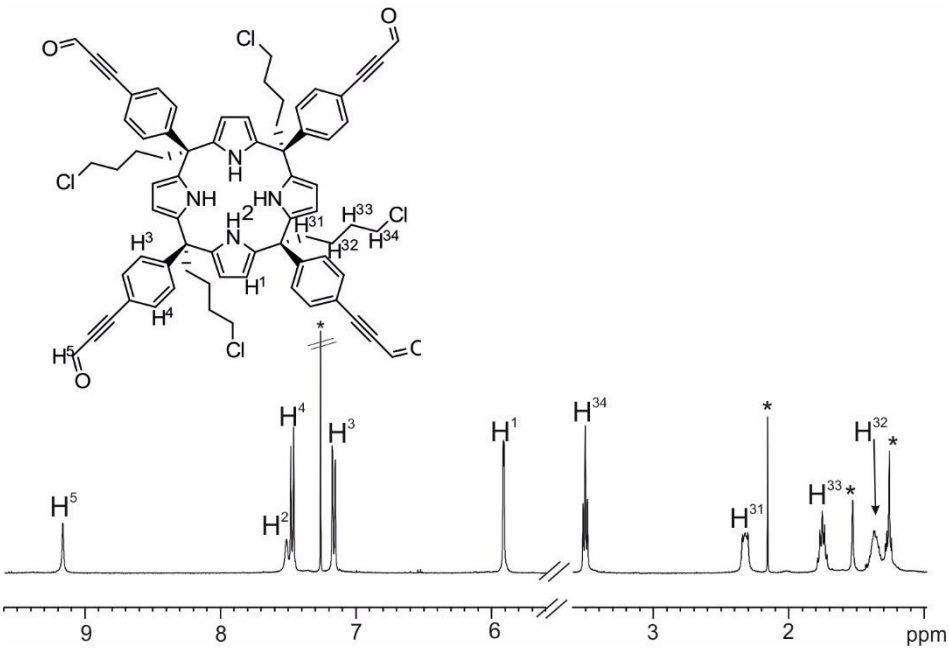

Figure 2.27. ^1H NMR spectrum (400 MHz, at 298 K, $CDCl_3$) of tetra-aldehyde calix[4]pyrrole **2**. (*) Indicates residual solvents.

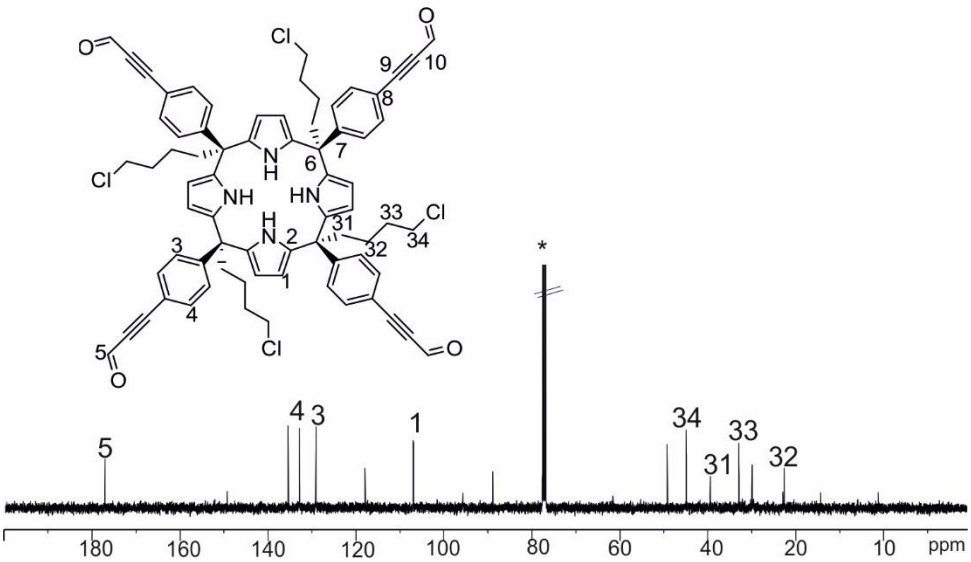

Figure 2.28. ^{13}C NMR (100 MHz, at 298 K, $CDCl_3$) of tetra-aldehyde calix[4]pyrrole **2**. (*) Indicates residual solvents.

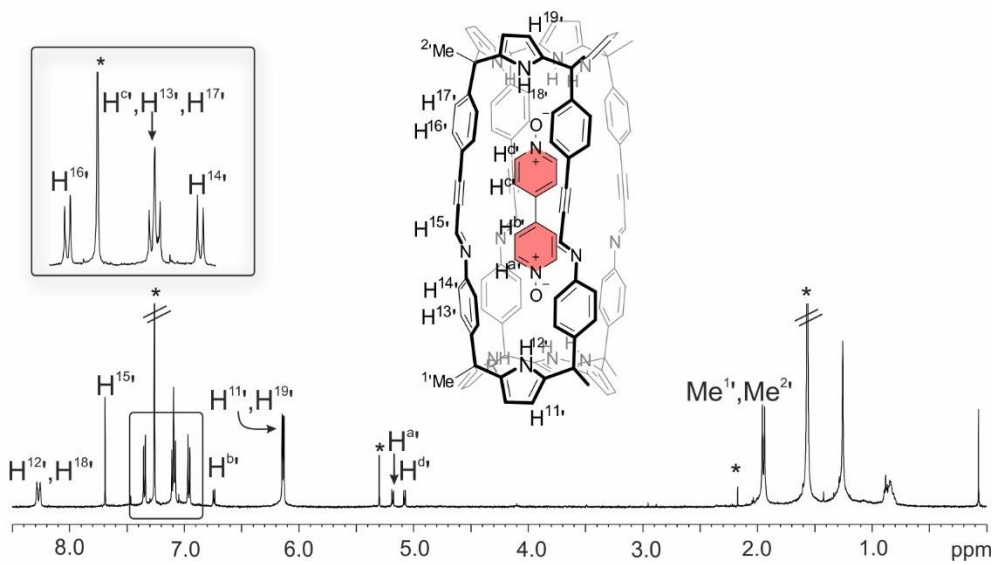

Figure 2.29. ^{1}H NMR spectrum (500 MHz, at 298 K, $CDCl_3$) of a 1:1:1 equimolar mixture of tetra-aldehyde calix[4]pyrrole **1**,tetra-amino calix[4]pyrrole **3** and **5** after 24h at r.t. (imine cage complex **5⊂6**). (*) Indicates residual solvents.

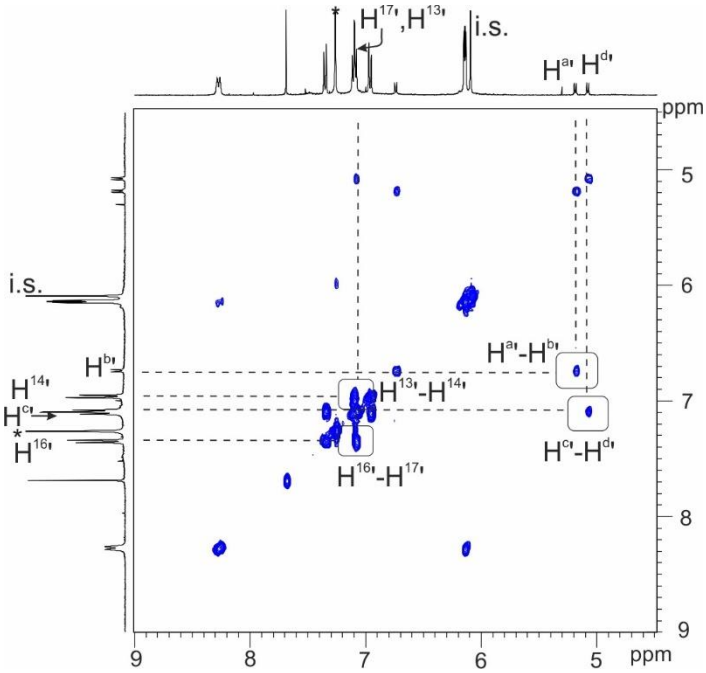

Figure 2.30. Selected region of 2D COSY NMR (400 MHz, at 298 K, $CDCl_3$) of a solution containing imine cage complex **5⊂6**. See Figure 2.29 for protons assignment. (*) Indicates residual solvents.

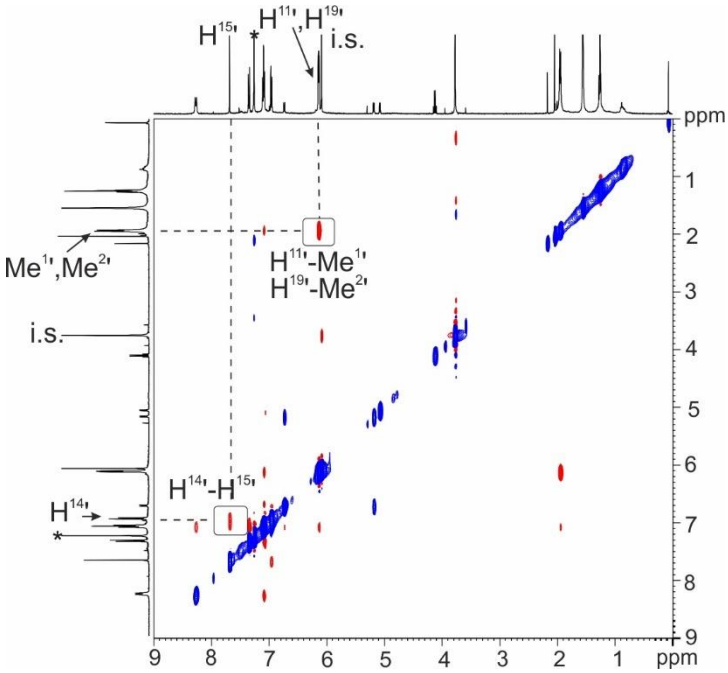

Figure 2.31. 2D ROESY NMR(400 MHz, at 298 K, $CDCl_3$) of solution containing a imine cage complex **5⊂6**. See Figure 2.29 for protons assignment. (*) Indicates residual solvents.

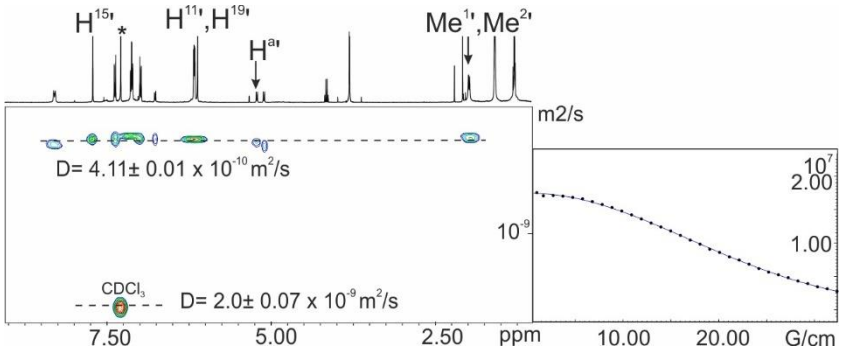

Figure 2.32.[1]H pseudo-2D DOSY NMR (400 MHz, at 298 K, $CDCl_3$, big delta 0.15 s, little delta 0.001 s) solution containing imine cage complex **5⊂6**. See Figure 2.29 for protons assignment. (*) Indicates residual solvents

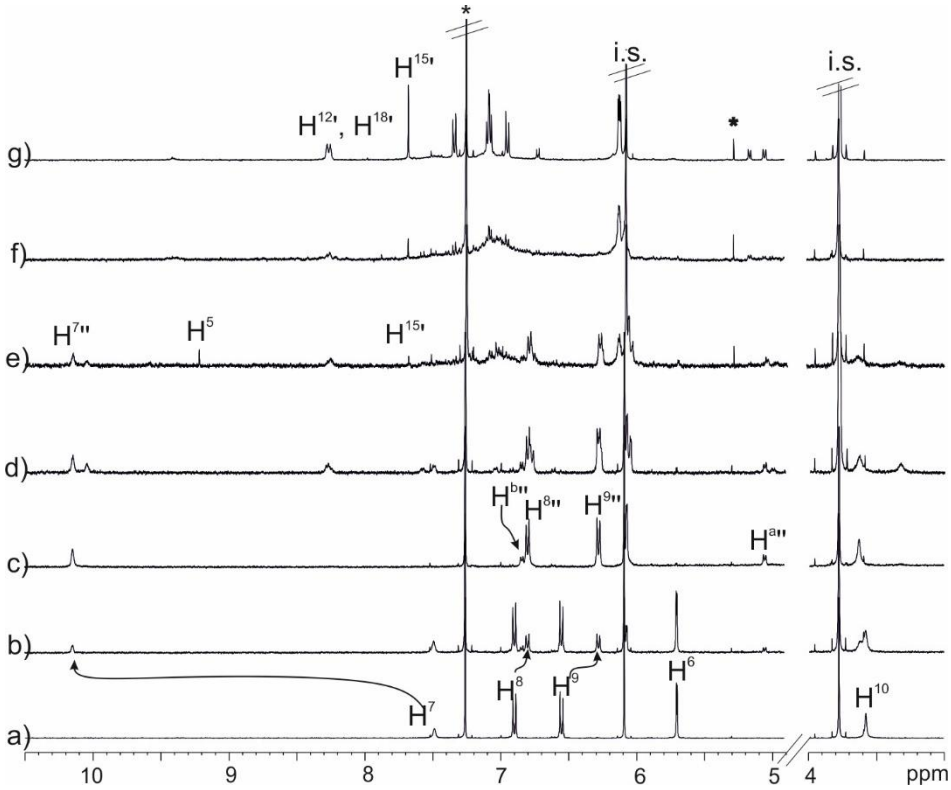

Figure 2.33. Selected region of [1]H NMR (400 MHz, at 298 K, $CDCl_3$) titration of a 1 mM solution of (a) tetra-amino calix[4]pyrrole **3** upon addition of (b) ca. 0.2 equiv. of **5**; (c) ca.0.6 equiv. of **5**; (d) ca.0.8 equiv. of **5**; (e) ca.1 equiv. of **5** and ca. 0.5 equiv. of **1**; (f) ca. 1.2 equiv. of **1**; (g) ca. 1.2 equiv. of **1** after 24h (imine cage complex **5⊂6**); (h) **5**. Primed letters indicate the bound host and guest in the 1:1 cage complex, double primed letters indicate the bound host and guest in the 2:1 dimeric complex. See Figure 2.29 for protons assignment. (*) Indicates the residual solvents.

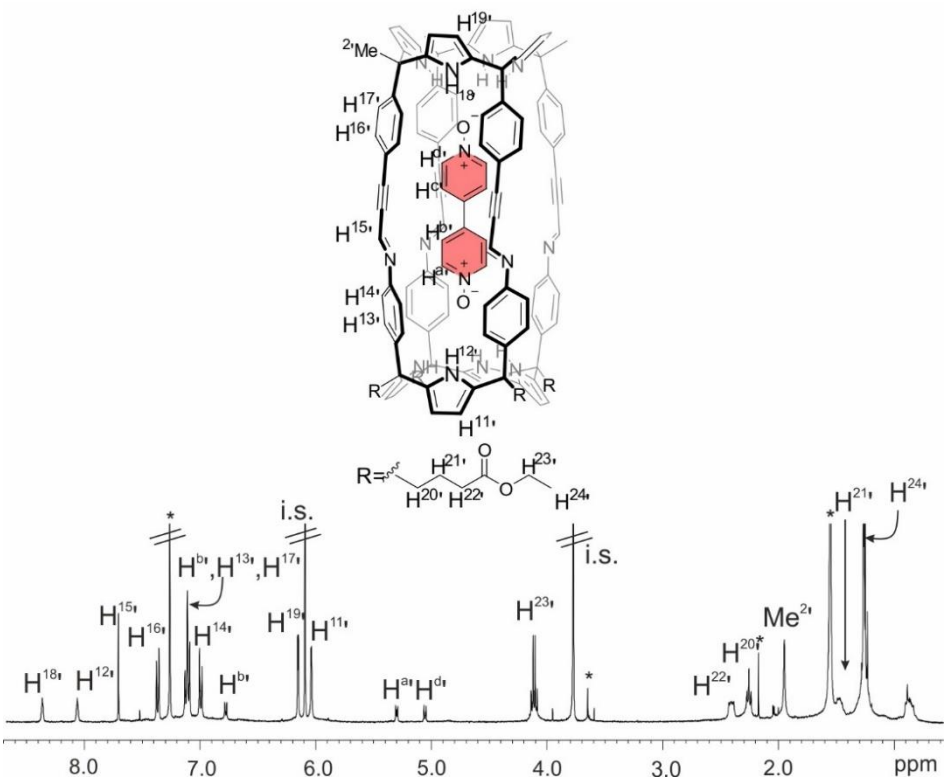

Figure 2.34. ^{1}H NMR spectrum (400 MHz, at 298 K, $CDCl_3$) of solution containing imine cage complex **5⊂7**. (*) Indicates residual solvents.

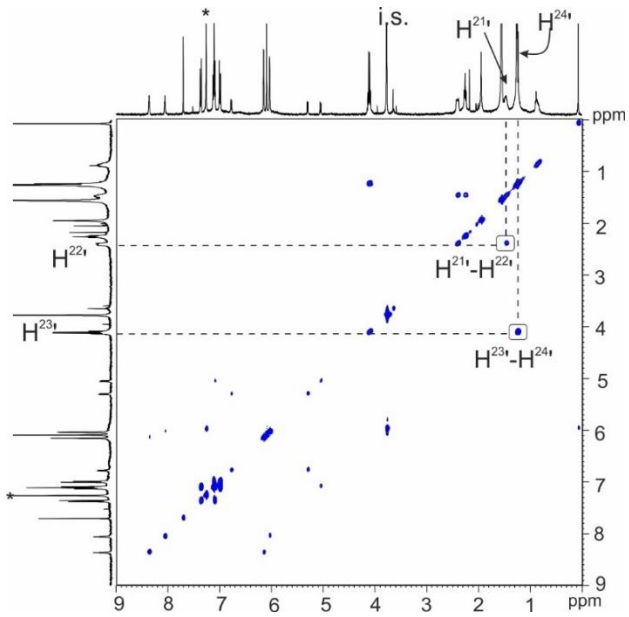

Figure 2.35.2D COSY NMR (400 MHz, at 298 K, $CDCl_3$) of a solution containing imine cage complex **5⊂7**. See Figure 2.34 for protons assignment. (*) Indicates the residual solvents.

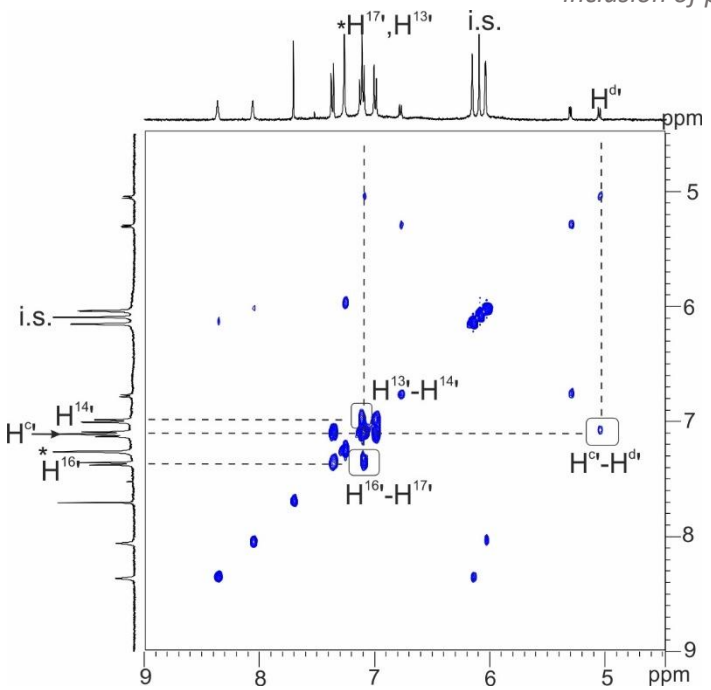

Figure 2.36. Selected region of 2D COSY NMR (400 MHz, at 298 K, $CDCl_3$) of a solution containing imine cage complex **5⊂7**. See Figure 2.34 for protons assignment. (*) Indicates the residual solvents.

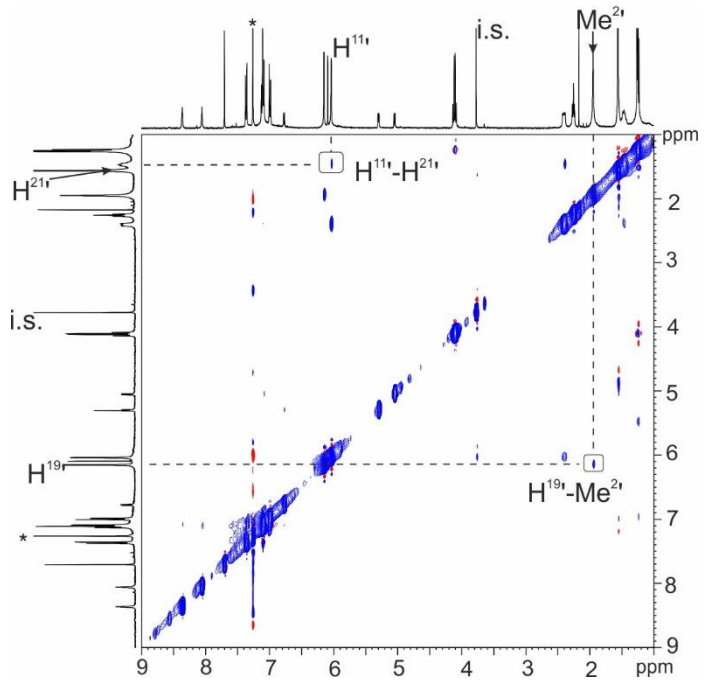

Figure 2.37. 2D NOESY NMR (400 MHz, at 298 K, $CDCl_3$, d_8= 0.3 s) of a solution containing imine cage complex **5⊂7**. See Figure 2.34 for protons assignment. (*) Indicates the residual solvents.

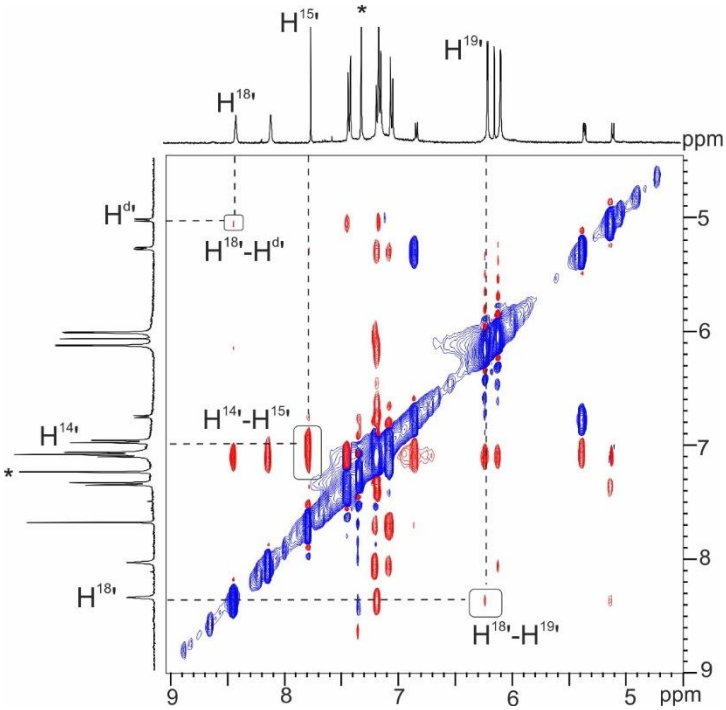

Figure 2.38. Selected region of 2D ROESY NMR (400 MHz, at 298 K, $CDCl_3$, p15= 0.3 s) of a solution containing imine cage complex **5⊂7**. See Figure 2.34 for protons assignment. (*) Indicates the residual solvents.

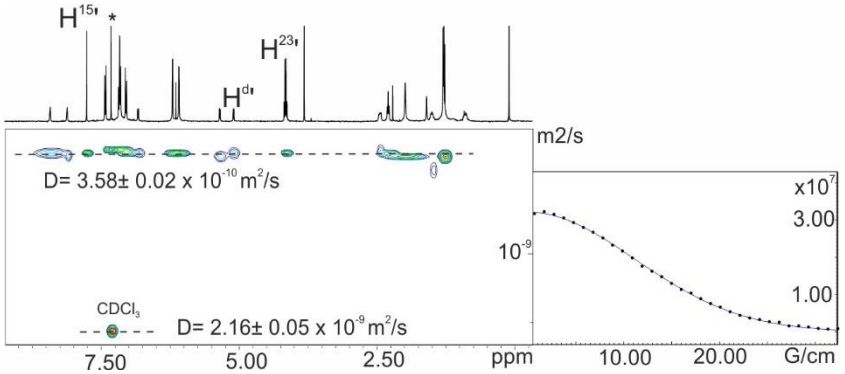

Figure 2.39. ^1H pseudo-2D DOSY NMR (400 MHz, at 298 K, $CDCl_3$, big delta 0.1 s, little delta 0.002 s) of a solution containing imine cage complex **5⊂7**. See Figure 2.34 for protons assignment. (*) Indicates the residual solvents.

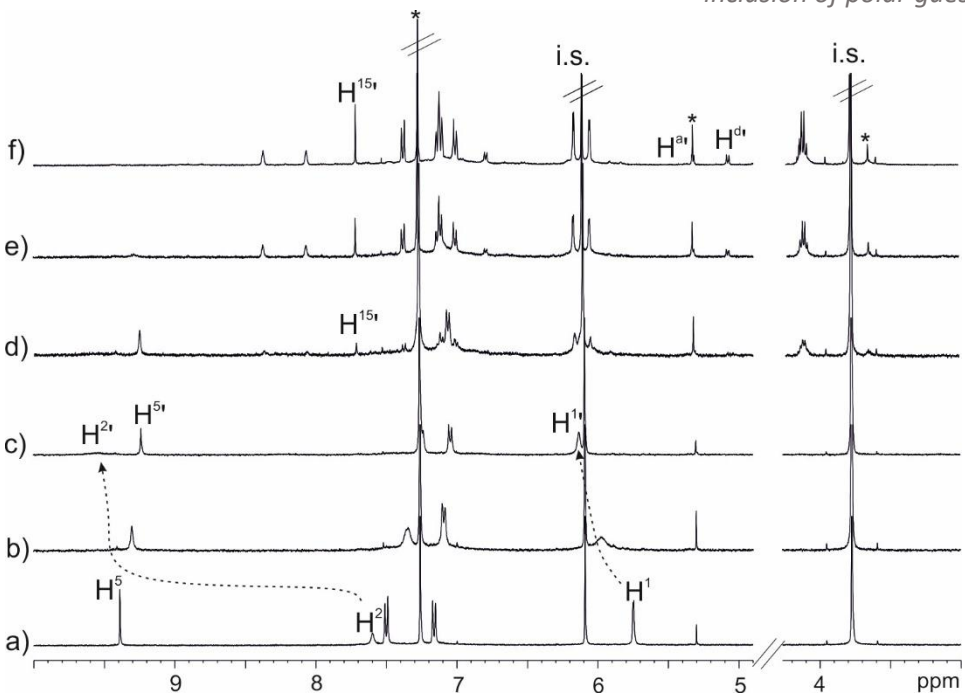

Figure 2.40. Selected region of ^{1}H NMR (400 MHz, $CDCl_3$, 298 K) titration of a 1mM solution of (a) tetra-aldehyde calix[4]pyrrole **1**, (b) ca.0.8 equiv. of **5**; (c) ca.1 equiv. of **5**; (d) ca. 0.5 equiv. of **4**; (e) ca. 1.2 equiv. of **4** (f) after 15 h. Primed letters indicate the bound host and guest respectively. See Figure 2.34 for protons assignment. (*) Indicates the residual solvents.

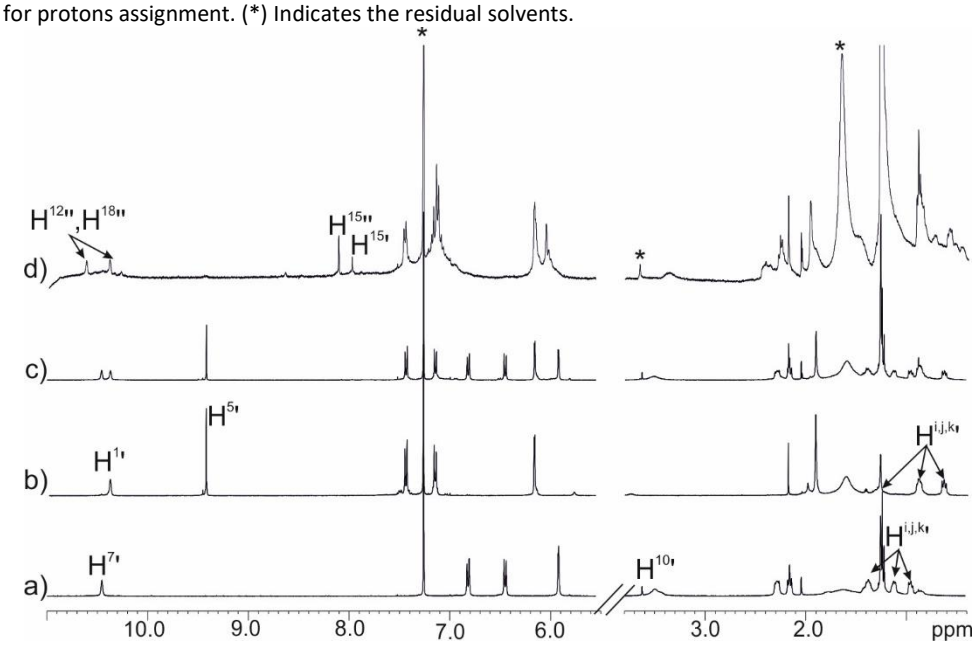

Figure 2.41. ^{1}H NMR spectra (400 MHz, at 298 K, $CDCl_3$) of (a) 1:1 complex **11⊂1**, (b) 1:1 complex **11⊂4**, (c) equimolar solution of **11⊂1** and **11⊂4** at r.t., (d) after one week at r.t. Primed letters indicate bound host and guest in the 1:1 complex; double primed letters indicate the bound host and guest in the 2:1 complex. See Scheme 2.1 for protons assignment. (*) indicates residual solvents.

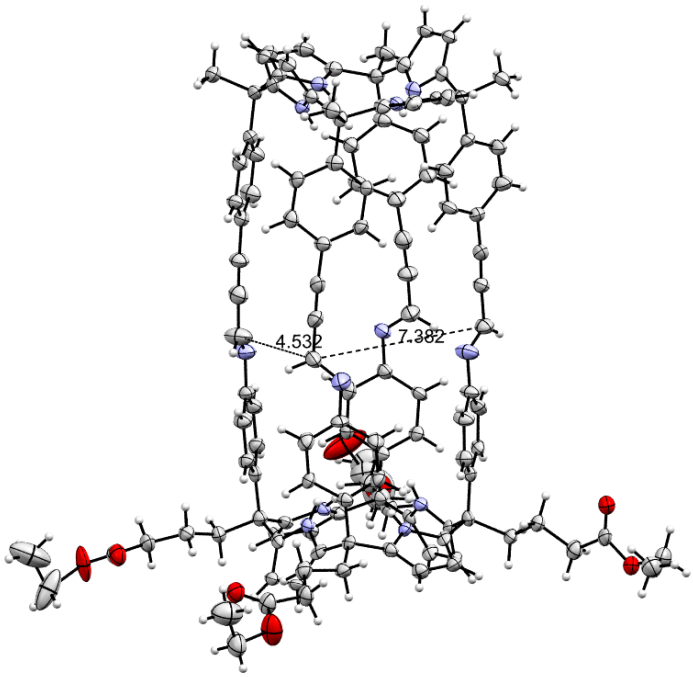

Figure 2.42. X-ray crystal structure of tetra-imine cage **7** (single crystals obtained for slow evaporation of 1,2-difluoro benzene in a $CDCl_3$:CD_3CN 9:1 equimolar mixture of calix[4]pyrroles **1** and **4**). Solvent molecules and encapsulated guest are omitted for clarity.

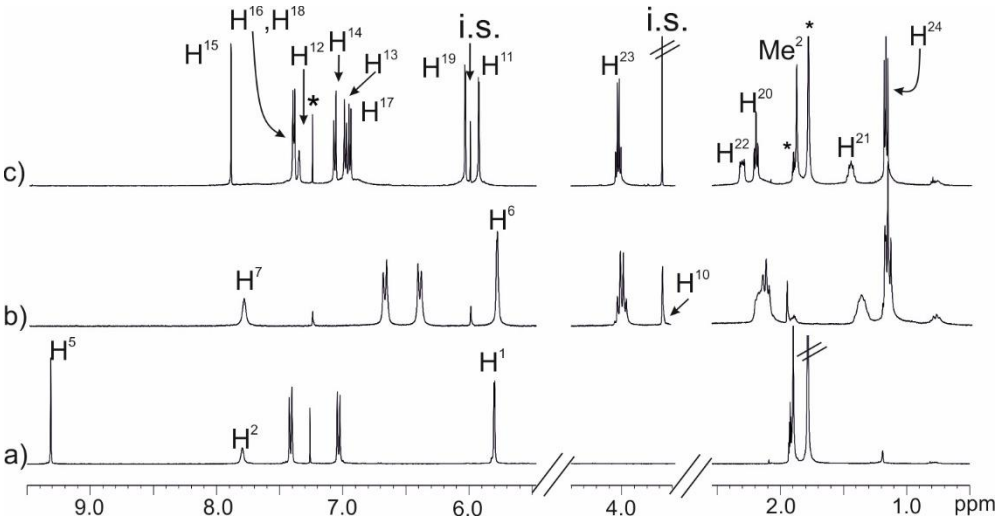

Figure 2.43. Selected regions of ^{1}H NMR spectra (400 MHz, at 298 K, $CDCl_3$:CD_3CN 9:1 mixture) of (a) **1**, (b) **4**, (c) an equimolar mixture of **1** and **4** after 24h at r.t. (imine cage **7**).See Scheme 2.1 and Figure 2.34 for protons assignment. (*) Indicates the residual solvents.

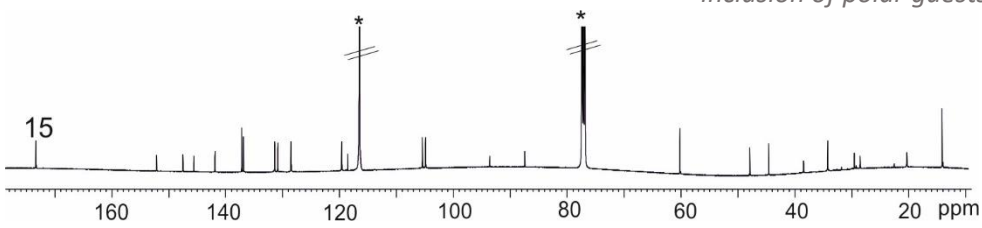

Figure 2.44. ^{13}C NMR (120 MHz with cryprobe, at 298 K, $CDCl_3$:CD_3CN 9:1 mixture) of a solution containing imine cage **7**. Imine carbon is indicated. (*) Indicates residual solvents.

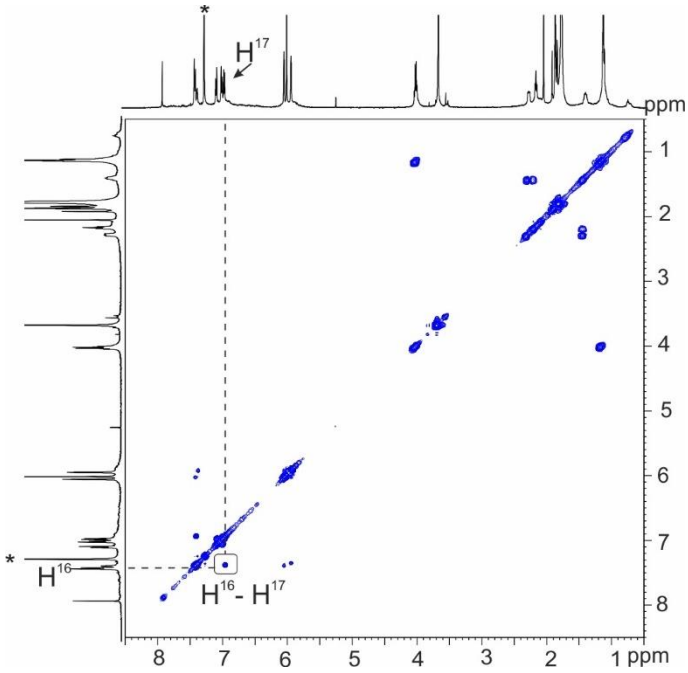

Figure 2.45. 2D COSY NMR (400 MHz, at 298 K, $CDCl_3$:CD_3CN 9:1 mixture) of a solution containing imine cage **7**. See Figure 2.34 for protons assignment. (*) Indicates residual solvents.

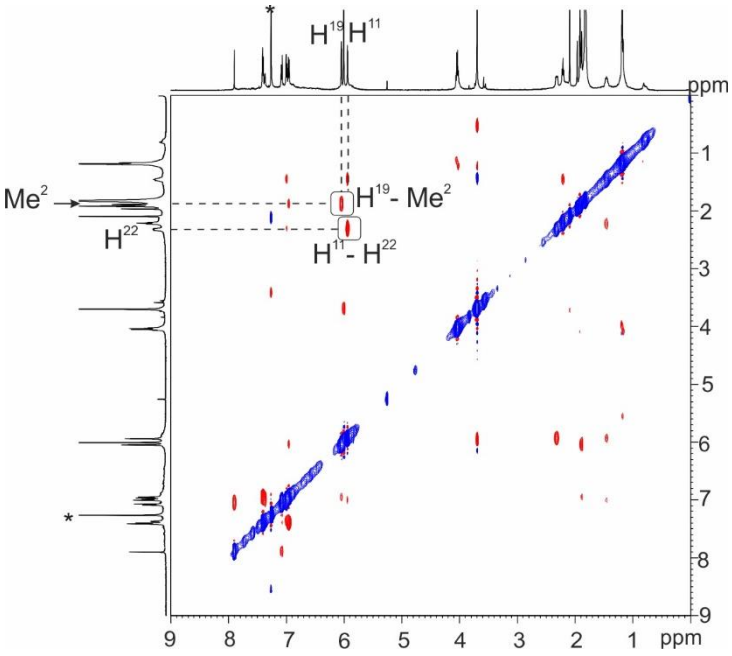

Figure 2.46. 2D ROESY NMR (400 MHz, at 298 K, $CDCl_3$:CD_3CN 9:1 mixture, p15= 0.3 s) of imine cage **7**. See Figure 2.34 for protons assignment. (*) Indicates residual solvents.

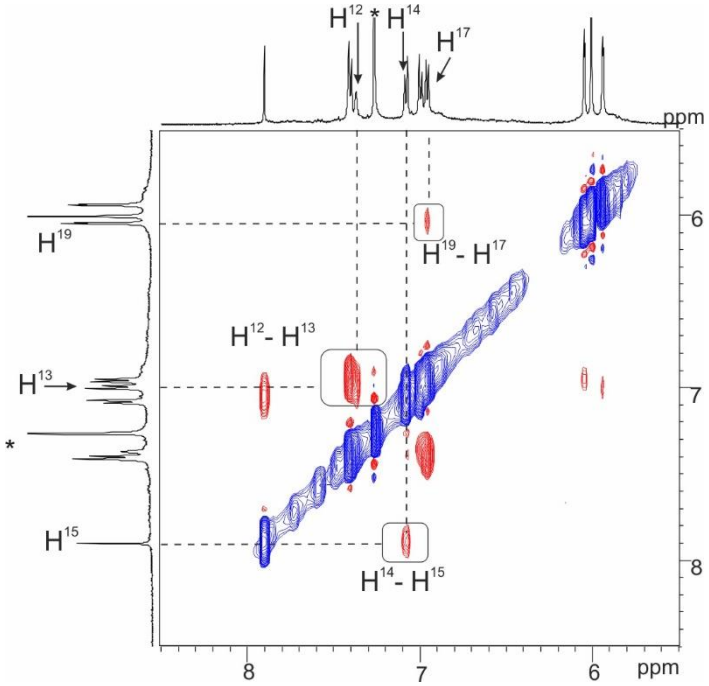

Figure 2.47. Selected region of 2D ROESY NMR (400 MHz, at 298 K, $CDCl_3$:CD_3CN 9:1 mixture, p15= 0.3 s) of imine cage **7**. See Figure 2.34 for protons assignment. (*) Indicates residual solvents.

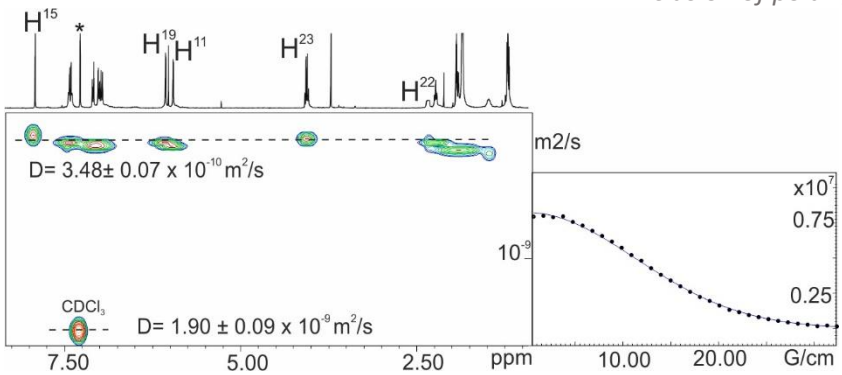

Figure 2.48. ^{1}H pseudo-2D DOSY NMR(400 MHz, at 298 K, $CDCl_3$:CD_3CN 9:1 mixture, big delta 0.1 s, little delta 0.002 s) of imine cage **7**. See Figure 2.34 for protons assignment (*) Indicates residual solvents.

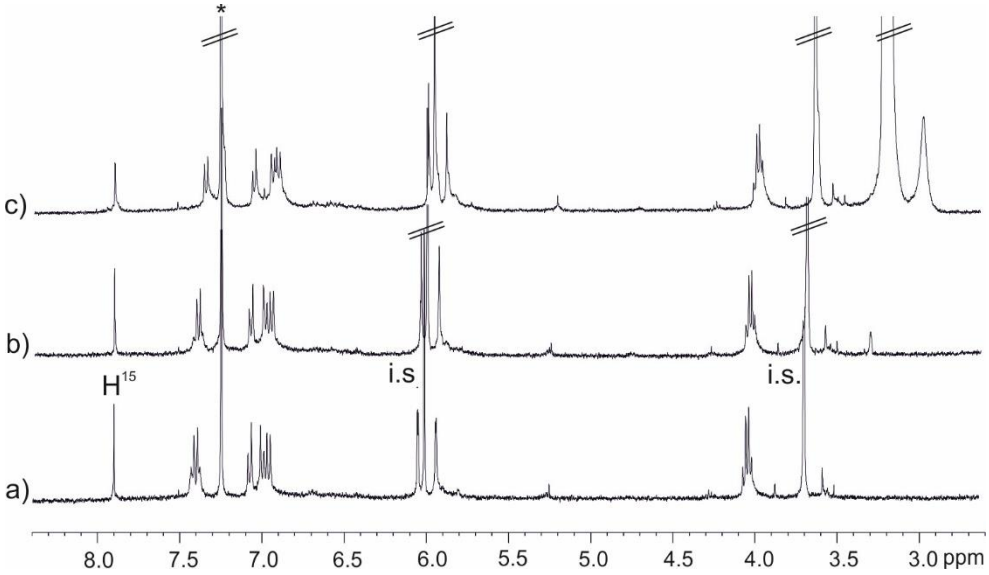

Figure 2.49. Selected regions of the ^{1}H NMR spectra (400 MHz, at 298 K, $CDCl_3$:CD_3CN 9:1 mixture) of (a) a solution containing imine cage **7**, (b) after addition of 1% of MeOH; (c) after addition of 10% of MeOH. See Figure 2.34 for protons assignment. (*) Indicates residual solvents.

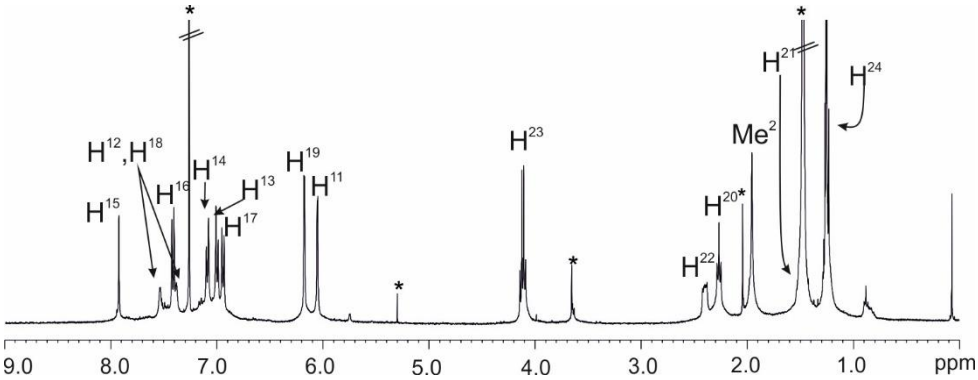

Figure 2.50. ^{1}H NMR spectrum (400 MHz, at 298 K, $CDCl_3$) of an equimolar mixture of tetra-aldehyde calix[4]pyrrole **1** and tetra-amino calix[4]pyrrole **4** after 48h at 308 K (imine cage **7**). See Scheme 2.1 and Figure 2.34 for protons assignment. (*) Indicates residual solvents.

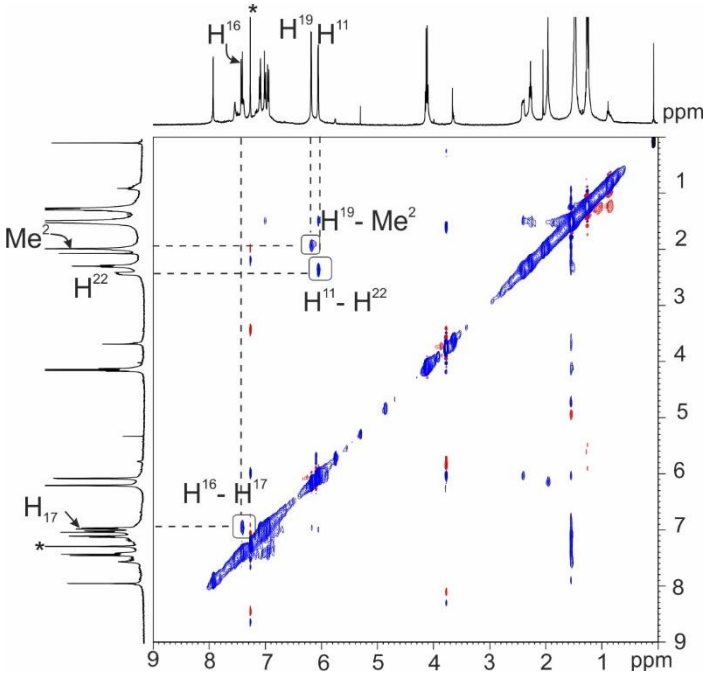

Figure 2.51. 2D NOESY NMR (400 MHz, at 298 K, $CDCl_3$, d_8= 0.3 s) of a solution containing imine cage **7**. See Figure 2.34 for protons assignment. (*) Indicates residual solvents.

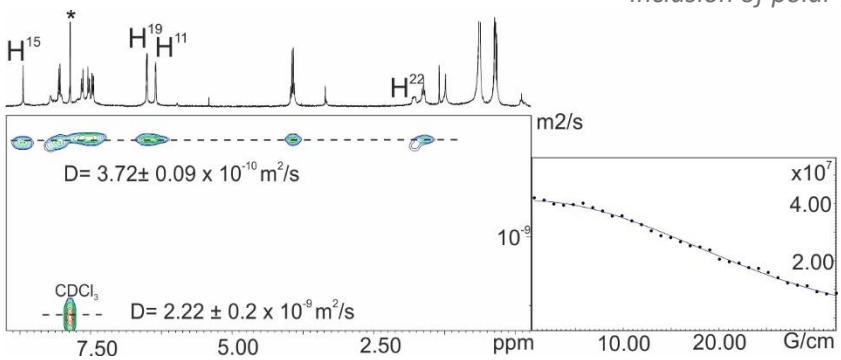

Figure 2.52. ^{1}H pseudo-2D DOSY NMR(400 MHz, at 298 K, $CDCl_3$, big delta 0.15 s, little delta 0.001 s) of a solution containing imine capsule **7**. See and Figure 2.34 for protons assignment. (*) Indicates residual solvents.

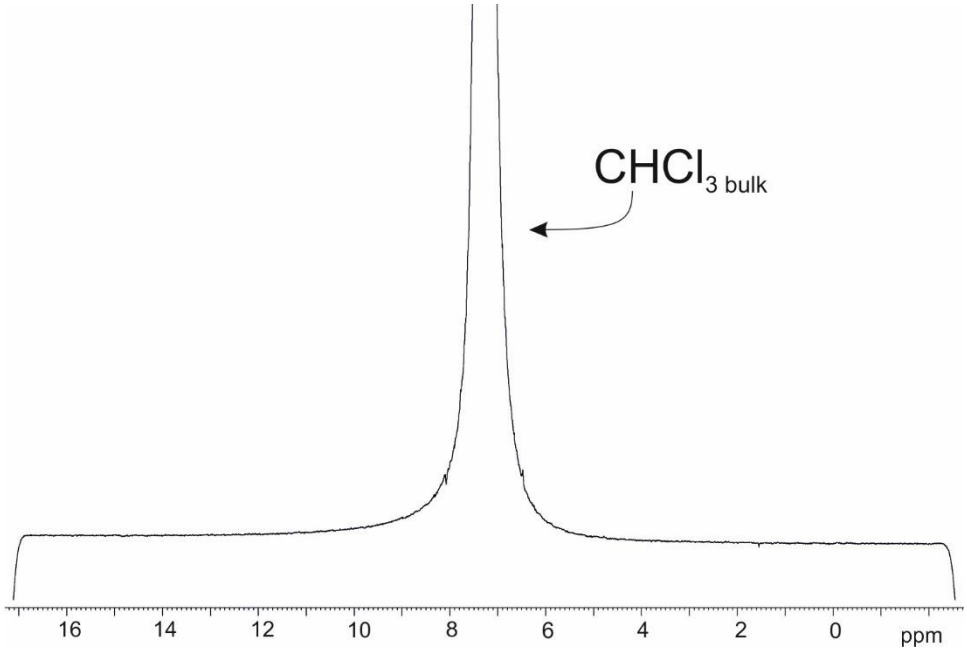

Figure 2.53. ^{1}H GOESY NMR (500 MHz, at 298 K, 9:1 $CHCl_3$:$CDCl_3$ mixture) of **7** with selective excitation at 7.28 ppm (signal of the bulk solvent). The absence of exchange peaks suggest a fast exchange between the solvent molecule inside the cage and the bulk solvent.

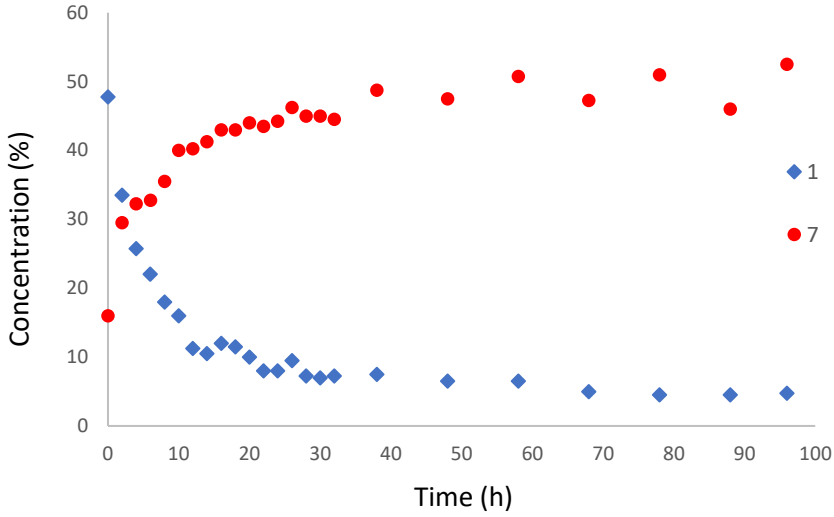

Figure 2.54. Imine capsule **7** formation by condensation between tetra-aldehyde calix[4]pyrrole **1** and tetra-amino calix[4]pyrrole **4** , as a function of time to reach the equilibrium in $CDCl_3$. The final solution is 0.6 mM.

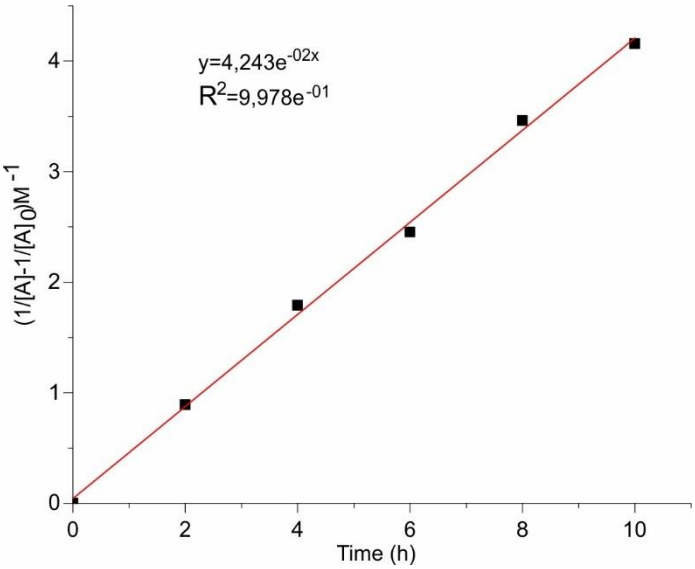

Figure 2.55. Representative linear least-squares fit ($\frac{1}{[A]} - \frac{1}{[A]0}$ vs. t) of the imine cage formation by condensation between tetra-aldehyde calix[4]pyrrole **1** and tetra-amino calix[4]pyrrole **4**, in $CDCl_3$. Kinetic studies were conducted monitoring the reaction progress at 303 K by ^1H NMR, by signal integration with respect to the signal of the I.S (1,3,5-Trimethoxy benzene), estimating an error in the integration of ±5%. Over the initial stages of reaction, when the reverse dissociation of the imine bonds could be ignored, the time dependence of the concentrations provided a good fit to simple second order kinetics.

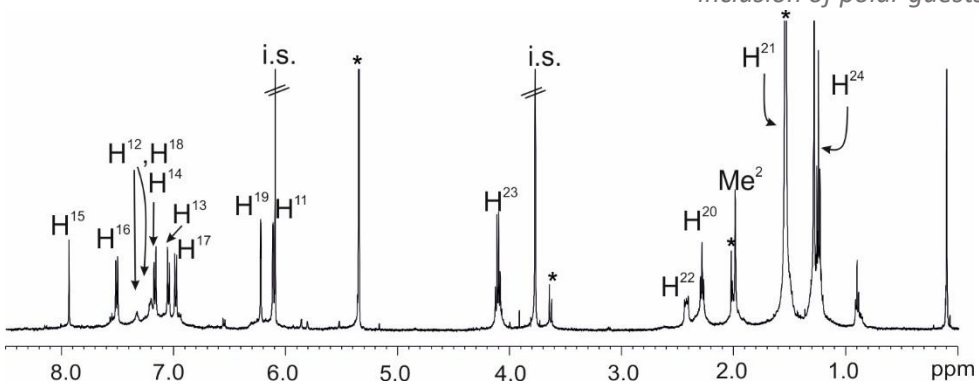

Figure 2.56. ^{1}H NMR spectrum (400 MHz, at 298 K, CD_2Cl_2) of an equimolar mixture of **1** and **4** after 72h at 303 K (imine cage **7**). See Scheme 2.1 and Figure 2.34 for protons assignment. (*) Indicates residual solvents.

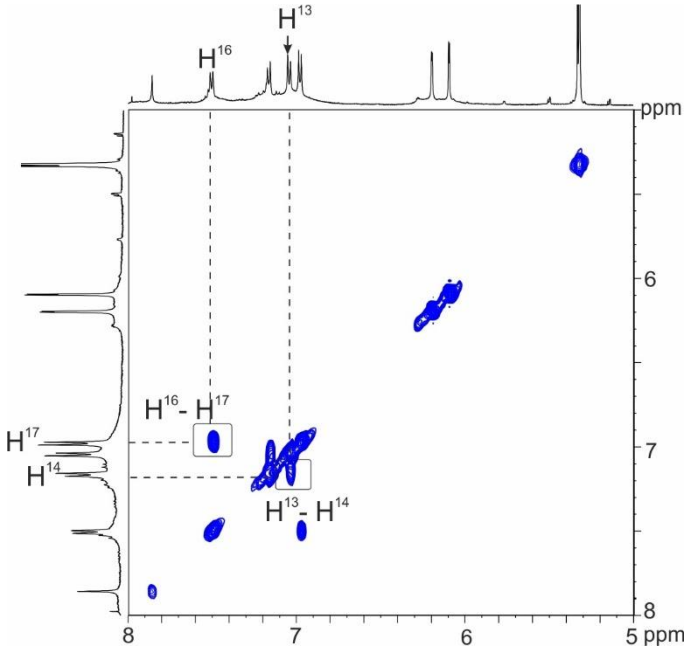

Figure 2.57. Selected region of 2D COSY NMR (400 MHz, at 298 K, CD_2Cl_2) of a solution containing imine cage **7**. See Figure 2.34 for protons assignment. (*) Indicates residual solvents.

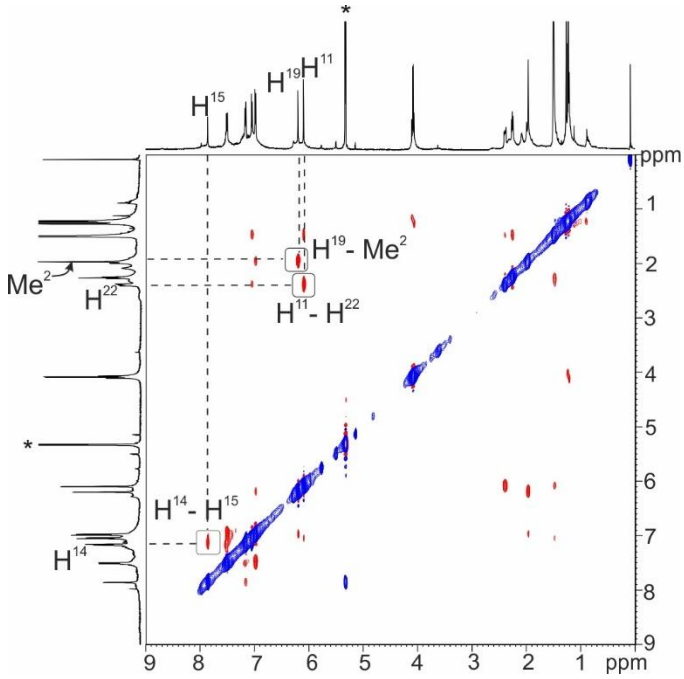

Figure 2.58. Selected region of 2D ROESY NMR (400 MHz, at 298 K, CD_2Cl_2, p15= 0.3 s) of a solution containing imine cage **7**. See Figure 2.34 for protons assignment. (*) Indicates residual solvents.

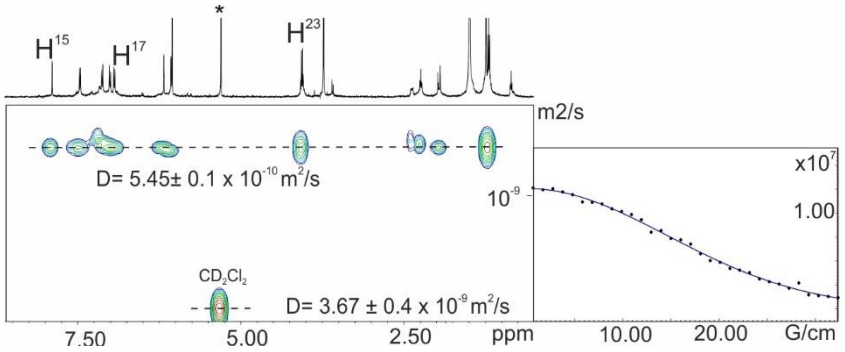

Figure 2.59. ^{1}H pseudo-2D DOSY NMR(400 MHz, at 298 K, CD_2Cl_2 , big delta 0.15 s, little delta 0.001 s) of a solution containing imine cage **7**. See Figure 2.34 for protons assignment. (*) Indicates residual solvents.

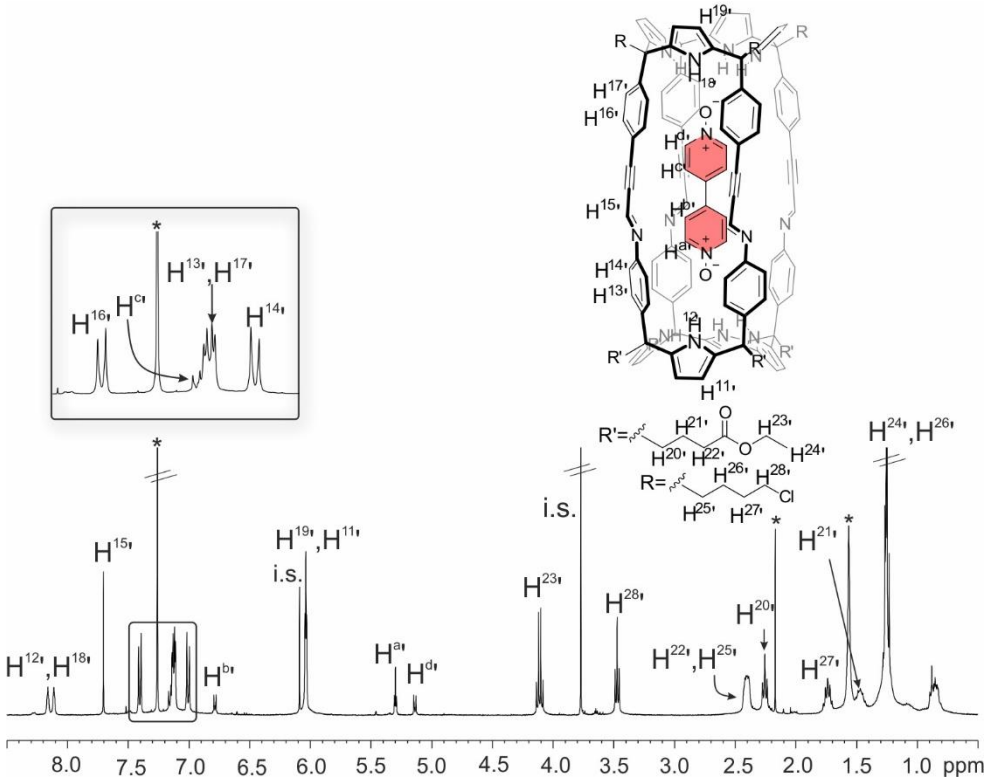

Figure 2.60. ^{1}H NMR spectrum (400 MHz, at 298 K, $CDCl_3$) of a 1:1:1 equimolar mixture of tetra-aldehyde calix[4]pyrrole **2**, tetra-amino calix[4]pyrrole **4** and **5** after 12h at r.t. (imine cage complex **5⊂8**). (*) Indicates residual solvents.

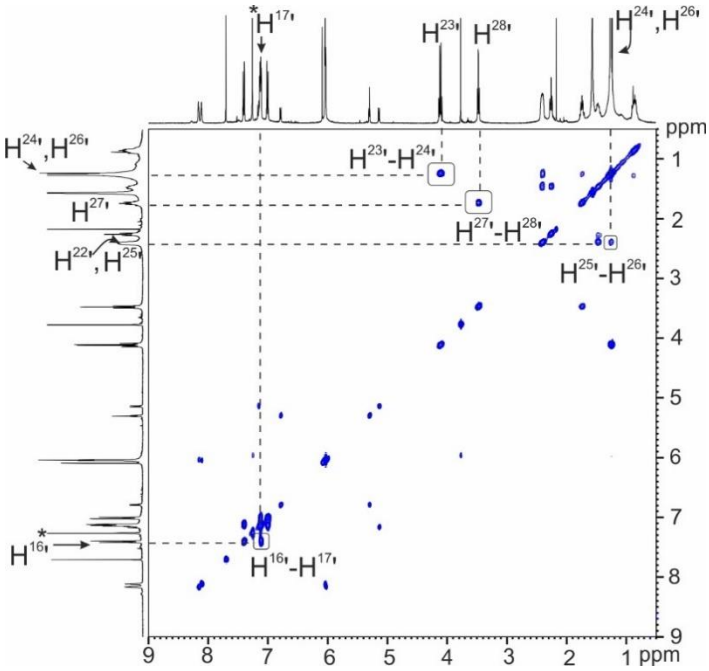

Figure 2.61. 2D COSY NMR (400 MHz, at 298 K, $CDCl_3$) of a solution containing imine cage complex **5⊂8**. See Figure 2.60 for protons assignment. (*) Indicates residual solvents.

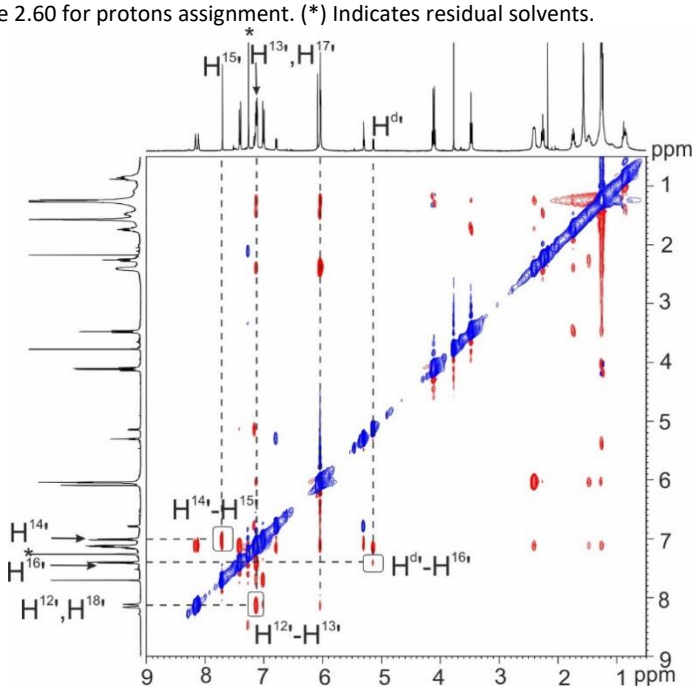

Figure 2.62. 2D ROESY NMR (400 MHz, at 298 K, $CDCl_3$, p15= 0.3 s) of a solution containing imine cage complex **5⊂8**. See Figure 2.60 for protons assignment. (*) Indicates residual solvents.

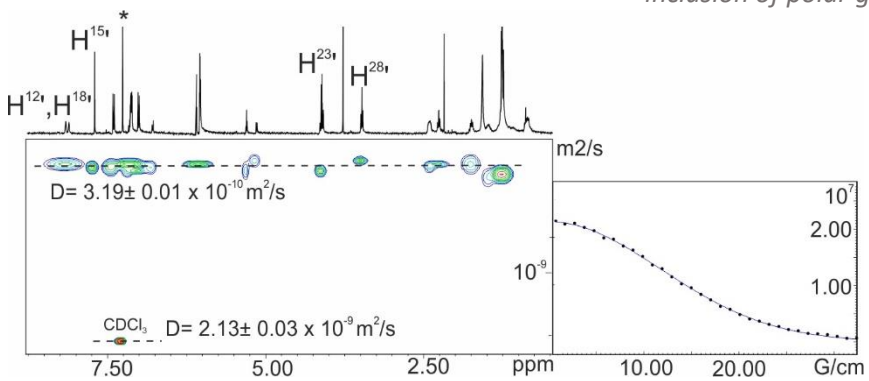

Figure 2.63. ^{1}H pseudo-2D DOSY NMR (400 MHz, at 298 K, $CDCl_3$, big delta 0.1 s, little delta 0.002 s) of a solution containing imine cage complex **5⊂8**. See Figure 2.60 for protons assignment. (*) Indicates residual solvents.

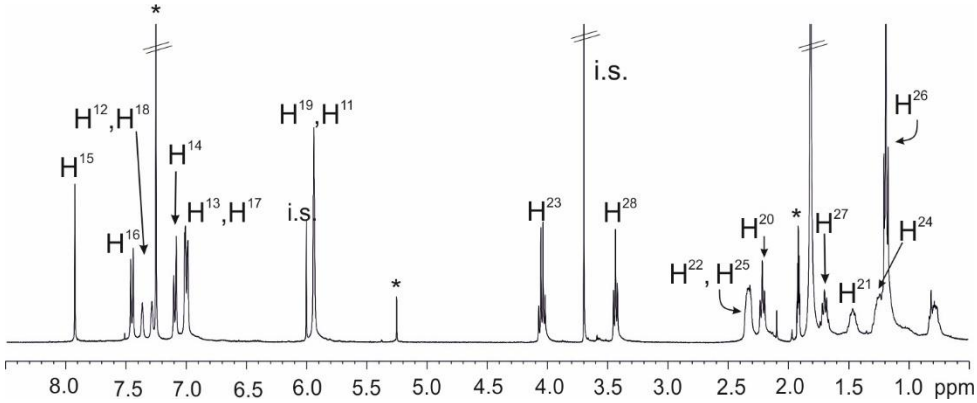

Figure 2.64. ^{1}H NMR spectrum (400 MHz, at 298 K, $CDCl_3$:CD_3CN 9:1 mixture) of a 1:1 equimolar mixture of tetra-aldehyde calix[4]pyrrole **2** and tetra-amino calix[4]pyrrole **4** after 12h at r.t. (imine cage **8**). See Figure 2.60 for protons assignment. (*) Indicates residual solvents.

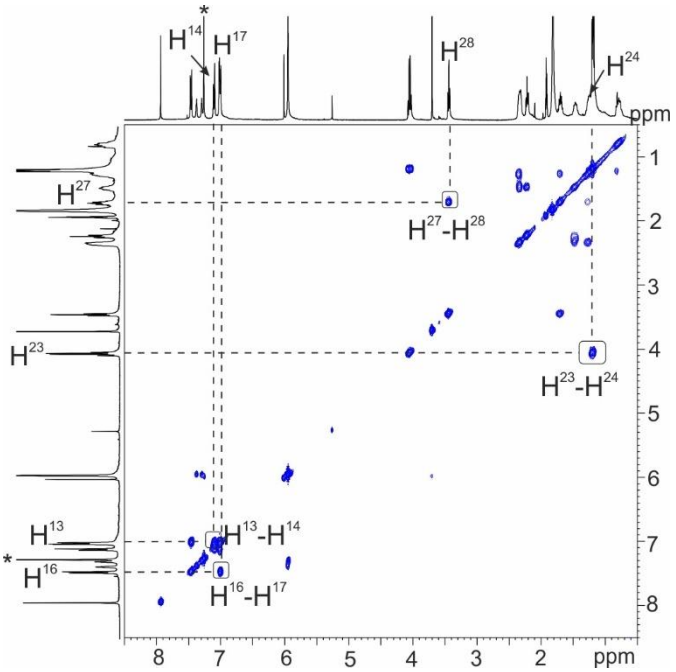

Figure 2.65. 2D COSY NMR (400 MHz, at 298 K, $CDCl_3$:CD_3CN 9:1 mixture) of a solution containing imine cage **8**. See Figure 2.64 for protons assignment. (*) Indicates residual solvents.

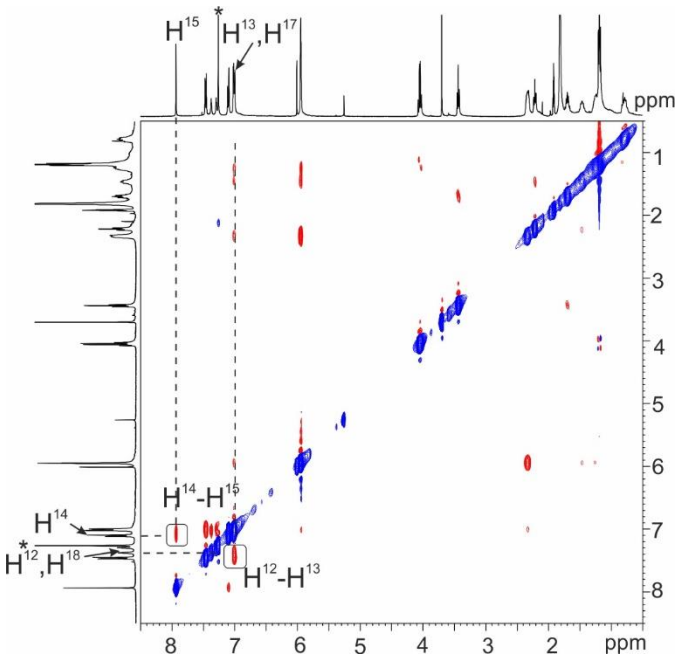

Figure 2.66. 2D ROESY NMR (400 MHz, at 298 K, $CDCl_3$:CD_3CN 9:1 mixture, p15= 0.3 s) of a solution containing imine cage **8**. See Figure 2.64 for protons assignment. (*) Indicates residual solvents.

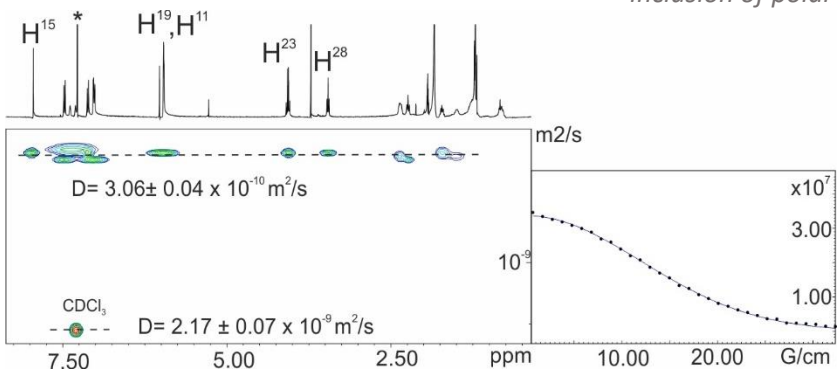

Figure 2.67. ^{1}H pseudo-2D DOSY NMR (400 MHz, at 298 K, $CDCl_3$:CD_3CN 9:1 mixture, big delta 0.1 s, little delta 0.002 s) of a solution containing imine cage **8**. See Figure 2.64 for protons assignment. (*) Indicates residual solvents.

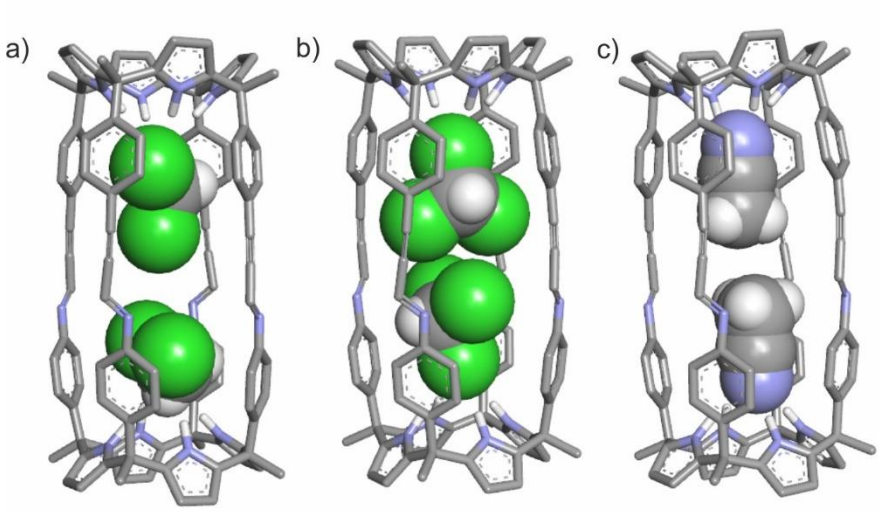

Figure 2.68. Energy minimized structures (MM3) of **7** in (a) CD_2Cl_2, (b) $CDCl_3$, (c) ACN.

Solvent	V **7**(Å^3)	V solvent (Å^3)	PC%
DCM	246	60	48
Chloroform	265	74	55
ACN	241	48	40

Table 2.2. Packing coefficient (PC%= (Vguests/Vhost)× 100) of the complex obtained from the energy minimized structure (MM3) considering the inclusion of two solvent molecules. The volumes of the capsules and solvents were calculated using SwissPDB Version 4.10.

2.4.3 Binding studies

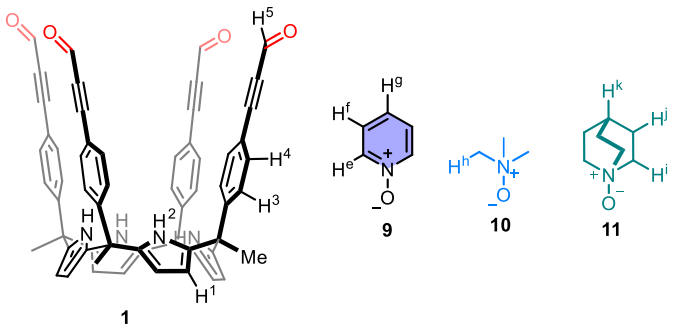

Scheme 2.3. Schematic representation of tetra aldehyde calix[4]pyrrole **1** and the *N*-oxide guests used for the binding studies

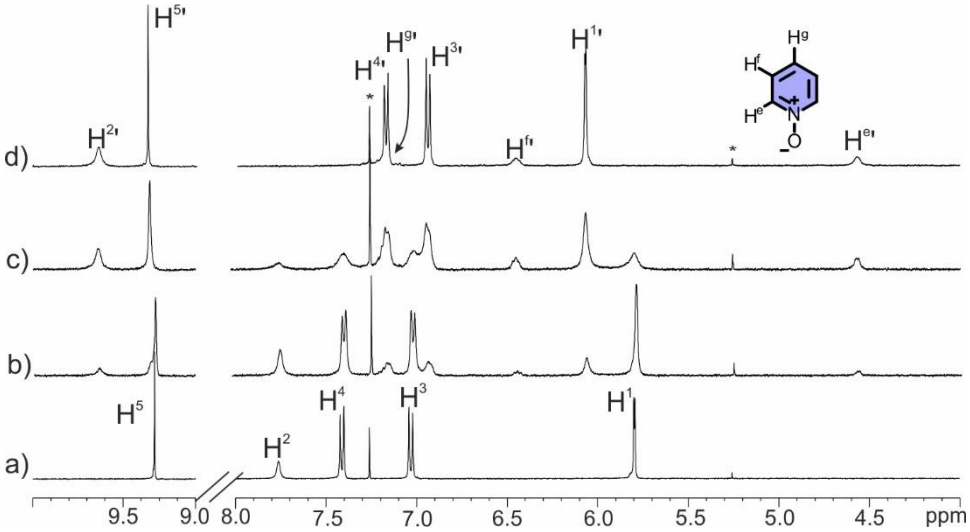

Figure 2.69. ^{1}H NMR (400 MHz, at 298 K, $CDCl_3$:CD_3CN 9:1 mixture) titration of a 2 mM solution of (a) tetra-aldehyde calix[4]pyrrole **1**, upon addition of (b) ca. 0.2 equiv. of **9**; (c) ca. 0.6 equiv. of **9**; (d) ca. 1 equiv. of **9**. Primed letters indicate the bound host and guest respectively. See Scheme 2.3 for protons assignment. (*) Indicates residual solvents. The quantitative formation of a 1:1 inclusion complex when ca. 1 equiv. of guest is added to the host solution allows to estimate a K_a larger than 10^4 M^{-1}.

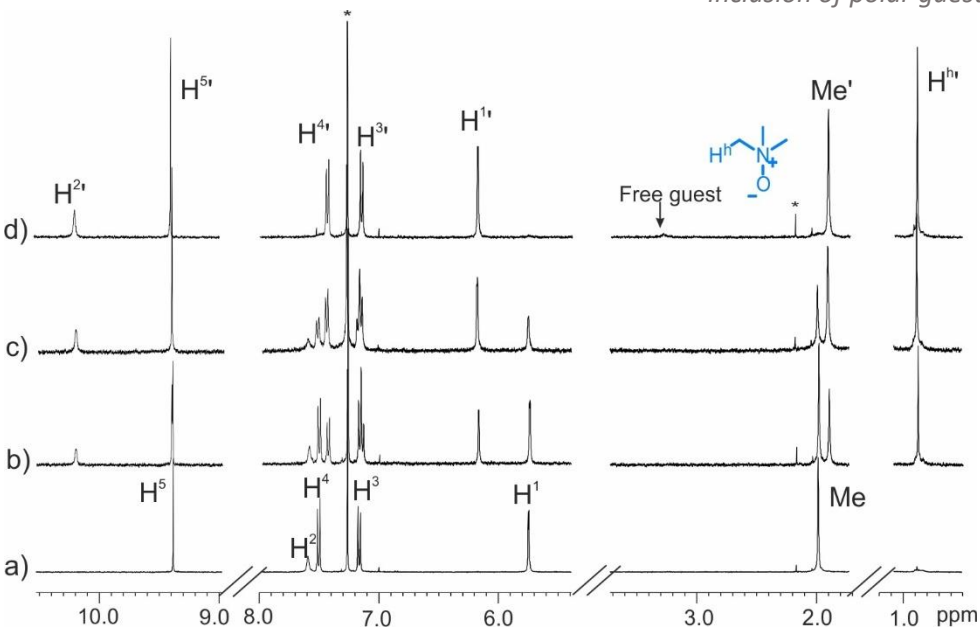

Figure 2.70. ^{1}H NMR (400 MHz, at 298 K, $CDCl_3$) titration of a 1 mM solution of (a) tetra-aldehyde calix[4]pyrrole **1**, upon addition of (b) ca. 0.4 equiv. of **10**; (c) ca. 0.8 equiv. of **10**; (d) ca. 1.1 equiv. of **10**. Primed letters indicate the bound host and guest respectively. See Scheme 2.3 for protons assignment. (*) Indicates residual solvents. The quantitative formation of a 1:1 inclusion complex when ca. 1 equiv. of guest is added to the host solution allows to estimate a K_a larger than 10^4 M^{-1}.

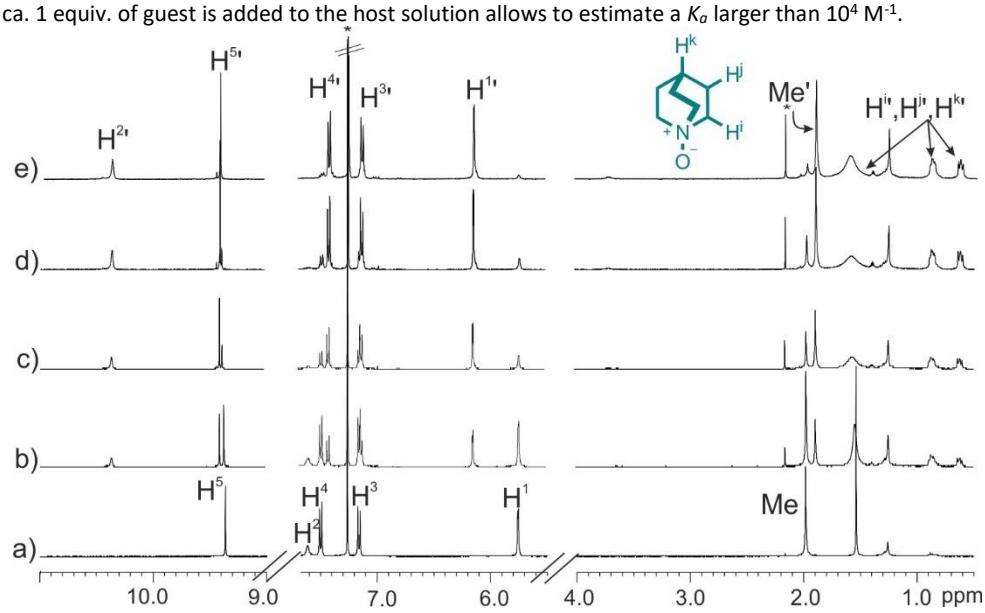

Figure 2.71. ^{1}H NMR (400 MHz, at 298 K, $CDCl_3$) titration of a 2 mM solution of (a) tetra-aldehyde calix[4]pyrrole **1**, upon addition of (b) ca. 0.4 equiv. of **11**; (c) ca. 0.8 equiv. of **11**; (d) ca.1 equiv. of **11**; (e) ca. 1.2 equiv. of **11**. Primed letters indicate the bound host and guest. See Scheme 2.3 for protons assignment. (*) Indicates residual solvents. The almost quantitative formation of a 1:1 inclusion complex when ca. 1.2 equiv. of guest are added to the host solution allows to estimate a K_a in the order of 10^4 M^{-1}.

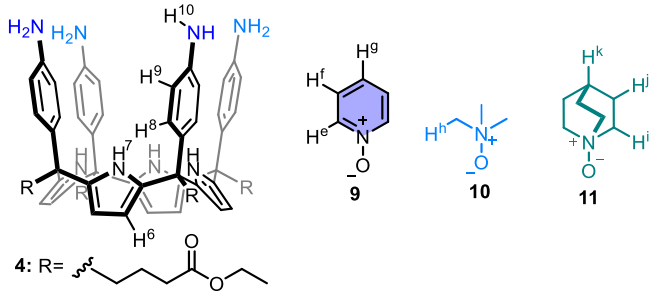

Scheme 2.4. Schematic representation of tetra aldehyde calix[4]pyrrole **1** and the *N*-oxide guests used for the binding studies.

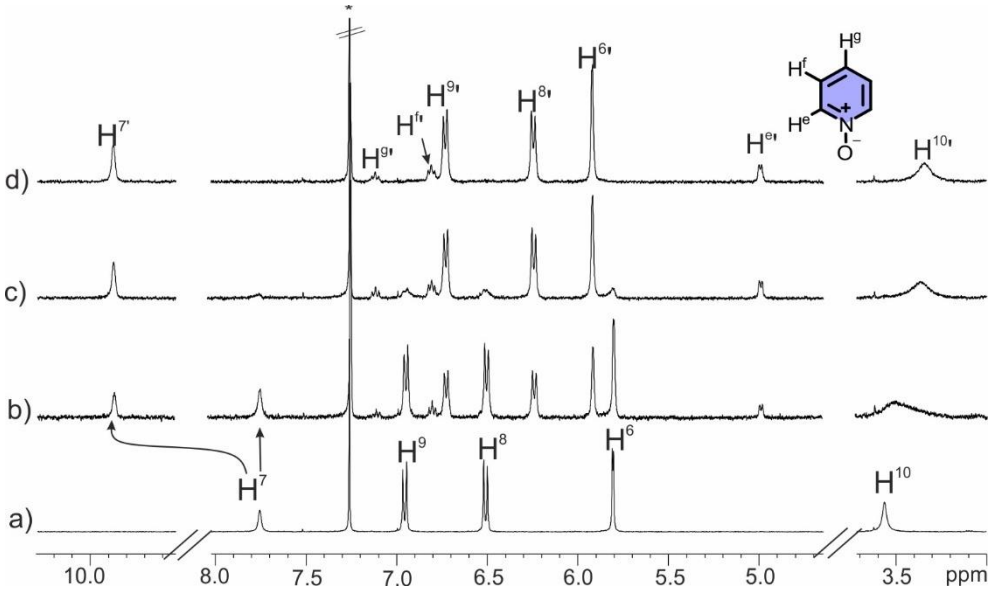

Figure 2.72. ^{1}H NMR (400 MHz, at 298 K, $CDCl_3$) titration of a 1.5 mM solution of (a) tetra-amino calix[4]pyrrole **4**, upon addition of (b) ca. 0.4 equiv. of **9**; (c) ca. 0.8 equiv. of **9**; (d) ca.1 equiv. of **9**. Primed letters indicate the bound host and guest. See Scheme 2.4 for protons assignment. (*) Indicates residual solvents. The quantitative formation of a 1:1 inclusion complex when ca. 1 equiv. of guest is added to the host solution, allows to estimate a K_a larger than 10^4 M^{-1}.

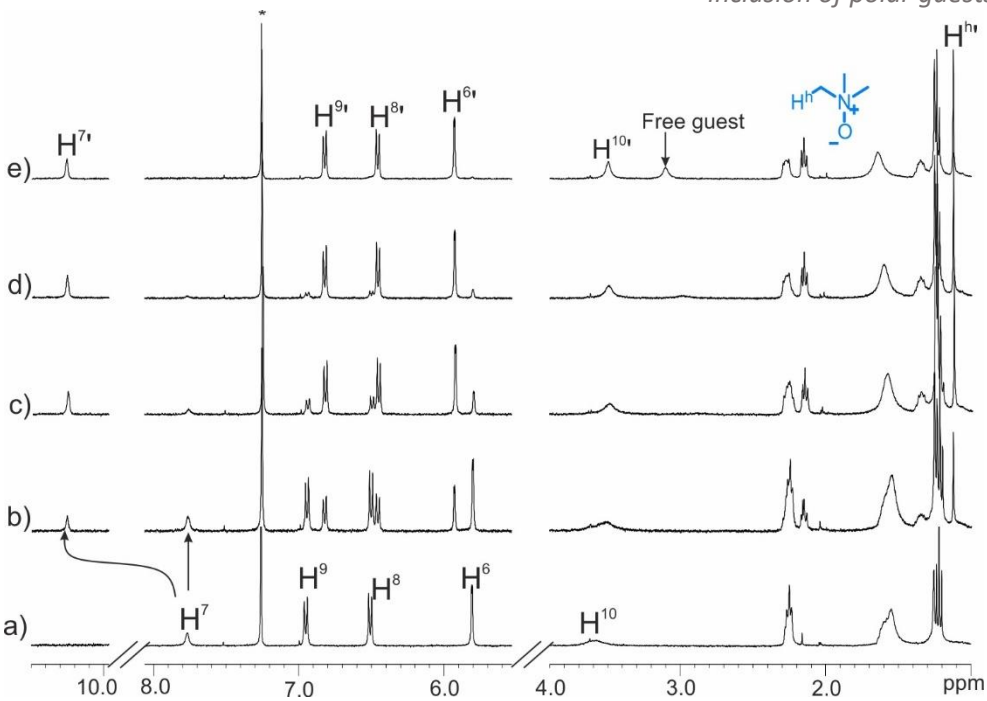

Figure 2.73. ^{1}H NMR (400 MHz, at 298 K, $CDCl_3$) titration of a 1.5 mM solution of (a) tetra-amino calix[4]pyrrole **4**, upon addition of (b) ca. 0.4 equiv. of **10**; (c) ca. 0.8 equiv. of **10**; (d) ca.1 equiv. of **10**; e) ca.1.5 equiv. of **10**. Primed letters indicate the bound host and guest. See Scheme 2.4 for protons assignment. (*) Indicates residual solvents. The almost quantitative formation of a 1:1 inclusion complex when ca. 1. equiv. of guest is added to the host solution, allows to estimate a K_a in the order of 10^4 M^{-1}.

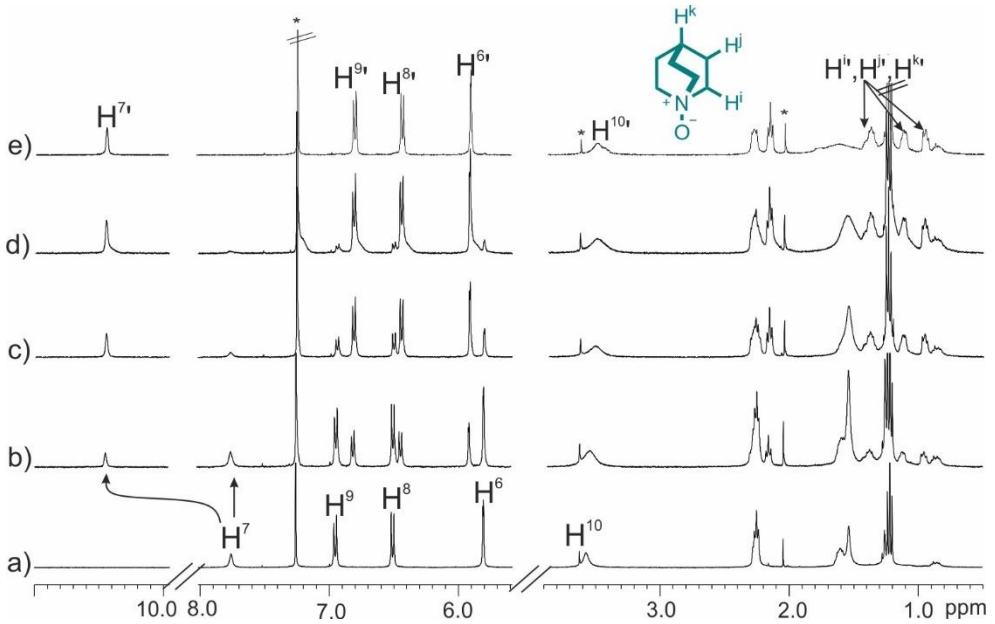

Figure 2.74. ^{1}H NMR (400 MHz, at 298 K, $CDCl_3$) titration of a 2 mM solution of (a) tetra-amino calix[4]pyrrole **4**, upon addition of (b) ca. 0.4 equiv. of **11**; (c) ca. 0.8 equiv. of **11**; (d) ca.1 equiv. of **11**; (e) ca. 1.2 equiv. of **11**; f) **11**. Primed letters indicate the bound host and guest. See Scheme 2.4 for protons assignment. (*) Indicates residual solvents. The almost quantitative formation of a 1:1 inclusion complex when ca. 1. equiv. of guest are added to the host solution allows to estimate a K_a in the order of 10^4 M^{-1}.

2.4.3.1 *Kinetic studies of inclusion of N-oxides*

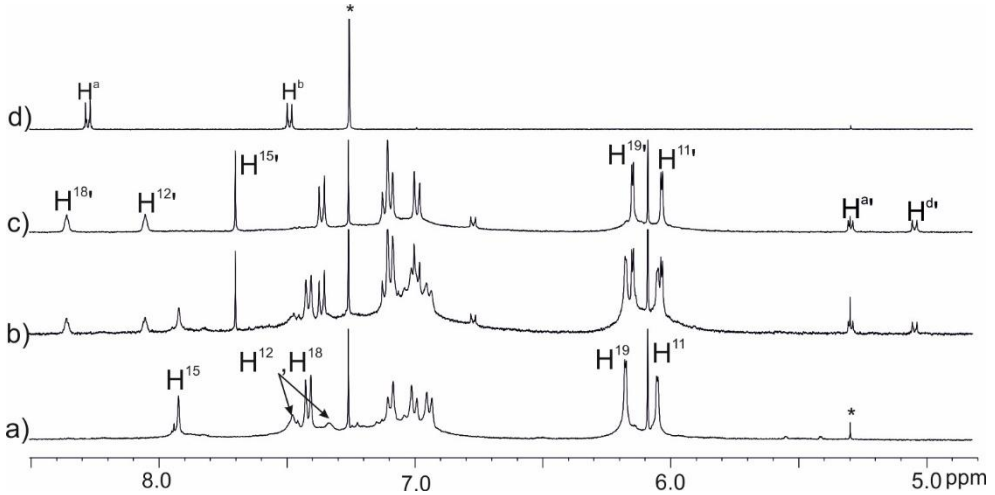

Figure 2.75. Selected ^{1}H NMR region of spectra (400 MHz, at 298 K, $CDCl_3$) of (a) a solution containing imine cage **7**, (b) immediately after addition of **5** (1 equiv.), (c) 20 min after addition of **5**, (d) **5**. Primed letters indicate the bound host and guest. See Scheme 2.1 for protons assignment. (*) Indicates residual solvents.

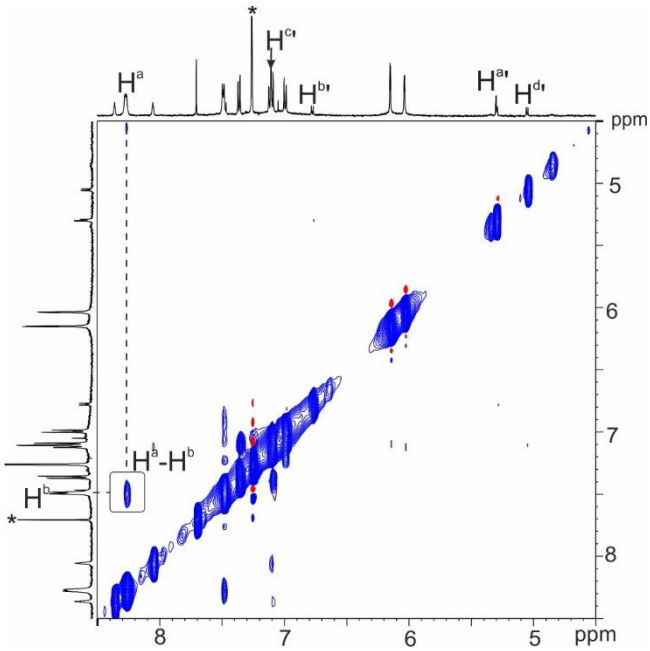

Figure 2.76. Selected region of the ^{1}H-^{1}H-EXSY NMR (400 MHz, $CDCl_3$, at 298 K, d_8= 0.3 s) of a solution containing imine cage **7** in presence of an excess of **5** (2 equiv.). The spectrum does not show cross-peaks between free and bound guest. This is indicative of a slow chemical exchange process between free and bound components on the EXSY NMR timescale. See Scheme 2.1 for protons assignment. (*) Indicates residual solvents.

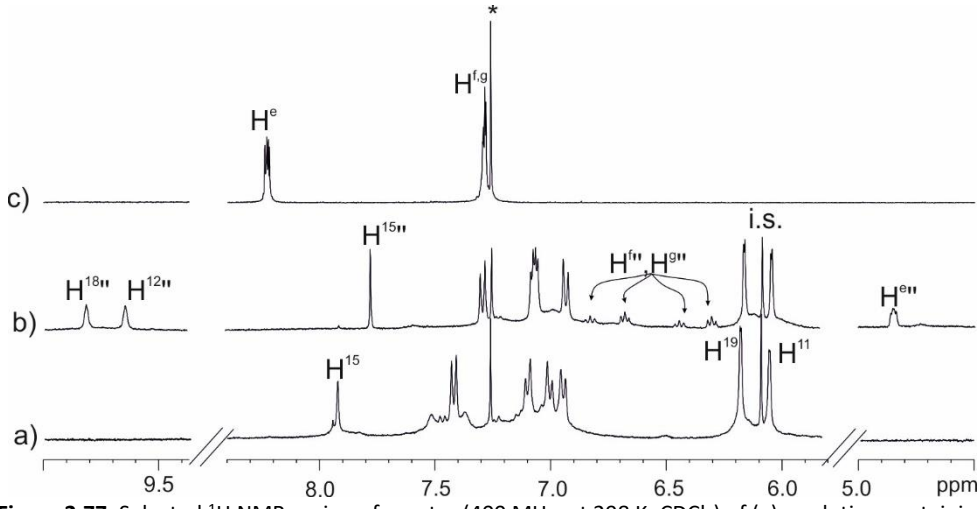

Figure 2.77. Selected ^{1}H NMR region of spectra (400 MHz, at 298 K, $CDCl_3$) of (a) a solution containing imine cage **7**, (b) immediately after addition of **9** (2 equiv.), (c) **9**. Double primed letters indicate the bound host and guest. See Scheme 2.1 for protons assignment. (*) Indicates residual solvents.

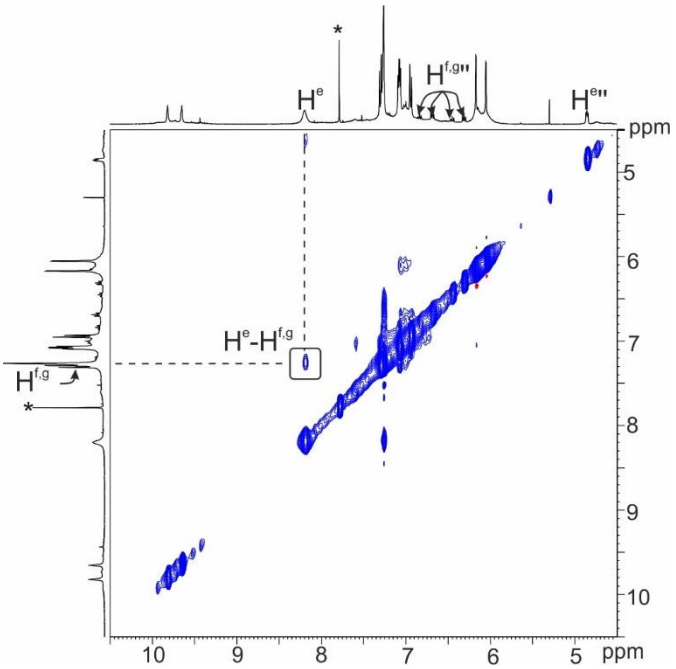

Figure 2.78. Selected region of the ^{1}H-^{1}H-EXSY NMR (400 MHz, $CDCl_3$, at 298 K, d_8= 0.3 s) solution containing imine cage **7** in presence an excess of **9** (3.5 equiv.). The spectrum does not show cross-peaks between free and bound guest. This is indicative of a slow chemical exchange process between free and bound components on the EXSY NMR timescale. See Scheme 2.1 for protons assignment. See Scheme 2.1 for protons assignment. (*) Indicates residual solvents.

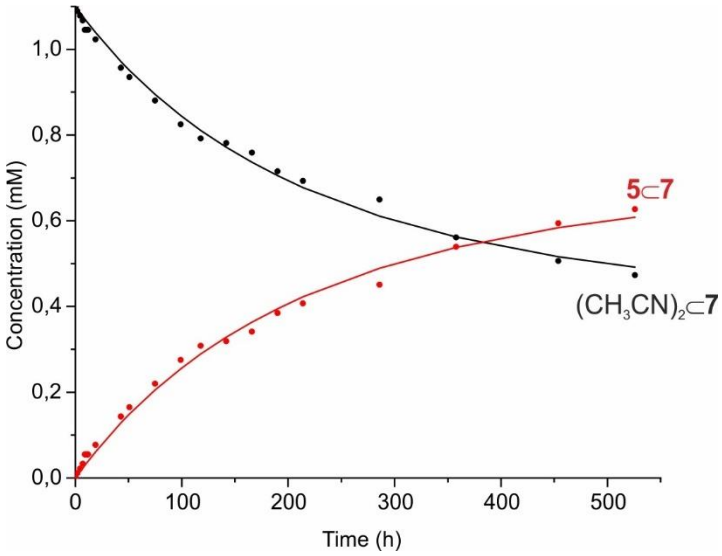

Figure 2.79. Kinetic of encapsulation of guest **5** inside capsule **7** cavity in $CDCl_3$:CD_3CN 8:2 mixture reported as mM [$(CH_3CN)_2$⊂**7**], [**5**⊂ **7**] vs time.

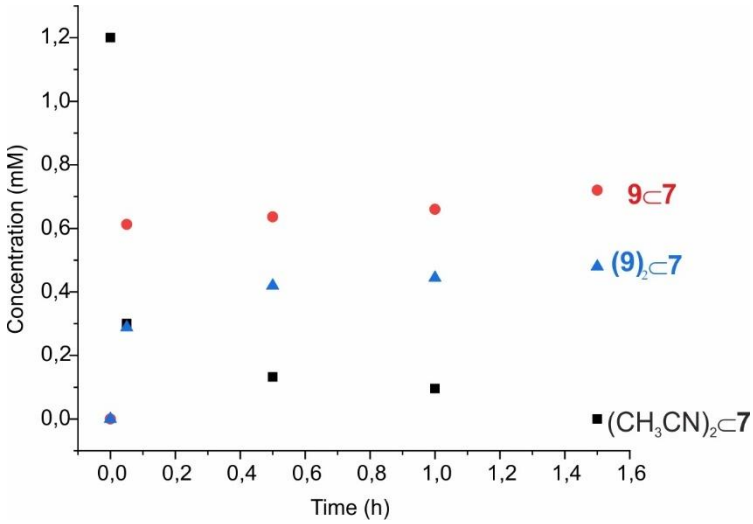

Figure 2.80. Kinetic of encapsulation of guest **9** inside capsule **7** cavity in $CDCl_3$:CD_3CN 9:1 mixture reported as mM [$(CH_3CN)_2$⊂**7**], [**9**⊂ **7**], [$(\mathbf{9})_2$⊂ **7**] vs time.

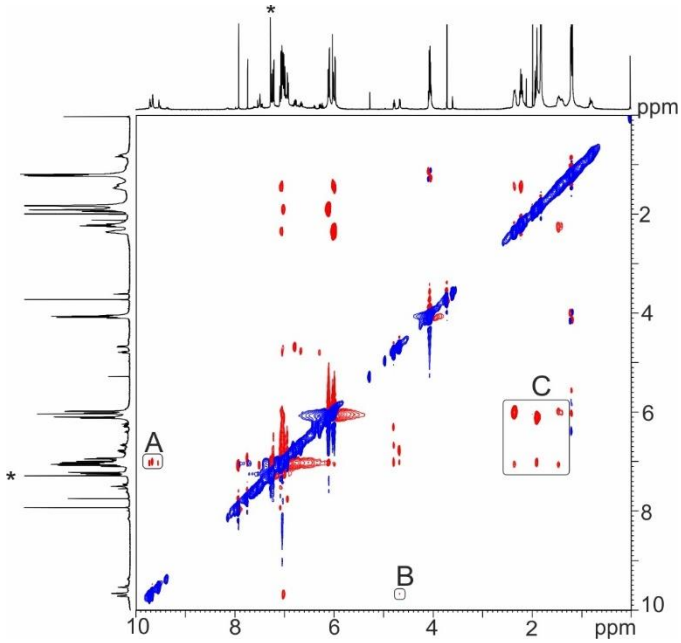

Figure 2.81. 2D ROESY NMR (400 MHz, at 298 K, $CDCl_3$:CD_3CN 9:1 mixture, p15= 0.3 s) of a solution containing imine cage **7** in presence of **9** (2 equiv.). See Scheme 2.1 for protons assignment. (*) Indicates residual solvents.

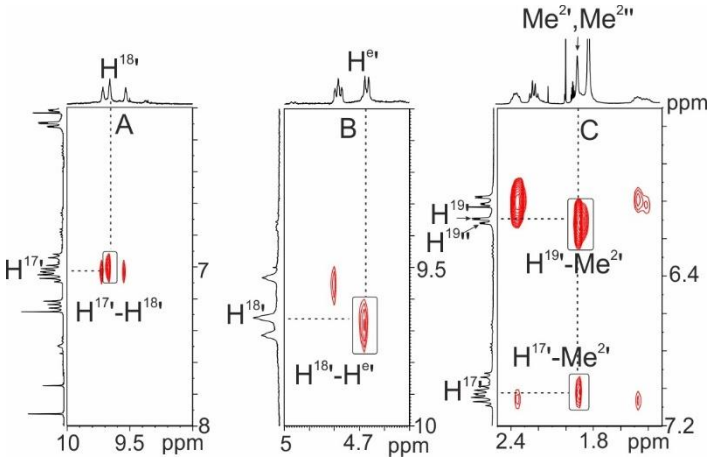

Figure 2.82. Selected region of 2D ROESY NMR (400 MHz, at 298 K, $CDCl_3$:CD_3CN 9:1 mixture, p15= 0.3 s) of a solution containing imine cage **7** in presence of **9** (2 equiv.). See Scheme 2.1 for protons assignment. (*) Indicates residual solvents.

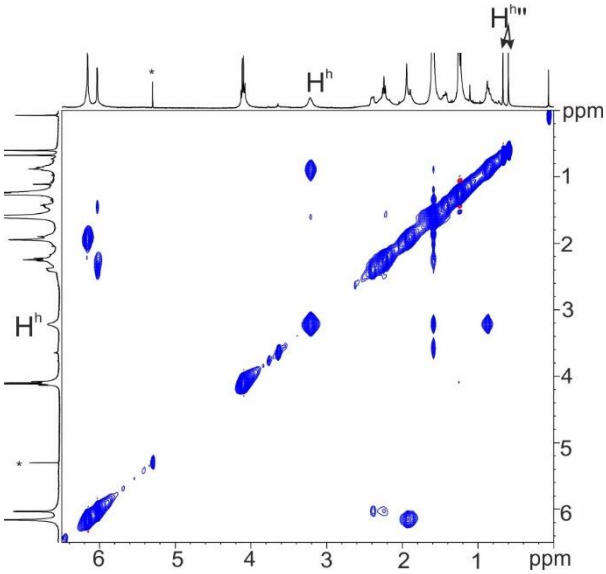

Figure 2.83. Selected region of the ^1H-^1H-EXSY NMR (400 MHz, $CDCl_3$, 298 K, d_8= 0.3 s) of a solution containing imine cage **7** in presence of **10** (3 equiv.). The spectrum does not show cross-peaks between free and bound guest. This is indicative of a slow chemical exchange process between free and bound components on the EXSY NMR timescale. See Scheme 2.1 for protons assignment. (*) Indicates residual solvents.

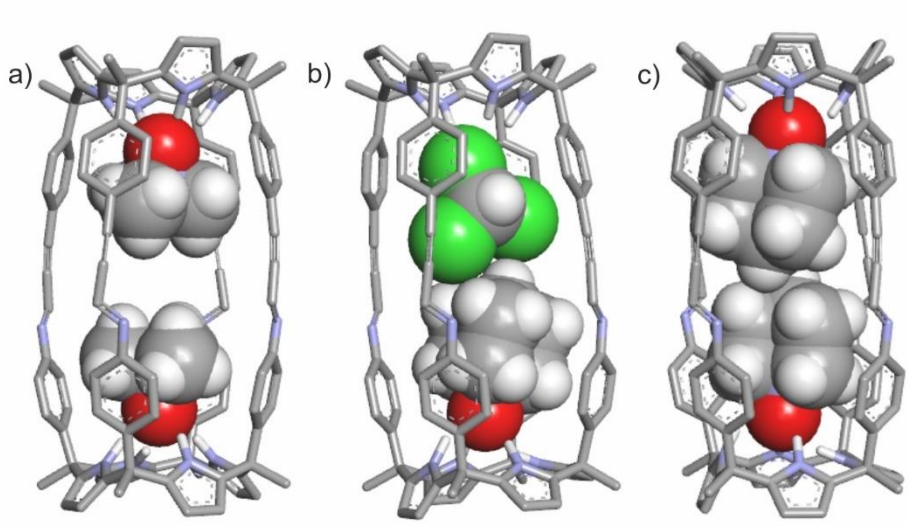

Figure 2.84. Energy minimized structures (MM3) of (a) **(10)$_2$⊂7**, (b) **11-CDCl$_3$⊂7** , (c) **(11)$_2$⊂7**.

Entry	V **7** (Å^3)	V guest(Å^3)	PC (%)
(10)$_2$⊂7	326	91	55
11⊂7	291	140	48*
(11)$_2$⊂7	357	140	78
9-ACN⊂7	284	89-40	45
(9)$_2$⊂7	294	89	60

Table 2.3. Packing coefficient (PC%= (Vguests/Vhost)× 100) of the complex obtained from the energy minimized structure (MM3). The volumes of the capsules and solvents were calculated using SwissPDB Version 4.10. *The PC% calculated considering the co-encapsulation of $CDCl_3$ returned a value of 74.

2.4.4 Characterization in gas phase

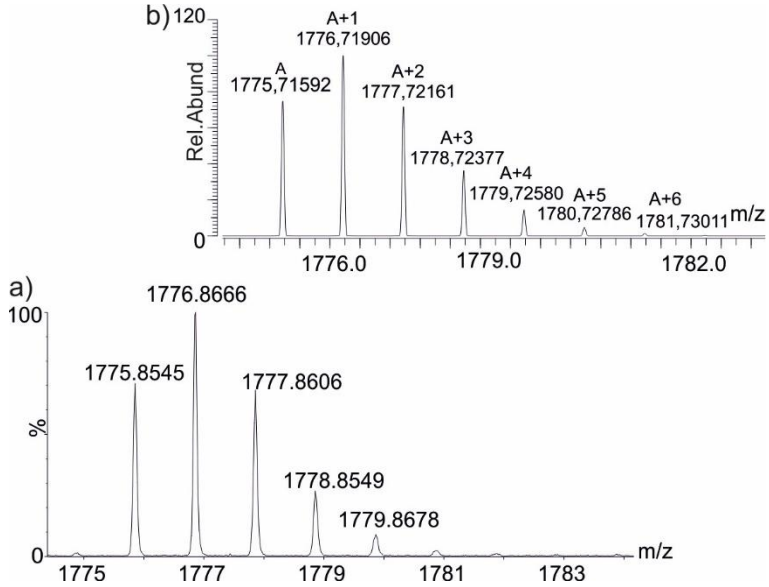

Figure 2.85. Experimental (a) and calculated (b) isotopic pattern of cage complex **[5⊂6+K]⁺.**

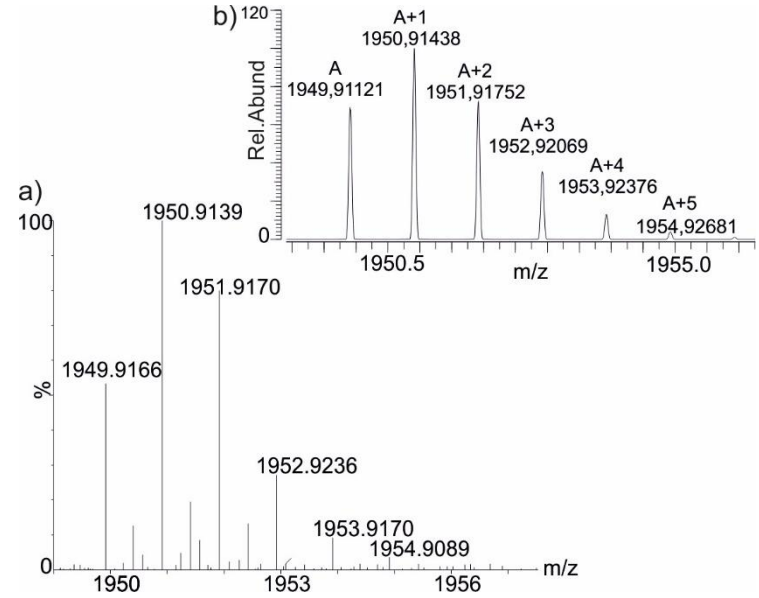

Figure 2.86. Experimental (a) and calculated (b) isotopic pattern of cage complex [**7**+H]⁺.

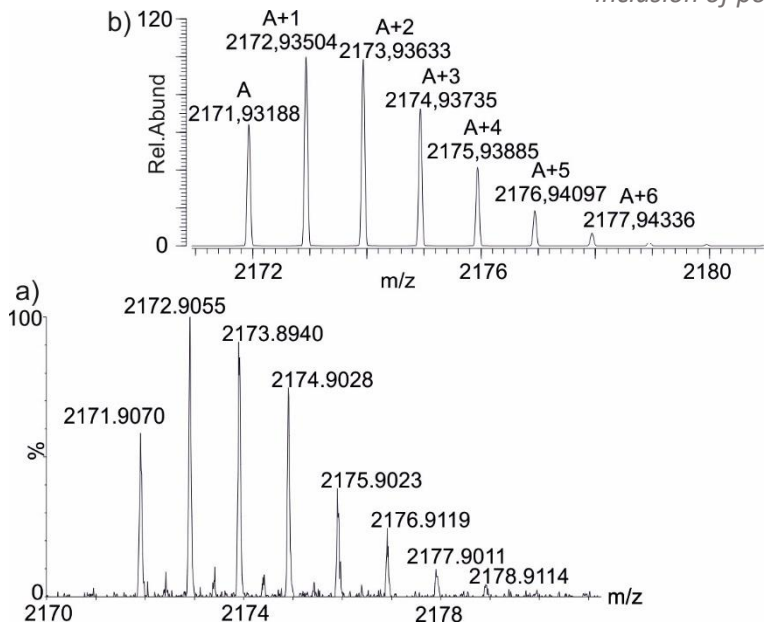

Figure 2.87. Experimental (a) and calculated (b) isotopic pattern of cage complex [**5⊂7**+Cl]$^-$.

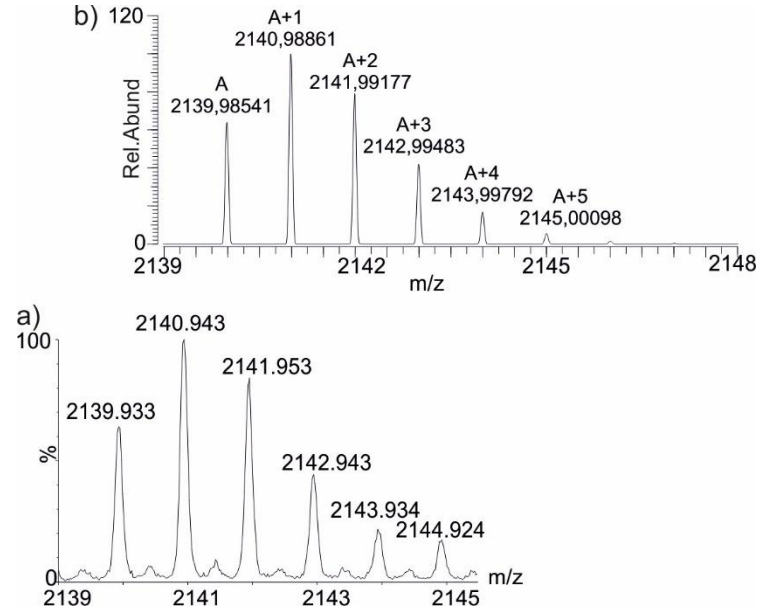

Figure 2.88. Experimental (a) and calculated (b) isotopic pattern of cage complex [(**9**)$_2$⊂**7**+H]$^+$.

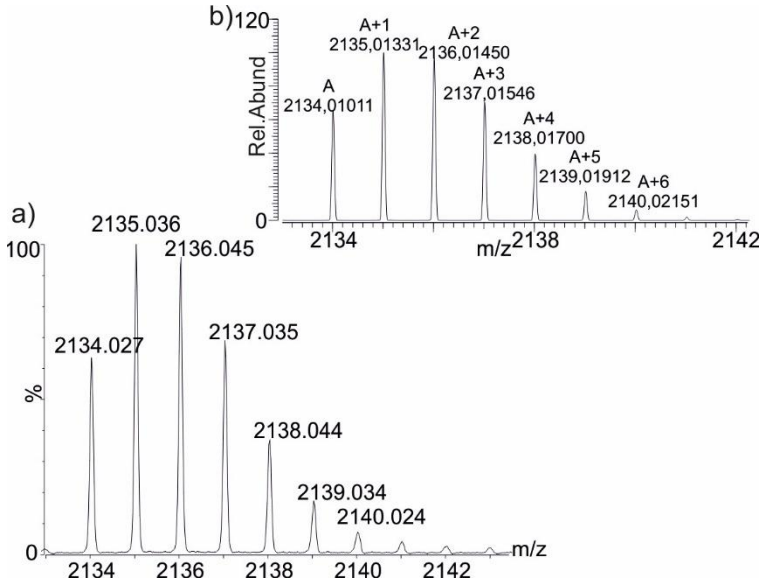

Figure 2.89. Experimental (a) and calculated (b) isotopic pattern of cage complex $[(\mathbf{10})_2 \subset \mathbf{7}+Cl]^-$.

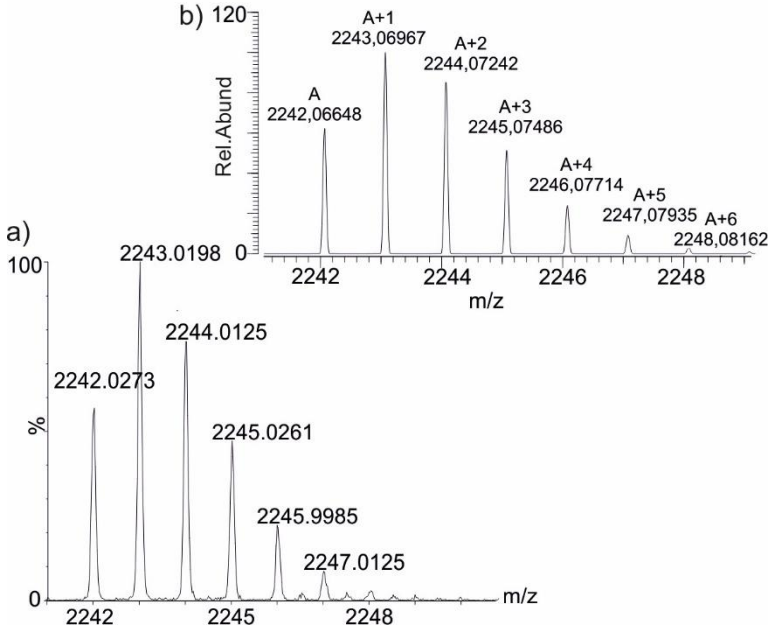

Figure 2.90. Experimental (a) and calculated (b) isotopic pattern of cage complex $[(\mathbf{11})_2 \subset \mathbf{7}+K]^+$.

2.5 References and notes

[1] F. Hof, S. L. Craig, C. Nuckolls, J. Rebek, Julius, *Angew. Chem. Int. Ed.* **2002**, *41*, 1488-1508.
[2] D. Fujita, *Pure Appl. Chem.* **2014**, *86*, 3-11.
[3] T. Iwasawa, R. J. Hooley, J. Rebek, *Science* **2007**, *317*, 493-496.
[4] R. Warmuth, *Eur. J. Org. Chem.* **2001**, *2001*, 423-437.
[5] A. Galan, P. Ballester, *Chem. Soc. Rev.* **2016**, *45*, 1720-1737.
[6] B. Breiner, J. K. Clegg, J. R. Nitschke, *Chem. Sci.* **2011**, *2*, 51-56.
[7] C. M. A. Gangemi, A. Pappalardo, G. Trusso Sfrazzetto, *RSC Advances* **2015**, *5*, 51919-51933.
[8] P. Ballester, A. Vidal-Ferran, P. W. N. M. van Leeuwen, in *Adv. Catal., Vol. 54* (Eds.: B. C. Gates, H. Knözinger), Academic Press, **2011**, pp. 63-126.
[9] D. J. Cram, S. Karbach, Y. H. Kim, L. Baczynskyj, G. W. Kallemeyn, *J. Am. Chem. Soc.* **1985**, *107*, 2575-2576.
[10] J. Atwood, L. Barbour, A. Jerga*, Vol. 35*, **2003**, pp. 153-175.
[11] J. Rebek, *Hydrogen-bonded Capsules*.
[12] O. Dumele, N. Trapp, F. Diederich, *Angew. Chem. Int. Ed.* **2015**, *54*, 12339-12344.
[13] F.-U. Rahman, D. Tzeli, I. D. Petsalakis, G. Theodorakopoulos, P. Ballester, J. Rebek, Y. Yu, *J. Am. Chem. Soc.* **2020**, *142*, 5876-5883.
[14] S. J. Dalgarno, N. P. Power, J. L. Atwood, *Coord. Chem. Rev.* **2008**, *252*, 825-841.
[15] B. J. Holliday, C. A. Mirkin, *Angew. Chem. Int. Ed.* **2001**, *40*, 2022-2043.
[16] S. J. Rowan, S. J. Cantrill, G. R. L. Cousins, J. K. M. Sanders, J. F. Stoddart, *Angew. Chem. Int. Ed.* **2002**, *41*, 898-952.
[17] K. Kobayashi, M. Yamanaka, *Chem. Soc. Rev.* **2015**, *44*, 449-466.
[18] M. Matache, E. Bogdan, N. D. Hădade, *Chem. Eur. J.* **2014**, *20*, 2106-2131.
[19] J.-M. Lehn, *Chem. Soc. Rev.* **2007**, *36*, 151-160.
[20] M. E. Belowich, J. F. Stoddart, *Chem. Soc. Rev.* **2012**, *41*, 2003-2024.
[21] L. Fabbrizzi, *J. Org. Chem.* **2020**, *85*, 12212-12226.
[22] N. M. Rue, J. Sun, R. Warmuth, *Isr. J. Chem.* **2011**, *51*, 743-768.
[23] M. L. C. Quan, D. J. Cram, *J. Am. Chem. Soc.* **1991**, *113*, 2754-2755.
[24] Y. Liu, X. Liu, R. Warmuth, *Chem. Eur. J.* **2007**, *13*, 8953-8959.
[25] J. Sun, R. Warmuth, *Chem. Commun. (Cambridge, U. K.)* **2011**, *47*, 9351-9353.
[26] N. Xu, K. Su, E.-S. M. El-Sayed, Z. Ju, D. Yuan, *Chem. Sci.* **2022**, *13*, 3582-3588.
[27] J. Zhu, Y. Han, Y. Ni, S. Wu, Q. Zhang, T. Jiao, Z. Li, J. Wu, *J. Am. Chem. Soc.* **2021**, *143*, 14314-14321.
[28] C. Bourguignon, D. Schindler, G. Zhou, F. Rominger, M. Mastalerz, *Org. Chem. Front.* **2021**, *8*, 3668-3674.
[29] J. C. Lauer, Z. Pang, P. Janßen, F. Rominger, T. Kirschbaum, M. Elstner, M. Mastalerz, *ChemistryOpen* **2020**, *9*, 183-190.
[30] H. Xie, V. W. L. Gunawardana, T. J. Finnegan, W. Xie, J. D. Badjić, *Angew. Chem. Int. Ed.* **2022**, *61*, e202116518.
[31] A. V. Davis, K. N. Raymond, *J. Am. Chem. Soc.* **2005**, *127*, 7912-7919.
[32] D. Ajami, J. Rebek, *Nature Chem.* **2009**, *1*, 87-90.
[33] P. Ballester, *Isr. J. Chem.* **2011**, *51*, 710-724.
[34] L. Adriaenssens, P. Ballester, *Chem. Soc. Rev.* **2013**, *42*, 3261.

[35] A. Díaz-Moscoso, D. Hernández-Alonso, L. Escobar, F. A. Arroyave, P. Ballester, *Org. Lett.* **2017**, *19*, 226-229.
[36] A. Galán, E. C. Escudero-Adán, P. Ballester, *Chem. Sci.* **2017**, *8*, 7746-7750.
[37] A. Galán, G. Aragay, P. Ballester, *Chem. Sci.* **2016**, *7*, 5976-5982.
[38] L. Escobar, P. Ballester, *Org. Chem. Front.* **2019**, *6*, 1738-1748.
[39] K. Sonogashira, Y. Tohda, N. Hagihara, *Tetrahedron Lett.* **1975**, *16*, 4467-4470.
[40] P. Ballester, G. Gil-Ramírez, *PNAS* **2009**, *106*, 10455-10459.
[41] L. Escobar, F. A. Arroyave, P. Ballester, *Eur. J. Org. Chem.* **2018**, *2018*, 1097-1106.
[42] Z. Lin, J. Sun, B. Efremovska, R. Warmuth, *Chem. Eur. J.* **2012**, *18*, 12864-12872.
[43] Y. Lei, Q. Chen, P. Liu, L. Wang, H. Wang, B. Li, X. Lu, Z. Chen, Y. Pan, F. Huang, H. Li, *Angew. Chem. Int. Ed.* **2021**, *60*, 4705-4711.
[44] Y. Chen, G. Wu, B. Chen, H. Qu, T. Jiao, Y. Li, C. Ge, C. Zhang, L. Liang, X. Zeng, X. Cao, Q. Wang, H. Li, *Angew. Chem. Int. Ed.* **2021**, *60*, 18815-18820.
[45] L. Escobar, G. Aragay, P. Ballester, *Chem. Eur. J.* **2016**, *22*, 13682-13689.
[46] L. Avram, Y. Cohen, *Chem. Soc. Rev.* **2015**, *44*, 586-602.
[47] J. H. Billman, A. C. Diesing, *J. Org. Chem.* **1957**, *22*, 1068-1070.
[48] D. Sinnaeve, *Concepts in Magnetic Resonance Part A* **2012**, *40A*.
[49] G. Gil-Ramírez, E. C. Escudero-Adán, J. Benet-Buchholz, P. Ballester, *Angew. Chem. Int. Ed.* **2008**, *47*, 4114-4118.
[50] M. Holsten, S. Feierabend, S. M. Elbert, F. Rominger, T. Oeser, M. Mastalerz, *Chem. Eur. J.* **2021**, *27*, 9383-9390.
[51] A. Asadi, D. Ajami, J. Rebek, *Chem. Sci.* **2013**, *4*, 1212-1215.
[52] Y. Chen, Y. Lei, L. Tong, H. Li, *Chem. Eur. J.* **2022**, *28*, e202102910.
[53] L. Escobar, E. C. Escudero-Adán, P. Ballester, *Angew. Chem. Int. Ed.* **2019**, *58*, 16105-16109.
[54] S. Hoops, S. Sahle, R. Gauges, C. Lee, J. Pahle, N. Simus, M. Singhal, L. Xu, P. Mendes, U. Kummer, *Bioinformatics* **2006**, *22*, 3067-3074.
[55] J. P. Perdew, *Phys. Rev. B* **1986**, *33*, 8822-8824.
[56] A. D. Becke, *Phys. Rev. A* **1988**, *38*, 3098-3100.
[57] S. Grimme, J. Antony, S. Ehrlich, H. Krieg, *J. Chem. Phys.* **2010**, *132*, 154104.
[58] F. Furche, R. Ahlrichs, C. Hättig, W. Klopper, M. Sierka, F. Weigend, *WIREs Comput Mol Sci* **2014**, *4*, 91-100.
[59] M. Von Arnim, R. Ahlrichs, *J. Comput. Chem.* **1998**, *19*, 1746-1757.
[60] D. J. Cram, M. T. Blanda, K. Paek, C. B. Knobler, *J. Am. Chem. Soc.* **1992**, *114*, 7765-7773.
[61] F. Liu, R. C. Helgeson, K. N. Houk, *Acc. Chem. Res.* **2014**, *47*, 2168-2176.
[62] S. Mecozzi, J. Rebek, Julius, *Chem. Eur. J.* **1998**, *4*, 1016-1022.
[63] S. Ro, S. J. Rowan, A. R. Pease, D. J. Cram, J. F. Stoddart, *Org. Lett.* **2000**, *2*, 2411-2414.
[64] B. Baytekin, H. T. Baytekin, C. A. Schalley, *Org. Biomol. Chem.* **2006**, *4*, 2825-2841.
[65] L. Cera, C. A. Schalley, *Chem. Soc. Rev.* **2014**, *43*, 1800-1812.
[66] Z. Qi, T. Heinrich, S. Moorthy, C. A. Schalley, *Chem. Soc. Rev.* **2015**, *44*, 515-531.
[67] K. Caprice, M. Pupier, A. Kruve, C. A. Schalley, F. B. L. Cougnon, *Chem. Sci.* **2018**, *9*, 1317-1322.
[68] A. Kruve, K. Caprice, R. Lavendomme, J. M. Wollschläger, S. Schoder, H. V. Schröder, J. R. Nitschke, F. B. L. Cougnon, C. A. Schalley, *Angew Chem Int Ed Engl* **2019**, *58*, 11324-11328.

Chapter 3

Self-assembly of [4+2] octa-imine capsules and their post-assembly modifications

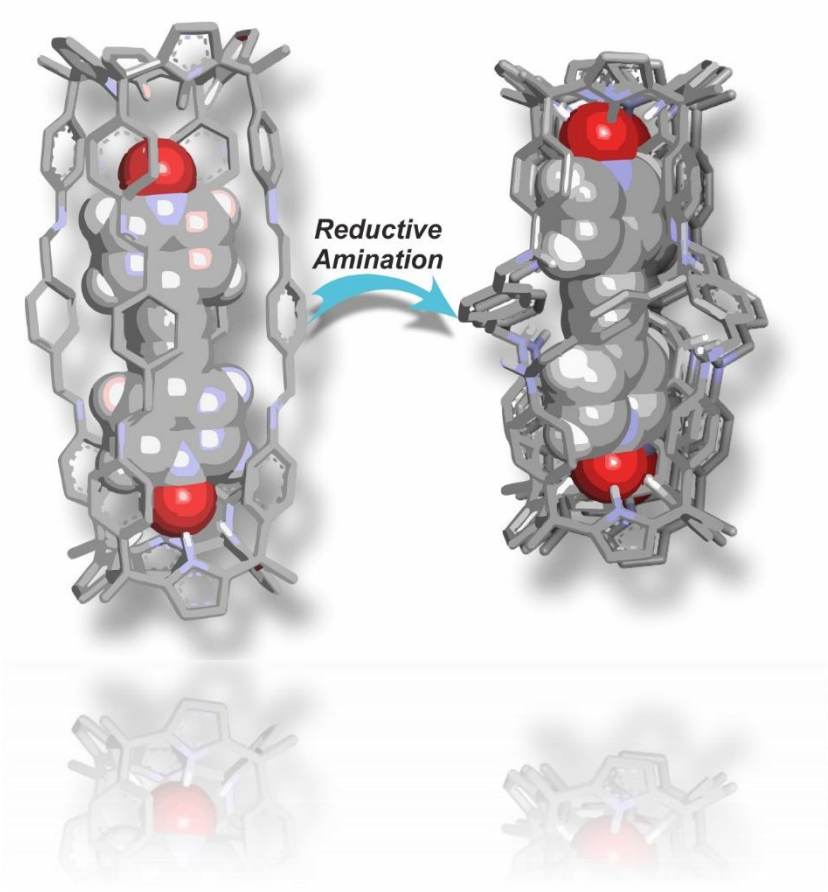

Unpublished results

3.1 Introduction

Since the first example of a poly-imine *hemicarcerand* assembled via dynamic covalent chemistry in 1991 (DCC),[1] this research area has witnessed significant progress.

The selection of the right precursors and the use of imine reversible bonds allowed the preparation of a plethora of molecular capsules and cages displaying different sizes and geometries.[2,3]

In particular, the self-assembly of capsular aggregates allows to create a nano-environment resembling the active sites of enzymes. In these environments, molecules are reversibly isolated from the bulk solvent and bound in a controlled and specific manner.[4]

For example, Rebek *et al*. reported the self-assembly of extended capsular containers featuring sizable and cylindrical cavities. The synthetic containers were held together by dynamic covalent bonds: eight imines (Figure 3.1).[5] The capsules allowed multiple molecular arrangements including accommodation of multiple guests and acid–base pairs in a confined space. The encapsulation complexes showed slow exchange rates on the chemical shift timescale for the bound guests allowing their complete characterization using ^{1}H NMR spectroscopy.

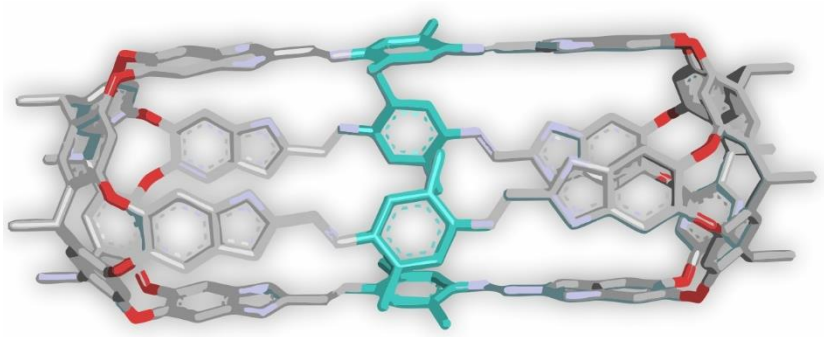

Figure 3.1. Energy minimized structure (MM3) of an extended resorcin[4]arene based poly-imine capsule assembled by [4+2] condensation of its molecular components (adapted from ref. 5). Alkyl chains at lower rim ($C_{11}H_{23}$) are here omitted for clarity.

The reversibility featured by the dynamic covalent capsular aggregates also facilitates their conversion into different architectures triggered by external stimuli. In doing so, the molecular function of an initial capsular aggregate *i.e*. uptake/release of guest molecules can be altered.

For example, a selective and reversible interconversion of calix[4]arene-based poly-imine aggregates in response to the presence of Na^{+} ions in solution was recently

reported.[6] Salicylaldehyde calix[4]arene derivatives self-assembled into macrocyclic [3+3] trimers by condensation reaction with 1,3-propanediame. The complexation of Na^+ cations with the lower-rim amide groups effectively altered the flattened cone conformation of the calixarene units to the spread cone counterpart. The induced conformational change was associated with the disassembly of the trimer and the formation of a [4+2] capsular-shaped dimeric cage.

Imine chemistry is also considered as a useful tool to synthesize covalent containers through post-assembly modifications. This methodology overcomes some of the limitations of covalent bonds which are formed in not reversible conditions, generating the desired products in low yields.[7]

Post-synthetic modification strategies have been applied to transform chemically labile poly-imine organic cages into more stable poly-amine derivatives. In addition to the common use of $NaBH_4$ as the reducing agent,[8] milder reducing agents such as $NaBH(OAc)_3$ have been recently used to reduced chiral poly-imine cages to furnish more stable chiral poly-amine counterparts.[9]

Mastalerz and coworkers reported several post-assembly modifications' strategies to endow shape persistent dynamically covalent cages with a high level of stability.[10,11,12] Among them, the transformation of the imine bonds into hydrocarbons[13] and carbamates[14] were of great relevance.

To the best of our knowledge, there are only a few examples of imine and amine-based capsules featuring polar cavities. The cavities of these constructs are endowed with convergent functional groups able to interact with encapsulated polar molecules either neutral or charged.

The incorporation of calix[4]pyrrole scaffolds in poly-imine capsular architectures provide aromatic cavities with polar functions. These structures are better suited to mimic biological receptors (*e.g*. proteins).[15]

Inspired by previous works,[15] we investigated the self-assembly of cylindrical capsules through a thermodynamically driven reversible condensation of 6 components (*i.e*. [2 amines + 4 bis-aldehydes]). The rational strategy of the self-assembly process made use of the template effect. The template guest was not only accommodated in the aromatic cavity of the self-assembled capsule, but it also pre-organized and brought together its molecular building blocks facilitating their inter- and intra-molecular reversible covalent reactions.[16,17]

We assembled [4+2] poly-imine capsules by condensation of two tetra amino-calix[4]pyrrole units with four 1,4-dicarboxyaldehyde-benzene linkers in the presence of 4',4'-bipyridyl-*N,N'*-dioxide as template. We also investigated the use of

solvent molecules (*i.e*. CD_3CN) as templates. In doing so, the resulting poly-imine capsules were suited for molecular recognition studies of polar guests. We also evaluated the capsule's mechanisms for the uptake and exchange of the encapsulated guests.

We used $NaBH_4$ as reducing agent for the post-assembly modification for the conversion of the labile octa-imine capsule into the octa-amine covalent counterpart.

Finally, we studied and compared the binding properties of the octa-imine capsule and its octa-amine analogue towards monotopic and ditopic *N*-oxides.

3.2 Results and discussion

3.2.1 Design and synthesis

Octa-imine capsules **5** and **6** (Scheme 3.1) were designed in order to assemble cylindrical containers having a larger polar cavity than that of the previously

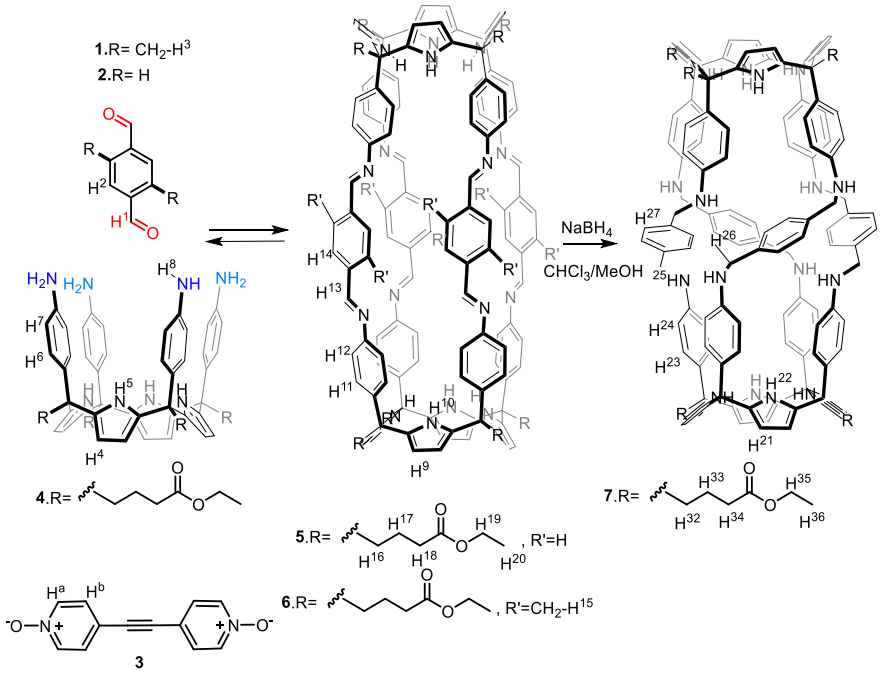

Scheme 3.1. Synthetic scheme of the self-assembly process for the preparation of calix[4]pyrrole octa-imine and octa- amine capsules.

synthesized tetra-imine hetero-dimeric cage discussed in Chapter 2.

The significant increase in the capsule's cavity compared to the [1+1] tetra-imine cages described in the previous chapter, would facilitate their use as molecular-

reactors to mediate bimolecular reactions. Molecular reactivity in confined spaces differs in many aspects from that conducted in bulk solution.[18,19,20]
Considering the need of pre-organizing and locating in proximity at least two of the six molecular components of the octa-imine capsules, we first investigated the use of a ditopic template in pure $CDCl_3$ solution. Molecular modelling studies indicated that 4,4'(1,2-ethynyl)-bis-pyridine-1,1-dioxide **3**[15,21] had a reasonably good fit for the polar aromatic cavity of octa-imine capsules **5** and **6**.
However, bis-*N*-oxide **10** having a buta-1,3-diynyl spacer (Figure 3.5) could fit even better the cavity of octa-imine capsules. We synthesized bis-*N*-oxide **10** from the Hay coupling reaction of 4-ethynylpyridine *N*-oxide **12**. In turn, 4-ethynylpyridine *N*-oxide **12** was obtained by *N*-oxidation of 4-ethynylpyridine with oxone®.

3.2.1.1 *Template-assisted synthesis of octa-imine capsules **5** and **6***

Firstly, we explored the ability of bis-*N*-oxide **3** to induce the self-assembly of the octa-imine capsules **5** and **6**. As mentioned above, molecular modeling studies (Figure 3.2) showed that **3** had a reasonably good fit in the cylindrical cavities of the capsules. Nevertheless, its length was slightly too short to establish a perfect ditopic interaction with the two-polar calix[4]pyrrole binding sites of the capsules.
In any case and considering the easy synthetic availability of **3**, we decided to experimentally investigate its use as template for the capsule's assembly. We monitored the self-assembly processes of the capsules by ^{1}H NMR spectroscopy.
The addition of 0.5 equiv. of bis-*N*-oxide **3** to a 2 mM solution of the tetra-amino calix[4]pyrrole **4** in $CDCl_3$ solution produced the quantitative assembly of the $\mathbf{3}\subset(\mathbf{4})_2$ inclusion complex (Figure 3.2 b). The ^{1}H NMR spectrum of the complex is in agreement with apparent D_{4h} symmetry. The downfield shifts experienced by the pyrrole NHs H_5'' ($\Delta\delta$= 0.46) indicated their involvement in hydrogen bonding interactions with the oxygen atoms of the *N*-oxide knobs of the template bis-*N*-oxide **3**. The aromatic protons of encapsulated **3** (H^{a}'', H^{b}'') resonated upfield owing to their deep inclusion in the calix[4]pyrrole aromatic cavity where they experience the strong shielding of the four *meso*-aromatic panels. Encapsulated **3** also interacted through CH-π and π-π interactions with the aromatic walls of the two calix[4]pyrrole units. The relative integral values of selected proton signals of the complex supported the 2:1 stoichiometry of the complex. The addition of 2 equiv. of 1,4-di-carboxyaldehyde benzene linker **1**, provoked the broadening of most proton signals. Most likely, this is due to the initial formation of oligomeric species. Heating the solution of the mixture at 310 K for 12 h, resulted in a ^{1}H NMR spectrum

with sharp and well-resolved proton signals. The signals assigned to the protons of the aldehyde (H^1) and the amine groups ($H^{5''}$) were no longer detected. Two

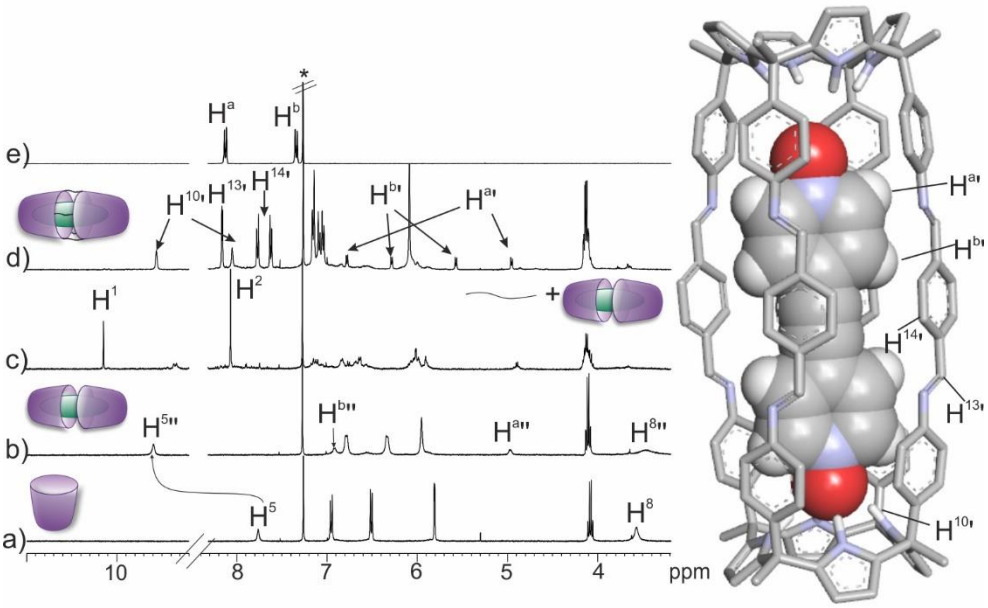

Figure 3.2. (Left) Selected region of the ^{1}H NMR spectra (400 MHz, at 298 K, $CDCl_3$) of (a) tetra-amino calix[4]pyrrole **4**, (b) capsular complex **3⊂(4)$_2$**, (c) 1:0.5:2 mixture of tetra-amino calix[4]pyrrole **4**, guest **3** and di-aldehyde linker **1**, (d) 1:0.5:2 mixture of tetra-amino calix[4]pyrrole **4**, guest **3** and dialdehyde linker **1** after reaction at 310 K for 12h to give imine capsular complex **3⊂5**, (e) bis-pyridyl *N*-oxide **3**. Primed and double primed letters indicate the signals of bound host and guest in the 1:1 and 2:1 complex, respectively. (*) Indicates residual solvents. (Right) Energy minimized (MM3) structure of imine capsular complex **3⊂5**. Ester chains at the lower rim were omitted for clarity.

overlapped singlets for the imine CH protons emerged at δ= 8.1 ppm ($H^{13'}$) indicating the assembly of the octa-imine capsule **5** (Figure 3.2 d). We observed that the pyrrole NHs of **5** resonated as two separate broad singlets at δ= 9.5 and 8.0 ppm ($H^{10'}$), demonstrating the encapsulation of one molecule of the bis-*N*-oxide **3**. These chemical shift values were smaller than expected for pyrrole NHs forming ideal hydrogen bonding interactions with an oxygen atom of a pyridyl-*N*-oxide. In addition, the aromatic protons of the encapsulated bis-*N*-oxide **3** appeared upfield as four doublets resonating between 4.80 ppm and 6.80 ppm. The encapsulated guest experienced the shielding effect of the aromatic components of capsule **5**. The ^{1}H NMR spectrum of **3⊂5** was not in agreement with an apparent D_{4h} symmetry. This finding indicated that the bis-*N*-oxide **3** was too short to establish ideal ditopic hydrogen-bonding interactions with the two hemispheres of capsule **5**. Most likely, **3** was co-encapsulated with one molecule of water bridging the gap between one

of its *N*-oxide ends and one calix[4]pyrrole binding site. The *N*-oxide **3** experienced a shuttling motion inside the capsule that was slow on the chemical shift timescale. The energy minimized structure (MM3) of the capsular complex **3⊂5** (Figure 3.2 right) supported the reduced size complementarity between the dimensions of capsule's cavity and the used *N*-oxide. The **3⊂5** complex was further characterized in solution by a set of 1D and 2D NMR spectroscopy and DOSY experiments.

Aiming at better understanding the origin of the lack of symmetry of the octa-imine capsular assembly **3⊂5**, we assembled the analogous **3⊂6** encapsulation complex using the dialdehyde linker **2**. Linker **2** contained two methyl groups *ortho* to the 1,4-aldehyde groups. Our expectations were that the methyl groups of the linkers should resonate as two diastereotopic signals in response to the reduced symmetry of the complex. As expected, the ^{1}H NMR spectrum of the **3⊂6** capsular complex (Figure 3.17) showed two signals for the methyl groups for the linker.

Single crystals of the **3⊂5** encapsulation complex suitable for X-ray diffraction grew from the slow diffusion of *p*-xylene into a $CDCl_3$:CD_3CN 9:1 mixture of solvents. The solution of the diffracted data revealed a preliminary structure of the **3⊂5** complex in the solid state. The octa-imine **5** completely surrounded the surface of encapsulated bis-pyridyl-*N*-oxide **3**. Unfortunately, the structure of the encapsulated guest showed a significant disorder of the atoms. Most likely, this is due to shuttling motion of the encapsulated *N*-oxide even at the lower temperature used during the X-ray diffractions (193 K) or to the existence of multiple positions of the guest in the crystal lattice of the encapsulation complex. The analysis of the diffracted data hinted to the co-encapsulation of one molecule of water as mentioned above.

The results of a 2D EXSY experiment[5,22,23] allowed us to calculated an energy barrier of 17.1 Kcal/mol for the shuttling motion of the encapsulated bis-*N*-oxide **3** (Figure 3.15). We observed cross-peaks due to chemical exchange between pyrrole NHs assigned to the two different hemispheres of the **3⊂5** complex. We hypothesized that the shuttling motion of the bis-*N*-oxide guest **3** in the cavity of **5** involves a coupled exchange with a water molecule either intra- or inter-molecularly.

3.2.1.2 *Solvent-templated synthesis of capsules **5** and **6***

We explored the self-assembly of octa-imine capsules **5** and **6** in the absence of a template. Instead, we decided to use acetonitrile as co-solvent.

We previously described that the binding of one acetonitrile molecule in the cavity of α,α,α,α-aryl extended calix[4]pyrroles pre-organized the receptor scaffold into the cone conformation.[24, 25]

A mixture of calix[4]pyrrole **4** (2 mM) and dialdehyde linker **1** (4mM) in a 1:2 molar ratio produced a solution in a $CDCl_3$:CD_3CN 9:1 blend of solvents. The ^1H NMR spectrum of the solution acquired immediately after mixing the two compounds showed broad proton signals that were indicative of the formation of oligomeric aggregates.

After heating the solution for 24h at 310 K, the ^1H NMR spectrum of the solution displayed sharp proton signals that were in agreement with an apparent D_{4h} symmetry for the capsular assembly **5** (Figure 3.4 a). The diagnostic signal of the imine protons, H^{13}, appeared at δ= 8.37 ppm. We also observed the disappearance of the signals attributed to aldehyde protons of linker **1** (H^1) and amino protons of calix[4]pyrrole **4** (H^1).

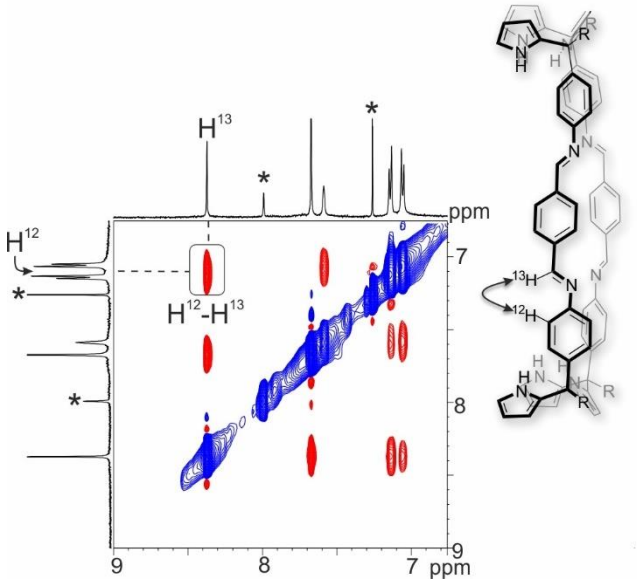

Figure 3.3. 2D ROESY NMR (400 MHz, at 298 K, $CDCl_3$:CD_3CN 9:1 mixture) spectrum of the self-assembled capsule **5**. The initial solution contained a mixture of tetra-amino calix[4]pyrrole **4** and dialdehyde linker **1** in a 1:2 molar ratio and was heated for 24 h at 310 K. (*) Indicates residual solvents and unreacted dialdehyde **1**.

The structure of capsule **5** in solution was characterized by 2D NMR spectra and ^1H DOSY experiments $CDCl_3$:CD_3CN 9:1 solvent mixture. For example, a ROESY experiment showed nOe cross peaks between the imine proton (H^{13}) and protons of *meso* aromatic panels (H^{12}) (Figure 3.3). A DOSY experiment assigned a diffusion

constant of 3.10± 0.07× 10^{-10} m^2s^{-1} to the protons of capsule **5**. This value is agreement with the one determined for the octa-imine capsular complex **3⊂5** (3.21± 0.06× 10^{10} m^2s^{-1}) in $CDCl_3$.

The yield of the self-assembly process of capsule **5** was determined as 70% based on the ratio of the integral values of selected signals of the assembly and those of an internal standard (1,3,5-trimethoxy-benzene). Most likely, the remaining 30% of the starting materials was engaged in the formation of non-capsular polymeric aggregates that were not visible in the ^{1}H NMR spectrum (*i.e*. signals broaden beyond detection).[26] Attempts to self-assemble capsule **5** using larger initial concentrations of its molecular components and maintaining the 1:2 molar ratio produced lower yields.

Most likely, the formation of aggregates is favoured when larger concentrations of the molecular components are used.[7] Heating the solution of molecular components **4** and **1** at 310 K for 24 h produced a higher yield of self-assembled cage **5** than using r.t.

We synthesized capsule **5** in a 20 mg scale using a 4 mM concentration of tetra-amino calix[4]pyrrole **4** and 8 mM concentration of the di-aldehyde linker **1**. We calculated a self-assembly yield of 55% using an internal standard. Capsule **5** did not show signs of degradation when stored in solution for more than a month at 281 K. Using an identical procedure, the solution of tetra-amine **4** and di-aldehyde linker **2** in 1:2 molar ratio in a 9:1 $CDCl_3$:CD_3CN solvent mixture produced the self-assembled octa-imine capsule **6** in similar yields.

3.2.2 Post-assembly reductive amination

Following described procedures for related poly-imine cages, we converted the octa-imine capsule **5** into the chemically more stable octa-amine derivative **7** by reductive amination.[27] To capsule **5**, self-assembled in a 9:1 $CDCl_3$:CD_3CN solvent mixture, we added 10% of CD_3OD and 43 equiv. of $NaBH_4$ (ca. 5 equiv. for imine group). We monitored the progress of the reaction using ^{1}H NMR spectroscopy.

After 26 h of reaction we did not observe additional changes in the ^{1}H NMR spectrum of the mixture.[28] Interestingly, the signal of the imine protons of capsule **5** resonating at δ= 8.37 ppm had totally disappeared. We detected the appearance of new signals in the region of 3.50 to 4.20 ppm (Figure 3.4 b). We assigned these signals to the amine and the benzylic methylene protons (H^{25}, H^{26}) of the octa-amine **7**. The relative integral values of the signals coincided with 8 and 16 protons. These finding were indicative of the positive outcome of the reductive amination reaction.

The octa-amine capsule **7** was isolated by simply washing the organic phase with water. After drying and evaporating the organic phase we obtained a solid containing capsule **7**. We analyzed the solid using HPLC-MS. Capsule **7** was characterized by a

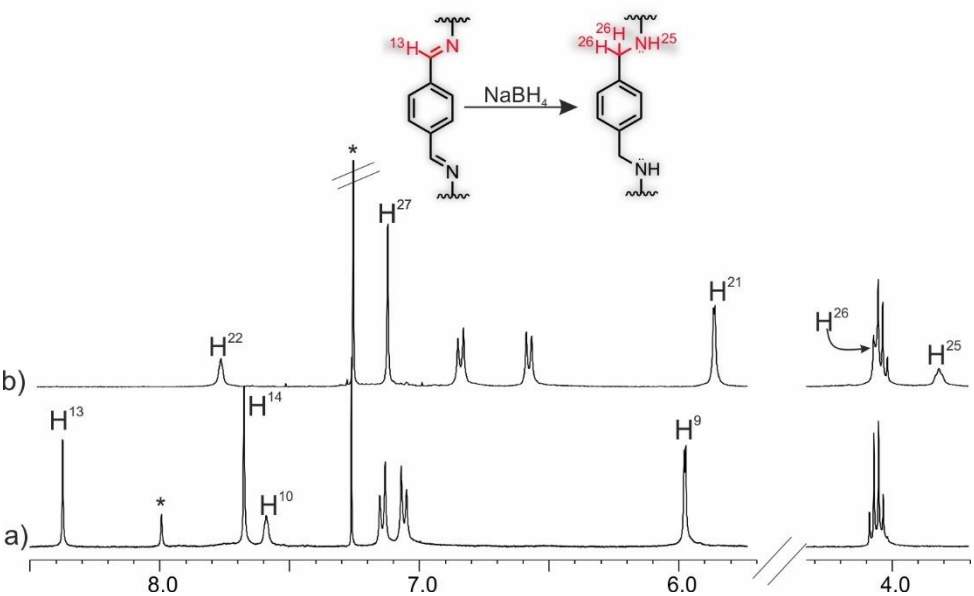

Figure 3.4. Selected region of ^{1}H NMR spectra (400 MHz, at 298 K, $CDCl_3$:CD_3CN 9:1 mixture) of (a) octa-imine capsule **5**, (b) octa-amine capsule **7**. See Scheme 3.1 for protons assignment. (*) Indicates residual solvents and unreacted dialdehyde **1**.

complete set of high-resolution spectra (^{1}H- ^{13}C-NMR and 2D NMR spectroscopy). Unfortunately, all our attempts to purify the octa-amine capsule **7** by crystallization from slow evaporation of $CHCl_3$/toluene solvent mixtures failed.

Single crystals suitable for X-ray diffraction grew from the slow diffusion of toluene into a 9:1 $CDCl_3$:CD_3CN solution containing the octa-amine capsule **7**. The analysis of the diffracted data revealed the structure the octa-amine capsule **7** in the solid-state encapsulating a ditopic *N*- oxide compound (Figure 3.11). Further evidences of the successful reductive amination, come from the value of averaged bond angle between C^{37},N^{25} and C^{26}extracted from the X-ray structure. This value is of 106° indicating the change in hybridization of N and C atoms from sp^2 to sp^3. The encapsulated guest formed four convergent hydrogen bonds between its two oxygen atoms and four pyrrole NHs of the two equivalent calix[4]pyrrole hemispheres of capsule **7** adopting the cone conformation.

3.2.3 Binding properties of the octa-imine capsule **5** towards a series of *bis*-pyridine-*N*-oxides (ditopic) and mono-*N*-oxide derivatives (monotopic) as guests

Having assembled the octa-imine capsule **5** in the absence of a pyridyl- *N*-oxide as template, we decided to investigate the capsule's binding properties using a series of bis-pyridine-*N*-oxides (ditopic) and mono-*N*-oxide derivatives (monotopic) as guests (Figure 3.5). The thermodynamic and kinetic characterization of the binding properties of capsule **5** are key in relation to its potential use as a molecular reactor (Chapter 4). Moreover, the use of different sized mono- and di-topic pyridyl-*N*-oxide derivatives is expected to further shine some light on the symmetry of the **3⊂5** encapsulation complex.

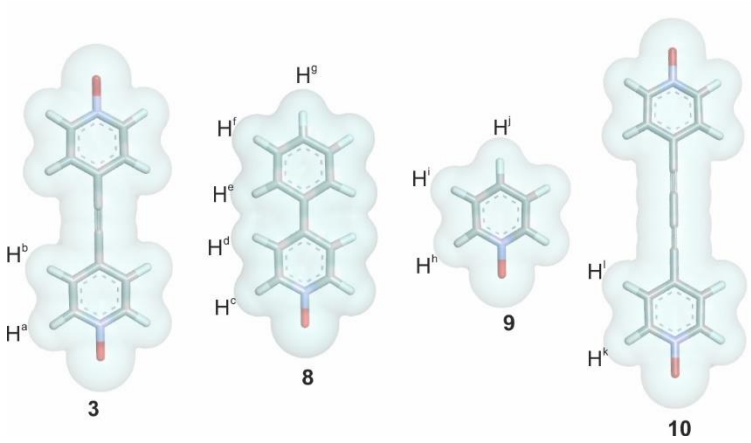

Figure 3.5. Ditopic and monotopic pyridyl-*N*-oxide guests used to investigate the binding features of the octa-imine capsule **5**.

Considering that during the self-assembly of capsule **5** non-capsular aggregates can also be formed and involved in the binding of the pyridyl-*N*-oxide guests, we performed the binding studies using the pyridyl-*N*-oxide guests in concentrations assuming the quantitative formation of the capsule or even slightly higher.

Firstly, we investigated the binding of the 4,4'-bis-pyridine-*N*,*N'*-dioxide **3** by the self-assembled capsule **5** in 9:1 $CDCl_3$:CD_3CN solvents mixture. We expected to obtain the **3⊂5** encapsulation complex formed when **3** was used as template in the self-assembly of **5** in the same solvent mixture (Figure 3.2). We were intrigued by the kinetics of the uptake of **3** by **5**, as well as if the yield of the **3⊂5** encapsulation complex would increase with respect to that of the initial concentration of free **5** (template amplification in DCL).

We performed ^{1}H NMR titrations adding small aliquots of **3** in $CDCl_3$:CD_3CN 9:1 mixture to a solution of **5** in the same mixture of solvents.

The addition of sub-stoichiometric amounts of bis-*N*-oxide **3** produced the immediate observation of separate signals for the protons of the free octa-imine **5** and the encapsulation complex **3⊂5** in the ^{1}H NMR spectra of the solution mixture (Figure 3.26). In the presence of 1.2 equiv. of **3**, we only detected the proton signals for the **3⊂5** complex (Figure 3.6 b).

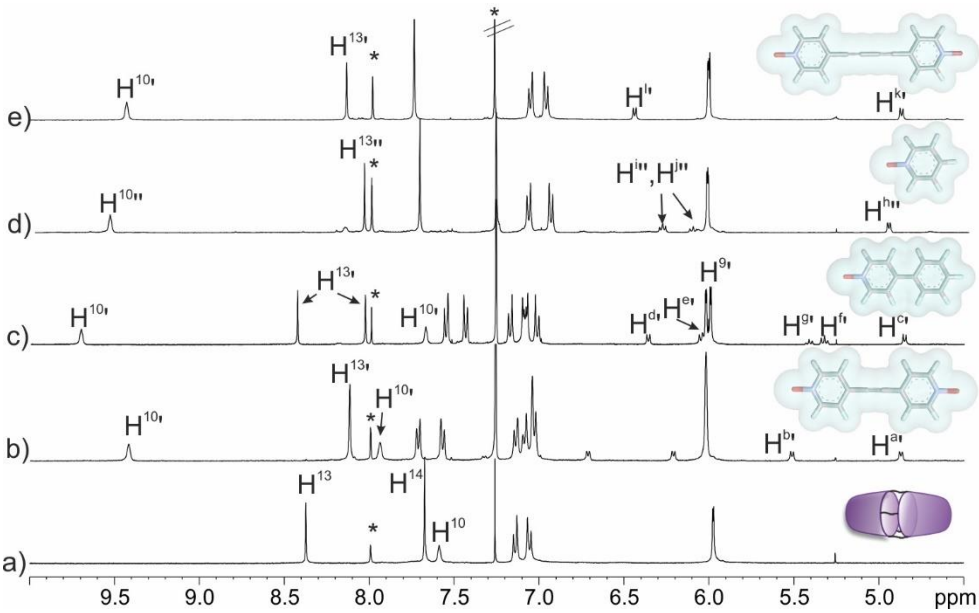

Figure 3.6. Selected regions of the ^{1}H NMR spectra (400 MHz, at 298 K, $CDCl_3$:CD_3CN 9:1 mixture) of (a) octa-imine capsule **5**, (b) upon addition of **3** (1.2 equiv.), (c) upon addition of **8** (1.2 equiv.), (d) upon addition of **9** (2.2 equiv.), (e) upon addition of **10** (excess). Primed and double primed letters indicate bound host and guest in the 1:1 and 2:1 complexes, respectively. (*) Indicates residual solvents and unreacted dialdehyde linker **1**. See Scheme 3.1 and Figure 3.5 for protons assignment.

All together, these observations indicated that the binding constant of the **3⊂5** complex can be estimated as larger than 10^4 M^{-1}. The dynamic of exchange of the binding equilibrium was slow on the chemical shift timescale. The uptake of **3** by **5** took place relatively fast on the human timescale (< 20 min) suggesting a low energy barrier of the inclusion process.

Secondly, we probed the binding of pyridine *N*-oxide **9** and phenyl pyridine *N*-oxide **8** with the octa-imine capsule **5** also using ^{1}H NMR spectroscopy.

The addition of sub-stoichiometric amounts of pyridine *N*-oxide **9** to a solution of the capsule **5** in 9:1 $CDCl_3$: CD_3CN mixture of solvents produced the observation of three sets of proton signals for the capsule's protons. We assigned the three sets of

signals to the free capsule **5** and the corresponding 1:1 and 2:1 encapsulation complexes with pyridine *N*-oxide **9**, **9⊂5** and (**9**)$_2$**⊂5**, respectively. The three species are involved in binding equilibria featuring slow dynamics on the ^{1}H chemical shift timescale (Figure 3.28). The ^{1}H NMR spectrum of the (**9**)$_2$**⊂5** encapsulation complex is in agreement with an apparent D_{4h} symmetry. In the presence of *ca.* 2.2 equiv. of the pyridine-*N*-oxide **9**, we detected exclusively the proton signals of the (**9**)$_2$**⊂5** complex (Figure 3.6 d). These observations allowed us to estimate the binding constants of the **9⊂5** and (**9**)$_2$**⊂5** complexes as larger than 10^4 M^{-1} and 10^8 M^{-2}, respectively. The pyrrole NHs of the (**9**)$_2$**⊂5** complex were highly downfield shifted (δ= 9.8 ppm) compared to the same protons in the free host, indicating that the two pyridine-*N*-oxide molecules included in the cavity of **5** established almost optimal hydrogen bonding interactions.

Finally, we investigated the encapsulation of *p*-phenyl-pyridine-*N*-oxide **8** in the cavity of octa-imine **5**. Based on molecular modelling studies *N*-oxide **8** seems too large for the formation of 2:1 complexes. The addition of 0.5 equiv. **8** to a solution of capsule **5** produced the appearance of a new set of signals for the container in the ^{1}H NMR spectrum of the mixture. We attributed the new set of proton signals to the formation of the 1:1 encapsulation complex **8⊂5** (Figure 3.27). The aromatic signals of the encapsulated *N*-oxide moved upfield in response to the shielding caused by the aromatic panels of the capsule.

The addition of 1 equiv. of **8** produced the exclusive observation of the proton signals of the 1:1 complex. Consequently, the K_a of the **8⊂5** complex can be estimated as higher than 10^4 M^{-1}. The addition of a small excess of **8** did not produce noticeable changes in the signals of the proton of the **8⊂5** encapsulation (Figure 3.6 c).

We performed molecular modelling studies, in order to find a suitable bis-*N*-oxide guest capable to fill the distance gap existing between the two polar hemispheres of capsule **5**. Bis-*N*-oxide **10** having a buta-1,3-diynyl spacer was selected. Bis-*N*-oxide **10** showed a reduced solubility in the in 9:1 $CDCl_3$: CD_3CN solvents mixture. For this reason, we performed the binding study with capsule **5** using a solid-liquid extraction experiment. To a mM solution of **5** in a 9:1 $CDCl_3$: CD_3CN solvent mixture, we added **10** as a solid. The resulting suspension was sonicated and filtered. The ^{1}H NMR spectrum of the filtrate showed sharp protons signals in agreement with an apparent D_{4h} symmetry that were diagnostic of the quantitative formation of the **10⊂5** complex. As could be expected, the aromatic proton signals of the encapsulated **10** resonated at the upfield region as two separate doublets (Figure 3.6 e).

This result evidenced that the bis-*N*-oxide **3** was too short to gap the distance between the two calix[4]pyrrole hemispheres of capsule **5**. It also showed that capsule **5** is conformationally rigid and cannot easily adapt to the dimensions of the encapsulated guests.

We performed ^{1}H DOSY experiments of all the encapsulation complexes described above: **3**⊂**5**, (**9**)$_2$⊂**5**, **8**⊂**5** and **10**⊂**5**. In all cases, the fit of the decay of the proton signals to a mono exponential function assigned an identical diffusion coefficient to the molecular components of the encapsulation complex. This proved that they were involved in the same supramolecular species. In addition, the diffusion constants of the complexes were almost 3.0×10^{-10} m^2s^{-1} and coincided with that of the free capsule **5** in the same solvent mixture. The encapsulation of the guest did not modify the dimensions of the capsule.

Luckily, we obtained single crystals suitable for X- ray diffraction from slow diffusion of *p*-xylene into a 9:1 $CDCl_3$:CD_3CN solution of the **10**⊂**5** encapsulation complex. To our delight, the solution of the diffraction data revealed the structure of the **10**⊂**5** encapsulation complex in the solid state (Figure 3.7). It was observed that octa-imine capsule **5** nicely complemented and surrounded the surface of encapsulated bis-*N*-oxide **10**. Each oxygen atom of **10** formed four convergent hydrogen bonds with the four NHs at each calix[4]pyrrole hemisphere of the capsule (average distance of 2.95 Å for the H-N···O hydrogen bonds). All the imine bonds displayed *E*-configuration. Notably, the imine bonds of the two hemispheres are not unidirectionally oriented. Similarly, to the observations made in the structure of [1+1] tetra- amine cage in Chapter 2, the imine carbon atoms of adjacent groups faced one to another, thus defining two portals of different dimensions in each hemisphere (Portal1: averaged dCim1···Cim2= 6.6 Å; Portal2: averaged dCim1···Cim4= 5.1 Å). The imine protons are outwardly directed with respect to the aromatic cavity of capsule **5**. The symmetry of the cage in the solid state is an apparent D_{2h} instead of the D_{4h} observed in solution. This result indicated that in solution the aromatic panels of the capsules are freely rotating around their single bonds.

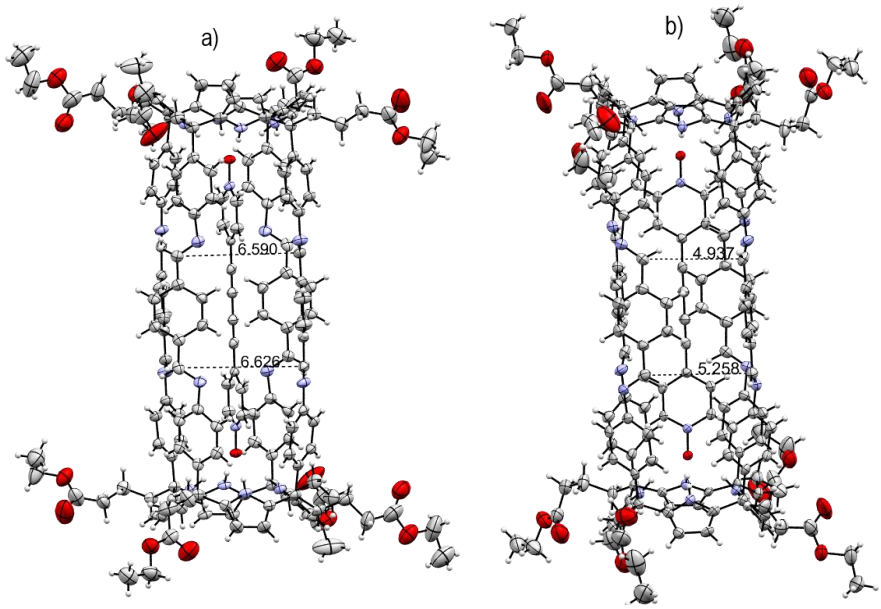

Figure 3.7. Different side views of X-ray structure of imine capsular complex **10⊂5** showing the two different portals.

3.2.3.1 *Structural differences between **3⊂5** and **3⊂7** encapsulation complexes.*

Having capsules **5** (octa-imine) and **7** (octa-amine) at hand, we were interested in comparing their structural properties upon encapsulation of guest **3**. As described in literature, the conversion of the imine bond into the corresponding covalent amine increases the conformational flexibility of shape persistent cages.[12] We selected bis-*N*-oxide **3** that is too short to undergo an ideal ditopic interaction with the two hemispheres of capsule **5**. The proton signals for the encapsulated guest **3** appear as four doublets upfield shifted compared to the free counterpart. The formed **3⊂5** capsular complex showed an apparent C_{4v} symmetry instead of the expected apparent D_{4h}.

The addition of an excess of bis-*N*-oxide **3** to a 1 mM solution of octa-amine capsule **7** in 9:1 $CDCl_3$:CD_3CN solvent mixture produced a ^{1}H NMR spectrum displaying a completely new set of signals in agreement with an apparent D_{4h} symmetry. We assigned the new set of signals to the quantitative assembly of the **3⊂7** complex (Figure 3.8).

The pyrrole NH proton signals of **7** moved downfield in the **3⊂7** complex ($H^{22'}$) indicating their involvement in hydrogen bonding interactions. As expected, the aromatic protons of encapsulated **3** appeared as two upfield shifted doublets.

Using 2D NMR spectroscopy and VT NMR experiments we assigned all the signals of the ^{1}H NMR spectrum to the protons of the **3⊂7** encapsulation complex. The encapsulated bis-*N*-oxide retained an apparent C_{2v} symmetry indicating that it established identical interactions with the two hemispheres. We assumed that the higher conformational flexibility of the octa-amine capsule **7** allowed its adaptability to the reduced dimensions of the encapsulated guest **3**. In order to do so, capsule **7** adopted an helicoidal conformation in the **3⊂7** complex as was derived from its electronic structure calculations at the DFT level. Considering the helical twist, the capsular complex can exist as two conformational enantiomers depending on the sense of rotation of the amine groups (*M* or *P*).

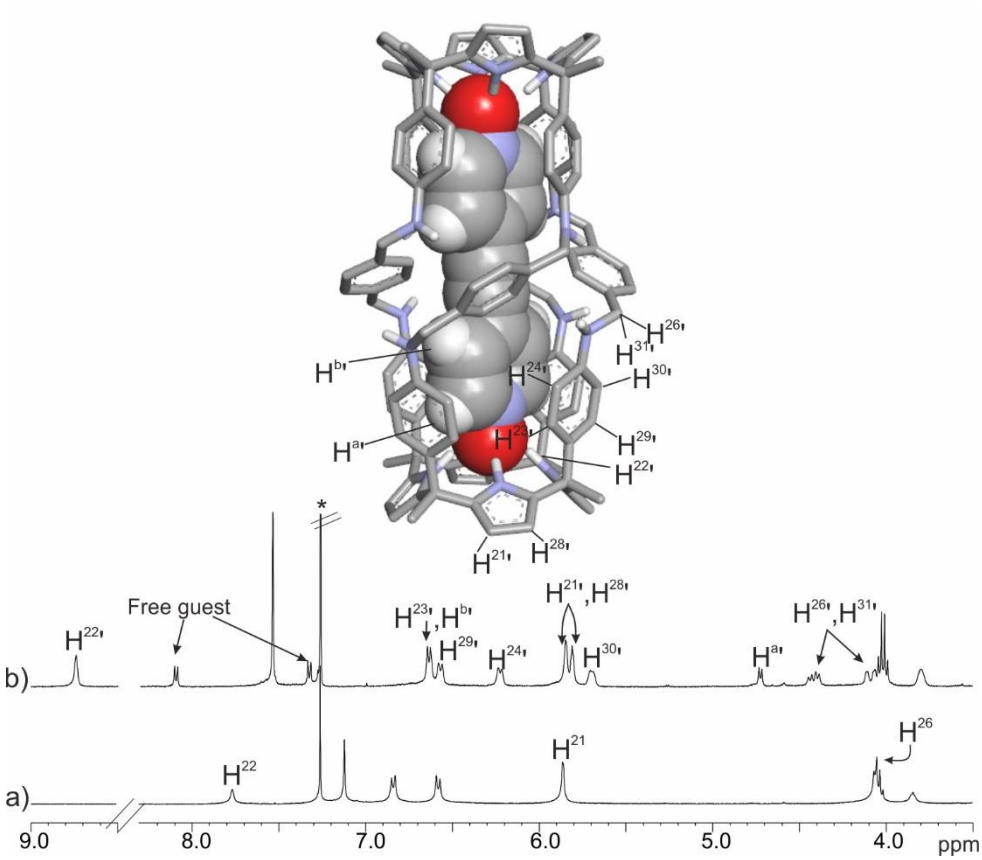

Figure 3.8. (Top panel) Energy minimized structure (BP86[29,30]-D3[31]-def2-TZVP using Turbomole v7.0 [32,33]) of octa-amine capsular complex **3⊂7**. Ester chains at the lower rim are omitted for clarity. (Bottom panel) Selected regions of the ^{1}H NMR spectra (500 MHz, at 298 K, $CDCl_3$:CD_3CN 9:1 mixture) of (a) octa-amine capsule **7** (1 mM solution), (b) upon addition of excess of **3**. Primed letters indicate diastereotopic protons of the 1:1 complex. (*) Indicates residual solvents.

The encapsulation of guest **3** provoked a slow rotation in the ^{1}H NMR timescale of *meso* aromatic walls of calix[4]pyrrole units around the single bond. Consequently, we could detect two signals for the diastereotopic *ortho* and *meta* protons in the aromatic panels ($H^{23'}$, $H^{29'}$, $H^{24'}$ and $H^{30'}$). Similarly, we could also detect two signals for the β pyrrole protons ($H^{21'}$, $H^{28'}$) and two double doublets for the diastereotopic benzylic protons ($H^{26'}$, $H^{31'}$).

We performed variable temperature ^{1}H NMR experiments to a solution of octa-amine capsular complex **3⊂7** in 9:1 $CDCl_3$:CD_3CN solvents mixture (Figure 3.29). The increase of temperature up to 323 K, only caused the broadening of signals relative to the *meso* aromatic panels, the β pyrrole protons and benzylic protons of the linker portion. However, due to experimental limitations we could not further increase the temperature to fasten the exchange process and reach the coalescence of the diastereotopic proton signals.

On the other hand, lowering down the temperature to 233 K only caused the splitting of the signal at δ= 6.7 ppm, attributed to the overlap of encapsulated guest signal ($H^{b'}$) and proton $H^{23'}$ of the capsule.

3.2.4 Gas phase characterization

We became also interested in analysing the host-guest chemistry of the octa-imine cage **5** in the gas phase. The stability of charged complexes formed by polar interactions is expected to be affected by the absence of solvent molecules.[34,35,36]

We performed ESI-MS analysis of solutions of **5** and **3⊂5** both in positive and negative mode. We further studied the complex stability using collision induced dissociation (CID)[37] experiments, which partially reflected what observed in solution.

For this purpose, we prepared a $CDCl_3$:CD_3CN solution of **5** at μM concentration containing 1 equiv. of **3** and 0.5% of TFA when operating in positive mode. The positive monocharged ion $[M+H]^+$ and the double charged $[M+2H]^{2+}$ were frequently detected, most likely due to the protonation of one or two imine groups.

In CID experiments in positive mode of the [**3⊂5**+H]$^+$ (m/z= 2878.437) selected ion, we observed that when the applied voltage was around 25 V it caused a significative loss of encapsulated guest **3** generating the [**5**+H]$^+$ (m/z=2666.289) ion (Figure 3.9). The voltage necessary to reduce up to 50% the intensity of the parent ion [**3⊂5**+H]$^+$ (25 V) was comparable to the one observed in the CID experiments for the encapsulation complex of a bis-*N*-oxide with the tetra-imine cage described in the

previous chapter. This result suggested that both capsular complexes have similar thermodynamic stabilities in the gas phase.

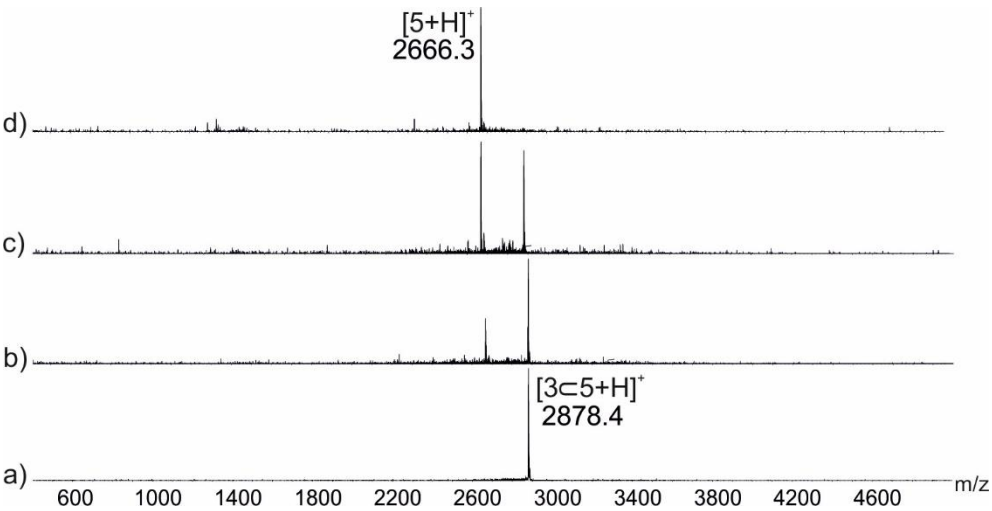

Figure 3.9. CID experiment performed with the mass selected ion [**3⊂5**+H]$^{+}$ with CE of (a) 0V, (b)15 V, (c) 25V, (d) 40 V.

We also performed Ion Mobility Mass Spectrometry (IMS)[38]- CID experiments in order to gain insight into the size of the complexes and the resulting ions upon increasing the voltage. When the parent ion [**3⊂5**+2H]$^{2+}$ was selected and subjected to fragmentation, we observed the appearance of a second signal having a smaller

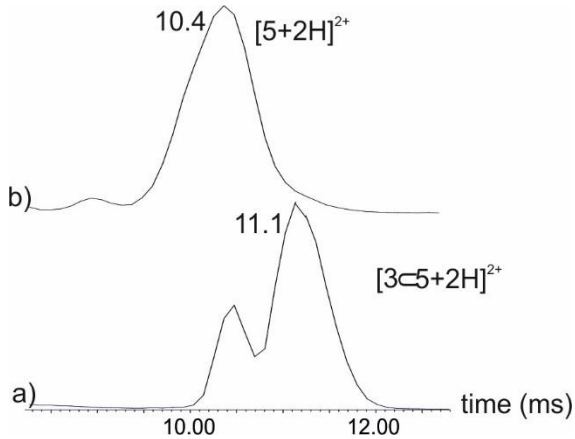

Figure 3.10. Arrival time distribution of ions [**3⊂5**+2H]$^{2+}$ and [**5**+2H]$^{2+}$ obtained in IMS-CID experiments of [**3⊂5**+2H]$^{2+}$ at (a) 4V and (b) 40V.

arrival time (Figure 3.10). At a voltage of 40 V, in the gas phase the second ion is exclusively detected. We assigned the peak to the doubly protonated ion [**5**+2H]$^{2+}$.

The small difference in arrival time might be related to a small difference in size of the two ions. We hypothesized that when **3** is expelled from the parent ion [**3**⊂**5**+2H]$^{2+}$, the resulting ion [**5**+2H]$^{2+}$ having an empty cavity experienced a small size reduction.

3.3 Conclusions

We describe the assembly of [4+2] octa imine capsules via condensation reaction between four units of aldehyde linkers (**1** or **2**) and two units of aryl-extended tetra amino-calix[4]pyrrole **4** in a 9:1 $CDCl_3$:CD_3CN solvents mixture. The use of a coordinating solvent such as acetonitrile allowed to template and pre-organize the calix[4]pyrrole cavity in the cone conformation and favor the formation of the capsular entity in good yields. We successfully obtained the octa-amine capsule **7** counterpart via simple reductive amination of imine bonds in presence of $NaBH_4$.

The capsules featuring weakly bound acetonitrile molecules were used as receptors for monotopic and ditopic *N*-oxide guests to produce thermodynamically (K_a larger than 10^4 M^{-1}) and kinetically stable complexes. The polar cavity of [4+2] octa-imine capsules is larger than the tetra-imine analogues and allowed the encapsulation of larger guests.

The ^{1}H NMR binding studies of octa-imine capsule **5** with two ditopic *N*-oxides of different lengths showed different symmetries of the resulting capsular complexes. On the one hand, the capsular complex with the shorter guest (4,4'(1,2-ethynyl)-bis-pyridine-1,1-dioxide **3**) **3**⊂**5** displays an apparent C_{4v} symmetry suggesting that the guest is too short to bind the two hemispheres of the capsule. On the other hand, the ^{1}H NMR of the capsular complex with the larger guest **10** (*i.e.* **10**⊂**5**) shows an apparent D_{4h} symmetry. This result confirmed that the length of guest **10** is good enough to fill the distance gap existing between the two polar hemispheres of capsule.

The X-ray analysis of single crystals of the capsular complexes **3**⊂**5** and **10**⊂**5** confirmed what we observed in solution. We hypothesize the co-encapsulation of the short guest **3** in the cavity of **5** with a molecule of water producing a C_{4v} symmetry complex.

In contrast, the more conformationally flexible octa-amine capsule **7** was able to adapt the cavity's dimensions to the short guest **3** producing a compact and stable encapsulation complex.

3.4 Experimental section

3.4.1 General information and instruments

Starting materials and reagents were purchased from commercial suppliers and used without any further purification. All reactions were performed under argon atmosphere and protected from light unless specified. Anhydrous solvents were obtained from a solvent purification system SPS-400-6 from Innovative Technologies. All solvents were of HPLC grade quality, commercially obtained and used without further purification.

^{1}H NMR, ^{13}C NMR and 2D NMR spectra were recorded on a Bruker Avance 400(400 MHz for ^{1}H NMR) and Bruker Avance500 (500 MHz for ^{1}H NMR). Deuterated solvents from Sigma Aldrich were used for NMR studies, previously dried for the synthesis of dynamic covalent capsules. Chemical shifts are given in ppm, relative to residual solvents.

Tetraamine calix[4]pyrrole **4**[39] synthesis was discussed in Chapter 2.

Mass spectrometric experiments were performed with a Synapt G2-S HDMS (Waters Co., Milford, MA, USA) travelling wave ion mobility mass spectrometer. All ions were generated by electrospray ionization (ESI) in the positive and negative mode. The parameters were optimized to get obtain the maximum abundance of the ions of interest.

3.4.2 Synthesis and characterization

3.4.2.1 *Synthesis of guest **10***

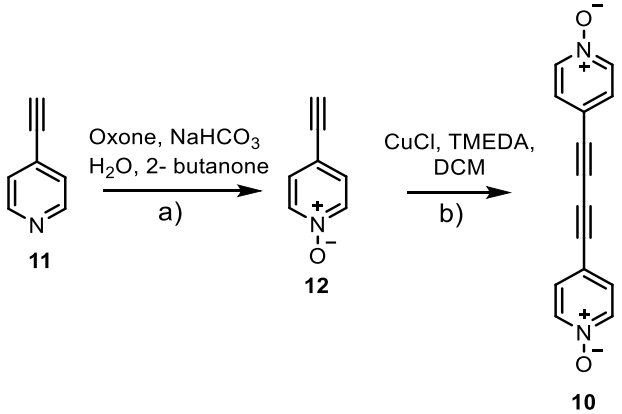

Scheme 3.2. Synthesis of bis-pyridyl *N*-oxide **10**.

a) 4-ethynylpyridine **11** (0.2 g, 1.94 mmol) was dissolved in a 1:1 mixture of water/2-butanone (60 ml) and $NaHCO_3$ (2.44 g, 29 mmol) was added under stirring. Then oxone® (2.38 mg, 3.88 mmol) was added dropwise as a water solution (20 mL). After 24h at r.t. (under Ar and protected from light), the crude mixture was extracted with chloroform (3x 60 mL). The organic layers were collected, dried over anhydrous Na_2SO_4 and concentrated under vacuum to afford pure **12** as a beige solid in 78% yield.
^{1}H NMR (400 MHz, $CDCl_3$) δ(ppm): 8.1 (d, *J*= 7.2 Hz, 2H), 7.3 (d, *J*= 7.2 Hz, 2H), 3.4 (s, 1H).
^{13}C [^{1}H] NMR (100 MHz, $CDCl_3$) δ(ppm): 139.2, 129.0, 119.6, 83.4, 79.9.
HR MS (APCI +) m/z: $[M+H]^+$ Calculated for $C_7H_6NO^+$= 120.0449, found 120.0447.

b) 4-ethynylpyridine *N*-oxide **12** (0.100 g, 0.84 mmol), CuCl (0.83 g, 8.4 mmol), and TMEDA (0.98 g, 8.4 mmol), were suspended in DCM (45 mL). The mixture was stirred at r.t. exposed to the air and protected from light. After 5.5 h the solvent was evaporated and adsorbed on neutral alumina. The reaction crude was purified by column chromatography (neutral alumina, chloroform: *i*-propanol 95:5 -> 50:50) to obtain bis-*N*-oxide **10** as a white solid in 25% yield.

^{1}H NMR (400 MHz, $CDCl_3$) δ(ppm): 8.14 (d, *J*= 7.1 Hz, 2H), 7.37 (d, *J*= 7.1 Hz, 2H).
HR MS (APCI +) m/z: $[M]^{+\cdot}$ Calculated for $C_{14}H_8N_2O_2^+$ =236.0586, found 236.0580.

3.4.2.2 *Synthesis of imine capsular complexes **3⊂5** and **3⊂6***

In a NMR tube containing 0.55 mL of a 2 mM solution of tetra-amino calix[4]pyrrole **4** in dry $CDCl_3$, we added 0.5 equiv. of guest **3** (prepared solubilizing **3** in a 2 mM solution of **4** to maintain constant the concentration of the host) to produce the capsular encapsulation complex **3⊂(4)$_2$**. Then 2 equiv. of terephtalaldehyde **1** or **2** (4 mM) were added to the solution and the mixture was heated up to 310 K for 12 h. The ^{1}H NMR spectrum showed the diagnostic proton signal for the formation of the octa-imine capsular complexes **3⊂5** or **3⊂6**, respectively in yield of 68 and 65% respectively.
3⊂5: ^{1}H NMR (400 MHz, $CDCl_3$) δ(ppm): 9.56 (br. s, 4H), 8.17 (s, 4H), 8.16 (s, 4H), 8.05 (br. s, 4H), 7.77 (d, *J*= 8.2 Hz, 8H) ,7.62 (d, *J*= 8.2 Hz, 8H), 7.18–7.00 (m, 32H), 6.77 (d, *J*= 7.0 Hz, 2H), 6.28 (d, *J*= 6.8 Hz, 2H), 6.08 (d, *J*= 2.6 Hz, 16H), 5.57 (d, *J*=7.0 Hz, 2H), 4.95 (d, *J*=6.8 Hz, 2H), 4.17–4.05 (m, 16 H), 2.50–2.40 (m, 16H), 2.28 (t, *J*= 7.5 Hz, 16 H), 1.65–1.46 (m, 16H, ov. with H_2O) 1.27–1.22 (m, 24H, ov. with grease).

MS (ESI TOF) m/z: $[M+2H]^{2+}$ Calculated for $C_{180}H_{178}N_{18}O_{18}^{2+}$ = 1439. 6677; Found 1439. 6631.

3⊂6: ^{1}H NMR (400 MHz, $CDCl_3$) δ(ppm): 9.62 (br.s, 4H), 8.55 (s, 4H), 8.45 (s, 4H), 8.17 (br. s, 4H), 7.78 (s, 4H), 7.61 (s, 4H), 7.19–6.99 (m, 26H), 6.96 (d, *J*= 7.4 Hz ,8H), 6.17 (d, *J*= 6.2 Hz, 2H), 6.08 (d, *J*= 2.5 Hz, 16H), 5.58 (d, *J*= 6.8 Hz, 2H), 4.88 (d, *J*= 6.8 Hz, 2H), 4.17– 4.05 (m, 16H), 2.50–2.40 (m, 16H), 2.32 (s, 12H, overl.), 2.30–2.24 (m, 16H overl.), 2.24 (s, 12H, overl.), 1.60–1.48 (m, 16H overl. with H_2O), 1.30–1.20 (m, 16H overl.).

3.4.2.3 *Synthesis of imine capsules **5** and **6***

Procedure A:

In a NMR tube, to 0.5 mL of a 2-4 mM solution of tetra-amino calix[4]pyrrole **4** in dry $CDCl_3$:CD_3CN 9:1 mixture, we added 2 equiv. of a solution of terephtalaldehyde **1** or **2** (4-8 mM) in the same mixture of solvents. The mixture was then heated up to 310 K for 24 h. The mixture turns into a yellow solution containing capsule **5** or **6** in 70% yield (according to the presence of an i.s. in solution).

5: ^{1}H NMR (400 MHz, $CDCl_3$:CD_3CN 9:1 mixture): 8.37 (s ,8H), 7.68 (s, 16H), 7.60 (br. s, 8H), 7.14 (d, *J* = 8.1 Hz,16H) ,7.06 (d, *J* = 8.1 Hz,16H), 5.96 (d, *J* = 2.6 Hz, 16H), 4.06 (q, *J* = 7.1 Hz,16 H), 2.39– 2.31 (m, 16H), 2.22 (t, *J* = 7.3 Hz,16H), 1.55– 1.44 (m, 16H) 1.20 (t, *J* = 7.1 Hz,24H).

MS (ESI TOF) m/z: $[M+2H]^{2+}$ Calculated for $C_{168}H_{170}N_{16}O_{16}^{2+}$ = 1333, 6485; Found 1333, 6630.

6: ^{1}H NMR (400 MHz, $CDCl_3$:CD_3CN 9:1 mixture) δ(ppm): 8.66 (s, 8H), 7.62 (br. s, 8H), 7.05 (s, 32H), 5.97 (d, *J* = 2.6 Hz, 16H), 4.06 (q, *J* = 7.1 Hz, 16H), 2.4–2.33 (m, 16H), 2.23 (t, *J* = 7.2 Hz, 16H), 1.96 (s, 24H), 1.55–1.45 (m, 16H), 1.19 (t, *J* = 7.1 Hz, 24H).

Procedure B (large scale):

In a dry Shlenk flask tetra-amino calix[4]pyrrole **4** (18 mg, 16.3 µmol) was dissolved in 4 mL of dry chloroform-acetonitrile 9:1 mixture and then terephtalaldehyde **1** (4.4 mg, 33 µmol, 2 equiv.) was added as a solid. A change in the color of the solution from beige to yellow was observed. The mixture was stirred at 310 K under Ar and protected from light for 48h to give capsule **5** in 55% yield (according to an i.s. in solution). Capsule **5** was obtained as a yellow solid after evaporation of the solvent.

3.4.2.4 *Synthesis of amine capsule **7** (one pot reductive amination)*

To a 4 mM solution of **5** in 4 mL of $CHCl_3$:CH_3CN 9:1 mixture, we added 0.4 mL of anhydrous MeOH. Then, $NaBH_4$ (27 mg, 0.7 mmol, 43 equiv. previously dried for 3 h under ultra-high vacuum) was added portion wise under Ar. A change in the solution color from yellow to white was observed. The mixture was stirred under Ar protected from light for 26h. If necessary the addition of portions of $NaBH_4$ can be repeated. The mixture was diluted with chloroform and washed with water (x3). The organic phase was dried over anhydrous Na_2SO_4, filtered and dried at low pressure. Octa-amine capsule **7** was obtained as a beige solid.

^{1}H NMR (500 MHz, $CDCl_3$:CD_3CN 9:1 mixture) δ(ppm): 7.77 (br. s, 8H), 7.12 (s, 16H), 6.84 (d, *J* = 8.2 Hz, 16H), 6.58 (d, *J* = 8.2 Hz, 16H), 5.86 (d, *J* = 2.7 Hz, 16H), 4.09–4.01 (m, 32H), 3.84 (br. s, 8H), 2.32–2.24 (m, 16H), 2.23–2.15 (m, 16H), 1.54–1.40 (m, 16H), 1.20 (t, *J* = 7.2 Hz, 24H).

^{13}C [^{1}H]NMR (126 MHz, $CDCl_3$:CD_3CN 9:1 mixture) δ(ppm): 173.5, 145.9, 137.6, 137.4, 130. 8, 128.9, 111.8, 103.9, 60.0, 49.2, 47.3, 38.7, 34.4, 29.5, 20.5, 14.1.

HR MS (ESI TOF) m/z: $[M+Na]^+$ Calculated for $C_{168}H_{184}N_{16}O_{16}Na^+$ = 2704.3970; Found 2704.4000.

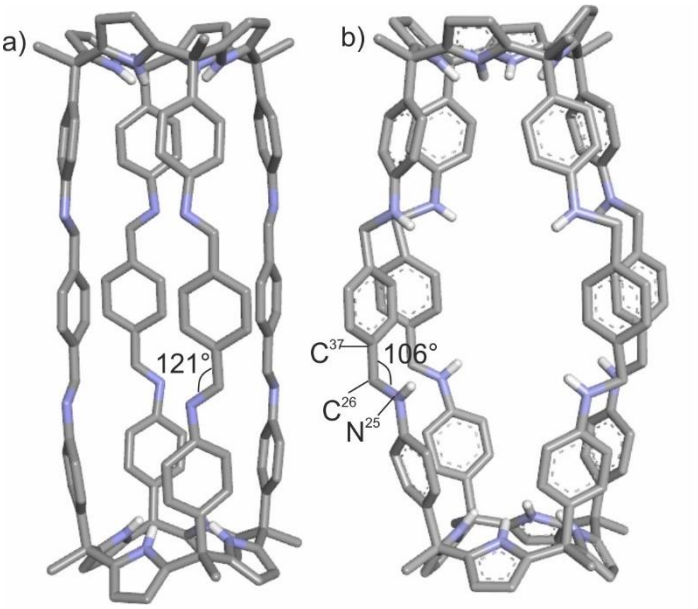

Figure 3.11 (a) Single crystal structure of a mixture of capsule **5** with guest **3** (encapsulated guest **3** was omitted for clarity); (b) preliminary single crystal structure of a mixture of capsule **7** with a ditopic triazole guest *N*-oxide (here omitted for clarity). Ester chains at lower rim and guest are omitted for clarity.

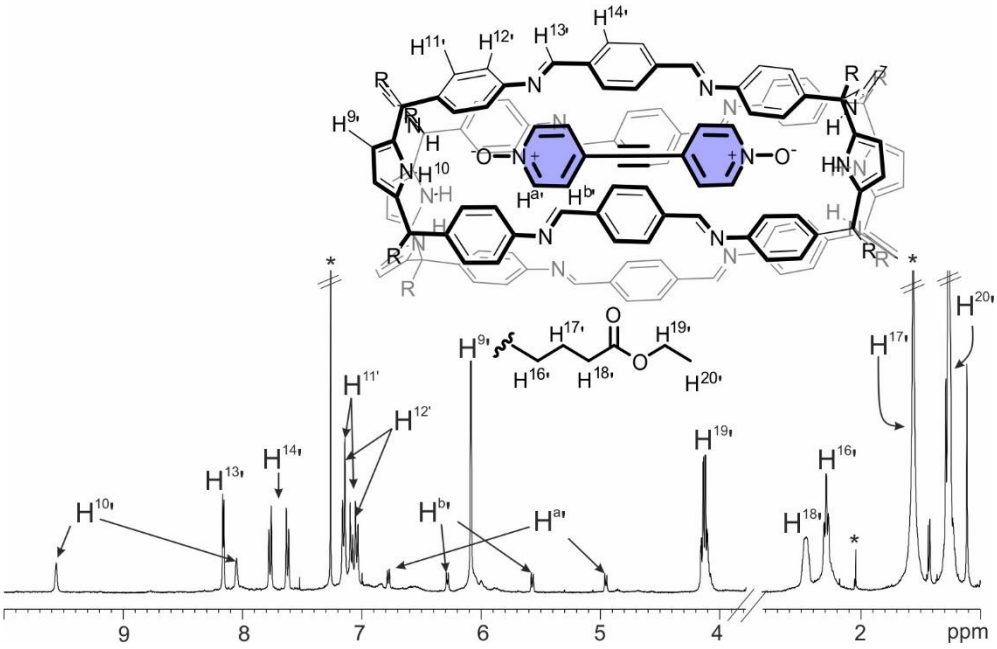

Figure 3.12. ^{1}H NMR spectrum (400 MHz, at 298 K, $CDCl_3$) of 1:0.5:2 mixture of tetra-amino calix[4]pyrrole **4**, bis pyridine *N*-oxide **3** and dialdehyde **1** after 12 h at 310 K to form the imine capsular complex **3⊂5**. Primed letters indicate bound host and guest in the 1:1 complex. (*) Indicates residual solvents.

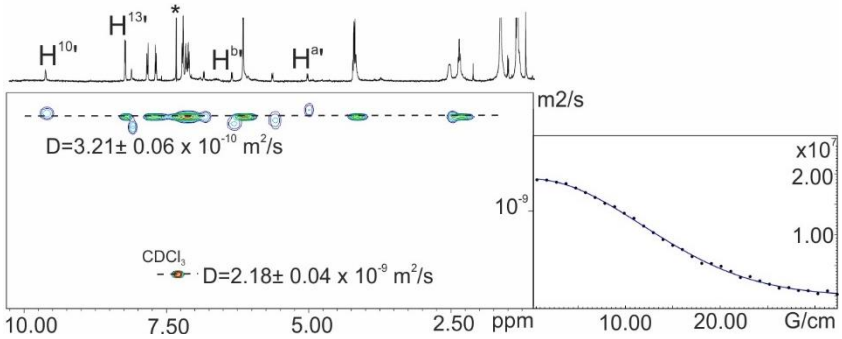

Figure 3.13. ^{1}H pseudo-2D DOSY NMR (400 MHz, at 298 K, $CDCl_3$, big delta= 0.1 s, little delta= 0.002 s) of imine capsular complex **3⊂5**. Primed letters indicate bound host and guest in the 1:1 complex. See Figure 3.12 for protons assignment. (*) Indicates residual solvents.

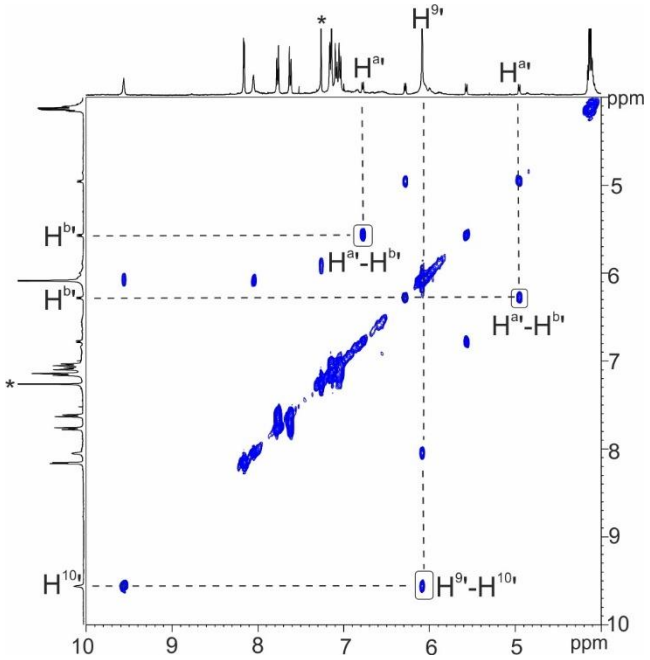

Figure 3.14. Selected region of 2D COSY NMR (400 MHz, at 298 K, $CDCl_3$) of imine capsular complex **3⊂5**. Primed letters indicate bound host and guest in the 1:1 complex. See Figure 3.12 for protons assignment.(*) Indicates residual solvents.

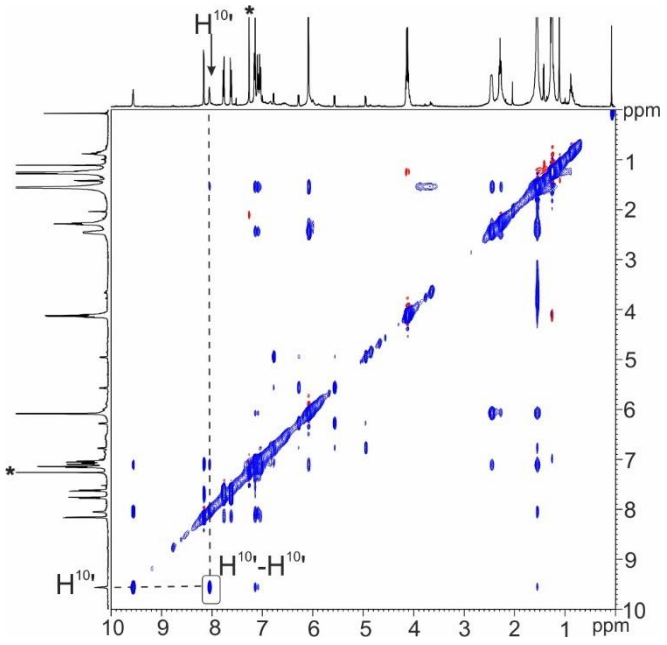

Figure 3.15. 2D EXSY NMR (400 MHz, at 298 K, $CDCl_3$, d_8= 0.3 s) of imine capsular complex **3⊂5**. Primed letters indicate bound host and guest in the 1:1 complex. See Figure 3.12 for protons assignment.(*) Indicates residual solvents. The exchange peak between pyrrole NHs proton signals indicates a fast exchange on the EXSY NMR timescale.

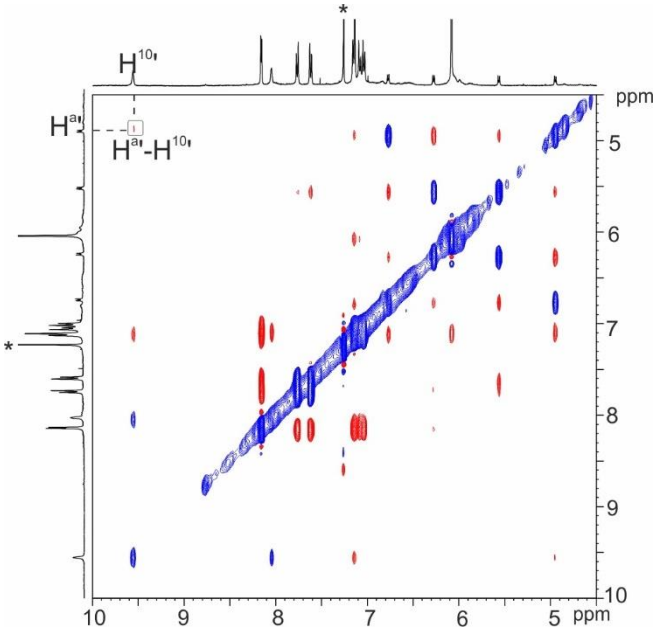

Figure 3.16. Selected region of 2D ROESY NMR (400 MHz, at 298 K, $CDCl_3$, p15= 0.3 s) of imine capsular complex **3⊂5**. Primed letters indicate bound host and guest in the 1:1 complex. See Figure 3.12 for protons assignment. (*) Indicates residual solvents.

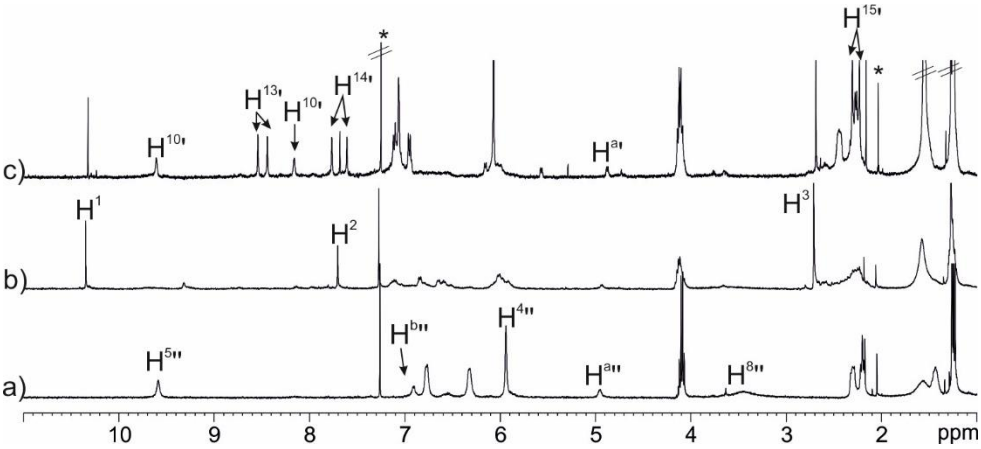

Figure 3.17. ^1H NMR spectra (400 MHz, at 298 K, $CDCl_3$) of (a) 1:0.5 mixture of tetra-amino calix[4]pyrrole **4** and bis pyridine *N*-oxide **3** (capsular complex **3⊂(4)$_2$**), (b) after addition of 2 equiv. of dialdehyde **1** (1:0.5:2 mixture of **4**:**3**:**1**), (c) after heating for 12h at 310 K the 1:0.5:2 mixture of **4**:**3**:**1** (imine capsular complex **3⊂6**). Primed and double primed letters indicate bound host and guest in the 1:1 and 2:1 complexes respectively. See Scheme 3.1 for protons assignment. (*) Indicates residual solvents.

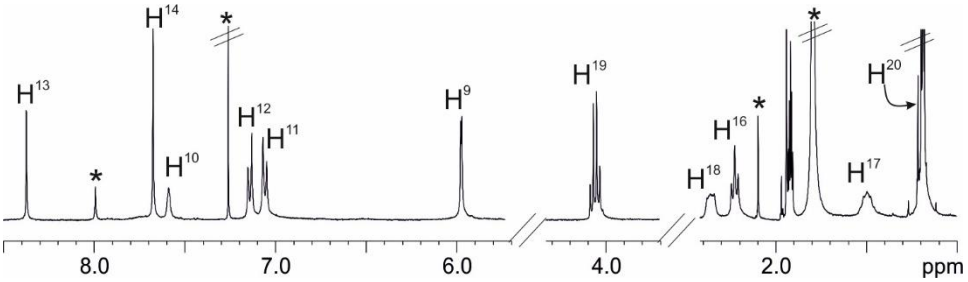

Figure 3.18 ^{1}H NMR spectrum (400 MHz, at 298 K, $CDCl_3$:CD_3CN 9:1 mixture) of a 1: 2 mixture of tetra-amino calix[4]pyrrole **4** and dialdehyde **1** after 24h at 310 K (imine capsule **5**). See Figure 3.12 for protons assignment. (*) Indicates residual solvents and unreacted dialdehyde **1**.

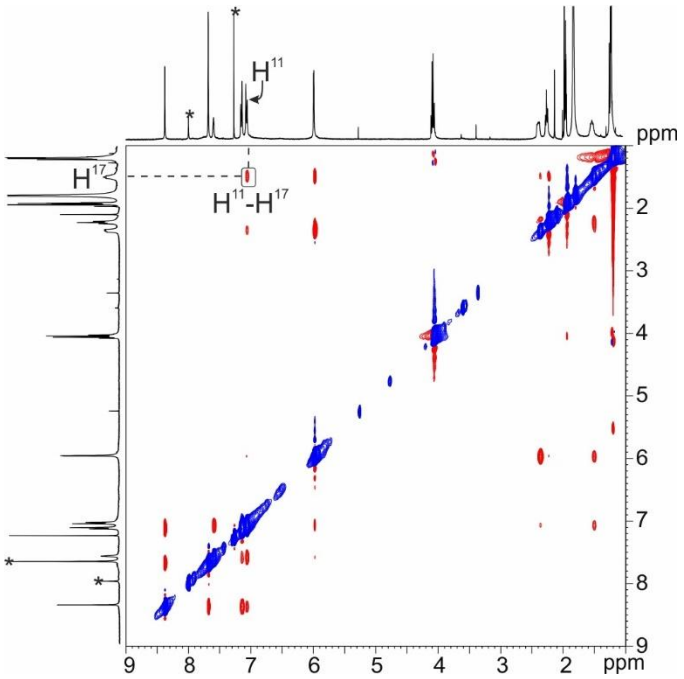

Figure 3.19. 2D ROESY NMR (400 MHz, at 298 K, $CDCl_3$:CD_3CN 9:1 mixture, p15= 0.3 s) of a solution containing imine capsule **5**. See Figure 3.12 for protons assignment. (*) Indicates residual solvents and unreacted dialdehyde **1**.

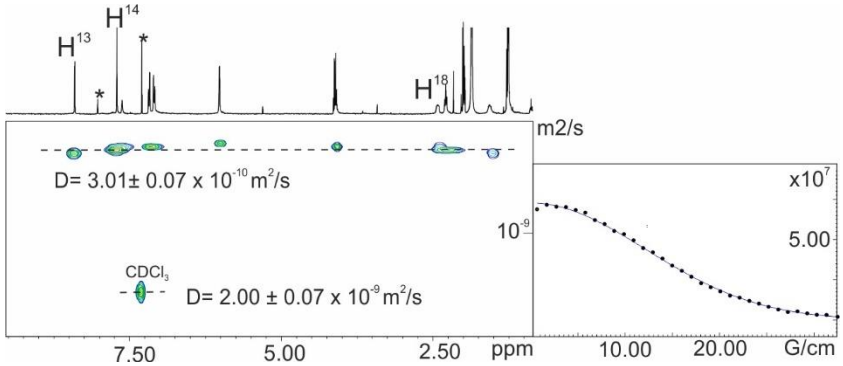

Figure 3.20. ^{1}H pseudo-2D DOSY NMR (400 MHz, at 298 K, $CDCl_3$:CD_3CN 9:1 mixture , big delta= 0.1 s, little delta= 0.002 s) of a solution containing imine capsule **5**. See Figure 3.12 for protons assignment. (*) Indicates residual solvents and unreacted dialdehyde **1**.

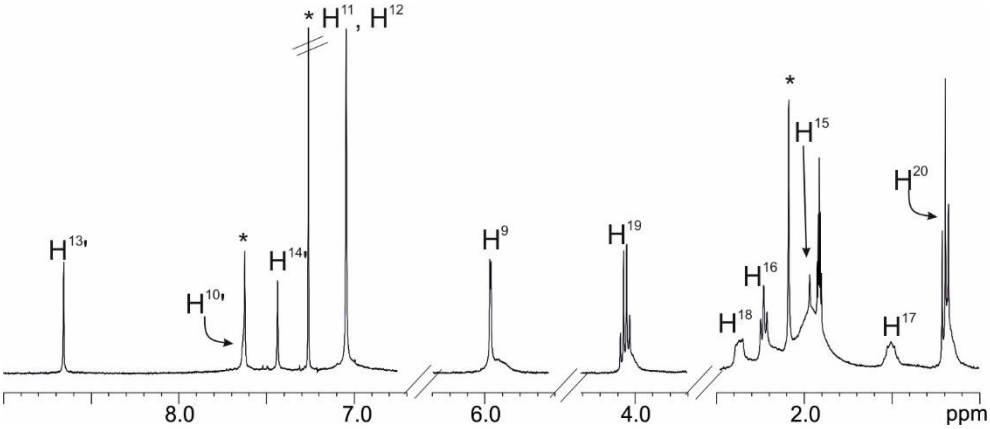

Figure 3.21. ^{1}H NMR spectrum (400 MHz, at 298 K, $CDCl_3$:CD_3CN 9:1 mixture) of a 1:2 mixture of tetra-amino calix[4]pyrrole **4** and dialdehyde **2** after 24h at 310 K (imine capsule complex **6**). Primed letters indicate bound host and guest in the 1:1 complex. See Scheme 3.1 for protons assignment. (*) Indicates residual solvents and unreacted dialdehyde **2**.

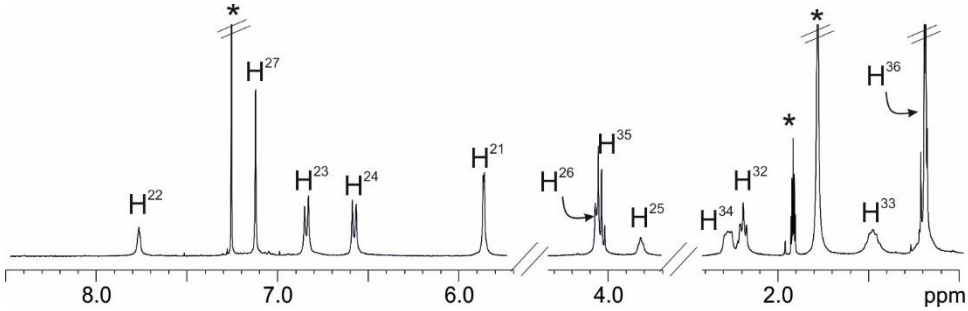

Figure 3.22. ^{1}H NMR spectrum (400 MHz, at 298 K, $CDCl_3$:CD_3CN 9:1 mixture) of octa-amine capsule **7**. See Scheme 3.1 for protons assignment. (*) Indicates residual solvents.

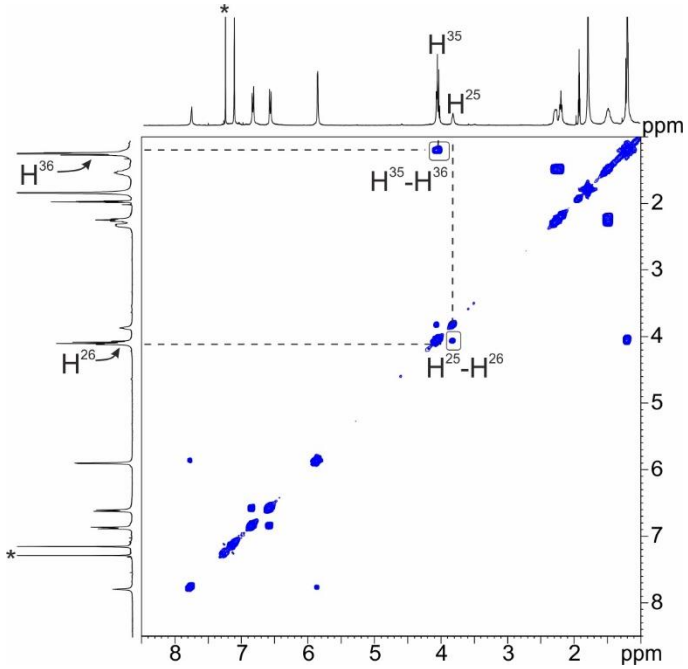

Figure 3.23. 2D COSY NMR (400 MHz, at 298 K, $CDCl_3$:CD_3CN 9:1 mixture) of octa-amine capsule **7**. See Scheme 3.1 for protons assignment. (*) Indicates residual solvents.

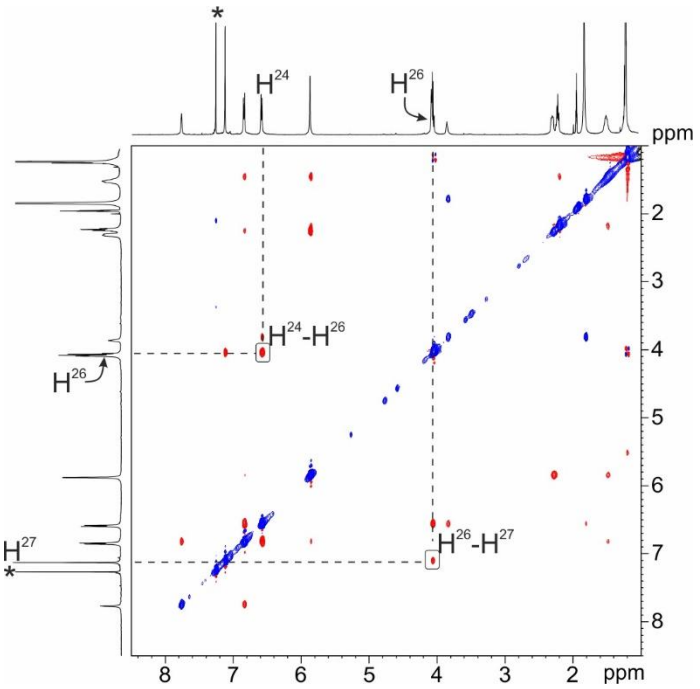

Figure 3.24. 2D ROESY NMR (500 MHz, at 298 K, $CDCl_3$:CD_3CN 9:1 mixture, p15= 0.3 s) of octa-amine capsule **7**). See Scheme 3.1 for protons assignment. (*) Indicates residual solvent.

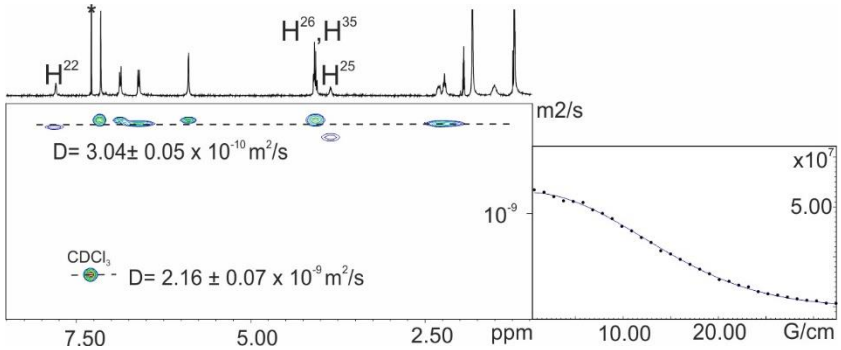

Figure 3.25. ^{1}H pseudo-2D DOSY NMR (400 MHz, at 298 K, $CDCl_3$:CD_3CN 9:1 mixture , big delta= 0.1 s, little delta= 0.002 s) of octa-amine capsule **7**. See Scheme 3.1 for protons assignment. (*) Indicates residual solvents.

3.4.3 Binding studies in $CDCl_3$:CD_3CN 9:1 mixture

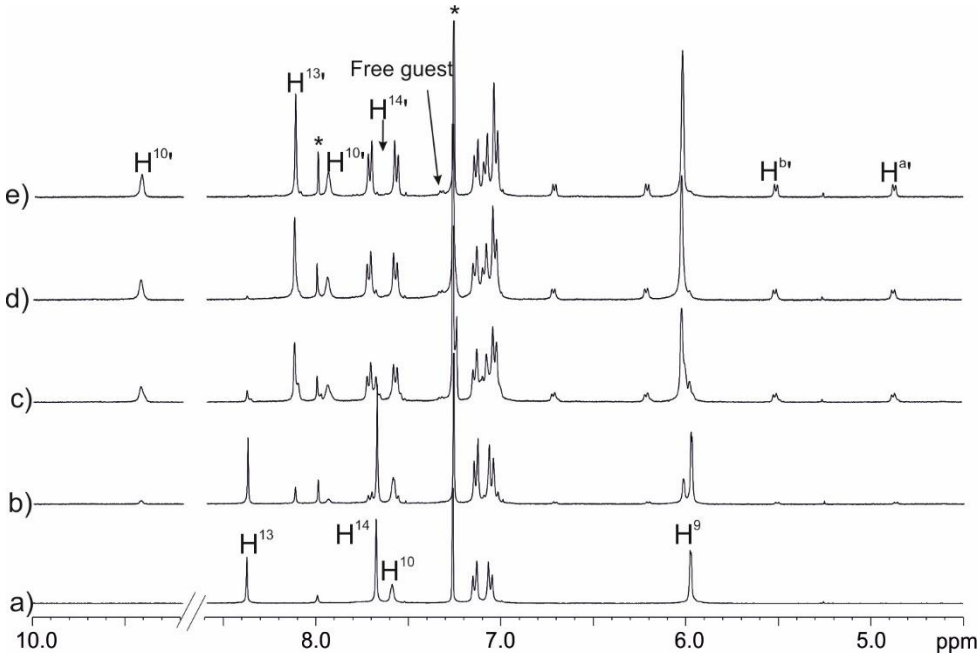

Figure 3.26. Selected ^{1}H NMR region of spectra (400 MHz, at 298 K, $CDCl_3$:CD_3CN 9:1 mixture) of (a) capsule **5**, (b) immediately after addition of 0.4 equiv. of **3**, (c) upon addition of 0.8 equiv. of **3**, (d) upon addition of 1.2 equiv. of **3**, (e) 15 min. after addition of 1.2 equiv. of **3**. Primed letters indicate the bound host and guest in the 1:1 complex. See Scheme 3.1 and Figure 3.5 for protons assignment. (*) Indicates the residual solvents and unreacted aldehyde linker **1**.

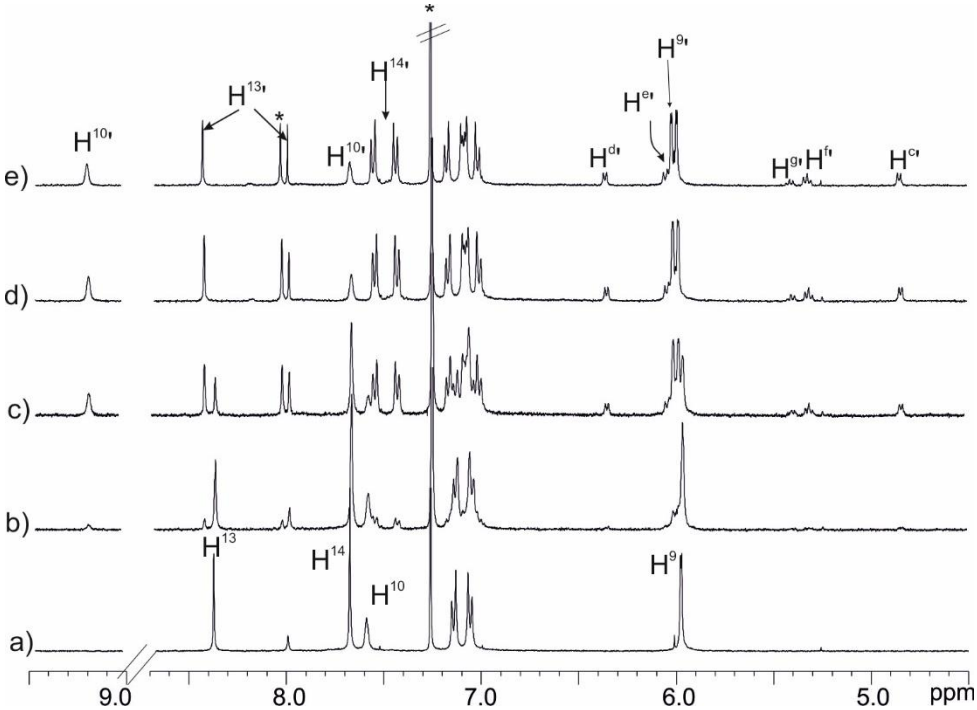

Figure 3.27. Selected ^{1}H NMR region of spectra (400 MHz, at 298 K, $CDCl_3$:CD_3CN 9:1 mixture) of (a) capsule **5**, (b) immediately after addition of 0.3 equiv. of **8**, (c) upon addition of 0.6 equiv. of **8**, (d) upon addition of 1 equiv. of **8**, (e) 10 min after addition of 1.2 equiv. of **8**. Primed letters indicate the bound host and guest in the 1:1 complex. See Scheme 3.1 and Figure 3.5 for protons assignment. (*) Indicates the residual solvents and unreacted aldehyde linker **1**.

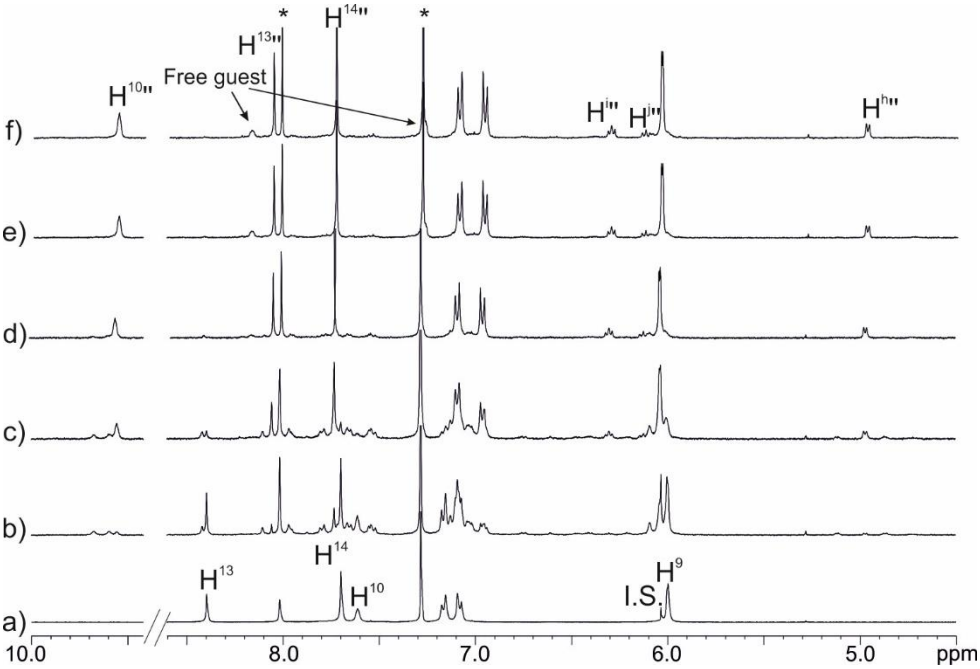

Figure 3.28. Selected ^{1}H NMR region of spectra (400 MHz, at 298 K, $CDCl_3$:CD_3CN 9:1 mixture) of (a) capsule **5**, (b) immediately after addition of 0.8 equiv. of **9**, (c) upon addition of 1.2 equiv. of **9**, (d) upon addition of 2 equiv. of **9**, (e) upon addition 2.2 equiv. of **9**, (f) 15 min. after addition of 2.2 equiv. of **9**. Double primed letters indicate the bound host and guest in the 1:2 complex. See Scheme 3.1 and Figure 3.5 for protons assignment. (*) Indicates the residual solvents and unreacted aldehyde linker **1**.

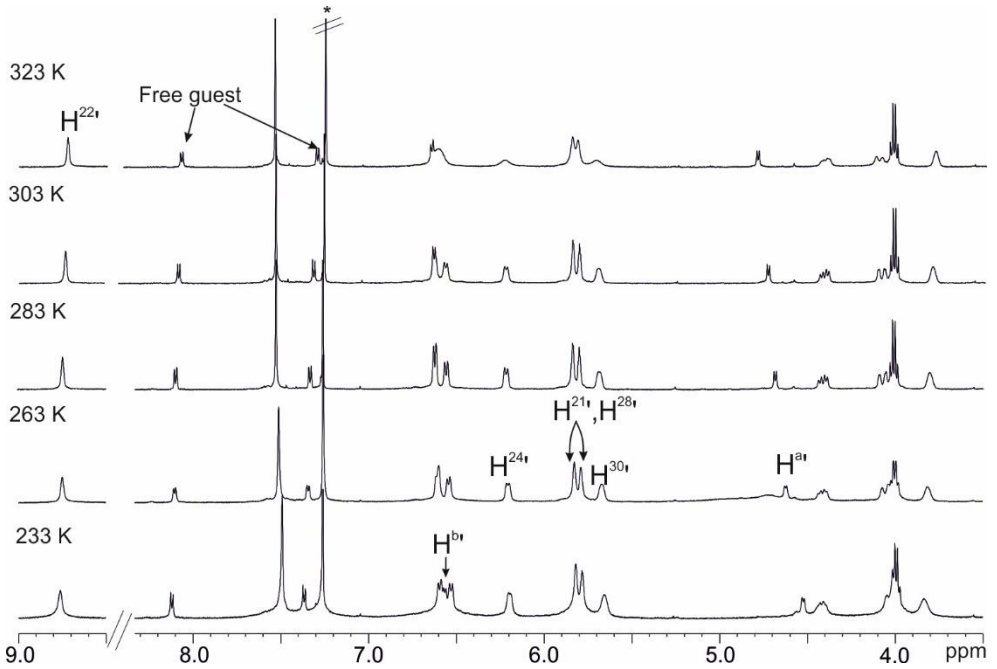

Figure 3.29. Variable temperature ^{1}H NMR spectra (500 MHz, $CDCl_3$:CD_3CN 9:1 mixture) of a solution of **7** (1 mM) with excess of **3**. See Scheme 3.1 and Figure 3.8 for protons assignment. Primed letters indicate the bound host and guest in the 1:1 complex. (*) Indicates the residual solvents.

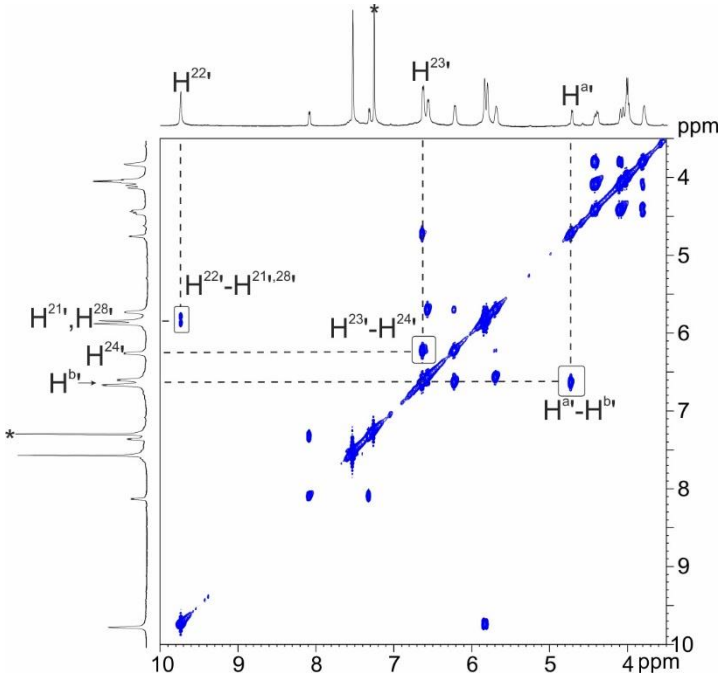

Figure 3.30. 2D COSY NMR (500 MHz, at 298 K, $CDCl_3$:CD_3CN 9:1 mixture) of octa-amine capsular complex **3⊂7.**See Scheme 3.1 and Figure 3.8 for protons assignment. Primed letters indicate the bound host and guest in the 1:1 complex. (*) Indicates the residual solvents.

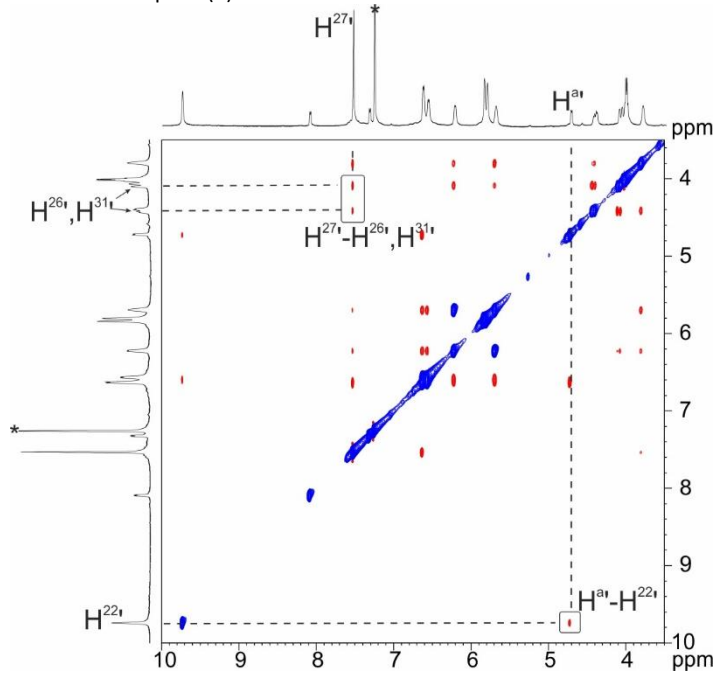

Figure 3.31. 2D ROESY NMR (500 MHz, at 298 K, $CDCl_3$:CD_3CN 9:1 mixture, p15= 0.3s) of a octa-amine capsule **7** solution with 2 equiv. of **3**. See Scheme 3.1 and Figure 3.8 for proton assignment. Primed letters indicate the bound host and guest in the 1:1 complex. (*) Indicates residual solvents.

3.4.4 Characterization in gas phase

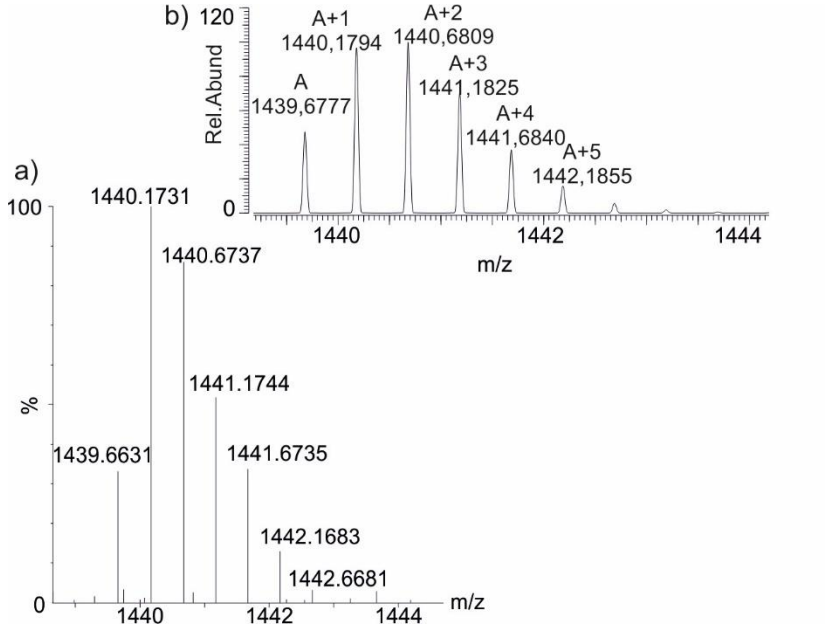

Figure 3.32. Experimental (a) and calculated (b) isotopic pattern of capsular complex [**3**⊂**5**+2H]$^{2+}$**.**

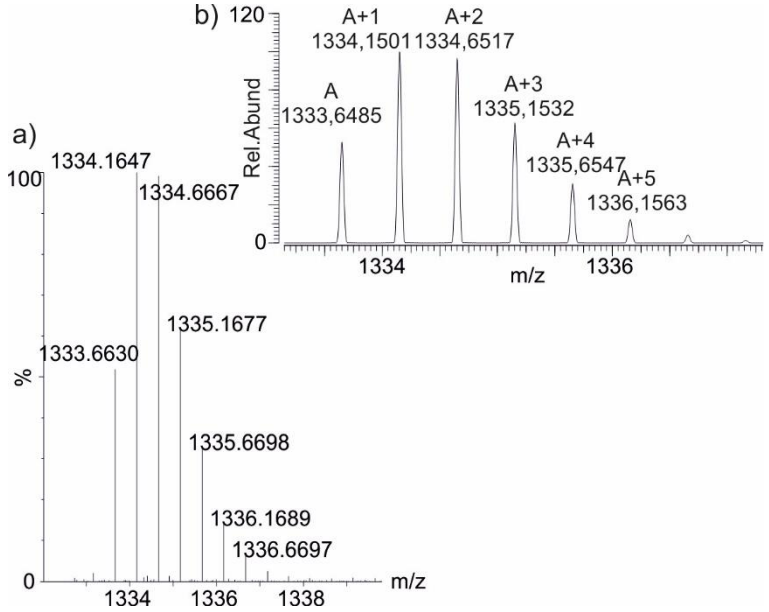

Figure 3.33. Experimental (a) and calculated (b) isotopic pattern of capsule [**5**+2H]$^{2+}$.

3.5 References and notes

[1] M. L. C. Quan, D. J. Cram, *J. Am. Chem. Soc.* **1991**, *113*, 2754-2755.
[2] J.-M. Lehn, *Chem. Soc. Rev.* **2007**, *36*, 151-160.
[3] M. Kołodziejski, A. R. Stefankiewicz, J.-M. Lehn, *Chem. Sci.* **2019**, *10*, 1836-1843.
[4] L. Adriaenssens, P. Ballester, *Chem. Soc. Rev.* **2013**, *42*, 3261.
[5] A. Asadi, D. Ajami, J. Rebek, *Chem. Sci.* **2013**, *4*, 1212-1215.
[6] Y. Sakata, R. Tsuyuki, S. Sugimoto, S. Akine, *Chem. Commun. (Cambridge, U. K.)* **2021**, *57*, 13510-13513.
[7] S. J. Rowan, S. J. Cantrill, G. R. L. Cousins, J. K. M. Sanders, J. F. Stoddart, *Angew. Chem. Int. Ed.* **2002**, *41*, 898-952.
[8] J. H. Billman, A. C. Diesing, *J. Org. Chem.* **1957**, *22*, 1068-1070.
[9] E. Ramakrishna, J.-D. Tang, J.-J. Tao, Q. Fang, Z. Zhang, J. Huang, S. Li, *Chem. Commun. (Cambridge, U. K.)* **2021**, *57*, 9088-9091.
[10] A. S. Bhat, S. M. Elbert, W.-S. Zhang, F. Rominger, M. Dieckmann, R. R. Schröder, M. Mastalerz, *Angew. Chem. Int. Ed.* **2019**, *58*, 8819-8823.
[11] P.-E. Alexandre, W.-S. Zhang, F. Rominger, S. M. Elbert, R. R. Schröder, M. Mastalerz, *Angew. Chem. Int. Ed.* **2020**, *59*, 19675-19679.
[12] M. Mastalerz, *Chem. Commun. (Cambridge, U. K.)* **2008**, 4756-4758.
[13] T. H. G. Schick, J. C. Lauer, F. Rominger, M. Mastalerz, *Angew. Chem. Int. Ed.* **2019**, *58*, 1768-1773.
[14] X.-Y. Hu, W.-S. Zhang, F. Rominger, I. Wacker, R. R. Schröder, M. Mastalerz, *Chem. Commun. (Cambridge, U. K.)* **2017**, *53*, 8616-8619.
[15] A. Galán, E. C. Escudero-Adán, P. Ballester, *Chem. Sci.* **2017**, *8*, 7746-7750.
[16] F. Aricó, J. D. Badjic, S. J. Cantrill, A. H. Flood, K. C. F. Leung, Y. Liu, J. F. Stoddart, in *Templates in Chemistry II: -/-* (Eds.: C. A. Schalley, F. Vögtle, K. H. Dötz), Springer Berlin Heidelberg, Berlin, Heidelberg, **2005**, pp. 203-259.
[17] C. D. Meyer, C. S. Joiner, J. F. Stoddart, *Chem. Soc. Rev.* **2007**, *36*, 1705-1723.
[18] G. Olivo, G. Capocasa, D. Del Giudice, O. Lanzalunga, S. Di Stefano, *Chem. Soc. Rev.* **2021**, *50*, 7681-7724.
[19] Y. Lyu, P. Scrimin, *ACS Catal.* **2021**, *11*, 11501-11509.
[20] A. B. Grommet, M. Feller, R. Klajn, *Nat. Nanotechnol.* **2020**, *15*, 256-271.
[21] A. Galán, G. Aragay, P. Ballester, *Chem. Sci.* **2016**, *7*, 5976-5982.
[22] C. L. Perrin, T. J. Dwyer, *Chem. Rev. (Washington, DC, U. S.)* **1990**, *90*, 935-967.
[23] A. Pastor, E. Martínez-Viviente, *Coord. Chem. Rev.* **2008**, *252*, 2314-2345.
[24] A. Díaz-Moscoso, D. Hernández-Alonso, L. Escobar, F. A. Arroyave, P. Ballester, *Org. Lett.* **2017**, *19*, 226-229.
[25] G. Gil-Ramírez, E. C. Escudero-Adán, J. Benet-Buchholz, P. Ballester, *Angew. Chem. Int. Ed.* **2008**, *47*, 4114-4118.
[26] Especially when the capsule is assembled in absence of a guest, we often observed an excess of aldehyde in solution. When we use a little defect of dialdehyde linker, we observed the formation of a not fully closed species. We then kept working using **1** and **4** in a 2:1 ratio. The free aldehyde linker in solution does not interfere with binding processes.

[27] X. Liu, Y. Liu, G. Li, R. Warmuth, *Angew. Chem. Int. Ed.* **2006**, *45*, 901-904.
[28] When capsule **6** is similarly treated to get the amino derivative, only a partial reduction of amino groups is observed. We also observed that reductive amination under the conditions used works better when performed on a NMR tube scale.
[29] J. P. Perdew, *Phys. Rev. B* **1986**, *33*, 8822-8824.
[30] A. D. Becke, *Phys. Rev. A* **1988**, *38*, 3098-3100.
[31] S. Grimme, J. Antony, S. Ehrlich, H. Krieg, *J. Chem. Phys.* **2010**, *132*, 154104.
[32] F. Furche, R. Ahlrichs, C. Hättig, W. Klopper, M. Sierka, F. Weigend, *WIREs Comput Mol Sci* **2014**, *4*, 91-100.
[33] M. Von Arnim, R. Ahlrichs, *J. Comput. Chem.* **1998**, *19*, 1746-1757.
[34] B. Baytekin, H. T. Baytekin, C. A. Schalley, *Org. Biomol. Chem.* **2006**, *4*, 2825-2841.
[35] L. Cera, C. A. Schalley, *Chem. Soc. Rev.* **2014**, *43*, 1800-1812.
[36] Z. Qi, T. Heinrich, S. Moorthy, C. A. Schalley, *Chem. Soc. Rev.* **2015**, *44*, 515-531.
[37] K. Caprice, M. Pupier, A. Kruve, C. A. Schalley, F. B. L. Cougnon, *Chem. Sci.* **2018**, *9*, 1317-1322.
[38] A. Kruve, K. Caprice, R. Lavendomme, J. M. Wollschläger, S. Schoder, H. V. Schröder, J. R. Nitschke, F. B. L. Cougnon, C. A. Schalley, *Angew Chem Int Ed Engl* **2019**, *58*, 11324-11328.
[39] L. Escobar, F. A. Arroyave, P. Ballester, *Eur. J. Org. Chem.* **2018**, *2018*, 1097-1106.

Chapter 4

[4+2] Octa-imine capsule and its octa-amino derivative as supramolecular nanoreactors

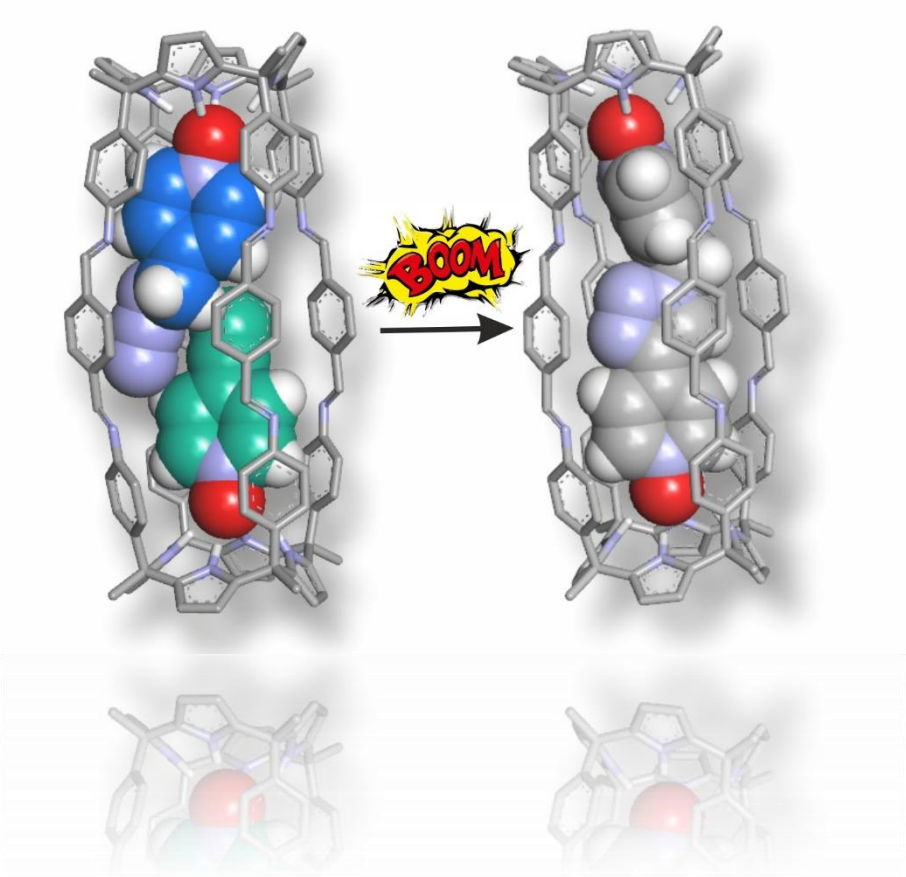

Unpublished results

4.1 Introduction

The inclusion of size, shape and function complementary guests in the cavities of synthetic molecular containers enables not only selective molecular recognition but also controlling the properties and reactivities of the bound substrates. These functions mimic those of the binding pockets of the enzymes.[1,2] Intra- and inter-molecular reactions have been promoted in the cavities of synthetic molecular containers with rate enhancements that, in some cases, were comparable to those of the biological counterparts.[3] Consequently, the applications of synthetic molecular containers for the stabilization of reactive species/intermediates,[4] accelerate reactivity, enhance or -invert regio- and stereoselectivity, and sometimes even promote new reactions constitute current topics of interest in chemical research.[5,6] The function of the containers as nano-reactors occurs because the molecules bound in their cavities orient in specific ways or fold into unusual high energy conformations, favouring intra- and inter-molecular reactions. In addition, effective substrate concentrations are increased by several orders of magnitude compared to the bulk solvent due to confinement of the reactant in the container's cavities. On the other hand, the stabilization effect played by the molecular containers is related to the impossibility of the substrate/s to achieve the reaction transition state owing to its tight confinement.

Supramolecular catalysis covers many different approaches to affect chemical reactivity. When using molecular containers to mediate or accelerate chemical reactions, two general approaches can be considered: a) location of catalytic centre/s close to the container's cavity (binding site) and b) binding the reactants in the container's cavity by forming a supramolecular ternary complex. In this latter case, the reaction rate can be accelerated not only by stabilization of the transition state (enthalpy) but also by the simply increase of the effective local concentrations of the reactants (entropy).[5]

As an example of the first approach, that is molecular containers decorated with catalytic units, Yuan and co-workers recently reported two porous poly-imine organic cages (POCs) based on a tetraformyl-functionalized calix[4]resorcinarene and different diamine linkers endowed with appended chiral proline moieties. The [4+8] and [3+6] assembled cages were shown to be effective supramolecular nanoreactors for the asymmetric aldol reaction.[7] Although, in principle, the reaction could take place inside the cavity or in the external surface of the cages, the authors designed thoughtful experiments to demonstrate that the majority of the catalytic

reaction took place inside the cavity. Substrates that according to their size and shape could not be encapsulated in the cage's cavity showed reduced rate accelerations.

In the second approach of the use of molecular containers in mediating chemical reactivity, the rate acceleration is mainly provided by the increase in local concentration of the two reactants caused by their inclusion in the container's cavity (effective molarity).[8] Other factors influencing the reaction rate, as elimination of the reorganization of the solvent molecules or stabilization of the transition state, are possible but difficult to evidence. A classic example of this approach is the use of Rebek's tennis ball[9] to accelerate the rate of a Diels-Alder reaction of cyclohexadiene and *p*-quinone.[10] Remarkably, one encapsulation species dominated the ^{1}H NMR spectrum of the mixture after addition of the reactants. Only a signal for the encapsulated quinone was observed and no signals unique to encapsulated cyclohexadiene were detected. However, some cyclohexadiene must be co-encapsulated with the quinone because the signals of the encapsulated adduct

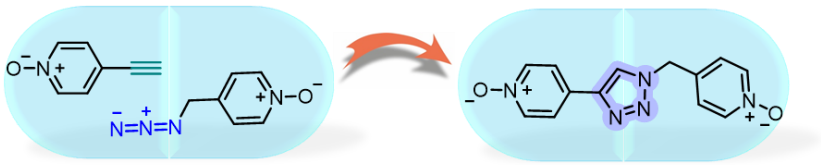

Figure 4.1. Schematic representation of a Huisgen azide-alkyne 1,3-dipolar cycloaddition in a confined space.

appeared after one day. These signals grew at the expense of the signal of bound quinone. The probable precursor to the encapsulated adduct is the ternary complex, which can be regarded as the counterpart of the Michaelis complex, as it converts to products in a first-order process. The rates showed saturation kinetics suggesting that the reaction was taken place inside the capsule. Control experiments demonstrated that other forms of conventional catalysis *i.e*. acid catalysis were not operative. The authors performed studies of size selectivity and product inhibition. The obtained results are consistent with the encapsulation of the transition state. The accelerating effect of the encapsulation of two reactants in the self-assembled capsule was interpreted as an increase of their local concentration rather than some special stabilization of the transition state. An effective molarity (EM = k_{intra}/k_{inter}) value of 2.4 M for the reactants was determined that is consistent with the estimated 5 M concentrations for the reactants ($V_{capsule}$ = 300 Å^3).

A similar effect was observed for the Huisgen azide-alkyne 1,3-dipolar cycloaddition[11,12] (lately included in the family of "click reactions"[13]) when performed in the cavity of a cucurbit[6]uril[14] and a resorcin[4]arene based self-assembled dimeric capsule.[15] In both cases, the regioselectively of the reaction was also altered, compared to the bulk solution, providing exclusively the 1,4-cycloaddition isomer. The cucurbit[6]uril binds the azide and alkyne reactants by establishing electrostatic interactions between their alkyl ammonium substituents and the carbonyl groups at the portals of the container. The two reacting groups were oriented and fully encapsulated in the hydrophobic cavity of the container.
In the case of the cylindrical capsule formed by dimerization of a resorcin[4]arene cavitand, the azide and alkyne reagents were equipped with a phenyl group to anchor them in the cavity of the container. The capsule can accommodate two copies of the reactants and constrain their orientation to edge-to-edge approaches. The disproportionation of the 2:1 homo-capsular complexes produced an unsymmetrical hetero-capsule involving one azide and one alkyne (Michaelis-Menten complex) that was the major species. The estimated increase in local concentrations of the substrates are 3.7 M for the capsule and 10 M for the cucurbit[6]uril. The cucurbit[6]uril induced a rate acceleration that was quantified to be of the order of 10^5 fold, however the reaction inside the capsule was calculated to proceed only 240 times faster than outside. This difference might be attributed to the different orientations of the reactants in the two containers. No reasons were put forward to support that the transition state was better bound than the reactants.

In this chapter, we will describe the application of the octa-imine and octa-amine [4+2] capsules based on calix[4]pyrrole scaffolds as supramolecular reaction vessels.[16] As discussed in the previous chapter, pyridine-*N*-oxides are excellent guests for encapsulation in the aforementioned capsules. We hypothesized that the co-encapsulation[17] of two pyridine-*N*-oxides properly functionalized with azide and alkyne groups, in the capsules (Michaelis complex) would promote their inter-molecular Huisgen azide-alkyne 1,3-dipolar cycloaddition (Figure 4.1). The reactants will be bound in the capsule's cavity mainly by establishing hydrogen bonding interactions between oxygen atom of pyridine *N*-oxides and the pyrrole NHs of the two hemispheres. This will result in a constrained convergence of their *p*-pyridyl reacting substituents favouring the exclusive formation of the 1,4-isomer. We investigated the kinetic of the reaction taking place inside the capsule and compared it with that of the reaction occurring in the bulk solution.

We also performed a series of size and function selectivity control experiments. To this end, we used substrates that could not produce ternary co-encapsulation complexes or lacked the polar groups required for encapsulation.

4.2 Results and discussion

4.2.1 Design and synthesis

We previously disclosed (Chapter 3) the binding properties of the octa-imine and octa-amine capsules containing calix[4]pyrrole hemispheres in the encapsulation of

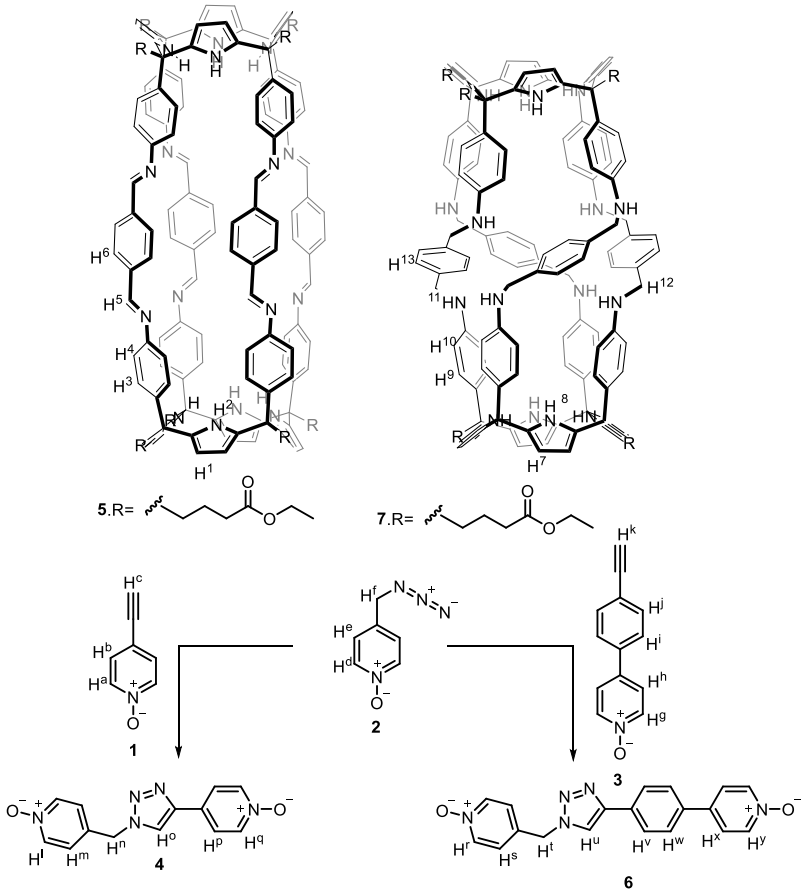

Figure 4.2. (Top) Octa-imine and octa-amine capsules as nanoreactors for Huisgen cycloaddition between 4-(ethynyl)-pyridine-*N*-oxide **1** and 4-(methylazide)-pyridine-*N*-oxide **2**. (Bottom) Synthetic schemes for the preparation of Huisgen cycloaddition products **4** and **6** in the bulk solution catalysed by Cu(I).

mono- and bis-pyridyl-*N*-oxide derivatives. In this chapter, we investigate their binding properties with *p*-functionalized pyridine *N*-oxides equipped with azide and

alkyne groups (**1**–**3**, Figure 4.2). Molecular modelling studies (MM3) indicated that the co-encapsulation of 4-(ethynyl)-pyridine-*N*-oxide **1** and 4-(azidomethyl)-pyridine-N-oxide **2** in the [4+2] octa-imine capsule will nicely fulfil all the complementary size, shape, function and volume requirements (Figure 4.3 c)

The encapsulated guests showed the *p*-peripheral substituents in close contact. This arrangement seemed to be appropriate to engage the reacting groups in the transition state of the cycloaddition reaction. Moreover, the two substrates were anchored in the capsule's cavity mainly by establishing hydrogen bonding interactions between their *N*-oxides knobs and the calix[4]pyrrole hemispheres. The guests' inclusion constrained their relative orientation to the one confronting the reacting groups.

We also modelled octa-imine **5** in order to select a competitive guest of 4-(ethynyl)-pyridine-*N*-oxide **1** that does not allow the formation of the ternary complex with 4-(methylazide)-pyridine-*N*-oxide **2**. For this purpose, we selected 4-(4-ethynylphenyl)-pyridine-*N*-oxide **3**. This *N*-oxide will be useful for the control studies of the capsule's size selectivity and reaction inhibition experiments.

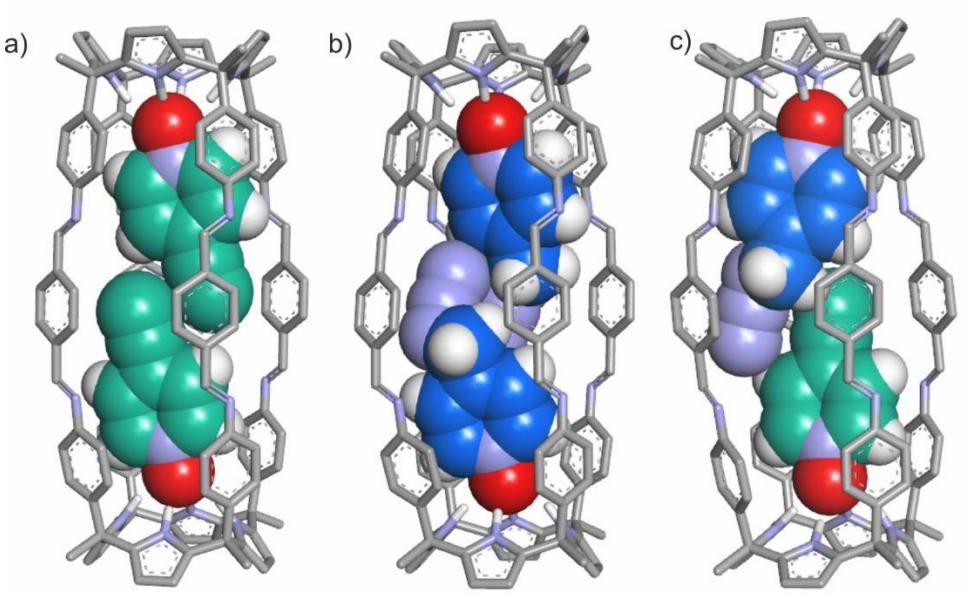

Figure 4.3. Energy minimized structure (MM3) of the ternary octa-imine homo- and hetero-encapsulation complexes a) (**1**)$_2$⊂**5**, b) (**2**)$_2$⊂**5**, c) **1-2**⊂**5**. *Meso*-alkyl-ester chains are pruned to methyl groups for clarity.

Briefly, 4-(methylazide)-pyridine was synthesised by reacting 4-(bromomethyl)pyridine hydrobromide with NaN_3 in DMF solution and, in the presence of K_2CO_3 as base, using a slightly modified reported procedure.[18] Next, the

isolated pyridine azide obtained was *N*-oxidized using oxone® in a water:2-butanone 1:1 solvent mixture affording 4-(methylazide)-pyridine-*N*-oxide **2** as a yellow oil in 45% yield.
Similarly, *N*-oxides **1** and **3** were synthesised by oxidation with oxone® of the ethynyl pyridine precursor derivatives.[19]
Compounds **1**–**3** have not been described previously.

The separate Cu(I) catalyzed cycloaddition reaction of pyridine *N*-oxide alkyne **1** and **3** with pyridine *N*-oxide azide **2** in CH_2Cl_2 solution and using tris-(benzyltriazolylmethyl)amine (TBTA) as ligand rendered the corresponding "click" triazole products, **4** and **6**, as pure 1,4-isomers. The 1,4-triazole isomers precipitated from solution as the reaction progressed.

4.2.2 Cycloaddition reaction mediated by the octa-imine capsule **5**

4.2.2.1 *Preparation of the homo-encapsulation complexes: (1)₂⊂5 and (2)₂⊂5*

Firstly, we investigated the binding properties of the octa-imine capsule **5** for the selected pyridine *N*-oxide derivatives: alkyne substituted **1** and azide substituted **2**. We assembled capsule **5** in a 9:1 $CDCl_3$:CD_3CN solvent mixture as described in Chapter 3. We divided the solution in two NMR tubes and performed separate ^{1}H NMR titration experiments of capsule **5** by adding incremental amounts of guests **1** and **2**.

The ^{1}H NMR spectrum of a *ca.* 1.5 mM solution of capsule **5** containing 2.2 equiv. of 4-(methylazide)-pyridine-*N*-oxide **2** showed the diagnostic signals for the quantitative formation of the 1:2 complex. We did not detect any remaining proton signal of free **5** (Figure 4.4 c). Molecular modelling studies (MM3) showed that two molecules of the azide **2** were a perfect fit for the capsule's interior.

The steric clashes that might be produced due to the proximity of the azide substituents of **2** in the 1:2 encapsulation complex (**2**)$_2$⊂**5**, can be alleviated by rotation through the single bonds connecting the pyridine ring and the azide group.

In contrast, the ^{1}H NMR spectrum of a ca. 1.5 mM solution of **5** containing 2.2 equiv. of the pyridine-*N*-oxide alkyne derivative **1** displayed multiple signals for the bound capsule, especially in the regions of the imine and NH protons (Figure 4.4 b). This observation indicated that the assembly of the 1:2 homo-capsular complex (**1**)$_2$⊂**5** was not quantitative and was accompanied by the formation of the 1:1 counterpart. Most likely, this result is caused by unavoidable steric clashes between the alkyne

groups of the two encapsulated *N*-oxides **1** owing to their conformational rigidity or unfavourable dipole-dipole interactions. In short, under stoichiometric control the (**1**)$_2$⊂**5** complex was only partially assembled.

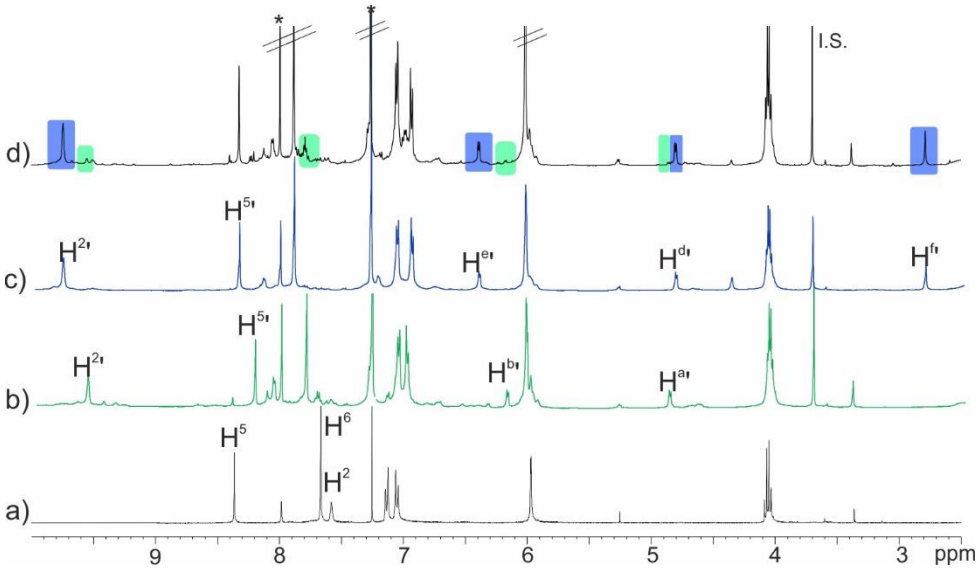

Figure 4.4. Selected region of the ^{1}H NMR spectra (500 MHz with cryoprobe, at 298 K, $CDCl_3$:CD_3CN 9:1 mixture) of (a) octa-imine capsule **5**; (b) solution (a) after the addition of 2.2 equiv. of ethynyl pyridine-*N*-oxide **1** (encapsulation complex (**1**)$_2$⊂**5** major species in solution); (c) solution (a) after the addition of 2.2 equiv. of azide pyridine-*N*-oxide **2** (quantitative formation of the encapsulation complex (**2**)$_2$⊂**5**); (d) solution mixture containing the encapsulation complexes (**1**)$_2$⊂**5** (indicated with green boxes) and (**2**)$_2$⊂**5** (indicated with blue boxes) prepared in (b) and (c). See Figure 4.2 for protons assignment. Primed letters indicate the signals of the complexes. (*) Indicates residual solvents and unreacted dialdehyde linker (at δ= 8 ppm used to assemble capsule **5**).

4.2.2.2 *Evaluation of cycloaddition reaction in the cavity of octa-imine capsule **5***

To study the putative role played by capsule **5** in promoting the cycloaddition reaction of **1** and **2**, we mixed the two solutions containing the homo-encapsulation 2:1 complexes (**1**)$_2$⊂**5** and (**2**)$_2$⊂**5**). Although, the initial concentration of capsule **5** was identical in the two solutions (*ca.* 1.5 mM concentration), we showed above that the homo-encapsulation complexes were assembled to different extent (Figure 4.4 c). The ^{1}H NMR of the mixture of homo-encapsulation complexes revealed that the (**2**)$_2$⊂**5** was the major species in solution. The signals of the protons in the (**1**)$_2$⊂**5** complex were also visible but with a reduced intensity. We did not observe proton signals that could be directly assigned to the hetero-encapsulation complex **1·2**⊂**5** (Michaelis complex).

However, it may be present in solution because the ^{1}H NMR spectrum of the mixture acquired after 30 min revealed the emergence of a new set of proton signals that perfectly matched with those of the encapsulation complex of the 1,4-triazole isomer of the Huisgen cycloaddition of **1** and **2**, that is the **4⊂5** complex (Figure 4.5 a). It is worth noting here that we prepared **4** by the Cu(I) catalysed cycloaddition of **1** and **2** in dichloromethane and characterized, separately, its encapsulation complex with **5**.

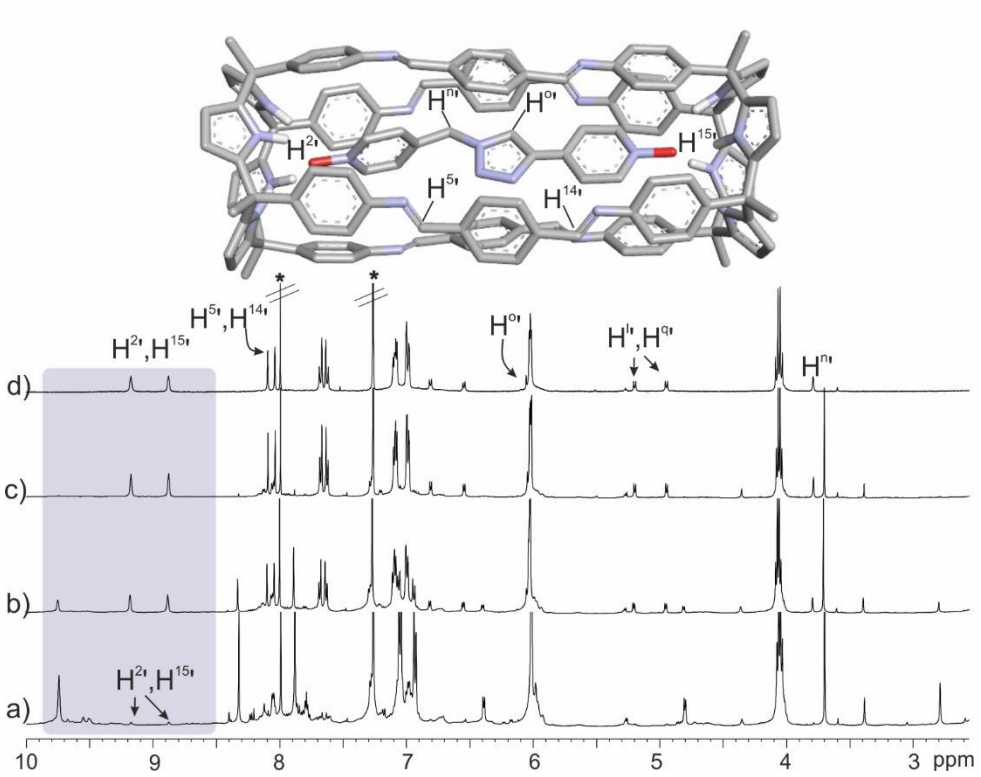

Figure 4.5. (Top) MM3 Energy minimized structure of the octa-imine complex **4⊂5**. (Bottom) Selected regions of the ^{1}H NMR spectra (500 MHz with cryoprobe, at 298 K, $CDCl_3$: CD_3CN 9:1 mixture) of (a) mixture of encapsulation complexes (**1**)$_2$⊂**5** and (**2**)$_2$⊂**5** solution after 30 min; (b) solution (a) after 20h; (c) solution (a) after 100 h; (d) **4⊂5** complex. See Figure 4.2 for protons assignment. Primed letters indicate the signals of the complexes. (*) Indicates residual solvents and unreacted dialdehyde linker (at δ= 8 ppm).

Approximately, after 100 h of reaction only the signals related to the **4⊂5** complex are observed in the ^{1}H NMR spectrum (Figure 4.5 c). The ^{1}H NMR spectrum of the encapsulation complex **4⊂5** displayed the encapsulated triazole proton H$^{o'}$ at δ= 6.05 ppm (slightly overlapped with the β pyrroles protons signal). The rest of the protons of the encapsulated product **4** appeared as five signals resonating between δ=6.80–3.78 ppm. The pyrrole NH protons of capsule **5** (H$^{2'}$, H$^{15'}$) experienced a

downfield shift (δ= 9.18 and 8.88 ppm) compared to the free capsule due to the formation of eight hydrogen bonding interactions with the non-symmetric encapsulated "click product" **4**.

The reason why the disproportionation equilibrium of the homo-complexes, (**1**)$_2$⊂**5** and (**2**)$_2$⊂**5**, did not produce the hetero-complex **1·2**⊂**5** (Michaelis complex) to an extent suitable for its detection by ^{1}H NMR spectroscopy is not clear to us. One could argue that this intermediate does not accumulate because its reaction rate is faster than that of its formation. Alternatively, the **1·2**⊂**5** may be high in energy, thus explaining its reduced formation. Without knowing the exact concentration of the ternary complex, it is not possible to calculate an accurate rate constant for the pseudo-first order cycloaddition taking place inside the capsule. This also limits the calculation of the effective molarity (EM) of the reaction in the cavity (EM = k_{in}/k_{out}). EM represents the theoretical concentration of the reactants necessary for observing an intermolecular reaction rate identical to that measured for the intramolecular counterpart.[8]

We determined the initial rate of the cycloaddition reaction, by calculating the slope of the line of the plot of changes in concentration of the encapsulation complex **4**⊂**5** *versus* time at t=0 ([**4**⊂**5**]= v_{in}t). We obtained an initial rate of v_{in}= 9.72 × 10^{-9} Ms^{-1} (Figure 4.6).
Similarly, the initial rate for the cycloaddition reaction of **1** with **2** at r.t. in the bulk solvent was v_{out}= 5.8 × 10^{-11} M s^{-1}. In this case, we used the slowly reacting compounds at 20 mM initial concentration. This translate into a rate constant of k_{out}= of 1.47 × 10^{-7} M^{-1} s^{-1} (k_{out}= v_{out}/[**1**] [**2**]= 5.8× 10^{-11} M s^{-1}/(20× 10^{-3} M × 20× 10^{-3} M)) corresponding to a half-life (at 20 mM of each component) of 10 years ($t_{1/2}$=1/(k_{out} [**1**]) for a bimolecular reaction).
Assuming that the concentration of the hetero-complex is below the detection limit of ^{1}H NMR spectroscopy (< 1 × 10^{-4} M), we estimated a rate constant for the reaction taking place in capsule **5** to be larger than 9.72 × 10^{-5} s^{-1}. Thus, the EM of the intramolecular reaction can be estimated to be larger than 660 M.

Alternatively, the effect of capsule **5** in mediating the cycloaddition can be estimated by considering that the rate of the reaction outside the capsule at the 1.5 mM concentration reagents used for the experiment is v= k_{out} [**1**] [**2**]= 1.47 × 10^{-7} M^{-1} s^{-1} × 1.5× 10^{-3} M × 1.5 × 10^{-3} M = 3.3 × 10^{-13} Ms^{-1} (where k_{out} is the rate constant measured in the absence of the capsule). This rate is around 30000 times lower than the one estimated inside the capsule **5** (v_{in}/v_{out}= 9.72 × 10^{-9} Ms^{-1}/3.3 × 10^{-13}Ms^{-1}).

Unfortunately, the strong non-covalent interactions established between the cycloaddition product **4** and the capsule led to product inhibition of the catalyst. In short, the catalytic capsule did not show turnover. The reaction stops when capsule **5** is filled with the product. For this reason, we are forced to use capsule **5** in stoichiometric amount with respect to the reagents.

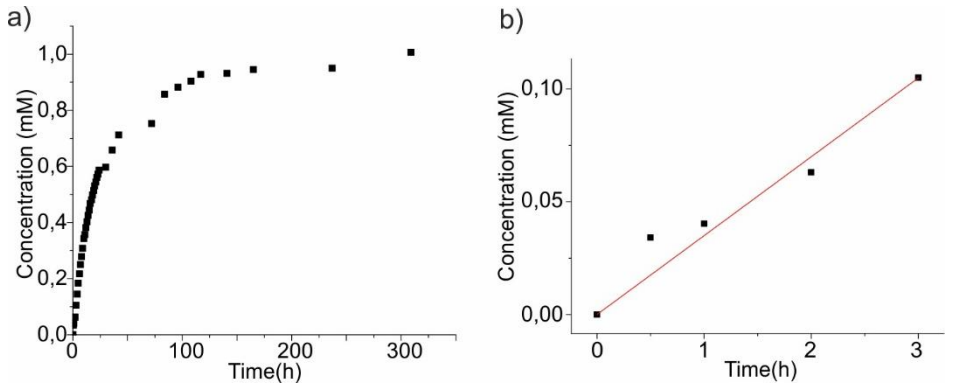

Figure 4.6. (a) Plot of the concentrations of encapsulation complex [**4⊂5**] in $CDCl_3$: CD_3CN 9:1 mixture *vs* time, (b) linear fit of the plot of the initial concentrations of the complex [**4⊂5**] in $CDCl_3$:CD_3CN 9:1 mixture *vs* time used to determine the initial reaction rate.

We also performed an analogous kinetic experiment in pure $CDCl_3$ solution. We wondered if in the absence of acetonitrile (which presents a larger binding affinity than $CHCl_3$ for the calix[4]pyrrole hemispheres[20,21]) the 2:1 homo-complexes of the capsule (especially (**1**)$_2$⊂**5**) would be formed to a larger extent.
We assembled the [4+2] octa-imine **5** in separate NMR tubes using pure $CDCl_3$ and 2 equiv. of pyridine-*N*-oxides **1** and **2** as templates. The resulting solutions were heated to 310 K for 24h and analysed after this time using ^{1}H NMR spectroscopy.

The 2:1 octa-imine complex with pyridine *N*-oxide azide **2**, (**2**)$_2$⊂**5**, was quantitatively assembled (*ca.* 1 mM concentration). In contrast, the 2:1 homo-encapsulation complex with pyridine-*N*-oxide alkyne **1**, (**1**)$_2$⊂**5**, although being the most abundant species in solution was not exclusively observed (Figure 4.19). These results are in complete agreement with the observations made in the 9:1 $CDCl_3$:CD_3CN mixture of solvents. Mixture of the two solutions containing the encapsulation complexes, (**2**)$_2$⊂**5** and (**1**)$_2$⊂**5**, assembled to a different extent, led to the observation of the proton signals of the encapsulation complex of the cycloaddition product, **4**⊂**5**, in the ^{1}H NMR spectrum acquired after 30 min.
We determined an initial reaction rate value of 9.49×10^{-9} Ms^{-1}, which is almost coincident with the one determined in 9:1 $CDCl_3$:CD_3CN solvent mixture.

4.2.2.3 *Control experiments*

In order to demonstrate that the cycloaddition reaction of **1** with **2** was taking place inside the cavity of capsule **5** and was not affected by other conventional forms of catalysis (*i.e*. organocatalysis), we performed additional control experiments.
To test the hypothesis that the capsule was not acting as an organocatalyst, we used two pyridine derivatives bearing the same reacting groups, alkyne and azide **8** and **9**. The pyridine derivatives do not have an intrinsic affinity for the calix[4]pyrrole hemispheres and remained in the bulk solution (Figure 4.7).

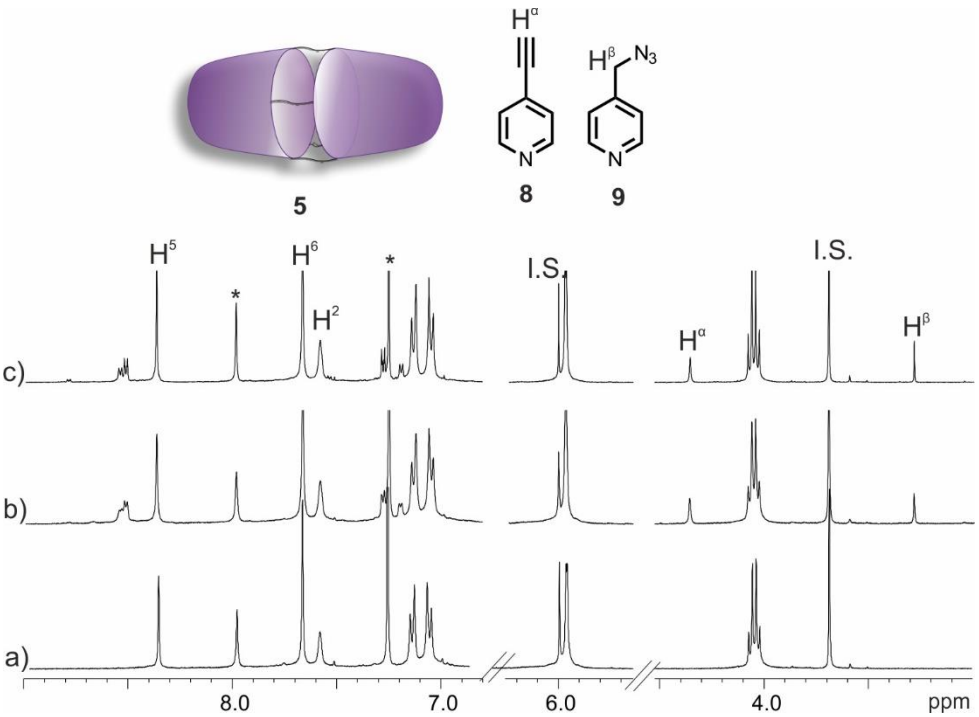

Figure 4.7. Selected region of the ^{1}H NMR spectra (400 MHz, at 298 K, $CDCl_3$:CD_3CN 9:1 mixture) of (a) imine based capsule **5**; (b) upon addition of 1 equiv. of **8** and 1 equiv. of **9**; (c) after 24 days. See Figure 4.2 for protons assignment. (*) Indicates residual solvents and unreacted dialdehyde linker (used to assemble capsule **5**).

Capsule **5** did not accelerate the cycloaddition reaction of **8** with **9**. Accordingly, we can exclude organocatalysis as the core of the acceleration.

We also performed a size selectivity experiment. The 4-(4'ethynylphenyl)-pyridine *N*-oxide **3** is too large to be co-encapsulated in **5** with the 4-(methylazide)-pyridine-*N*-oxide **2** and the corresponding reaction product **6** was not observed in a 1:1:1 mixture of **1**, **2** and **3** (Figure 4.8).

The cycloaddition product **6** is a lousy fit for the cavity of **5**. The addition of **6** to a solution of **5** produced a complex ^{1}H NMR spectrum suggesting the formation of poly-imine aggregates with ill-defined structures (Figure 4.8 f).

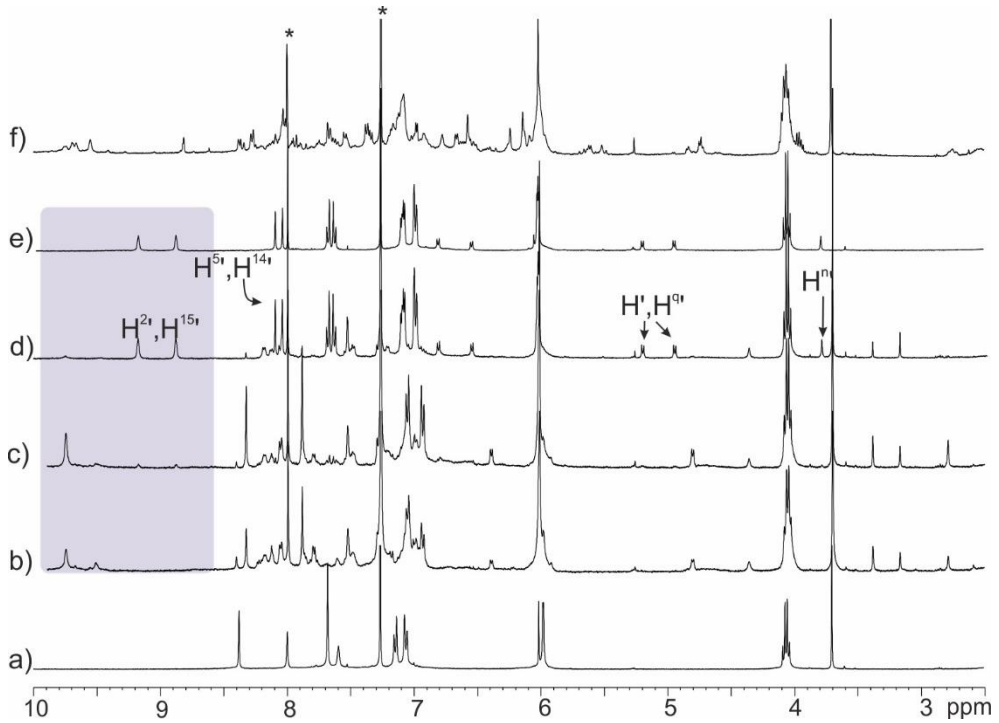

Figure 4.8. Selected region of the ^{1}H NMR spectra (400 MHz, at 298 K, $CDCl_3$:CD_3CN 9:1 mixture) of (a) imine based capsule **5**; (b) upon addition of a 1:1:1 mixture of **1**, **2** and **3**; (c) after 6 h; (d) after 24 d; (e) **4⊂5** complex; (f) 1:1 mixture of capsule **5** and click product **6** after equilibration for 5 days at r. t. See Figure 4.2 for protons assignment. (*) Indicates residual solvents and unreacted dialdehyde linker (at δ= 8 ppm).

In agreement with our previsions, we did not observe any cycloaddition product **6**. The presence of **3** in solution, which competes with **1** and **2** for the binding inside the cavity of **5**, produced an inhibition effect to the cycloaddition reaction of **1** with **2**. We observed that after 12 h the **4⊂5** complex was formed in a 26% yield when the competitive *N*-oxide **3** was present compared to the 47% obtained in its absence. The factors of size selectivity and reaction inhibition supported the encapsulation of the transition state.

4.2.3 Cycloaddition reaction mediated by the amine-based capsule **7**

4.2.3.1 *Preparation of the homo-encapsulation complexes: (**1**)$_2$⊂**7** and (**2**)$_2$⊂**7***

Considering the differences in conformational flexibility of the octa-imine **5** and octa-amine **7** capsules demonstrated in Chapter 3 for the binding of rigid bis-pyridine-*N*-oxides, we became interested in comparing their acceleration effect in the cycloaddition reaction between **1** and **2**.
We speculated that the larger conformational flexibility of octa-amine **7** may better adapt to geometric requirements of the transition state and influence favourably the reaction kinetics.

We prepared the homo-encapsulation complexes (**1**)$_2$⊂**7** and (**2**)$_2$⊂**7** by adding 2.2 equiv. of **1** or **2** to separate 0.7 mM solutions of the octa-amine capsule **7** in 9:1 $CDCl_3$:CD_3CN solvent mixture. We monitored the assembly of the complexes using ^{1}H NMR spectroscopy (Figure 4.9).

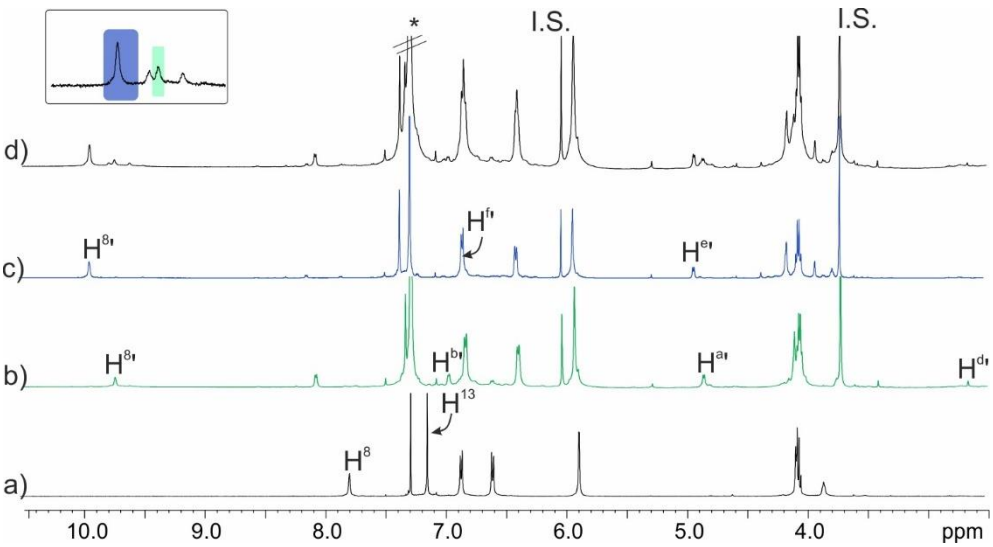

Figure 4.9. Selected region of the ^{1}H NMR spectra (500 MHz with cryo probe, at 298 K, $CDCl_3$: CD_3CN 9:1 mixture) of (a) amine based capsule **7**; (b) upon addition of 2.2 equiv. of **1** (capsular complex (**1**)$_2$⊂**7**); (c) upon addition of equiv. of 2.2 equiv. of **2** (capsular complex (**2**)$_2$⊂**7**); (d) 1:1 mixture of capsular complexes (**1**)$_2$⊂**7** (green box) and (**2**)$_2$⊂**7** solution (blue box). See Figure 4.2 for protons assignment. Primed letters indicate the signals of the complexes. (*) Indicates residual solvents.

The octa-amine capsule **7** formed quantitatively the homo-complexes (**1**)$_2$⊂**7** and (**2**)$_2$⊂**7**. We did not observe the signals of the protons of free **7**. The protons of the encapsulated *N*-oxides experienced the expected upfield shifts. Some remaining

signals for the free *N*-oxides were detected. The quantitative self-assembly of the (**1**)$_2$⊂**7** is at odds with the observation made for the (**1**)$_2$⊂**5** octa-imine counterpart. Most likely, the higher flexibility of the octa-amine capsule **7** compared to the octa-imine parent **5**, allowed the minimization of steric clashes of the ethynyl groups in the (**1**)$_2$⊂**7** complex.

4.2.3.1 *Evaluation of cycloaddition reaction inside octa-amine capsule* ***7***

We mixed the two solutions containing the (**1**)$_2$⊂**7** and the (**2**)$_2$⊂**7** homo-encapsulation complexes. We analysed the solution and the progress of the cycloaddition reaction using ^{1}H NMR spectroscopy (Figure 4.10).

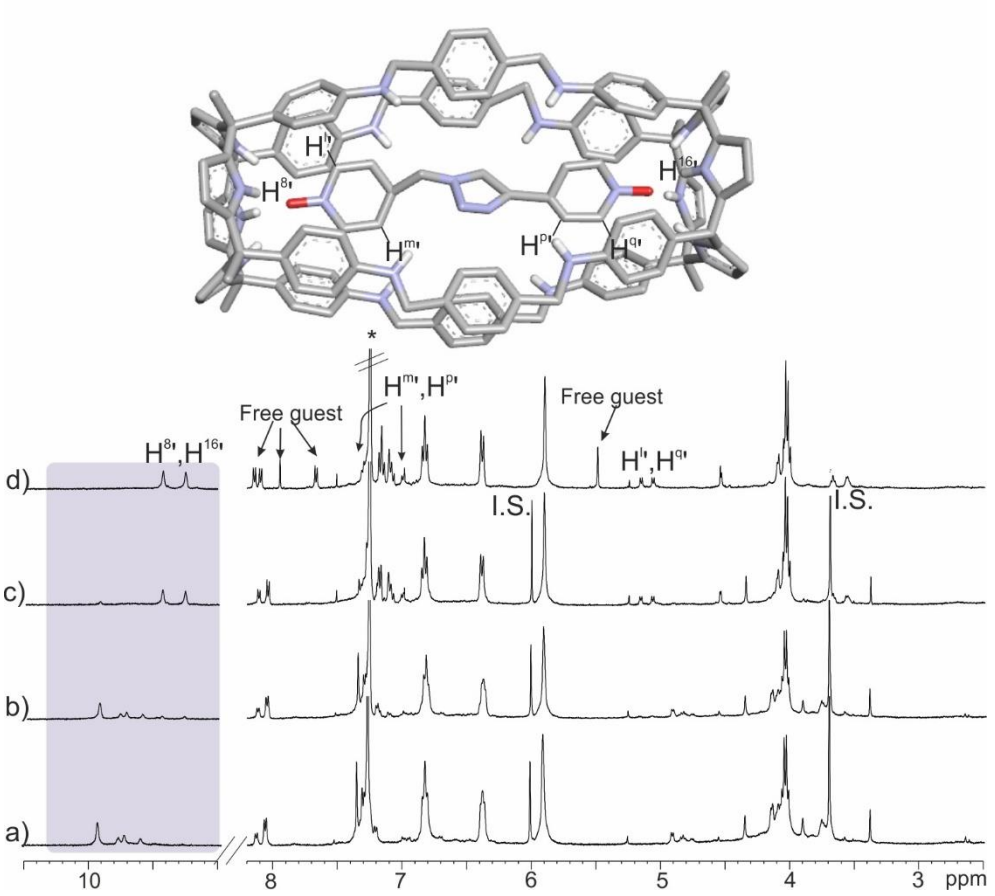

Figure 4.10. (Top) Preliminary X-ray structure of amine based capsular complex **4**⊂**7**. (Bottom) Selected region of the ^{1}H NMR spectra (500 MHz with cryoprobe, at 298 K, $CDCl_3$: CD_3CN 9:1 mixture) of (a) 1:1 mixture of capsular complexes (**1**)$_2$⊂**7** and (**2**)$_2$⊂**7** solution; (b) after 4 h; (c) after 92 h; (d) 1:1 mixture of capsule **7** and guest **4** (amine capsular complex **4**⊂**7**). See Figure 4.2 for protons assignment. Primed letters indicate the signals of the complexes. (*) Indicates residual solvents.

To our surprise, the concentration of the two homo-encapsulation complexes in the mixture, based on the integral values of the pyrrole NHs, was significantly different. We observed the appearance of two new pyrrole NHs that were assigned to the hetero-encapsulation complex **1·2⊂5** (Michaelis complex) formed by the rapid disproportionation equilibrium of the homo-encapsulation counterparts. Interestingly, after 4 hours of reaction, we detected the emergence of the proton signals of the encapsulation complex with the cycloaddition product **4⊂7**. We prepared separately the **4⊂7** encapsulation complex for comparison purposes.

The signals of the **4⊂7** complex increased at the expenses of those of the homo- and hetero-ternary counterparts. This result indicates that the formation of the hetero-encapsulation complex **1·2⊂5** (disproportionation rate) is faster than the reaction rate producing the **4⊂7** complex. This allowed its observation in the equilibrium with the homo-encapsulation complex precursors.

The initial rate of the cycloaddition reaction was calculated to be 6.38×10^{-9} Ms^{-1}. This value is, in the bulk part, of the same order of magnitude than the one obtained for the mediated reaction using the rigid octa-imine capsule **5**. However, at this point, we refrain in doing direct comparison of reaction rates because the concentrations used in the two experiments are not identical and even the molar ratio of the homo-encapsulation complexes are substantially different.

Remarkably, single crystals suitable for X-ray diffraction grew from the slow diffusion of toluene into a solution of the 9:1 $CDCl_3$:CD_3CN solvent mixture containing an equimolar ratio of octa-amine capsule **7** and the *N*-oxides **1** and **2**. Before the diffusion of toluene, the mixture was left reacting for a month at r.t.

The preliminary analysis of the diffracted data showed the structure of the octa-amine capsule **7** encapsulating a highly disordered bis-*N*-oxide guest (Figure 4.10 top). The refinement of the electronic density of the atoms of the encapsulate guest revealed the presence of a triazole ring. We also observed that each oxygen atom of the ditopic *N*-oxide guest formed four convergent hydrogen bonding interactionswith the pyrrole NHs of the distal hemispheres of octa-amine capsule **7** (average distance of 2.98 Å for the H-N···O hydrogen bonds). The average hydrogen-bonding distance in the solid-state is not very different from the average distance calculated for the energy minimized structure (Figure 4.5 top) of the octa-imine counterpart **5⊂7** complex (3.13 Å).

4.3 Conclusions

The [4+2] octa-imine capsule **5** and the fully covalent octa-amine capsule **7** were used as supramolecular reaction vessels to promote the Huisgen azide-alkyne 1,3-dipolar cycloaddition. For this purpose, we describe the syntheses of three pyridine *N*-oxides guests featuring either alkyne (**1** and **3**) or azide (**2**) terminal groups.
Binding studies of octa-imine capsule **5** with 2 equiv. of 4-(azidomethyl)-pyridine-*N*-oxide **2** produced exclusively the 2:1 capsular complex. In contrast, analogous experiments performed with the alkyne derivative **1** show the coexistence of 1:1 and 2:1 capsular complexes in solution. We propose that the existence of steric clashes or unfavourable dipole-dipole interactions between the alkyne moieties of the two encapsulated guests in the $(\mathbf{1})_2\subset\mathbf{5}$ 2:1 complex most likely disfavours its quantitative assembly.
The formation of the 1:1:1 complex $\mathbf{1}\cdot\mathbf{2}\subset\mathbf{5}$ was not observed in the ^{1}H NMR. However, pleasantly the mixture of $(\mathbf{1})_2\subset\mathbf{5}$ and $(\mathbf{2})_2\subset\mathbf{5}$ 2:1 complexes produced the progressive formation of the encapsulation complex of the 1,4-triazole isomer of the Huisgen cycloaddition product of the initial included guests. The kinetic studies performed by monitoring the formation of the "click" product showed a 10^4-fold acceleration of the reaction rate in the presence of the octa-imine capsule **5** compared to the same reaction in the bulk solution (absence of capsule **5**).
Analogous experiments performed in the presence of octa-amine capsule **7** revealed similar behaviour in rate acceleration compared to the reaction in the bulk. However, we could not establish direct comparisons of reaction rates with the octa-imine counterpart because the experiments were performed at slightly different concentrations.
In any case, beside the acceleration rate observed in the presence of both capsules, we demonstrated that the cycloaddition reaction taking place inside the capsules' cavity selectively produces the 1,4-cycloaddition regioisomer without the need to use a Cu(I) catalyst or high temperature.

Unfortunately, the application of the octa-imine and octa-amine capsules as molecular nanoreactors did not show turnover. This is attributed to the strong binding of the ditopic Huisgen cycloaddition product in the cage cavity.

4.4 Experimental section

4.4.1 General information and instruments

Starting materials and reagents were purchased from commercial suppliers and used without any further purification. All reactions were performed under argon atmosphere and protected from light unless specified. Anhydrous solvents were obtained from a solvent purification system SPS-400-6 from Innovative Technologies. All solvents were of HPLC grade quality, commercially obtained and used without further purification.

^{1}H NMR, ^{13}C NMR and 2D NMR spectra were recorded on a Bruker Avance 400(400 MHz for ^{1}H NMR) and Bruker Avance500 (500 MHz for ^{1}H NMR). Deuterated solvents from Sigma Aldrich were used for NMR studies, previously dried for the synthesis of dynamic covalent capsules. Chemical shifts are given in ppm, relative to residual solvents.

Capsules **5**, **7** and guest **1** synthetic procedures were reported in Chapter 3.

4.4.2 Synthesis and characterization

4.4.2.1 *Synthesis of guest **2***

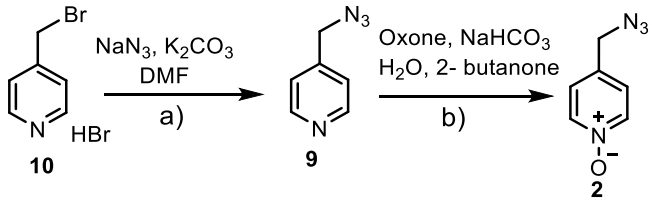

Scheme 4.1. Synthetic procedure for the preparation of pyridine *N*-oxide **2**.

a) Pyridine azide **9** was prepared by adapting a procedure reported in the literature.[18] 4-(bromomethyl)pyridine hydrobromide **10** (0.3 g, 1.2 mmol) was sonicated in 3 mL of DMF and K_2CO_3 (0.12 g, 1.8 mmol, 1.5 equiv.) was added. The mixture was stirred for 15 min. Then NaN_3 (0.25 g, 1.8 mmol, 1.5 equiv.) was added and the reaction was stirred for 4h at r.t., under Ar and protected from the light.

CH_2Cl_2 and cold water were added to the yellow suspension. The aqueous layer was extracted with CH_2Cl_2 (5× 10 mL) and the combined organic layers were washed with cold water (3×10 mL). The organic phase was then dried over anhydrous Na_2SO_4, filtered and the solvent was evaporated under reduced pressure. Pyridine azide **9**

was obtained as an orange oil in 40% yield and it was immediately used for the next synthetic step without further purification.
The ^{1}H NMR data is in agreement with the one reported in literature.

b) Pyridine azide **9** (80 mg, 0.8 mmol) was dissolved in a 1:1 mixture of water/2-butanone (20 ml) and $NaHCO_3$ (1.5 g, 17.9 mmol, 30 equiv.) was added under stirring. Oxone® (1.47g, 2.4 mmol, 4 equiv.) was added dropwise as a solution in water (ca. 10 ml) and the reaction was stirred under Ar protected from light for 24 h. After 24 h the mixture was diluted with chloroform (20 mL) and the water phase was washed with chloroform (3x20 mL). The organic layers were collected, dried over anhydrous Na_2SO_4, filtered and concentrated under reduced pressure. Pyridine *N*-oxide azide **2** was obtained as a yellow oil in 90% yield without any further purification.
^{1}H NMR (400 MHz, $CDCl_3$) δ(ppm): 8.18 (d, *J*= 7.2 Hz, 2H), 7.22 (d, *J*= 7.2 Hz, 2H), 4.39 (s, 1H).
^{13}C [^{1}H] NMR (100 MHz, $CDCl_3$) δ(ppm): 139.5, 134.4, 125.3, 52.6.
HR MS (APCI +) m/z: $[M+H]^+$ calculated for $C_{13}H_{10}NO^+$= 151.0620, found 151.0613.

4.4.2.2 *Synthesis of guest **3***

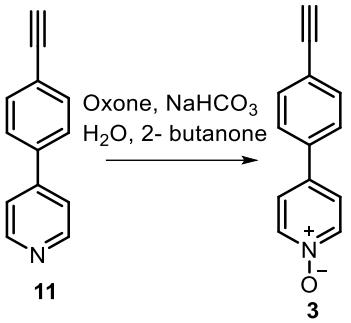

Scheme 4.2. Synthetic procedure for the preparation of pyridine *N*-oxide **3**.

Pyridine alkyne **11** was synthesized using a reported procedure.[19]
11 (0.1 g, 0.56 mmol) was dissolved in a 1:1 mixture of water/2- butanone (20 ml) and $NaHCO_3$ (1.4 g, 17mmol, 30 equiv.) was added under stirring. Oxone® (1.37 g, 2.2 mmol, 4 equiv.) was added dropwise as a solution in water (ca. 7 ml) and the reaction was left stirring under Ar protected from light.

After 24 h the mixture was diluted with chloroform (20 ml) and the water phase was washed with chloroform (3x20 ml). The organic layers were collected, dried over anhydrous Na_2SO_4, filtered and concentrated under reduced pressure. The crude

was adsorbed on celite and purified by column chromatography (neutral alumina, chloroform: *i*-propanol 95:5 -> 50:50) to obtain the product as a white solid in 40% yield.

^{1}H NMR (400 MHz, $CDCl_3$) δ(ppm): 8.25 (d, *J*= 7.3 Hz, 2H), 8.59 (d, *J*= 8.4 Hz, 2H), 7.54 (d, *J*= 8.4 Hz, 2H), 7.49 (d, *J*= 7.3 Hz, 2H), 3.19 (s, 1H).

^{13}C [^{1}H] NMR (100 MHz, $CDCl_3$) δ(ppm):139.6, 137.6, 136.5, 133.2, 126.4, 123.8, 123.2, 82.9, 79.3.

HR MS (APCI +) m/z: $[M+H]^+$ calculated for $C_{13}H_{10}NO^+$= 196.0762, found 196.0761.

4.4.2.3 *Synthesis of cycloaddition products **4** and **6***

Pyridine *N*- oxide alkyne **1** or **3**, (0.13 mmol), pyridine *N*-oxide azide **2** (0.13 mmol), tetrakis-(acetonitrile)copper(I) hexafluorophosphate (7.6 µmol, 0.06 equiv.) and TBTA (7.6 µmol, 0.06 equiv.), were dissolved in a vial with 5 mL of dry CH_2Cl_2. The reaction mixture was stirred for 12 h at r.t. protected from light.

The white precipitate was collected via filtration and washed with cold CH_2Cl_2, giving **4** or **6** as beige solids in 45% yield.

4: ^{1}H NMR (400 MHz, $CDCl_3$:CD_3CN 9:1 mixture) δ(ppm): 8.16 (d, *J*= 6.8 Hz, 2H), 8.11 (d, *J*= 6.8 Hz, 2H), 7.96 (s, 1H), 7.68 (d, *J*= 6.4 Hz, 2H), 7.16 (d, *J*= 6.4 Hz, 2H), 5.51 (s, 2H).

6: ^{1}H NMR (400 MHz, $CDCl_3$) δ(ppm): 8.27 (d, *J*= 7.2 Hz, 2H), 8.23 (d, *J*= 7.1 Hz, 2H), 7.95 (d, *J*= 8.3 Hz, 2H), 7.83 (s, 1H), 7.67 (d, *J*= 8.3 Hz, 2H), 7.54 (d, J= 7.2 Hz, 2H), 7.20 (d, J= 7.1 Hz, 2H), 5.60 (s, 2H).

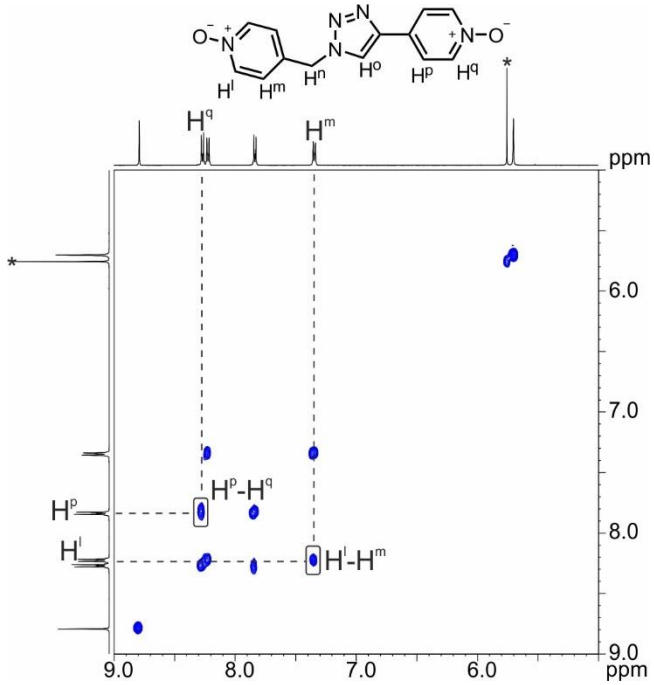

Figure 4.11. Selected region of 2D COSY NMR (400 MHz, at 298 K, DMSO-d_6) of click product **4**. (*) Indicates residual solvents.

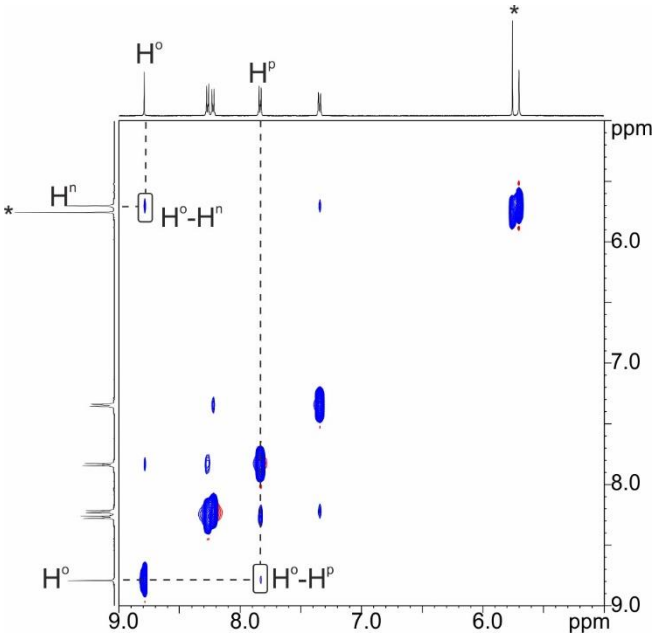

Figure 4.12. Selected region of 2D NOESY NMR (400 MHz, at 298 K, DMSO-d_6, d8= 0.6 s) of click product **4**. (*) Indicates residual solvents. See Figure 4.11 for proton assignment.

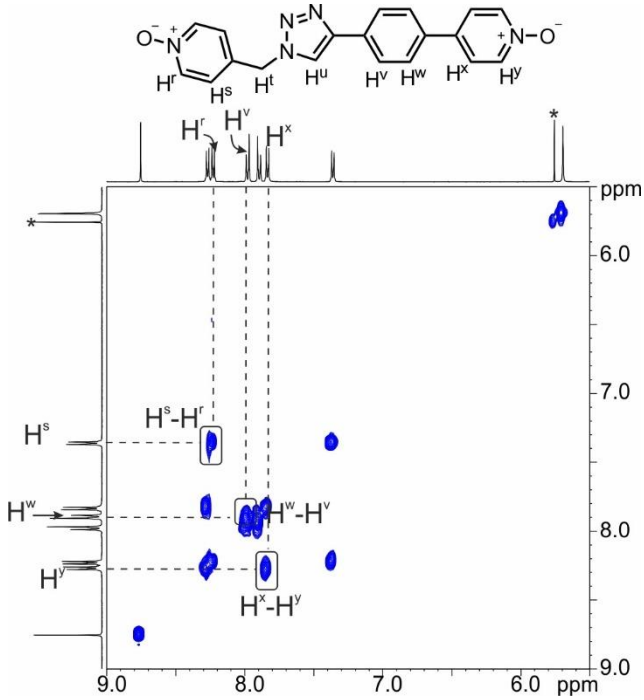

Figure 4.13. Selected region of 2D COSY NMR (400 MHz, at 298 K, DMSO-d_6) of click product **6**. (*) Indicates residual solvents.

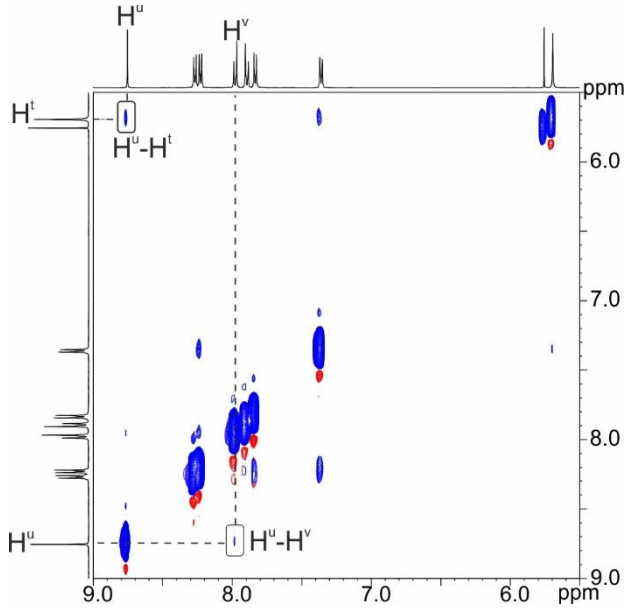

Figure 4.14. Selected region of 2D NOESY NMR (400 MHz, at 298 K, DMSO-d_6, d8= 0.6 s) of click product **6**.(*) Indicates residual solvents. See Figure 4.13 for protons assignment.

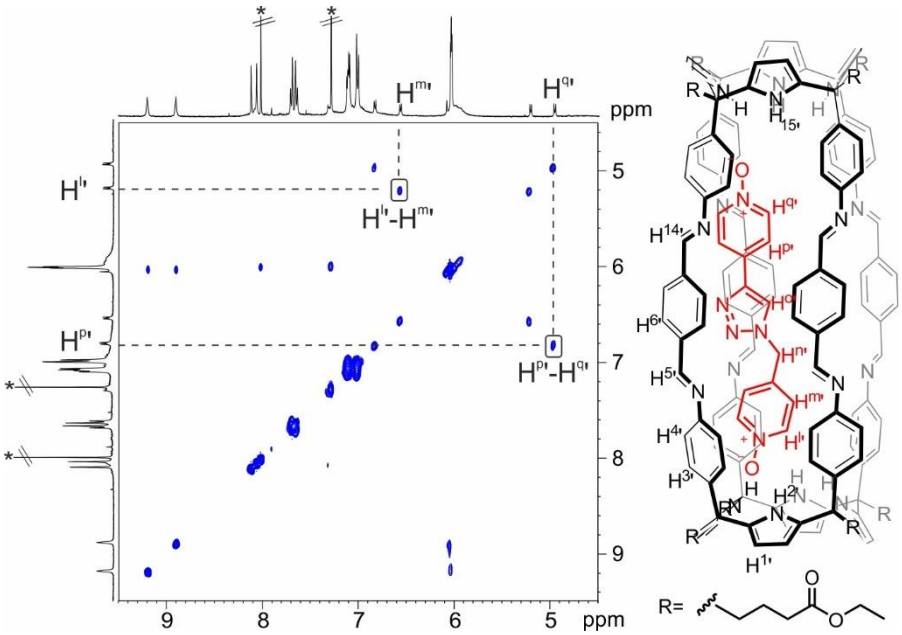

Figure 4.15. Selected region of 2D COSY NMR (400 MHz, at 298 K, $CDCl_3$: CD_3CN 9:1 mixture) of imine capsular complex **4⊂5**.(*) Indicates residual solvents and unreacted aldehyde used for the capsule assembly.

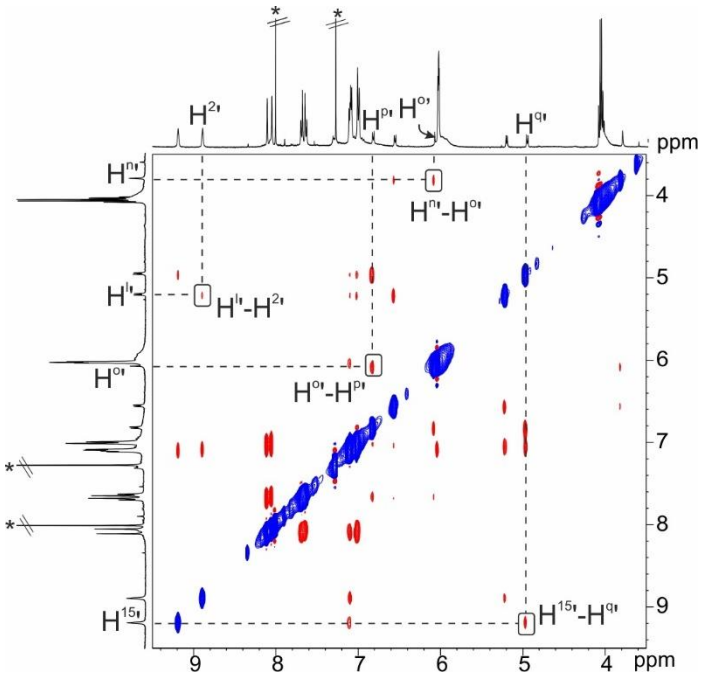

Figure 4.16. Selected region of 2D ROESY NMR (400 MHz, at 298 K, $CDCl_3$:CD_3CN 9:1 mixture, p15= 0.3 s, $CDCl_3$: CD_3CN 9:1 mixture) of imine capsular complex **4⊂5**. (*) Indicates residual solvents and unreacted aldehyde used for the capsule assembly. See Figure 4.15 for protons assignment.

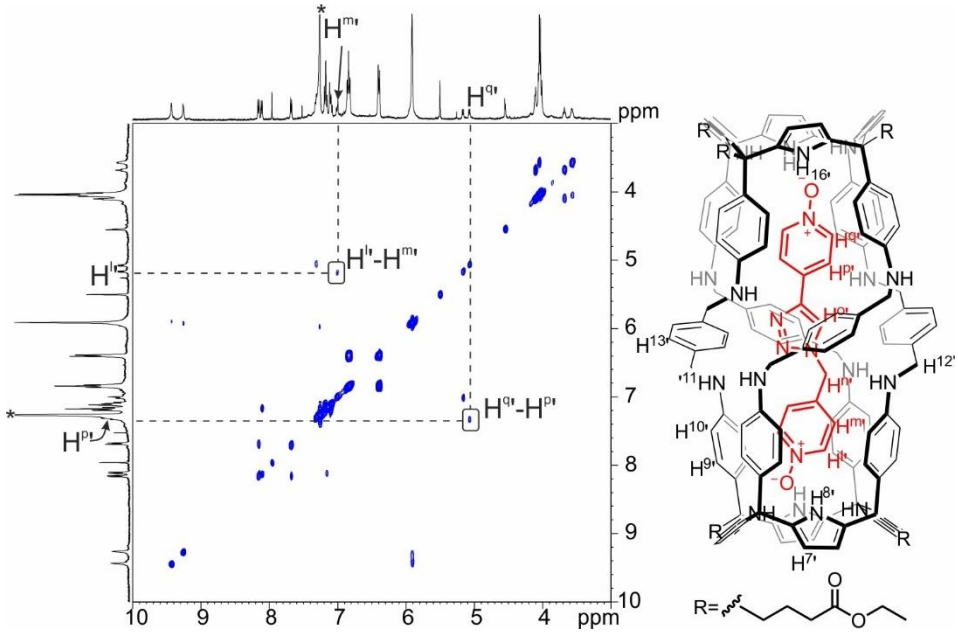

Figure 4.17. Selected region of 2D COSY NMR (400 MHz, at 298 K, $CDCl_3$:CD_3CN 9:1 mixture) of amine capsular complex **4⊂7**. (*) Indicates residual solvents.

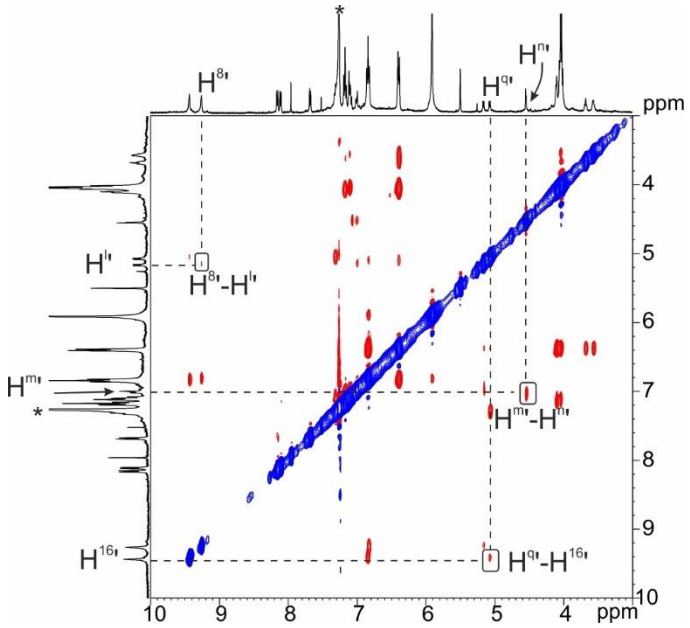

Figure 4.18. Selected region of 2D ROESY NMR (400 MHz, at 298 K, p15= 0.3 s, $CDCl_3$:CD_3CN 9:1 mixture) of imine capsular complex **4⊂7**. (*) Indicates residual solvents and unreacted aldehyde used for the capsule assembly. See Figure 4.17 for protons assignment.

4.4.3 Kinetic characterization of cycloaddition reaction

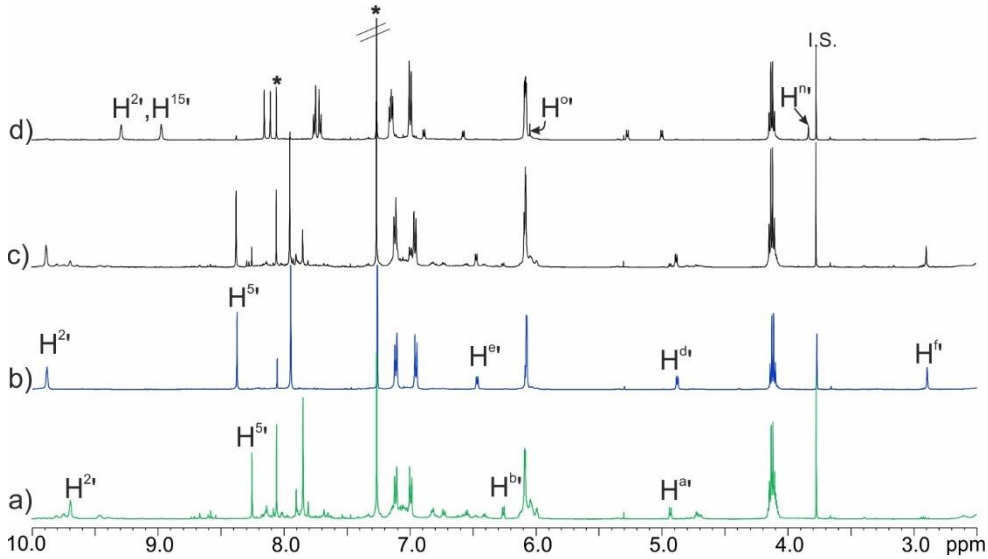

Figure 4.19. Selected region of the ^{1}H NMR spectra (500 MHz with cryo probe, at 298 K, $CDCl_3$) of (a) imine capsular complex assembled in presence of **1** ((**1**)$_2$⊂**5** complex major product); (b) imine capsular complex assembled in presence of **2** ((**2**)$_2$⊂**5** complex); (c) 1:1 mixture of (a) and (b); (c) 1:1 mixture of a) and b) after 13 days. See Figure 4.15 for protons assignment. Primed letters indicate the signals of the complexes. (*) Indicates residual solvents and unreacted dialdehyde used for the capsule assembly.

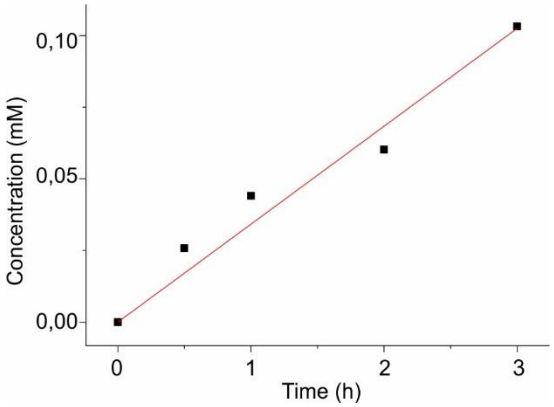

Figure 4.20. Linear fit of the plot of initial concentrations of capsular complex [**4**⊂**5**] in $CDCl_3$ *vs* time used to determine the initial reaction rate.

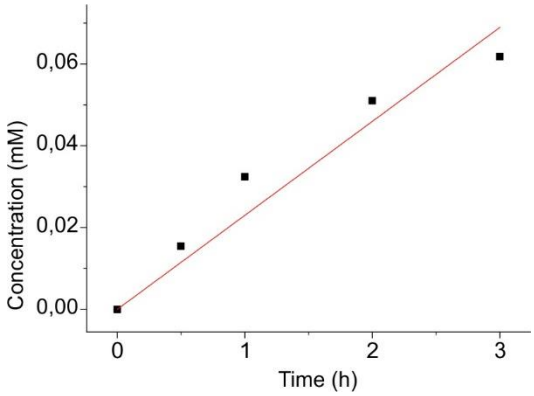

Figure 4.21. Linear fit of the plot of initial concentrations of capsular complex [**4⊂7**] in $CDCl_3$:CD_3CN 9:1 mixture *vs* time used to determine the initial reaction rate.

4.5 References and notes

[1] Y. Lyu, P. Scrimin, *ACS Catal.* **2021**, *11*, 11501-11509.
[2] M. Raynal, P. Ballester, A. Vidal-Ferran, P. W. N. M. van Leeuwen, *Chem. Soc. Rev.* **2014**, *43*, 1734-1787.
[3] G. Olivo, G. Capocasa, D. Del Giudice, O. Lanzalunga, S. Di Stefano, *Chem. Soc. Rev.* **2021**, *50*, 7681-7724.
[4] A. Galan, P. Ballester, *Chem. Soc. Rev.* **2016**, *45*, 1720-1737.
[5] P. Ballester, A. Vidal-Ferran, P. W. N. M. van Leeuwen, in *Adv. Catal., Vol. 54* (Eds.: B. C. Gates, H. Knözinger), Academic Press, **2011**, pp. 63-126.
[6] D. Fiedler, D. H. Leung, R. G. Bergman, K. N. Raymond, *Acc. Chem. Res.* **2005**, *38*, 349-358.
[7] N. Xu, K. Su, E.-S. M. El-Sayed, Z. Ju, D. Yuan, *Chem. Sci.* **2022**, *13*, 3582-3588.
[8] R. Cacciapaglia, S. Di Stefano, L. Mandolini, *Acc. Chem. Res.* **2004**, *37*, 113-122.
[9] R. S. Meissner, J. Rebek, J. d. Mendoza, *Science* **1995**, *270*, 1485-1488.
[10] J. Kang, J. Rebek, Jr., *Nature* **1997**, *385*, 50-52.
[11] R. Huisgen, *Angew. Chem., Int. Ed. Engl.* **1963**, *2*, 565-598.
[12] V. V. Rostovtsev, L. G. Green, V. V. Fokin, K. B. Sharpless, *Angew. Chem. Int. Ed.* **2002**, *41*, 2596-2599.
[13] H. C. Kolb, M. G. Finn, K. B. Sharpless, *Angew. Chem. Int. Ed.* **2001**, *40*, 2004-2021.
[14] W. Mock, *Org. Chem* **1983**, *48*, 3619.
[15] J. Chen, J. Rebek, *Org. Lett.* **2002**, *4*, 327-329.
[16] A. V. Davis, R. M. Yeh, K. N. Raymond, *PNAS* **2002**, *99*, 4793-4796.
[17] J. Rebek Jr., *Angew. Chem. Int. Ed.* **2005**, *44*, 2068-2078.
[18] M. Piccinno, G. Aragay, F. Y. Mihan, P. Ballester, A. Dalla Cort, *Eur. J. Inorg. Chem.* **2015**, *2015*, 2664-2670.
[19] H. L. Ozores, M. Amorín, J. R. Granja, *J. Am. Chem. Soc.* **2017**, *139*, 776-784.
[20] G. Gil-Ramírez, E. C. Escudero-Adán, J. Benet-Buchholz, P. Ballester, *Angew. Chem. Int. Ed.* **2008**, *47*, 4114-4118.
[21] A. Díaz-Moscoso, D. Hernández-Alonso, L. Escobar, F. A. Arroyave, P. Ballester, *Org. Lett.* **2017**, *19*, 226-229.

General conclusions

In this thesis work, we describe the design, the synthesis of molecular components, the self-assembly and the study of the binding properties of [1+1] and [4+2] supramolecular cages and capsules containing two calix[4]pyrrole hemispheres. The supramolecular capsules and cages are self-assembled using dynamic covalent chemistry, more specifically, as a result of imine condensation reactions (Schiff-base). We also report the post-assembly modification of the [4+2] octa-imine capsule to obtain a chemically more robust octa-amine capsule derivative.
We investigate the kinetics of the uptake and release of planar di-topic and mono-topic pyridyl-*N*-oxides, as well as of the sterically more demanding quinuclidine-*N*-oxide. The obtained results provided insights of the mechanisms of encapsulation and release of the guests by the dynamically covalent and fully covalent capsules.
We also demonstrated the ability of the [4+2] octa-imine capsule and the octa-amine derivative to promote the reactivity (1,3-dipolar cycloaddition) of two substrates confined in their cavity.

We draw the following conclusions from the results obtained in this work:

1) Dynamically covalent [1+1] tetra- and [4+2] octa-imine capsules are assembled in good yields by encapsulating a template guest or two copies of solvent molecules. The included solvent molecules can be polar (*e.g.* acetonitrile) or non-polar (*e.g*. chloroform or dichloromethane). The weakly bound solvent molecules are conveniently displaced by the encapsulation of pyridyl-*N*-oxides. The oxygen atoms of the encapsulated *N*-oxides strongly interact with the pyrrole NHs of capsule's calix[4]pyrrole hemispheres by establishing an array of hydrogen bonding interactions and complementary CH-π and π-π interactions, etc.
2) The rate of the encapsulation processes of mono-topic pyridine-*N*-oxide and di-topic 4',4'-bipyridine *N*,*N*-dioxide in the [1+1] tetra-imine capsule was influenced by the solvent's nature. Binding studies performed in 9:1 $CDCl_3$:CD_3CN solvent mixture featured encapsulation kinetics that were slow on the human-time scale (it took from hours to days to reach equilibrium). The kinetics of the encapsulation process was further slowed down when the sterically more demanding quinuclidine *N*-oxide guest was used. In contrast, the use of pure chloroform as solvent produced fast encapsulation kinetics for the planar *N*-oxides. We conclude that the acetonitrile molecules actively participated in the encapsulation processes

by competing for the binding with the calix[4]pyrrole hemispheres with the incoming *N*-oxides. Most likely, the encapsulation mechanisms of the planar *N*-oxides (2D guests) and the quinuclidine-*N*-oxide (3D guest) in the [1+1] capsule are different.

3) The [4+2] octa-imine capsules displayed polar cavities larger than the [1+1] tetra-imine counterparts and are able to accommodate larger monotopic and ditopic pyridyl-*N*-oxides. The encapsulation of bis-*N*-oxide guests of different lengths produced encapsulation complexes featuring different apparent symmetries. The ^{1}H NMR spectrum of the complex with the longest bis-pyridine *N*-oxide guest displays an apparent D_{4h} symmetry. This demonstrated that the guest simultaneously binds the two hemispheres of the capsule through hydrogen bond interactions between the *N*-oxide knobs and the pyrrole NHs.

   In contrast, the encapsulation complex with the shortest bis-pyridine *N*-oxide shows an apparent C_{4v} symmetry. The observed symmetry suggests that the length of the guest is too short to bind at the same time the two hemispheres of the capsule. The X-ray crystal structure of the encapsulation complex revealed an highly disordered guest suggesting the co-encapsulation of a water molecule in the cavity of the octa-imine together with the short *N*-oxide.

4) Post-assembly modification of the [4+2] octa-imine capsule by simple reductive amination of the imine bonds produced the corresponding octa-amine derivative. The conformational flexibility imparted by the presence of single bonds in the octa-amine capsule's backbone allowed the adaptation of the dimensions of its cavity to those of short ditopic bis-*N*-oxide guest. This behaviour contrasted with the conformational rigidity detected for the octa-imine capsular precursor. The octa-amine capsule produced a more compact encapsulation complex by maximizing the non-covalent interactions between the calix[4]pyrrole NHs and the oxygen atoms of the *N*-oxide functions and optimizing the interactions' distances.

5) The [4+2] octa-imine capsule and the octa-amino derivative were used as supramolecular nano-reactors. The co-encapsulation of pyridine *N*-oxides having *p*-substituted alkyne and azide groups produced an acceleration in the rate of the Huisgen azide-alkyne 1,3-dipolar cycloaddition when compared to the reaction rate observed in the bulk solution. The cycloaddition reaction taking place inside the capsule cavity does not

require the use of a Cu(I) catalyst or high temperatures affording selectively the 1,4- cycloaddition regioisomer.

List of abbreviations

ACN	-	Acetonitrile
APCI	-	Atmospheric Pressure Chemical Ionization
CE	-	Collision Energy
CID	-	Collision Induced Dissociation
COSY	-	Correlated Spectroscopy
CPK	-	Corey-Pauling-Koltun model
DCC	-	Dynamic Covalent Chemistry
DCL	-	Dynamic Covalent Library
DCM	-	Dichloromethane
DIPA	-	*N,N*-Diisopropylamine
DFT	-	Density Functional Theory
DMF	-	Dimethylformammide
DMSO	-	Dimethylsulfoxide
DOSY	-	Diffusion Ordered Spectroscopy
Equiv.	-	Equivalent
ESI-MS	-	Electrospray Ionization Mass Spectrometry
GPC	-	Gel Permeation Chromatography
HPLC	-	High-Performance Liquid Chromatography
IMS	-	Ion-Mobility Mass Spectrometry
I.S.	-	Internal Standard
ITC	-	Isothermal Titration Calorimetry

K	-	Kelvin
kcal	-	Kilocalorie
MALDI	-	Matrix-Assisted Laser Desorption Ionization
MHz	-	MegaHertz
MS	-	Mass Spectrometry
mM	-	Millimolar
MM	-	Molecular Mechanics force field
MTBE	-	Methyl tert-butyl ether
NMR	-	Nuclear Magnetic Resonance
NOESY	-	Nuclear Overhauser Enhancement Spectroscopy
PC	-	Packing Coefficient
ROESY	-	Rotating-frame Enhancement Spectroscopy
r.t.	-	Room temperature
SPS	-	Solvent Purification System
TBACl	-	Tetrabutylammonium Chloride
TBAF	-	Tetrabutylammonium Fluoride
THF	-	Tetrahydrofuran
TFA	-	Trifluoroacetic Acid
TBTA	-	Tris(benzyltriazolylmethyl)amine
TMA	-	Trimethylamine
TMEDA	-	Tetramethylethylenediamine
Ts	-	Toluenesulfonyl

TS	-	Transition State
VT	-	Variable Temperature
µM	-	Micromolar

UNIVERSITAT
ROVIRA i VIRGILI

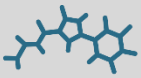

ICIQ

Institute
of Chemical
Research
of Catalonia